

Oscillatory and structural measures of connectivity in psychosis, psychosis-risk and the healthy population

Emily Lambe



Thesis submitted for the degree of
Doctor of Philosophy 2022

School of Psychology
Cardiff University

General Summary

Magnetoencephalography (MEG) and Diffusion Tensor Imaging (DTI) are important tools for probing functional and structural properties of the brain. The interactions between the brain's local and long-range circuitry could provide a key to understanding schizophrenia as a disorder of dysconnectivity and related risk factors in the healthy population.

The aim in the first chapters of this thesis was to understand how high frequency local visual circuitry and long-range low frequency connectivity can be best estimated from MEG data. It was shown that using a finer sampling grid in source estimation leads to improved measures of high frequency responses. Furthermore, that networks usually measured in the resting-state can be extracted from task data was another key discovery and has positive implications for data quality and participant comfort going forward.

The second aim of this thesis was to understand how specific local and global entities interact by investigating the relationships between local visual circuitry and long-range structural and oscillatory connectivity. An important finding was that the magnitude of local connectivity in the superficial layers of the visual cortex, as probed by gamma amplitude, was associated with reduced long-range connectivity beyond primary visual areas. The other novel finding was that the frequency of local visual oscillations was correlated with structural measures, possibly reflecting increased myelination.

The third aim of this work was to better understand how psychosis-risk relates to functional and structural connectivity in health and schizophrenia. Schizotypy was robustly correlated with reduced long-range functional connectivity but not structural connectivity. The opposite was true for correlations between polygenic risk and connectivity. However, the aforementioned risk factors were not robustly correlated with local functional connectivity. The last chapter showed novel but non-significant differences in local and global oscillatory connectivity that were related to excitatory-inhibitory copy number burden in patients.

Statements and Declarations

Statement 1 This thesis is being submitted in partial fulfilment of the requirements for the degree of PhD.

Signed.....Date.....29.03.2022.....

Statement 2 This work has not been submitted in substance for any other degree or award at this or any other university or place of learning, nor is it being submitted concurrently for any other degree or award (outside of any formal collaboration agreement between the University and a partner organisation)

Signed.....Date.....29.03.2022.....

Statement 3 I hereby give consent for my thesis, if accepted, to be available in the University's Open Access repository (or, where approved, to be available in the University's library and for inter-library loan), and for the title and summary to be made available to outside organisations, subject to the expiry of a University-approved bar on access if applicable.

Signed.....Date.....29.03.2022.....

Declaration This thesis is the result of my own independent work, except where otherwise stated, and the views expressed are my own. Other sources are acknowledged by explicit references. The thesis has not been edited by a third party beyond what is permitted by Cardiff University's Use of Third Party Editors by Research Degree Students Procedure.

Data collection

Data in Chapter 3 was collected by Dr Jennifer Brealy as part of the 100-Brains study. Data in Chapter 4 was collected as part of the MEG-Partnership study by Dr Lorenzo Magazzini and Dr Bethany Routley. In Chapters 5-9, the functional data was collected by Dr Jennifer Brealy, Dr Lorenzo Magazzini and Dr Bethany Routley. The structural data was collected by Dr Lisa Brindley, Dr Sonya Foley and the CUBRIC radiographers and operators. Data in Chapter 10 was collected by myself and Dr Gemma Williams.

Initial analysis

Pre-processing and co-registration of the 100-Brains data was completed by Jennifer Brealy. Pre-processing of the MEG-Partnership resting-state data was completed by Bethany Routley and co-registration was completed by Lorenzo Magazzini. Tractography and generation of the structural matrices was performed by Dr Eirini Messaritaki. The McDespot data was originally analysed by Sonya Foley. The ICA denoising of the resting-state data in Chapter 10 was carried out by Dr Diana Dima and Dr Elin Roberts. Polygenic Risk Score and Copy Number Variant information was courtesy of Dr Thomas Lancaster and Dr Elliot Rees, respectively. All other analyses were carried out by me.

Acknowledgements

There are a number of people at Cardiff University without whom this PhD would not have been possible. Foremost, I would like to express my sincere gratitude to my supervisor Krish Singh, for his support over the last 5 years, for his expertise in MEG imaging and analysis and relaxed nature.

I would also like to give special thanks to Alex Shaw, Eirini Messaritaki and Craig Hedge: Alex, thank you for your copious time and wisdom in programming and analysis; Eirini, thank you for sparking my interest in structural imaging and sharing your expertise with openness and support; to Craig I want to share my thorough appreciation for the helpful chats and your professional time also.

Next, I want to thank Kevin Murphy for his advice and the encouragement to write. Last but not least, thank you to James Walters for supporting me in undertaking this venture. I am very glad I did.

Beyond the university environment, I would like to give warm thanks to my family who have never wavered in their belief in me; I am eternally grateful. Let the phrase ‘onwards and upwards’ never fall on deaf ears.

Finally, to my friends, who have encouraged and listened to me in the hard times during this PhD, well done, we made it! To those friends, also, who made my time in Cardiff such fun; you know who you are! I will never forget your support and kindness.

My appreciation also goes to Cardiff University School of Psychology for funding my PhD.

Contents

| | |
|---|----|
| Chapter 1. Introduction | 1 |
| 1.1 General Aim | 1 |
| 1.2 Schizophrenia | 1 |
| 1.3 Dysconnectivity Theory | 2 |
| 1.4 Neuroimaging schizophrenia..... | 4 |
| 1.5 The visual cortex (VC)..... | 8 |
| 1.6 Beyond diagnostics | 9 |
| 1.7 What is an oscillation? | 11 |
| 1.8 Gamma oscillations and the healthy brain | 11 |
| 1.9 Local and global processes in the healthy brain-a commentary..... | 17 |
| 1.10 General aims and objectives..... | 22 |
| Chapter 2. General Methods | 24 |
| 2.1 Magnetoencephalography | 24 |
| 2.2 Structural Magnetic Resonance Imaging (MRI) | 32 |
| Chapter 3. An investigation of the optimal sampling grid resolution for MEG beamforming..... | 37 |
| 3.1 Rationale..... | 37 |
| 3.2 Introduction | 37 |
| 3.3 Method | 41 |
| 3.4 Results | 46 |
| 3.5 Discussion | 51 |
| Chapter 4. Extracting long-range networks from task data | 55 |
| 4.1 Rationale..... | 55 |
| 4.2 Introduction | 55 |
| 4.3 Method | 58 |
| 4.4 Results | 65 |
| 4.5 Discussion | 83 |
| 4.6 Appendix A | 87 |
| Chapter 5. Identifying sub-networks with Non-Negative Matrix Factorization: Initial results.... | 88 |
| 5.1 Rationale..... | 88 |
| 5.2 Non-Negative Matrix Factorization | 88 |

| | |
|---|-----|
| 5.3 Functional components | 89 |
| 5.4 Structural components (DTI measures)..... | 94 |
| Chapter 6. Relationships between local and global oscillatory measures of connectivity and structural connectivity in the healthy population..... | 100 |
| 6.1 Rationale..... | 100 |
| 6.2 Introduction | 100 |
| 6.3 Method | 107 |
| 6.4 Results | 116 |
| 6.5. Discussion | 132 |
| Chapter 7. Schizotypy and global functional and structural networks | 138 |
| 7.1 Rationale..... | 138 |
| 7.2 Introduction | 138 |
| 7.3 Method | 144 |
| 7.4 Results | 151 |
| 7.5 Discussion | 159 |
| Chapter 8. Polygenic Risk Score for Schizophrenia and structural and functional connectivity | 164 |
| 8.1 Rationale..... | 164 |
| 8.2 Introduction | 164 |
| 8.3 Method | 171 |
| 8.4 Results | 178 |
| 8.5 Discussion | 188 |
| Chapter 9. Schizophrenia risk factors and local visual gamma | 193 |
| 9.1 Rationale..... | 193 |
| 9.2 Background | 193 |
| 9.3 Method | 200 |
| 9.4 Results | 203 |
| 9.5 Discussion | 211 |
| Chapter 10. The effect of excitatory-inhibitory (E-I) CNV status on global oscillatory connectivity and visual gamma in psychosis | 215 |
| 10.1 Rationale..... | 215 |
| 10.2 Introduction | 215 |
| 10.3 Method | 222 |
| 10.4 Results | 230 |

| | |
|--|-----|
| 10.5 Discussion | 237 |
| 10.6 Appendix B | 244 |
| 1. GABA and glutamate CNVs in cases. | 244 |
| Chapter 11. General Discussion..... | 245 |
| 11.1 Summary of findings..... | 245 |
| 11.2 Implications | 247 |
| 11.3 Broader considerations..... | 256 |
| 11.4 General limitations and future directions | 258 |
| 11.5 Conclusion..... | 260 |
| References..... | 262 |

Chapter 1. Introduction

1.1 General Aim

Up to 1 percent of the population suffer with schizophrenia (NIMH, 2022). Though the prevalence is relatively low, the disorder is associated with several health, economic and social issues. Despite continued neurological discovery and theoretical advancements in the fields of psychiatry, psychology and academia, heterogeneity exists in the schizophrenia literature. This thesis will look beyond the classical diagnostic approach to schizophrenia (DSM-V, American Psychiatric Association, 2013), with the aim of identifying potential neuroimaging phenotypes which could help delineate differences between sufferers and in the literature. The overall aim is to investigate connectivity associated with schizophrenia-risk with a combination of functional task-based and resting-state paradigms, as well as structural connectivity measures. This will provide new mechanistic insights into the underlying neurobiological pathology that could help inform stratification of disease, treatment planning and novel drug discovery.

1.2 Schizophrenia

Schizophrenia is a severely debilitating disorder characterised by the presence of positive (e.g., hallucinations and delusions), negative (e.g., avolition and anhedonia), and cognitive symptoms (i.e., working memory and executive function deficits). Increased disease co-morbidity together with ineffective anti-psychotic medications and side effects, are among the factors that contribute to sufferers experiencing a poorer quality of life and significantly shortened life span; on average 15% (Buckley, Miller, Lehrer, & Castle, 2009; Fitzgerald & Watson, 2018). A higher incidence of suicide is also reported in groups with schizophrenia or related psychoses compared to those in the normal population, with ~1 in 3 people attempting suicide during their lifetime (Hor & Taylor, 2010; Pompili et al., 2007).

Recent evidence suggests that the Covid-19 pandemic disproportionately affected the mental health of young people (“COVID-19 mental health and wellbeing surveillance: report,” 2021), where the onset of psychosis is usual. Furthermore, suicide risk is especially elevated within the first year of presentation, at 12 times greater than in the healthy groups in Europe (Nordentoft et

al., 2004), suggesting that better interventions are required for those in the early stages of illness and in the at-risk population.

The primary medical intervention for schizophrenia continues to be anti-psychotic medications which target dopaminergic pathways in the brain. While these dopamine blockades have fundamental value in relieving acute psychosis, their usage over ~ 60 years has shown ineffectiveness in relieving negative and cognitive symptoms. There is now strong animal, genetic, pharmacological and imaging evidence to suggest that other systems are also involved (Egerton et al., 2020; Friston, Brown, Siemerikus, & Stephan, 2016; Krogmann et al., 2019; Legge et al., 2021; Pocklington et al., 2015; Zhao et al., 2018). Specifically, serotonergic, glutamatergic, gamma-aminobutyric acid (GABA), acetylcholinergic and inflammation factors have been implicated, with research on associated actions and interactions ongoing. Principally, the last 20 years has seen increasing support for disturbances of glutamatergic and GABAergic processes (Chung, Fish, & Lewis, 2016; Glausier & Lewis, 2017), which underpin the synaptic excitatory-inhibitory (E-I) balance of the healthy brain (Alan Anticevic & Lisman, 2017).

Proposed neurobiological mechanisms for schizophrenia fall largely into four categories; **1**) the dopaminergic hypothesis in which positive symptoms are associated with dopamine hyperactivity at D2 dopamine receptors in mesolimbic pathways, with medications antagonising D2 receptors there (Meltzer & Stahl, 1976; Winterer & Weinberger, 2004), **2**) the NMDA receptor hypo-function hypothesis where glutamate signalling is dysregulated in the limbic system and results in aberrant dopamine pathways and hypodopaminergia downstream (Snyder & Gao, 2013; Stahl, 2007), **3**) the dysfunction in neuromodulation of GABAergic receptors on inhibitory interneurons and subsequent dysregulation of pyramidal neuron firing (Guiotti et al., 2005; Lewis et al., 2005) and **4**) the inflammatory hypothesis, where a hyper-activated immune system influences serotonergic and glutamatergic neurotransmission (Müller, Weidinger, Leitner, & Schwarz, 2015).

1.3 Dysconnectivity Theory

Such mechanisms feature in Friston's theory of Dysconnectivity (Friston, 1998; Friston et al., 2016), which proposes that schizophrenia aetiology is, at least partly, due to impaired synaptic

connectivity both between and within brain regions, and is a popular mode of interpretation. Predictive Coding and Bayesian Inference are prominent components of the theory which successfully collate heterogeneous experiences of positive symptoms in patients. Here, the iterative interaction between bottom-up encoding processes (in superficial pyramidal cells) and top-down representations (in deep pyramidal cells) in the cortical hierarchy, is the process by which representations are updated and if disturbed can result in prediction errors and false representations. The idea that weights attributed to sensory versus internal representations during perception are unbalanced in schizophrenia, builds on previous theories such as Aberrant Saliency (Howes & Kapur, 2009), which postulate that dopamine dysregulation in psychosis results in perceptual attribution to stimuli otherwise extraneous. More recent evidence has also demonstrated that people with early psychosis have a disposition to favour existing knowledge over new sensory information (Teufel et al., 2015).

Synaptic gain is the excitability of neuronal populations (e.g., superficial pyramidal cells) one function of which is reporting prediction errors. GABA is the primary inhibitory neurotransmitter in the brain whereas glutamate is the primary excitatory neurotransmitter. Thus, beyond dopaminergic systems, GABA and glutamate are closely tied to modulated gain control. Computationally, abnormal gain control within local canonical circuits in schizophrenia has been demonstrated with Dynamic Casual Modelling (Adams et al., 2022; Friston, Harrison, & Penny, 2003; Friston, 2008; Pinotsis et al., 2017; Shaw et al., 2017; Shaw, Knight, et al., 2020).

Abnormal gain control, perhaps via impairments of these neurotransmitter systems, can also lead to desynchronised populations of neurons across the cortex, reflected in abnormal connectivity measures (Bowyer, 2016; Buzsaki & Draguhn, 2004; Friston, 2011). Interestingly, glutamate has been associated with positive, negative and cognitive symptoms in schizophrenia, and GABAergic inhibition is negatively associated with negative symptoms (Balu, 2016; Kantrowitz & Javitt, 2010; Krogmann et al., 2019; Shaw, Knight, et al., 2020; Stone, 2011; Tsai & Coyle, 2002; Uno & Coyle, 2019), such that the aforementioned neurotransmitter systems may be implicated in the full spectrum of schizophrenia symptomology.

1.3.1 Genetic contributors

Genetic studies show that both common and rare variation in genetics contribute to schizophrenia susceptibility (Rees et al., 2015). The latest Genome Wide Association Study (GWAS) found single nucleotide variants at 270 loci to be associated with schizophrenia (Consortium, Ripke, Walters, & O'Donovan, 2020). Consistent with described neurobiological models, a large study (N>26,000) found individuals with schizophrenia also have increased Copy Number Variant (CNV) burden on genes involved in inhibitory GABAergic and excitatory glutamatergic signalling, as compared with controls (Polkington et al., 2015).

Additionally, while heritability in schizophrenia is estimated at ~80 % (Owen, Sawa, & Mortensen, 2016), de novo mutations appear to be important, with new genetic changes being overrepresented among glutamatergic postsynaptic proteins comprising activity-regulated cytoskeleton-associated protein (ARC) and N-methyl-d-aspartate receptor (NMDAR) complexes (Fromer et al., 2014). A variety of genetic and neurodevelopmental factors are causally important and influence effective synaptic transmission (Owen et al., 2016), however faulty NMDA receptors have been heavily implicated in dysconnectivity (Balu, 2016; Friston et al., 2016; Harrison & Weinberger, 2005).

1.4 Neuroimaging schizophrenia

In the healthy brain, at the microscopic scale, axonal and dendritic connections and synaptic terminals connect neurons to other neurons forming both multicellular and local neuronal circuits. Meso- and macroscopic circuits comprise neural columns and largescale brain regions which are connected by close and long-range axonal white matter projections. Interactions between meso- and larger scale networks, studied under systems neuroscience, allow the complex functioning of the brain.

Neuroimaging is a dominant mode of systems neuroscience and has provided valuable pieces to the neuropathological puzzle that is schizophrenia. Functional connectivity comprises the dependencies of remote neurophysiological events (Friston, 2011) and can be captured by analysis of the oscillatory Magnetoencephalography (MEG) or Electroencephalography (EEG) signal, or by analysis of the slower Blood Level Oxygen Dependent (BOLD) signal obtained from functional Magnetic Resonance Imaging (fMRI). The slowness of the fMRI signal is

because it is reliant on the haemodynamic response and can therefore be confounded by respiratory and other physiological factors. Regardless, such methods, in addition to modelling techniques, have revealed both local and global functional dysconnectivity in schizophrenia using both task paradigms and investigations of the resting-state.

1.4.1 Resting-state studies

Resting-state paradigms are easily implemented in a neuroimaging protocol. By avoiding potential confounds related to the completion of a task, measuring connectivity at rest is useful in investigating spontaneous networks. That being said, because there is no task, it is difficult to know exactly what the participant is doing in the scanner and therefore some scans can be poorly controlled. Globally, fMRI studies have revealed reduced connectivity in schizophrenia (Pettersson-Yeo, Allen, Benetti, McGuire, & Mechelli, 2011; Yu et al., 2012; Zhou et al., 2007), whereas oscillatory connectivity measures have revealed both hyper- and hypo-connectivity, across the oscillatory frequency bands (Alamian et al., 2017b; Bowyer et al., 2015; Cetin et al., 2016; Hinkley et al., 2011; Uhlhaas & Singer, 2010a).

Among the most consistent findings are reduced frontal connectivity, aberrant fronto-parietal/occipital connectivity, particularly in the alpha band (Liu et al., 2019b; Trajkovic et al., 2021), and aberrant parieto-temporal connectivity (Alamian et al., 2017b; Houck et al., 2016; Maran, Grent-'t-Jong, & Uhlhaas, 2016). These findings are interesting in the context of schizophrenia symptoms, where deficits in executive functioning, working memory and auditory and visual hallucinations are common, and closely tied to the aforementioned areas.

One explanation for the differences in electrophysiological connectivity profiles is the effect of disease stage and duration (Liu et al., 2019a; Zhao et al., 2018). For example, Grent-'T-Jong (2018) found increased resting-state high gamma power, in clinical-high-risk (CHR) groups, over frontal and temporal structures, while schizophrenia groups showed reduced broadband gamma power, with first episode subjects also showing increase gamma power in the visual cortex (VC). In support, glutamatergic NMDAR-related gamma signatures associated with early and chronic disease stages have been shown to be distinct (Anticevic et al., 2015). Importantly, hyper-connectivity seen in At-Risk and First-Episode groups could comprise a precursor to

illness (Di Lorenzo et al., 2015; Krukow, Jonak, Grochowski, Plechawska-Wójcik, & Karakuła-Juchnowicz, 2020; Zhao et al., 2018), which could be exploited a clinical risk marker.

At present, it remains unclear to what extent the global connectivity network effects are driven by local aberrant connectivity. Graph theoretical descriptions (where brain areas are represented as a set of local nodes with connections between represented as edges) have helped, with metrics such as smallworldness, modularity, global efficiency and path length representing the local and global properties of neural networks. Most functional graph theory studies have focused on fMRI in the resting-state, with results showing disrupted smallworldness (quantified integration and segregation properties of neural populations), in patients (Liu et al., 2008), and reduced local efficiency and increased global efficiency (Yu et al., 2012).

1.4.2 Task-based studies

Task-based studies have also been fundamental to our understanding of domain specificity and task related integrative connectivity in schizophrenia. Visual grating, auditory steady state and sensory motor tasks are now common in schizophrenia imaging pipelines due to neurophysiological research showing disturbances in the corresponding visual gamma, auditory 40hz steady state response (SSR) and beta activity phenomena (Gascoyne et al., 2021; Shaw et al., 2017; Spencer, Salisbury, Shenton, & McCarley, 2008). Dynamic Causal Modelling (DCM) has provided a means by which such responses can be tied to excitatory and inhibitory connections within canonical microcircuits and at the meso- and macro-neuronal scale (Friston et al., 2003), and subsequently the opportunity to better non-invasively understand E-I imbalance in schizophrenia. DCM is based on Bayesian Inference, where essentially change in one region predicts rate of change in another and provides considerable support to Friston's Dysconnectivity theory (Friston et al., 2016).

Task-based studies have also been useful in unpicking cognitive symptoms that are at present poorly treated. For example, Nielsen (2017) found that fronto-parietal connectivity was modulated by working memory during an N-back task using DCM, and that modulation was reduced in FE patients. Exploiting time series data in this way has provided evidence that local

and global functional connectivity impairments seen in patients are causally involved in presentation.

Oscillatory functional connectivity disturbances have been related to positive, negative and cognitive symptoms in schizophrenia, though the nature of these relationship is also unclear with positive and negative trends being found (e.g., Chen et al., 2016; Fehr et al., 2001, 2003; Kim et al., 2014; Spencer et al., 2008; Sperling et al., 2002; Sperling et al., 2003). Interestingly, Manzano and colleagues (2017) found that MEG resting-state data in individuals with chronic schizophrenia had high frequency amplitude profiles across the cortex which could distinguish predominant symptom dimensions (i.e., disorganisation, reality disturbance and poverty slowness), suggesting that MEG oscillations could provide a unique opportunity for understanding functional systems across the different clinical domains (Manzano et al., 2017).

1.4.3 Structural connectivity

While functional connectivity is not isomorphic with structural connectivity, it is constrained by the structural connectome. ‘Connectomics’ is the study of the brain’s architecture and how it supports brain functioning (Fornito, Zalesky, Pantelis, & Bullmore, 2012; Sadaghiani, Brookes, & Baillet, 2021b). The structural connectome refers to the anatomical structure of the brain and its interconnections. It includes, though is not limited to, white matter projections, white matter volume and axonal microstructure, metrics for which are obtained through neuroimaging methods like Diffusion Tensor Imaging (DTI). DTI is a specific MRI sequence which utilises the signal generated from water molecules when combining radiofrequency pulses with magnetic field gradients. Alternating the direction of gradient pulses across different planes provides diffusivity metrics in 3 directions and allows structural pathways to be reconstructed with tractography modelling.

Structurally, individuals with schizophrenia show several abnormalities. Historical imaging studies have shown clear volumetric and morphological differences, including reductions in prefrontal, temporal and thalamus volume (Breier et al., 1992; Gaser, Nenadic, Buchsbaum, Hazlett, & Buchsbaum, 2004). More recent network studies have shown abnormalities in DTI measures such as Fractional Anisotropy (FA), Radial diffusivity (RD) and Axial Diffusivity

(AD), which index the movement of water within white matter tracts. Reductions in FA and increases in RD, representing reduced overall diffusivity and increased diffusivity in the perpendicular orientation of the tract, respectively, have most commonly been found in schizophrenia (Joo et al., 2018; Parnanzone et al., 2017). Graph theoretical studies have also shown increased clustering and modularity and increased path length, suggesting there could be increased segregation of areas connected by white matter tracts in patients (Fornito et al., 2012; Van Den Heuvel, P & Fornito, 2014). While these findings contrast functional evidence showing increased local efficiency in schizophrenia, their existence is not necessarily contradictory, as functional hyper-connectivity may also be pathological (Fornito & Bullmore, 2015; Friston et al., 2016).

1.5 The visual cortex (VC)

The VC, an extensively studied local modality of the brain, is highly implicated in schizophrenia on account of its role in processing bottom-up and top-down visual information (Lawrence, Norris, & De Lange, 2019). Both volume and neuron number are reduced in the VC of patients (Dorph-Petersen, Pierri, Wu, Sampson, & Lewis, 2007). Disrupted local interneuron circuitry and NMDA hypofunction in VC are also reflected in the high frequency oscillatory disturbances frequently reported in schizophrenia groups (Carlén et al., 2012; Gonzalez-Burgos, Cho, & Lewis, 2015; Grent-'t-Jong et al., 2016; Kujala et al., 2015). Furthermore, complementary to E-I theories (Lewis, Curley, Glausier, & Volk, 2012), GABA concentration is reduced in VC in patients (Yoon et al., 2019, 2010).

Persons with psychotic disorder show altered processing of contextual visual information, which is the background or context of the visual stimulus or activity in addition to existing top-down biases, knowledge or expectations (Glöckner & Moritz, 2008; Yang et al., 2013). In fact, even the earliest responses in V1 show contextual modulation (Seymour et al., 2013). Nevertheless, it has been suggested that the long-range integration of information is fundamentally disturbed in schizophrenia (Glöckner & Moritz, 2008; Northoff, Sandsten, Nordgaard, Kjaer, & Parnas, 2021), and is reflected in intra-area connectivity differences. For example, dysconnectivity between VC and amygdala has been associated with visual hallucinations (Ford et al., 2015) and

dysconnectivity between VC and thalamus has also been related to attentional impairments (Yamamoto et al., 2018).

Interestingly, the VC may be a therapeutic target for schizophrenia considering recent longitudinal work which has shown that visual acuity and visual impairment in childhood is associated with increased psychotic experience in 17–24-year-olds (Shoham, Hayes, Cooper, Theodorsson, & Lewis, 2021). This effect has also been shown in a cohort of 1 million Swedish men studied between adolescence and adulthood (40+ years) (Hayes et al., 2019). Such studies demonstrate the importance of understanding neuropathological inter- and intra- areal interactions in VC.

1.6 Beyond diagnostics

Friston's dysconnectivity hypothesis provides an excellent framework for reconciling schizophrenia imaging findings. However, studying the normal population with schizophrenia risk factors can also be beneficial for several reasons. For example, as Duration of Untreated Psychosis (DUP) is associated with poorer long-term outcomes (Murru & Carpiniello, 2018), acutely unwell individuals are usually fast-tracked onto antipsychotic medication. However, antipsychotics have structural and functional neural correlates which can compromise the reliability of findings in clinical cohorts (Tarcijonas & Sarpal, 2019). Furthermore, inflammation has been increasingly implicated in psychosis, as indexed by cytokines and C-reactive protein (Boozalis, Teixeira, Cho, & Okusaga, 2018; Fond, Lançon, Korchia, Auquier, & Boyer, 2020), and accumulating evidence suggests that inflammation affects E-I neural circuitry (Fourgeaud & Boulanger, 2010; Fourgeaud et al., 2010; Landek-Salgado, Faust, & Sawa, 2015). Finally, the nature of schizophrenia disorders is heterogeneous, with individuals exhibiting a diversity of symptoms differentially weighted by genetic, clinical, biological and neurodevelopmental factors.

The dimensional view of schizophrenia suggests genetic and clinical risk factors for schizophrenia are dispersed in the normal population (Grant, Green, & Mason, 2018). Clinical risk includes factors like symptom presentation and adverse circumstances (Paolo Fusar-Poli et al., 2013). Genetics risk refers to the presence of identified variants i.e., Single Nucleotide

Polymorphisms or CNVs associated with schizophrenia. Increasingly such factors have become targets for investigation as increased genetic or clinical burden is related to psychosis onset (Barrantes-Vidal, Grant, & Kwapil, 2015; Marshall et al., 2017; Nenadić et al., 2020) and will be discussed further in this thesis.

1.6.1 Identifying biomarkers and imaging markers in psychology and psychiatry

The aforementioned factors highlight the importance of investigating neuropathology beyond classical diagnostics. For this, the identification of bio-imaging markers in both the healthy brain and psychopathology has a considerable number of advantages. Firstly, probing the healthy brain provides an opportunity to further develop understanding of the brain's equilibrium, mechanisms and its associated physiological processes. Secondly, markers which differ in disease provide a key to identifying clinical, genetic and environmental differences between heterogeneous individuals and between disorders in general. And third, neurobiological impairment is common prior to the onset of clinical symptoms and in related groups; bio-imaging markers are a means to better understanding of risk and subsequent avenues for prevention.

1.6.2 Research Domain Criteria (RDoC)

The identification of biomarkers supports the 6-domain translational RDoC approach (Insel, 2014), which aims to understand the nature of mental health disorders in terms of biological systems and psychological mechanisms. At present, the 6 domains include: Positive Valence systems, Negative Valence Systems, Cognitive Systems, Arousal and Regulatory Systems, Social Processing and Sensorimotor Systems. These can be studied using different units of analysis, which include genetic, physiological, behavioural, and self-report assessments. The RDoC approach differs to the traditional diagnostic approach to research, where a binary categorisation system applies and tools such as the Diagnostic and Statistics Manual (American Psychiatric Association, 2013) and International Classification of Diseases (WHO, 2018) are employed.

Understanding specific neurobiological impairments under the umbrella term of 'schizophrenia' would facilitate the administration of individualistic care. Through this research process, it is hoped that functionally important mechanistic markers will be uncovered.

1.7 What is an oscillation?

Oscillations comprise rhythmic signals which represent neural fluctuations. In laboratories, intracellular single unit recordings measure the oscillatory activity of a neuron, while extracellular local field potentials measure the summation of oscillatory activity originating from a group of neurons. In humans, oscillations are typically recorded by scalp EEG and MEG (MEG) and occasionally by cortical and depth electrodes during surgery, which all yield complicated oscillatory waveforms comprised of energy in different frequency bands. Unlike animal recordings, scalp-recorded oscillations do not directly measure neuronal bursting, but instead measure fluctuations in neural activity. They are considered an assembly of local field potentials, which are thought to come mostly from post-synaptic potentials, representing the synchronous activity of a large set of neurons or neural circuits.

1.8 Gamma oscillations and the healthy brain

1.8.1 Gamma oscillations – Background

Since the early discovery of fluctuations in EEG signal in the human VC at ~ 10Hz associated with eyes open and eyes closed states (Berger, 1929) our understanding of neural oscillations has grown immensely. In 1989, Gray and colleagues were able to show that visual stimulation elicited synchronous inter-columnar neural oscillations at 40-60Hz, ‘the gamma range’, in the cat occipital cortex (Gray & Singer, 1989; Gray, König, Engel, & Singer, 1989a). Most importantly they were able to show that the nature of the oscillations was altered with the stimulus configurations. That is, different cortical columns in the VC were responsive and synchronised, to spatially separate features (Gray et al., 1989). They suggested this rhythmic synchronisation in the gamma range reflects the integration of these separate visual features. A cascade of research followed.

The findings were supported by studies of different species and different brain areas (Engel, König, Kreiter, & Singer, 1991; Kreiter & Singer, 1996, Gieselmann & Tiele, 2008) and led the Wolf Singer lab to propose the popular Binding By Synchrony (BBS) theory (1999). BBS postulates that synchronised activity acts as a binding tag, linking neurons and allowing representation of complex inputs. Multisite recordings in cat also demonstrated that these

oscillatory synchronisations were not only occurring in highly localised bundles of neurons but across structures in the cortex (Brecht, Singer, & Engel, 1998).

In the Communication Through Coherence theory, Fries (2005) proposed that the mechanism which governs the encoding of co-ordinated neural information is by synchronised, phase-locked, self-generated oscillations. Communication or ‘effective connectivity’ between neural assemblies, within and between brain regions, is underpinned by coherent rhythmic synchronisations. A later revision of theory proposed that connectivity has directedness, on basis that many studies have shown a non-zero, delayed, phase coherence; now so called ‘effective connectivity’ (Bastos et al., 2015; Bosman et al., 2012).

Generally, oscillations in the gamma band occur in highly localised neuronal groups, with plenty of research in support (Cardin et al., 2009; Gieselmann & Thiele, 2008; Hasenstaub et al., 2005; Sohal, Zhang, Yizhar, & Deisseroth, 2009). That being said, more recent studies have shown that connectivity exists at relatively high frequencies across inter-areal and intra-areal neuronal groups, which may relate to feedforward and feedback mechanisms (Bastos et al., 2015a; Bosman et al., 2012). Gamma oscillations are continuously modulated by excitatory and inhibitory factors, though the exact mechanisms remain unknown (see subsequent ‘Gamma Oscillations- a probe of local excitation-inhibition balance’). What is known is that excitability is not modulated by linear or sinusoidal rhythmic synchronisations but by a complex regularisation system calibrated by inhibitory and excitatory neurons and constituting a short excitation period with a long inhibition period (Fries, 2015; Merker, 2016).

1.8.2 The Role of Gamma Oscillations

Changes in band activity are functionally relevant and have been associated with different sensory and cognitive processes, in animals and humans (see reviews Moran & Hong, 2011; Uhlhaas & Singer, 2010). Gamma band activity (30-90Hz), occurs spontaneously across the cortex (Mitra, Nizamie, Goyal, & Tikka, 2015) and in response to stimulation. Stimulus related gamma can be broken into two temporal components of interest (Uhlhaas et al., 2006). Early evoked gamma is phase locked to the stimulus and events can be averaged over a number of trials. Evoked responses have a maximal amplitude and have inter- and intra-individual

reliability in the healthy population (Muthukumaraswamy, Singh, Swettenham, & Jones, 2010), which has made them popular candidates for investigation in clinical populations (Sensory Gating - Boutros, Korzyukov, Jansen, Feingold, & Bell, 2004). Being phase-locked to the stimulus suggests evoked gamma has a primary sensory role (Tallon-Baudry et al., 1996).

The second component of the gamma signal is the self-generated sustained, induced or oscillatory period, where the signal is not phase locked to the stimulus and would be essentially cancelled out through averaging across trials. This sustained/induced gamma is fundamental to Perceptual Binding Theory (Tallon-Baudry et al., 1996, 1998; Uhlhaas et al., 2006). Following the work of Wolf Singer and colleagues (1999), PBT states that bundles of firing of neurons, at gamma frequency, can each process different object feature and allow the integration of features over this specific time window. Hence, the number of representations that can be held at one time is multiplied considerably.

According to the PBT, stimulus specificity effects are shown in the sustained gamma period, induced at around 280msc after stimulus onset (Tallon-Baudry et al., 1996). Tallon-Baudry (1999) extended the theory to include integration over sensory modalities (e.g., visual-auditory), providing an explanation for gamma synchronisations found not just across intra-areal groups but distinct parts of the cortex. Top-down factors have also been included, involving integration from memory rather than bottom-up processes (Tallon-Baudry, 1999), without ignoring the role of attentional and perceptual mediators (Uhlhaas & Singer, 2006).

A subsequent body of research has implicated sustained gamma band activity in top-down and bottom-up local processes, especially attention (Fries, Reynolds, Rorie, & Desimone, 2001; Tallon-Baudry, Bertrand, Hénaff, Isnard, & Fischer, 2005) and perception (Gray, König, Engel, & Singer, 1989; Castelhana et al 2013). Consciousness (Melloni et al., 2007), synaptic plasticity (Wespatat, Tennigkeit, & Singer, 2004), pattern recognition and object recognition (Rodriguez et al., 1999; Tallon-Baudry & Bertrand, 1999), memory load (Howard et al., 2003), face recognition (Dobel, Junghöfer, & Gruber, 2011) and age dependent executive function (Paul et al., 2005), have also been associated. Importantly, considering early single electrode studies using the visual systems of anesthetized animals to generate gamma oscillations, changes in

gamma oscillations do not always require attention, suggesting likely top-down and bottom-up interactions in these processes.

That being said, the attribution of cognitive functions to oscillatory characteristics constitutes a ‘jump in the literature’ considering the continued uncertainty on the origins and mechanisms of oscillations. Recent thinking supports a more modest role for gamma oscillations in brain functioning, i.e., an intrinsic role in local processing via the excitation–inhibition balance rather than as a cognitive operator (Merker, 2016). In this case, findings of cognitive covariation are likely to represent relationships with the activation of local circuitry, rather than the oscillatory gamma signal itself. Despite disagreement over the higher order functions of gamma oscillations, what is generally accepted is the association with neurocircuitry and local synchrony, which is of relevance to this thesis.

1.8.3 Gamma oscillations – a probe of local inhibition-excitation balance

Healthy brain functioning requires an equilibrium in excitatory and inhibitory processes, that if disturbed can lead to dysfunction. The predominant cells in the cortex, the pyramidal cells, are glutamatergic and excitatory. Gamma-aminobutyric acid (GABA)-ergic inhibitory interneurons comprise about 20% of the cell population and prevent the over excitement of the cortex (Moore, Carlen, Knoblich, & Cardin, 2010). This process is particularly fine-tuned as inhibitory responses are co-ordinated in accordance with individual excitation levels (Xue, Atallah, & Scanziani, 2014).

Parvalbumin (PV) positive basket cells are fast-spiking interneurons that express the calcium-binding protein PV and receive *N*-methyl-D-aspartate (NMDA)-dependent excitatory input from pyramidal cells (Jones & Bühl, 1993). These cells have a key role in regulating gamma oscillations as they are inhibitory, and their genetic removal has been shown to lead to disturbed gamma activity (Carlén et al., 2012). PV interneurons also have a high sensitivity to pharmacological substances, such as ketamine, which antagonize NMDA receptors and have been shown to influence gamma oscillations (Ehrlichman et al., 2009; Jingyi Ma, 2000; Muthukumaraswamy et al., 2015).

The exact mechanisms behind gamma oscillation generation, however, are not clear. Putative mechanisms have been suggested via computer models in animals (Jensen & Lisman, 1996; Leung, 1982; Tiesinga & Sejnowski, 2009; Traub et al., 2001; Traub, Whittington, Stanford, & Jefferys, 1996; Wang & Buzsáki, 1996). This work supports two main circuit models for gamma rhythm generation, Inhibitory models (I-I) or Excitatory inhibitory models (E-I), specifically the Interneuron Network Gamma (ING) model and the Pyramidal Interneuron Network Gamma (PING) model (Buzsáki & Wang, 2012a; Whittington, Traub, Kopell, Ermentrout, & Buhl, 2000).

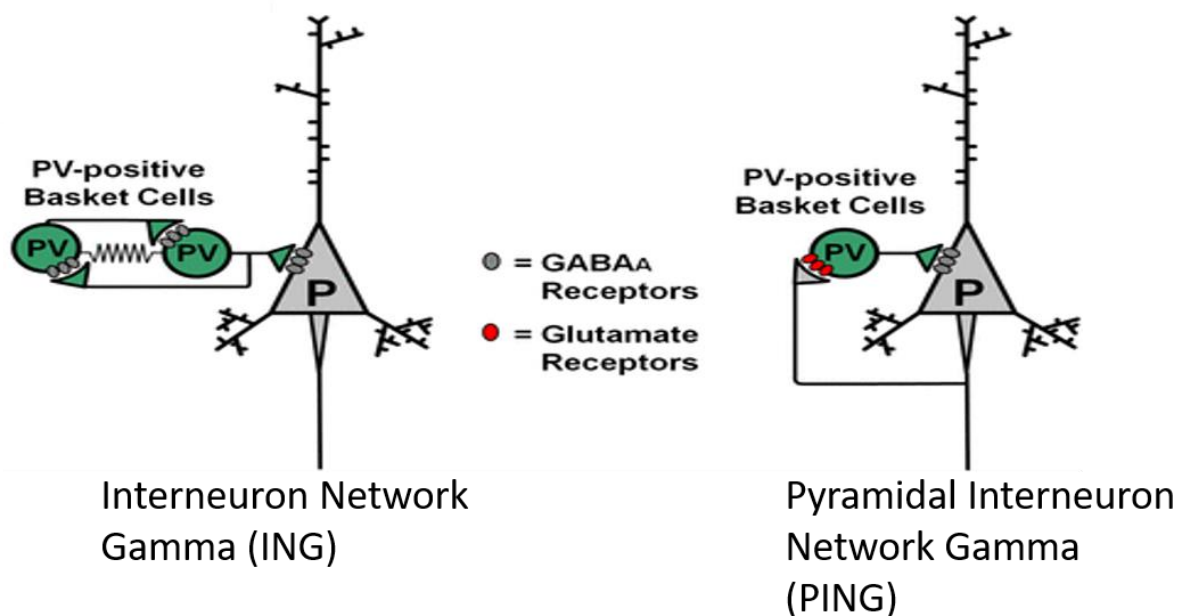


Figure 1.1. PING and ING gamma models¹.

The main difference between models is that in the PING model the pyramidal cells are directly involved in the gamma rhythm production. The pyramidal neurons are mediated by phasic excitatory glutamatergic currents which then trigger interneuron activation and feedback inhibition (Gonzalez-Burgos & Lewis, 2012). The ING model assumes some kind of continuous excitation current to the interneurons (non-glutamatergic). In this case, oscillations are

¹ Note: Adapted from Gonzalez-Burgos, G., & Lewis, D. A. (2012). NMDA receptor hypofunction, parvalbumin-positive neurons, and cortical gamma oscillations in schizophrenia. *Schizophrenia bulletin*, 38(5), 950-957.

modulated by the interaction between parvalbumin basket cells (GABAergic interneurons) and not by pyramidal neurons directly. Rather, the pyramidal cells are synchronised passively with the oscillation rhythm (Gonzalez-Burgos & Lewis, 2012). The consensus falls with the PING model as several lines of animal research suggest it is better supported (Börger, 2017; Gonzalez-Burgos & Lewis, 2012). For example, research with modified mice has supported the phasic excitation role of pyramidal cells in gamma oscillations (Fuchs et al., 2007). Furthermore, the genetic knock out of the I-I link in mice does not strongly affect hippocampal gamma power (Wulff et al., 2009).

The PING model proposes that gamma oscillations are generated in superficial layers (2/3) of the cortex and are mediated by fast GABA_A and AMPA receptors as well as slower NMDA receptors (Oke et al., 2010). Simulation studies have suggested gamma rhythms in neocortical layer 5 also have the potential to obscure simultaneous gamma in layer 2/3 (Lee & Jones, 2013). Nonetheless, AMPA and NMDA receptors are fundamental to glutamate-mediated circuitry. AMPA receptors have a large contribution as shown by animal studies (Fuchs et al., 2007; Oke et al., 2010). For example, the removal of AMPAR in rodent is associated with significantly reduced or eliminated gamma power (Fuchs et al., 2007). NMDA receptor antagonism is also consistently associated with aberrant gamma oscillations, usually with positive directionality in the animal literature (Gonzalez-Burgos & Lewis, 2012). Strong support comes from ontogenetic and pharmacological studies in vitro and in vivo (Hakami et al., 2009; Hong et al., 2010; Muthukumaraswamy et al., 2015a).

As mentioned, GABA is the major inhibitory neurotransmitter in the brain and has an essential role in local PING circuitry. Two types of GABA receptor exist (GABA_A & GABA_B) but inotropic GABA_A receptors are abundant on neurons and glial cells and mediate the majority of GABA inhibition (Kandel, Schwartz & Jessel, 2000). With the development of Magnetic Resonance Spectroscopy (MRS) techniques allowing measurement and advanced differentiation (GABA from creatine) of metabolites in vivo, the association between GABA concentration and gamma oscillations has become well established (Chen et al., 2014; Kujala et al., 2015; Kuki et al., 2015; Muthukumaraswamy, Edden, Jones, Swettenham, & Singh, 2009).

Associations between GABAergic inhibition and gamma have mostly been found in the VC (Muthukumaraswamy et al., 2009; Shaw et al., 2020) and paradigms which induce changes in occipital gamma oscillations have been commonly employed in electrophysiological research. The inference from the PING model is that these paradigms allow the local excitation-inhibition system to be passively perturbed. Support comes from Dynamic Causal Modelling work on the canonical microcircuit in V1 (Shaw et al, 2017). Specifically, the model suggests the main determinants of the amplitude of the visual gamma response (to a visual grating stimulus) are connections between pyramidal cells and interneurons in the superficial layers (2/3) of the cortex. Additionally, increased inhibition of pyramidal cells, with GABAergic tiagabine, was found to result in reduced amplitude and increase frequency of gamma activity (Shaw et al., 2017).

On this basis, induced gamma oscillations have been taken as a proxy for local circuitry in the VC. Furthermore, as key theories of schizophrenia propose an impairment of GABAergic and glutamatergic systems (Stone, Raffin, Morrison, & McGuire, 2010), oscillatory gamma has been a prime candidate for investigation in schizophrenia and schizophrenia-risk research.

1.9 Local and global processes in the healthy brain-a commentary

Some of the fundamental questions in neuroscience are to what extent and how are regional and inter-regional areas of the brain connected; what are the characteristics and functions of these relationships? These questions are on-going, with many approaches and accompanying jargon having been devised. For example, the study of micro-circuitry, mesocircuitry and macrocircuitry in physiologically informed research (Kennedy, Van Essen, & Christen, 2016), smallworldness properties in graph theory (Farahani, Karwowski, & Lighthall, 2019), local and global functional properties (Donner & Siegel, 2011; Gandal, Edgar, Klook, & Siegel, 2012; Siegel, Donner, & Engel, 2012), modelling systems specialisation and integration (Friston, Harrison, & Penny, 2003) and the connectome and cortices (Romme, de Reus, Ophoff, Kahn, & van den Heuvel, 2017) are all broadly concerned with these same questions.

Neuroimaging tools have been crucial to advancements in our understanding of functional connectivity in both health and disease; particularly in disorders such as schizophrenia where

through comparisons with healthy controls, both impairments in local visual areas and global networks have been found (Uhlhaas & Singer, 2010a). The consideration of these impairments is a key theme in this thesis, however to better place explorations of the relationship between local visual and global functioning in schizophrenia using MEG, here some current findings and hypotheses on local-global interactions in healthy individuals will be discussed.

The co-ordinated modulation of membrane potentials across a number of pyramidal cells in a network enables groups of neurons to fire synchronously, in the way that is reflected in measurable oscillatory activity. The central idea in the local-global story is that high frequency oscillatory activity (>30 Hz, gamma) is reflective of local processes, whereas lower frequency alpha and beta oscillations (8-12Hz, 13-30Hz) appear to be reflected in the synchronous communication of neurons over distant brain areas. Occurrences of synchronous gamma oscillations across brain areas have been observed, though the interpretation that this represents high frequency long- range connectivity is not well supported (see Buzsáki & Schomburg, 2015).

In the frequency domain, higher frequencies oscillations appear to travel shorter distances than slower frequency oscillations, the rates of which are modulated by neuronal conductance delays (Buzsáki & Draguhn, 2004). The generation of faster (gamma) and slower (beta) oscillations has been demonstrated in individual neuron work, via a reduced network of 2 excitatory and 2 inhibitory neurons (E-E & E-I connections), by Kopell and colleagues (2000). While an extremely reduced model, the principle has been considered to generalise to larger more realistic models or circuits (Kopell, Ermentrout, Whittington, & Traub, 2000b; Moran & Hong, 2011). Gamma oscillations, in particular, have been studied extensively in single- and multi-electrode work where an origin in intra- areal Excitation-Inhibition (E-I), spiking and Local Field Potential interactions, is suggested (Buzsáki & Schomburg, 2015a).

Evidence for gamma reflecting activation of local neuronal circuitry comes from the physiologically informed Dynamic Causal Modelling (DCM), based on the Pyramidal Interneuron Network Gamma (PING) model (Gonzalez-Burgos et al., 2015). In short, the PING model suggests that gamma oscillations are generated by the interaction between glutamatergic pyramidal cells and GABAergic parvalbumin interneurons (Shaw et al., 2017). This was found

with DCM based on a canonical microcircuit in V1 (a simple model of a cortical column). Specifically, the model suggests the main determinants of the visual gamma response (amplitude) are connections between pyramidal cells and interneurons in superficial layers (2/3). Increased inhibition of pyramidal cells, with GABAergic tiagabine, was also shown to result in reduced amplitude and increase frequency of gamma activity (Shaw et al., 2017). That being said, other DCM work has also suggested that deep layer cholinergic input enhances superficial layer activity in V1 (Pinotsis et al., 2017). Regardless, a subsequent study has shown visual gamma frequency is associated with the superficial layers and reduced in schizophrenia (Shaw et al., 2020).

Exactly how pyramidal- interneuron interactions result in the signals measured and analysed in global oscillatory connectivity analysis is not well understood. However, beta peak differences have also been shown to be predicted by between-subject differences in deep layer (5/6) pyramidal cells and interneurons using DCM (Shaw et al., 2017); with longer inhibition periods related to slower oscillations. A recent version of the model, including a thalamo-cortical parameter, shows reduced free energy along with the generation of an alpha peak (Shaw et al., 2020). This finding supports the notion that alpha is generated over more extensive areas, namely thalamo-cortical loops (Vijayan, Ching, Purdon, Brown, & Kopell, 2013; Vijayan & Kopell, 2012).

Prominent theories of brain organisation and cognition suggest that communication between brain areas arises by means of the synchronisation of distant groups of neurons. That is, the phase alignment of signal generated by regional excitatory-inhibitory units (Coupled synchrony- Florin & Baillet, 2015; Communication through coherence- Fries, 2015; Perceptual binding- Tallon-Baudry & Bertrand, 1999). With long-range connectivity measures (amplitude-amplitude, phase-amplitude coupling), this is often found in the alpha and beta band (von Stein & Sarnthein, 2000), in large scale patterns that are largely consistent with network patterns found at higher spatial resolution using fMRI (Brookes et al., 2011a; Brookes et al., 2011b).

The spatial characteristics of gamma, beta and alpha oscillations and the connectivity of the brain has prompted the consideration of oscillations as important in local and distance interactions

(Siegel et al., 2012); with gamma in particular being a proxy for local connectivity (Donner & Siegel, 2011).

Meso- and macroscopic modelling approaches have been particularly useful for investigating such interactions. For example, Cabral and colleagues (2011) sought to investigate the relationship between low frequency BOLD resting-state activity and local gamma oscillators. The model they provide is based on the Kuramoto model of phasic oscillators, wherein slow resting-state network functional dynamics can be seen as a product of dispersed local dynamics and structural connectivity. When gamma oscillators were simulated in nodes across the cortex, a network of rhythmic slow neural activity occurred. This arose in a pattern that correlated with empirical functional connectivity (BOLD) data when realistic conductance delays (axonal conductance) were added to the model, suggesting resting-state activity could be a function of local dynamics and interactions rather than a connectivity pattern per se.

With regard to electrophysiological findings, oscillations as communications along the biological (cortical) and conceptual hierarchy has become a popular mode of interpretation (Baillet, 2017; Friston, 2008; Michalareas et al., 2016). Taking the VC, both van Kerkoerle and Michalareas and colleagues were able to show, using a combination of human MEG (granger causality) and macaque anatomical projections, that gamma was causally implicated in feedforward projections, whereas alpha and beta were implicated in feedback projections (Kerkoerle et al., 2014a; Michalareas et al., 2016b). These studies also support existing evidence (Bastos et al., 2015) suggesting a primary sensory, bottom-up, influence of gamma, where projections up the cortical hierarchy (e.g., V1>v4) are reflected in gamma synchronisations. Correspondingly, beta and alpha oscillations are involved in top-down influences, in line with projections down the cortical hierarchy (Bastos et al., 2015; Michalareas et al., 2016).

The idea of a cortical hierarchy with feedforward and feedback influences is central to prediction error theory (Bastos et al., 2012; Bastos et al., 2015; Friston & Kiebel, 2009), which has become fundamental to our modern interpretation of brain functioning. Higher areas combine incoming evidence and prior knowledge to generate predictions, which then feedback to the sensory areas and are compared with sensory evidence in a continuous loop. The difference between sensory

evidence and predictions comprises prediction errors which are forwarded to higher areas. An efficient system would require prediction errors to move faster than predictions, which is consistent with feedforward processes being reflected in fast gamma oscillations and feedback or top-down processes being reflected in slower alpha and beta oscillations.

Oscillatory interactions have also been investigated in the form of frequency mediation effects, i.e., the extent to which oscillations mediate each other's top-down/bottom-up effects. Baillet's model of polyrhythmic integration considers hierarchical influences in the context of local-global questions, with a focus on MEG findings (Baillet, 2017). At a global level, gamma bursts occur in volleys at certain phases of lower frequency activity, alpha and below, and have been thought to have a modulatory effect, in the resting-state at least (Roux, Wibra, Singer, Aru, & Uhlhaas, 2013). Several studies have shown alpha-gamma coupling, suggesting that alpha oscillations, which are associated with attention, could regulate gain control and higher frequency activity (Keitel et al., 2019; Romei et al., 2008). However, a recent frequency tagging study found that the attentional control of alpha oscillations and the (high) frequency response in V1 were uncorrelated (Popov, Kastner, & Jensen, 2017), with the sources of alpha being downstream. Mechanisms behind the co-occurrence of alpha-gamma oscillations appear to be more complex than a direct modulation of cortical excitability.

Mesoscopic beta oscillations have not been found to be mediated by gamma and are most studied in the motor cortex. However, it is feasible that gamma and beta may exert similar bottom-up and top-down influences across the brain, as shown at regional level of the VC, with additional thalamus interactions (a dynamical relaying centre) (Baillet, 2017). The testability and mechanistic understanding of this postulation in humans is presently limited, though the concept is increasingly endorsed (Jaramillo, Mejias, & Wang, 2019; Markov et al., 2014; Sikkens, Bosman, & Olcese, 2019).

Interestingly, using a Hidden Markov Modelling approach, Hirschmann and colleagues (Hirschmann et al., 2020a) were able to show that spontaneous network activity (in the resting-state) in the beta range and below (<35Hz) accounts for variability in induced visual gamma response. In this approach, complex time series data can be filtered into brain 'states' much like

how components are derived in Independent Component Analysis (ICA). Rather than a static snapshot, these brain states represent recurring patterns of dynamic network activity. Resting states characterised by high alpha and beta power in central areas, predicted reduced visual gamma power. The opposite was true for a state characterised by widespread reduced alpha and beta power, i.e., it accounted for reduced visual response across participants. These findings support other work suggesting a convergence between local task-based activity and the resting-state (Cole, Bassett, Power, Braver, & Petersen, 2014; Smith et al., 2009).

A coincidence of bottom-up visual gamma and lower oscillatory feedback would seem fundamental to our experience of visual stimuli and our visual perception. Hierarchical predictive coding provides a framework by which the integration of higher order and sensory information allows us to make inferences and update beliefs (Friston, Brown, Siemerikus, & Stephan, 2016). If, as believed, oscillations are signatures of these interactions, the continued study of local and global oscillatory dynamics will provide important insight into these processes in both health and disease.

1.10 General aims and objectives

Though our understanding of structural and functional connectivity in healthy and in schizophrenia patients, and those with increased risk of psychosis, has developed considerably over the last 20 years, much ambiguity remains around the nature of neural impairments in different individuals and particularly the extent to which impairments are local or global. The primary aim of this thesis is to explore different oscillatory and structural connectivity measures in relation to factors associated with increased psychosis risk and thus aid the cohesion of neuroimaging evidence accumulated in the psychosis literature.

In support of this aim two methods chapters will be completed as optimal utility and analysis of data acquired with MEG is fundamental to its applications. Furthermore, reducing the duration of scanning sessions is critical for participant comfort and for quality data acquisition, particularly in clinical cohorts. Therefore Chapter 3 will explore the optimal beamformer sampling grid resolution for obtaining estimates of local gamma oscillations, keeping in mind the significance of identifying functional activity at its source. Chapter 4 of this thesis will explore the extraction

of global resting-state networks from task data, investigating the necessity of a resting-state paradigm. Chapter 5 explores the functional and structural connectivity data, that will be further described in chapters 6, 7 and 8, using a network reduction method called Non-Negative Matrix Factorisation.

Those with schizophrenia show both local and global functional impairments and understanding the interaction between which is of utmost importance. However, presently the nature of local and global functional interactions is still to be understood in healthy individuals. The sixth chapter of this thesis will explore the relationship between local functional connectivity in VC and global oscillatory connectivity and structural connectivity, in the healthy population. Local functional connectivity will be probed with a visual grating MEG paradigm while global functional connectivity will be probed with amplitude correlations based on the Hilbert envelope, throughout the thesis. A range of structural metrics derived with tractography will also be explored.

The simultaneous study of structural and functional impairments in schizophrenia is receiving increasing attention. Chapter 7 will investigate how the schizotypy trait, a clinical risk factor for psychosis, is related to global structural and functional connectivity. The eighth chapter will investigate how polygenic risk score (PRS), a genetic risk measure for schizophrenia, is related to global structural and functional connectivity. Chapter 9 will investigate local connectivity in VC in relation to PRS and schizotypy.

Recent models have proposed schizophrenia as a disorder of dysregulated synaptic gain or E-I balance. The last experimental chapter will explore the effect of GABAergic and glutamatergic CNVs on local and global functional connectivity.

Chapter 2. General Methods

2.1 Magnetoencephalography

All electrical currents, including those from neuronal activity, generate an associated magnetic field. Magnetoencephalography (MEG) is a non-invasive neuroimaging technique that detects magnetic fields generated by synchronous neuronal activity. As a direct measure of neuronal activity, as with Electroencephalography (EEG), the main advantage of MEG is its superior temporal resolution (<1ms). However, compared to EEG, MEG also has superior spatial resolution because, unlike the EEG signal, magnetic fields are undistorted by transmission through the brain, skull and scalp. Thus, the accuracy and resolution of MEG localisation in the superficial cortex is a few millimetres, depending on the signal-to-noise ratio. One of the main advantages of MEG is its utility in the mapping and characterisation of physiologically informed oscillatory activity, which is a limitation of its functional Magnetic Resonance Imaging (fMRI) counterpart. MEG is, therefore, an excellent tool for studying rapid and dynamic sensory and cognitive processes in the brain.

2.1.1 MEG Instrumentation

The MEG system is constructed of ~275 evenly distributed Super Conducting Quantum Inference Devices (SQUIDS) contained in a dewar unit above the head. SQUIDS consist of tiny loop(s) of superconducting material (metal or alloy) and many Josephson Junctions. A Josephson Junction is made up of two superconducting loops with a thin insulating layer between them. When cryogenically cooled, the Josephson Effect (Josephson, 1974) shows that current flows around the loops and across the insulating gap, with no voltage, making SQUIDS extremely sensitive detectors. As superconduction can normally only occur at exceptionally low temperatures the SQUIDS are encased in a liquid helium pool, with a vacuum-insulated dewar, which maintains them at -269 degrees. When an external magnetic field becomes large (exceeds a critical value), e.g., due to magnetic fields from neural activation, a voltage occurs across the Josephson Junction which is measurable at the ordinary (rather than quantum) scale.

SQUIDs are extremely sensitive devices, allowing them to pick up the small magnetic fields (< 10 femtotesla) generated by neuronal activity in the brain. However, the MEG system is limited by a low signal to noise ratio as SQUIDs are sensitive to external noise, such as construction, power lines and traffic, which is of several orders of magnitude higher than the biomagnetic brain signals of interest (Hämäläinen, Hari, Ilmoniemi, Knuutila, & Lounasmaa, 1993). Biological noise is also created from intrinsic processes such as blinks, heartbeat and muscle movements which requires consideration and steps taken in the preparation scanning and analysis to account for this.

2.1.2 Noise reduction

To minimise the interference in the MEG signal, due to external environmental sources, the scanner is housed in a sealable magnetically shielded room, made of many layers of aluminium and niobium. Each SQUID is also paired with a magnetometer/ gradiometer which enhances the magnetic brain signal received by the SQUID. Magnetometers are made of a single superconducting coil, whereas gradiometers are made up of two oppositely wound coils, either in an axial (vertical) or planar (horizontal) position to each other. Gradiometers are sensitive to inhomogeneous magnetic fields like those generated in the brain but insensitive to homogeneous magnetic fields such as distance noise sources (and uniform field gradients) which are essentially cancelled out due to the double coil configuration (Hämäläinen et al., 1993).

Furthermore, collecting simultaneous measures of biological signals such as Electromyography (EMG), Electrooculography (EOG) and Electrocardiography (ECG) and external noise using a reference electrode, together with visual data inspection and averaging across trials, allow biological artefacts to be mostly accounted for in the analyses. The system at Cardiff University Brain Research Imaging Centre is a CTF 275 axial gradiometer design. The inbuilt 275 channels and 3rd order noise cancellation provided by a reference superconducting quantum interference devices (SQUID) array in the dewar affords an enhanced signal to noise ratio and ample spatial resolution.

2.1.3 Signal origins

Normal brain functioning requires a balance in excitatory and inhibitory cellular mechanisms (E-I balance). Neuronal firing is commonly described in terms of spiking activity, bursting activity and post-synaptic potentials. Single spiking activity refers to very brief rapid neural activity, i.e., action potentials, and bursting activity refers to a short succession of spikes. Post-synaptic potentials are temporally slower and reflect changes in the post-synaptic terminal of the chemical synapse.

In this way, ionic currents generated by activated neurons can be split broadly by their temporal dynamics; fast and slow(er). In the former, sufficient net gain of positive charge mediated by sodium (Na⁺) -potassium (K⁺) transmission, leads to rapid depolarisation of the cell, triggering an action potential along the neuronal axon and dendrites and reflected in spiking and bursting activity.

Slower ionic currents are generated by the action of neurotransmitters at the synapse. These result in excitatory (positive ions in) or inhibitory (positive ions out or negative ions in) post-synaptic potentials (EPSPs or IPSPs), the bulk effect of which is measured with MEG. The type of post-synaptic potential generated is dependent on the neurotransmitters, receptor types and ionic interactions involved (Lopes Da Silva, 2010). Of note, GABA is the main inhibitory neurotransmitter in the brain and glutamate is the main excitatory neurotransmitter.

The net action of ionic currents can be thought of as electrical current dipoles which have an orientation and measurable magnitude. To understand the origin of the MEG signal requires consideration of the following factors:

- 1) The magnetic field generated by a single neuron is tiny, requiring detectable magnetic fields to be generated by the synchronous activity of bundles of (>10,000) neurons. Spikes are very brief and do not sum temporally (and spatially) to give a measurable signal.

- 2) MEG dipole source modelling relies on the principle of mutual orthogonality (the right-hand rule) i.e., that electrical current flows at a right angle to the generated magnetic field.
- 3) Radial sources of activity, i.e., where dipoles point out from the centre of the brain, will be poorly imaged with MEG. The reason is, due to the (roughly) spherical shape of the head secondary volume currents will largely cancel out the magnetic fields generated by radial dipoles. In reality, however, a fairly small proportion of the brain is oriented radially (e.g., the sulci).
- 4) Magnetic fields decay as a function of distance. Therefore, MEG is generally sensitive to cortical sources and insensitive to deeper sources.

(Hämäläinen et al., 1993; Hillebrand & Barnes, 2005, Hillebrand & Barnes, 2002)

The MEG signal is, therefore, thought to reflect magnetic fields generated by synchronous electrical activity from the dendrites of excitatory pyramidal cells. This is because pyramidal dendrites tend to be perpendicular to the cortical surface and provide detectable signal from the cumulative summation of the long asymmetrical dendritic extensions. When post synaptic potentials from millions of neurons fire together an excitatory or inhibitory Local Field Potential (LFP) is generated. The net effect of dendritic EPSP/IPSP activity, or LFP, is often insufficient to trigger action potentials, especially simultaneous action potentials, represented as a spike in the MEG signal, and is instead reflected in the slower oscillatory dynamics of the signal (Lopes Da Silva, 2010). MEG oscillations are therefore assumed to reflect the aggregate activity of populations of neurons represented by fluctuations in their extracellular LFPs.

2.1.4 MEG Analysis

The MEG signal can be analysed into various components depending on the process of interest. Broadly, these can be categorised as evoked signals or oscillatory signals. As discussed in Chapter 1, evoked signals appear to have a primary sensory role (Tallon-Baudry et al., 1996), whereas oscillations, reflected in the induced response, are implicated in connectivity and communication across the brain (Bastos et al., 2015b; Bowyer, 2016; Fries, 2005; Shaw et al.,

2017), as well as in cognition (Donner & Siegel, 2011; Siegel, Engel, & Donner, 2011). MEG analysis is generally conducted in two modes; 1) in sensor space, in which characteristics of the signals are viewed at the level of the sensor, and 2) in source space, which considers where the signal origin is localised in the brain.

Sensor space

The characteristics of oscillatory activity can be described in terms of phase, frequency and amplitude. Conventionally, decomposition of the MEG signal allows neuronal activity to be separated into frequency bands delta (<4 Hz), theta (4-8 Hz), alpha (8-12 Hz), beta (12-30 Hz), gamma (30 Hz+) over time. Using spectral analysis, oscillatory power (amplitude squared) can be represented as a function of frequency, rather than time, by means of a Fourier transform (frequency domain, power spectrum) (Boashash, 2003). The power spectrum is an efficient way of representing the magnitude of activity in relation to frequency, averaged over time, which can then be compared at different time points, for example between pre- and post-stimulus periods as in this thesis.

However, many psychological experiments are (also) interested in how neural responses and signals change over time. For this, time frequency analysis can be performed which involves splitting the signal into shorter segments in time and applying various transforms. For example, a Moving Window Fourier Analysis (Richardson et al., 2019), where the time window has a fixed length independent of frequency, Wavelets and Multi-Taper transforms (van Vugt, Sederberg, & Kahana, 2007), where the time window decreases in length with increased frequency, or by applying a Hilbert transform (Hilbert, 1912). Each of these methods produce representations of amplitude and frequency as a function of time.

Source analysis

MEG and EEG measures, where data are collected outside of the head, are subject to both forward and inverse problems. The forward problem involves calculating the sensor potential, or field, for a given source configuration, i.e., neuronal activity, at a known location. The inverse problem, i.e., inferring the unknown current distribution within the brain from the external measurements, is harder to solve. That is, without any given source information, the cumulative

signal detected at the sensor level could come from an infinite number of different combination of sources in the brain; a problem known as non-uniqueness.

Understanding the origin of activity of interest, in ‘source space’ is a key aim in neuroscience. Fortunately, the number of possible solutions is reduced with a-priori information about a likely source. An understanding of brain histology, structure, and physiology can be used to this end (Barnes et al., 2006). Furthermore, prior knowledge can be provided computationally in the form of a source covariance matrix and several inversion algorithms exist. A lot of work has been done on finding inversion algorithms which are insensitive to noise and provide an accurate solution (Hillebrand & Barnes, 2005).

Common methods include Simple Dipole Models, where one or few active sources are assumed, and distributed current models/current density models, which estimate the continuous distribution of current within the brain by assuming a minimum-norm solution. The beamformer algorithms, however, have been found to be a robust method for acquiring biologically plausible source reconstructions with minimum assumptions (Van Veen et al., 1997; Hillebrand, et al, 2005., Barnes et al., 2006). Beamforming fundamentally involves the generation of weights, which are a linear weighted combination of the MEG channels, and when combined with the sensor data provide estimates of time-varying activity at any given location.

2.1.5 Beamforming

The beamforming approach benefits from enhanced noise rejection by considering each area individually, as a linear weighted combination of the channels. Selectively weighting the contribution of each sensor to the overall output not only increases sensitivity to detect sources in an area of interest but does not require the a-priori specification for a fixed number of sources. Furthermore, for any given source with a particular signal-to-noise ratio, there will be a sampling resolution that is optimal for obtaining accurate estimates. This is likely to differ across different areas of the cortex (Barnes, Hillebrand, Fawcett, & Singh, 2004).

Beamforming is also particularly useful for studying the induced or oscillatory signal as it does not rely on phase-locking across trials (Hillebrand & Barnes, 2005). Before beamforming was

widely implemented, studies were often limited to acquiring the phase- and time-locked evoked responses, as in order to accurately localise any given source at the appropriate signal to noise ratio they needed to assume one or few known and repeatable sources.

Beamforming has one significant disadvantage which is that perfectly correlated sources are cancelled out. This could be unhelpful in certain situations. For example, where bilateral areas are simultaneously activated, or in studies of evoked activity where nearby sources are likely to be highly correlated. That being said, it would seem unlikely for the complexity of the brain to depend on linearly interacting sources (Hillebrand & Barnes, 2005). Beamforming also requires additional computational resources compared with traditional methods; however, this is not significant problem in the present day.

2.1.6 Modes of analysis

Considerable researcher degrees of freedom can be employed in selecting a MEG analysis methods, due to the wealth of information in the MEG signal, along with the variety of experimental paradigms that exist. Nonetheless, as mentioned above, analyses are generally concerned with the amplitude, frequency and/or phase of the signal. At the local level, this might involve selecting peak amplitude and frequency values from spectral analysis performed in a specific region, for example, the visual cortex, which is relevant to this thesis.

Alternatively, connectivity across different areas of the brain can be investigated with correlations between the amplitude and/or phase of oscillatory time series between voxels (Bowyer, 2016). Phase coherence refers to consistency in the phase of a signal of the same frequency. As shown in Figure 2.1, this can be at zero-time lag (left panel) or non-zero lag (right panel). Non-zero, delayed, phase coherence is often used to infer directionality of connectivity (Siegel et al., 2012). Amplitude-amplitude coupling refers to covariance between Hilbert envelopes that are generated around the signal extremes. Amplitude correlations can therefore be performed on signals of the same or different frequencies but do not comprise phase information. In fact, phase coherence and amplitude correlation are generally independent of one another

(Siegel et al., 2012).

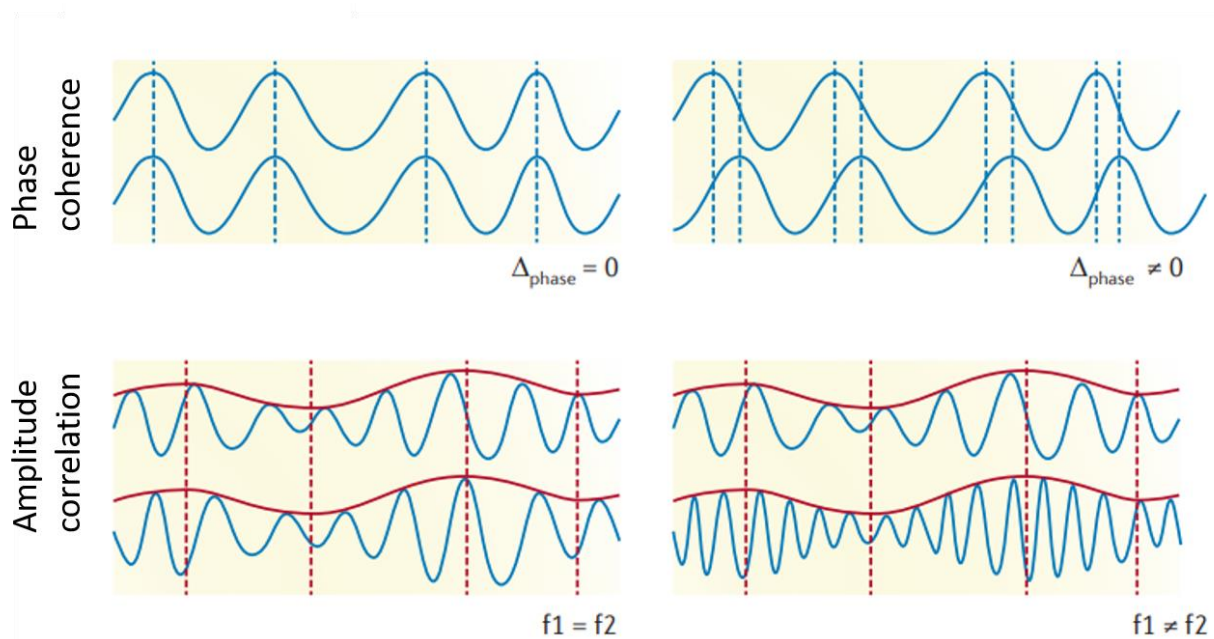


Figure 2.1. Correlations between phase and amplitude signals²: the top shows a correlation between the amplitude and phase of signals in two different areas of the brain and the bottom shows a correlation between the amplitude envelopes in two different areas of the brain.

Amplitude-amplitude correlations, particularly in the alpha and beta bands, have been shown to be robust and repeatable (Colclough et al., 2016) and are implemented in this thesis. In order to explore anatomically relevant networks, data can either be projected onto an atlas, such as the AAL atlas (AAL, Tzourio-Mazoyer et al., 2002), where 90 anatomical regions are pre-defined, or, explored using Independent Components Analysis (ICA) (Brookes, Woolrich, et al., 2011). Both ICA and atlas-based methods have revealed functionally relevant resting-state networks (Brookes, Woolrich, et al., 2011; Hillebrand, Barnes, Bosboom, Berendse, & Stam, 2012). However, an atlas-based approach can aid interpretation and comparison with other modalities (Hillebrand et al., 2012) and was the chosen approach for this work.

² Note: Adapted from Siegel, M., Donner, T. H., & Engel, A. K. (2012). Spectral fingerprints of large-scale neuronal interactions. *Nature Reviews Neuroscience*, 13(2), 121-134.

2.1.7 Further analysis

Various modelling techniques can be applied to MEG data including, Dynamic Causal Modelling (DCM), where MEG data is fitted to a physiologically informed model of a cortical microcircuit, and can elucidate relationships between specific connections and characteristics of the MEG data (Friston et al., 2003; Shaw et al., 2017; Shaw, Muthukumaraswamy, et al., 2020a), and Graph Theory, which is a mathematical technique that assesses the inter- and intra-connectedness of ‘hubs’ or specific areas of the brain (Bassett & Bullmore, 2006; Power, Fair, Schlaggar, & Petersen, 2010). Methods such as Non-Negative Matrix Factorisation (Lee & Seung, 1999) can also be applied to the connectivity data to reveal anatomically relevant sub-networks, as will be described in Chapter 5 of this thesis.

2.2 Structural Magnetic Resonance Imaging (MRI)

2.2.1 Basic principles of MRI

MRI is the most utilised non-invasive neuroimaging technique and has unchallenged spatial resolution. MRI operates by means of Nuclear Magnetic Resonance (NMR). The notion of ‘spin’ is critical to resonance and describes the rotation of subatomic particles around their axes. If a nucleus has an odd number of protons or neutrons, for example the hydrogen atom which has one proton and no neutrons, it will have a net spin or magnetic moment (magnetic strength and orientation) (Grover et al., 2015). Usually these spins are randomly oriented, however when placed in a strong magnetic field, i.e., in an MRI scanner (B_0), there is an increased tendency for these to align with the magnetic field and precess at a frequency proportional to the strength of the magnetic field (42.58 MHz/Tesla); the Larmor frequency (Larmor, 1897). It is the hydrogen atoms in water that are usually imaged with MRI, and these have a Larmor resonant frequency of 127.74 MHz at 3 Tesla.

Additional radiofrequency (RF) pulses (B_1), applied at the Larmor frequency, perpendicular to the B_0 gradient, perturb this system away from equilibrium. Once the RF pulses are turned off two occurrences happen 1) the spins return to alignment and the time taken is referred to as the longitudinal relaxation time (T_1), and 2) the precession of the spins differs between the protons because they experience slightly different magnetic fields. This loss of phase coherence is called the transverse relaxation time (T_2). The loss of energy from the perturbed system is recorded via

the receiver coils. Importantly, tissues in the brain have different water properties and it is the contrast between T1 and T2 in these tissues that allow the brain to be imaged. Three sets of gradient coils are used in nearly all MRI scanners and allow the spatial encoding of the MR signal in the x, y and z directions as the gradients induce a spatially-varying change in the resonant frequency. The application of a Fourier transform allows the signal to be interpreted as an image or a frequency spectrum (Grover et al., 2015).

2.2.2 Diffusion Tensor Imaging

Diffusion Tensor MRI is a neuroimaging method which allows the measurement of microstructure in vivo. It relies on the fact that the diffusion of water molecules in the brain is not unconstrained, but is influenced by the microenvironment (i.e., fibres, macromolecules, etc.) around the water molecules. In grey matter and in the cerebrospinal fluid (CSF) the diffusion is isotropic. In the white matter, however, the water molecules are constrained to move along the axons only, and that makes their diffusion movement highly anisotropic.

2.2.3 Acquisition and instrumentation

In humans, a diffusion-weighted sequence is implemented using a MRI scanner with a field strength of between 1.5 and 7 Tesla. To sensitize the MR scanner to diffusion, the magnetic field is varied within the scanner by a field gradient. Since precession is proportional to the magnetic field strength, the water molecules begin to precess at different rates, resulting in dispersion of the phase. Another gradient is subsequently applied, with the same magnitude but in the opposite direction to the original one, aiming to bring the spins back in phase. This refocusing is not perfect because the water molecules move due to diffusion during the time interval between the pulses, and the signal measured by the MRI scanner is reduced. By careful choice of the MRI sequence, therefore, images can be reconstructed which are sensitive to different directions of water diffusion within the brain. A basic sequence can be acquired in 5- minutes, however most experiments require more time.

2.2.4 The diffusion tensor (DT)

A diffusion tensor model is a 3-dimensional Gaussian model applied to each voxel in the diffusion-weighted images, which provides a description of the diffusion in the underlying tissue.

It is generated by modelling the displacement of molecules in three orthogonal directions (eigenvectors) and assigning three eigenvalues. This 3x3 matrix represents the DT, where the largest eigenvector signals the principal direction of diffusion along white matter tracts and the eigenvalues ($\lambda_1, \lambda_2, \lambda_3$) give the diffusivity in each direction. The tensor can be applied to the signal across the brain but looks quite different between the isotropic and anisotropic areas. The DT can also be represented as an ellipsoid of diffusion probability.

2.2.5 Analysis and tractography

A diffusion tensor model is generated at each voxel by comparing the reduced signal to the original signal (without the gradients). For the 3x3 DTI (6 independent values), the minimum number of images required would be 7: 6 images with diffusion weighting and 1 baseline image without diffusion weighting - in practice, however, many more images, with diffusion estimated in several different directions, are required to get a reliable estimate of the diffusion tensor. Information gathered from the Diffusion Weighted Image (DWI) can be represented as a scalar or as glyphs (ellipsoid visualisation). Scalar values represent some component of the magnitude of diffusivity. For example, axial diffusivity (AD) is the eigenvalue in the main direction of diffusivity and mean diffusivity (MD) is the average values of the three eigenvalues. Anisotropy measures represent the extent to which the DT differs from an isomorphic tensor i.e., a perfect sphere. Fractional anisotropy (FA) is the most common measure of anisotropy and represents the fraction of the tensor that is anisotropic or the normalised variance of the eigenvalues as shown in equation 2.1 (O'donnell & Westin, 2011).

$$FA = \sqrt{\frac{(\lambda_1 - \lambda_2)^2 + (\lambda_2 - \lambda_3)^2 + (\lambda_1 - \lambda_3)^2}{2(\lambda_1^2 + \lambda_2^2 + \lambda_3^2)}} \quad 2.1$$

Tractography is the process of reconstructing the trajectories of white matter tracts based on information gained from the DWI at each voxel. This is achieved by streamline reconstruction. The streamline curve is any curve whose tangent is parallel to the vector field representing the principal diffusion directions (Behrens, Sotiropoulos, & Jbabdi, 2014). The vector field can be visualised as a collection of arrows with magnitude and direction largely in the direction of the principal eigenvector in each voxel. Different fibre-tracking algorithms exist which piece

together information in the diffusion data to infer fibre trajectories (Jones & Cercignani, 2010). Deterministic algorithms assume one main diffusion direction in each voxel, and the tract is generated by defining a start point, propagating that direction across voxels and linking them. Probabilistic algorithms trace a large number of potential pathways from the start point, by considering many different diffusion directions compatible with the data and propagating them across voxels. Both result in a visual representation of the underlying white matter tracts or fibre bundles. The white matter tracts can then be weighted by different DW metrics. A variety of Region Of Interest (ROI) or whole brain analyses can follow, such as looking at individual tracts, or performing network analysis.

Obtaining estimates of myelin density in the white matter requires a different MRI sequence. The mcDESPOT sequence acquires 25 images for each participant. The fast (water constrained by myelin) and slow (free-moving water in intra- and extracellular space) components of the T1 and T2 times, and a nonexchanging free-water component were identified using a 3-pool algorithm (Deoni, Matthews, & Kolind, 2013; Zacharopoulos et al., 2017). The ratio of the myelin bound water to total water is calculated by taking advantage of T1 and T2 acquisitions. This is known as the Myelin Water Fraction.

2.2.6 Structural network generation

The structural data considered in this thesis was projected onto the same AAL atlas as the functional data (AAL, Tzourio-Mazoyer et al., 2002). Figure 2.2 shows a circular plot schematic of the 90 AAL regions. Edges of the networks were weighted by different structural measures: the number of streamlines measures from the tractography analysis, mean diffusivity (MD), radial diffusivity (RD), axial diffusivity (AD) and, finally, myelin content. These metrics will be further defined within the experimental chapters. Non-Negative Matrix Factorisation (Lee & Seung, 1999) was also applied to the structural connectivity matrices and will be explained further in Chapter 5.

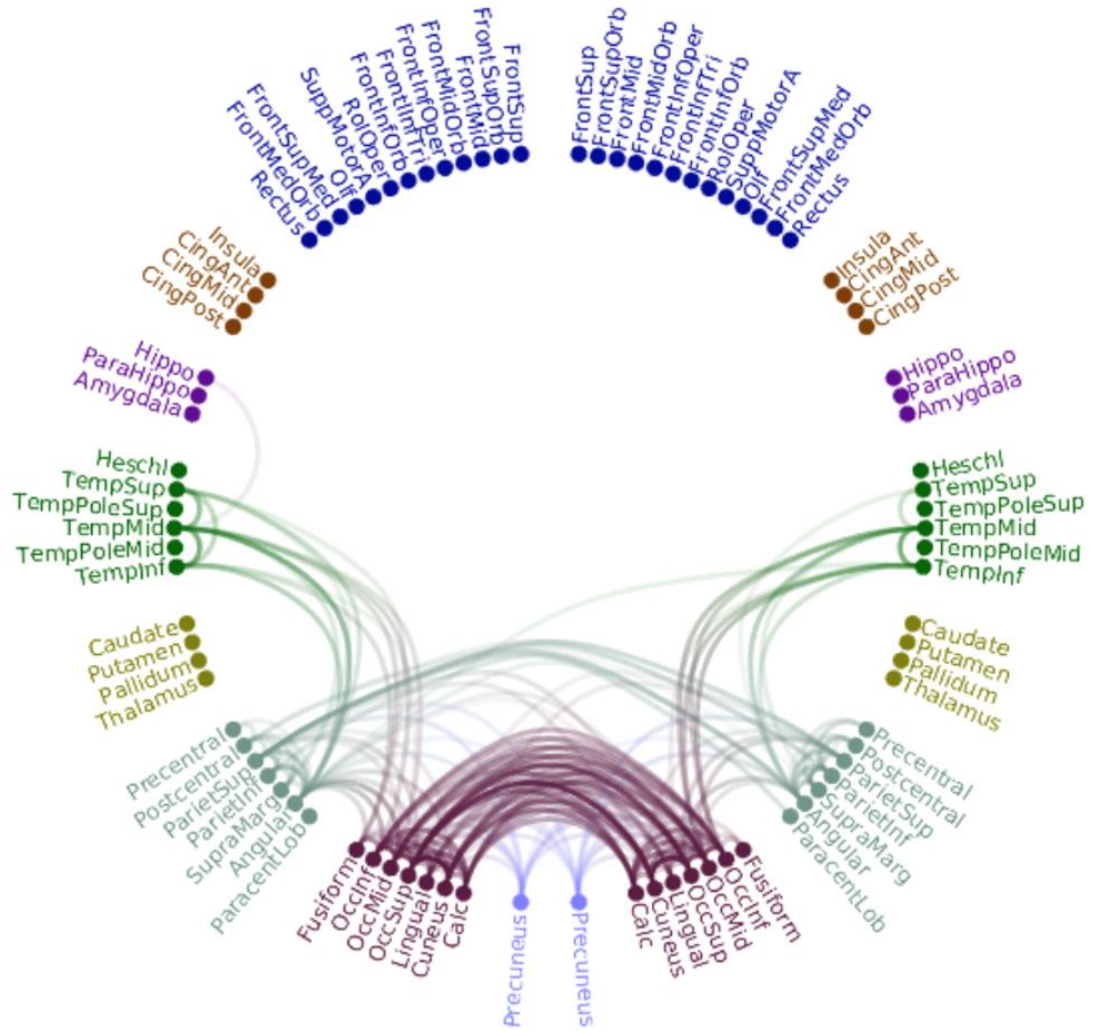


Figure 2.2. Anatomical labels for AAL regions on the connectivity plot. An example of valid connections. Blue: frontal, Gold: Insula/Anterior-Posterior cingulate, Purple: Medial temporal, Green: Temporal: Teal: Parietal and Sensorimotor, Maroon: occipital, Lilac: Precuneus. In house plot function (Singh, date).

Chapter 3. An investigation of the optimal sampling grid resolution for MEG beamforming

3.1 Rationale

MEG has excellent temporal resolution as shown in Chapter 2. However, improving the spatial resolution of MEG is an ongoing effort for researchers across hardware, methods and applied fields. In neuroscience, particular attention is given to localising signals of interest, such as gamma in the visual cortex. For this, several source-localisation algorithms exist, including beamforming. A beamformer applied at a higher spatial sampling resolution would be expected to give more accurate signal estimates, at the expense of computational resources. The aim of this chapter was to explore differences in gamma estimates obtained in the visual cortex, analysed with different (finer – coarser) sampling grids, to ascertain the optimal sampling resolution for source localisation in visual cortex.

3.2 Introduction

One of the fundamental problems in electrophysiological imaging is identifying neural activity at its source, by solving the inverse problem. In short, source analysis involves identifying spatial characteristics using a combination of the recorded signal, physiological assumptions and the electromagnetic forward model (estimating the sensor observations from a model with a given set of parameters) (Jaiswal et al., 2020). A number of approaches exist. Most commonly, dipole fitting has been applied, where a number of dipoles are specified (1 or 2 usually) at an expected ‘source’ location. Location and orientation are optimised and dipoles are considered collectively. Other methods include distributed source imaging which calculates source estimates across the whole source space (cortex) simultaneously. Well-known linear methods are eLORETA (low-resolution brain electromagnetic tomography-Pascual-Marqui, Michel, & Lehmann, 1994) and Minimum Norm Estimation MNE (Hämäläinen & Ilmoniemi, 1994). Non-linear versions also exist (Gramfort, 2013).

More recently beamforming algorithms have been increasingly advocated. Unlike the aforementioned methods, they operate adaptively, estimating the activity of each source as a linear, weighted combination of the channels. As such, beamformers are a spatial filter

comprised of source weights. The most common beamformer in the time domain, which is of particular interest in MEG research, is the Linearly Constrained Minimum Variance (LCMV - Sekihara, Hild, & Nagarajan, 2006; Spencer, Leahy, Mosher, & Lewis, 1992; Van Veen & Buckley, 1988). The LCMV beamformer estimates the activity at a point source per voxel, as defined by a pre-specified template grid, while simultaneously suppressing the contributions from sources at other locations, captured in the data covariance matrix.

As with all source localisation methods, however, beamforming is subject to the problem of non-uniqueness. That is, weightings between sensors and sources are not absolute, which requires consideration and constraint of the possibilities. This is done by providing the covariance of the sensor channels and the forward model. The forward model is essentially a mapping of currents per voxel, which asks if a current exists, what that would look like on the scalp. It is estimated using the conductance model, which considers how conductive the tissue between the area is, in combination with the geometry of the brain (usually measured using T1 weighted MRI). Conductance models come as part of popular LCMV tools, in packages such as Fieldtrip (Oostenveld, Fries, Maris, & Schoffelen, 2011), SPM12 (Litvak et al., 2011) and Brainstorm (Tadel, Baillet, Mosher, Pantazis, & Leahy, 2011).

While beamforming does assume non-temporally correlated sources i.e., perfectly correlated sources will mutually suppress each other, its principal merit is its relative lack of prior assumptions. A breadth of research questions in both task and rest data can be answered with beamforming because the weights are independent of sources in other regions. This is different to algorithms such as minimum norm, where reconstructions are dependent on the sources allowed in source space. Whole brain reconstructions are now commonplace due to the availability of computational resources, which were limited 20 years ago.

Recurrent questions in MEG methods research, however, concern achievable spatial resolutions, the spatial sampling resolutions required and how this affects analysis outputs. The smoothness of a reconstructed beamforming image depends on the characteristics of the sensor array (e.g., number of channels) and the signal to noise ratio of the data. Theoretically, the beamformer

image should be improved with a finer spatial sampling grid and conventionally studies have considered a 5-8mm sampling grid to be adequate.

However, Barnes and colleagues (Barnes et al., 2004) conducted an investigation using both simulated and experimental data (a visual grating paradigm) and found around 10% of the source space has a point spread function (FWHM) of less than 5 mm and 50% less than 8 mm. This problem could be considered a spatial equivalent to the Nyquist sampling theorem (Barnes et al., 2004), where use of an overly coarse grid will lead to under-sampling and missed information. In the paper by Barnes and colleagues (2004) this was particularly applicable to the occipital cortex, suggesting a 5+mm sampling grid might not be sufficient for investigation of this area. In fact, in a 64 electrode (.5mm spaced) electrocorticogram (ECoG) study of broadband gamma in the human motor cortex and superior temporal gyrus, Freeman and colleagues showed an optimal spatial sampling resolution of 1.25 mm, in avoiding undersampling and aliasing at the cost of computational resources (Freeman, Rogers, Holmes, & Silbergeld, 2000). The result of undersampling is reduced amplitude of the reconstructed source and potential misidentification of the true source. This is problematic for biomarker development and the identification of therapeutic targets, where source consistency is essential. Despite this, spatial sampling of ~6mm in MEG beamformer reconstructions is common.

To explore sampling resolution dependent differences in derived amplitude and frequency metrics, the same visual gamma data will be systematically explored from high (1mm) to low (6mm) spatial grid resolution. The visual gamma pipeline involves the insertion of a virtual electrode at the point of peak gamma power. Essentially, this process estimates what the time series would look like if an electrode was placed at the source of greatest amplitude in visual cortex. Visual gamma is related to local neuronal circuitry (Buzsáki, 2010; Buzsáki & Wang, 2012a; Donner & Siegel, 2011; Kopell, Ermentrout, Whittington, & Traub, 2000a; Shaw et al., 2017; Traub et al., 2001) and has been shown to be altered in clinical cohorts (Robinson & Mandell, 2015b), so, it is important that the sampling resolution and availability of information is optimal.

3.2.1 Aim and hypothesis

I sought to explore the optimal beamforming resolution for broadband (induced) visual gamma analysis (30- 80Hz) by comparing gamma output from 1mm, 2mm, 4mm and 6mm sampling grids and otherwise identical analysis pipelines. The hypothesis is that the use of a finer grid would provide more accurate (i.e., higher) visual gamma estimates of amplitude and frequency due to better sampling of the true sources.

3.3 Method

3.3.1 *Participants*

The 100-Brains project at Cardiff University Brain Imaging Centre (CUBRIC) was a large genetic and multimodal imaging study conducted in the healthy population (Brealy, 2015). There were 100 participants recruited of which 97 had MEG data. Participants were all right-handed (Edinburgh Inventory-Oldfield, 1971), absent of neuropsychiatric conditions (General Health Questionnaire, Goldberg & Williams, 1988), and of Caucasian ethnicity. Participants were university students (male 35%, female 65%) and, as such, similar in education level and age (m 24, SD 3.5). None of the participants had a history of drug or alcohol abuse.

3.3.2 *Task and data acquisition*

Visuomotor MEG data was acquired for 96 of the 97 participants. The paradigm involved 100 trials and lasted ~ 10 minutes. The visual grating stimulus was presented centrally. It comprised a vertical, stationary, maximum contrast square-wave grating with a spatial frequency of 3 cycles per degree ($8^\circ \times 8^\circ$ visual angle). The background was of mean grey luminance. Stimuli were jittered in length of between 1.5-2 seconds and followed by an inter-stimulus interval (ITI) of 2 seconds. Participants were required to push a button with their right hand every time the grating disappeared. Participants were notified if no response was detected after 750ms. Such tasks have been shown to induce large gamma responses in visual cortex (Muthukumaraswamy & Singh, 2013). The motor component of the response was not analysed here.

All data were acquired using the CTF-Omega axial gradiometer (275 channel) system, at Cardiff University Brain Research Imaging Centre (CUBRIC), which is placed inside a magnetically shielded room. Participants were sat upright in the scanner. Data were sampled at 1200Hz, with a 300Hz lowpass antialiasing filter. Three fiducial coils (nasion, left pre-auricular and right pre-auricular) were used for head localisation before and after the scan. For noise cancellation, data were acquired with 29 reference channels and were analysed in third-order gradiometer mode as recommended by Vrba and Robinson (2001).

3.3.3 Pre-processing

Data were pre-processed and co-registered by Jennifer Brealy. Data were pre-processed manually in DataEditor. Third-order gradient mode was applied, transforming the primary sensors for environmental noise reduction. Data were epoched into 4 second trials (-2, 2), around the stimulus onset. Each trial was inspected and those trials which contained large blink, motion or muscle artefacts were excluded.

Co-registration

MRIs (1mm- isotropic, T1 weighted), were acquired on the 3 Tesla General Electric system at CUBRIC. Co-registration was achieved by matching the MRI voxels that corresponded to the three fiducial coils using photographs taken in the MEG scanning session.

3.3.4 Visual gamma analysis

Data analysis was performed in Matlab (version 2017), using Fieldtrip (version 20190219) in house and custom scripts. Previously co-registered MRIs were defined in CTF co-ordinate space. The analysis was run 4 times. A weighted LCMV beamformer algorithm was used across the sampling grid manipulations (1mm, 2mm, 4mm & 6mm). Other than the change in sampling grid resolution, the analyses were identical.

The forward model

Using Fieldtrip, MRIs were segmented to distinguish ‘brain’, ‘skull’ and ‘scalp’ tissues. The outer brain surface was extracted from the MRI and a description of the brain surface (brainmask), created using vertices and triangles. This semi-realistic head model method was developed by Nolte (2003) and generates a single-shell headmodel. The headmodel, along with a description of tissue conductivity and derived mathematical parameters, comprises the volume conduction model.

A Montreal Neurological Institute (MNI) template grid was used in generating the source model. Data were transformed onto 1, 2, 4 and 6mm versions of the grid. The finer grid resolutions were employed at the cost of increased computational demand. To account for this, beamforming was conducted only on a sub-volume consisting of all bilateral visual areas from the AAL atlas

(Tzourio-Mazoyer et al., 2002); namely, Left Calcarine, Right Calcarine, Left Cuneus, Right Cuneus, Left Lingual, Right Lingual, Left Superior Occipital, Right Superior Occipital, Left Mid Occipital, Right Mid Occipital, Left Inferior Occipital, Right Inferior Occipital. At each location in this source grid, beamformer weights were calculated based on the covariance of the MEG data in a 30–80Hz bandwidth, over the whole dataset. The covariance time window was set to -1.5 – 1.5 s. A regularisation procedure (lambda 5%) was applied (Treder & Nolte, 2018).

Source power was projected separately for the baseline and stimulus periods in order to contrast them. The *sustained gamma* period was of primary interest here due to its oscillatory nature and a period between 0.3s- 1.5s after stimulus onset was selected (baseline -1.2 -0s). The percentage gamma power change between stimulus and baseline was then calculated. The coordinates of the source with the maximal percentage change in gamma power were extracted.

Reconstructing a virtual sensor

The timecourse at the peak source was calculated by multiplying the beamformer weights at the peak source location by the MEG timecourse of each trial. This virtual sensor (VS) timecourse was used to look at the gamma power spectra and time- frequency representations.

Power spectrum (frequency domain)

A slepian multi-taper method and frequency analysis was applied over the entire analysis window (4s trial epoch). The multi-taper method overcomes some issues associated with traditional Fourier Analysis, such as estimation bias in low trial analyses (Thomson, 1982). The multi-taper method increases signal to noise at the cost of temporal precision by averaging over the signal tapered in different ways (slepian method) and is helpful in identifying non-phase locked activity. Trial padding (1s, each side) and 2 Hz smoothing also was applied. The stimulus and baseline time-windows were analysed separately using a frequency-of-interest (FOI) window of 0-100Hz, padded to length of 2 seconds. The percentage change in power between them calculated and averaged over trials.

Time-frequency domain

Hilbert analysis was applied to each trial over ± 4 Hz wide, overlapping, frequency intervals, stepped from 0 Hz to 100 Hz in 0.5 Hz steps, generating a time-frequency spectrogram for each trial. Time-frequency spectrograms were averaged over trials and the percentage change between the mean of the baseline period and the whole trial was calculated. This resulted in a ‘single channel’ time-resolved time/frequency reconstruction for each participant, and at each reconstruction grid size.

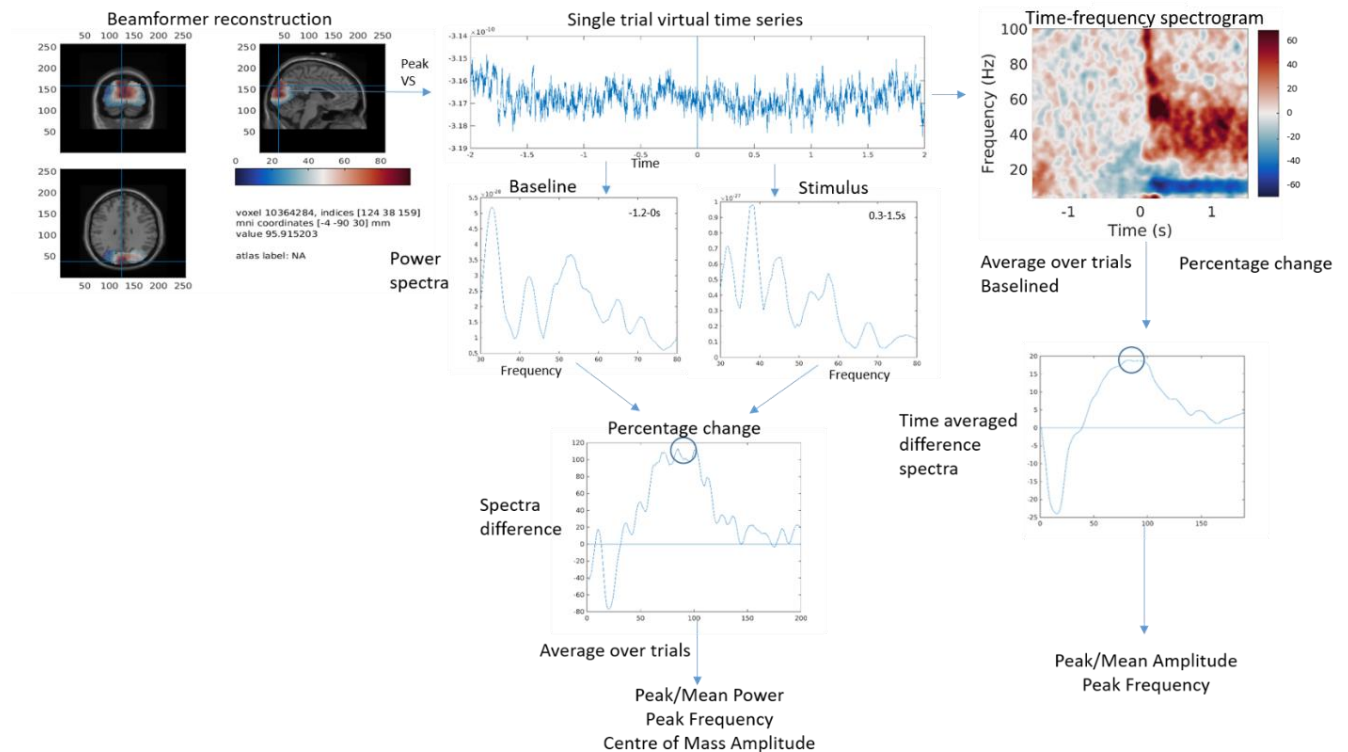


Figure 3.1. Visual gamma pipeline. Schematic denotes the generation of the multi-taper spectra (middle) and the time-frequency spectra (right).

Spectra in Figure 3.1 are smoothed with the Matlab ‘smooth’ function. This smooths data in column vector y using a moving average (default 5 data points). Furthermore, the beamformer is based on a 30-80 Hz window, however the reconstructed data is broadband. While not important to the analysis in this chapter, it should be acknowledged that slower signal may be the result of source leakage from another location(s).

3.3.5 Output Measures

Multi-taper Spectra Measures

- Peak Amplitude- largest gamma power change between stimulus and baseline at peak source (VS), collapsed across time.
- Mean Amplitude- mean power change collapsed across time at peak source.
- Peak Frequency- highest frequency value collapsed across time at peak source.
- Centre of Mass (weighted) Frequency (Lozano-Soldevilla, Ter Huurne, Cools, & Jensen, 2014a) . The centre of mass frequency was generated by calculating the mean frequency over the frequency window of interest (30-80=55Hz) as shown in equation 3.1. The mean is then weighted by the amplitude of the gamma response at each frequency. This finds the frequency values where the tendency of the peak to be maximal is.

$$f_c = \frac{\sum_{i=1}^N f_i \cdot P(f_i)}{\sum_{i=1}^N P(f_i)}$$

3.1

Time-frequency domain measures- Hilbert transform

- Peak Amplitude- largest gamma amplitude change between stimulus and baseline at peak source over time (highest intensity).
- Mean Amplitude- mean amplitude change over time.
- Peak Frequency- highest frequency value over time.

3.3.6 Statistical analysis

All statistics were completed in Matlab (version 2017) and IBM SPSS (25). To identify group differences due to the manipulation of the sampling grid, a repeated-measures ANOVA was used to compare estimates across the 4 levels (1mm, 2mm, 4mm & 6mm) of grid size. Grid size was the independent variable. Peak amplitude, peak frequency, centre of mass frequency and mean amplitude, estimates in the multi-spectra domain were dependent variables. Post hoc Bonferroni adjustment was applied for comparison of main effects.

Relationships between multi-taper and time-frequency spectrogram measures of peak amplitude, peak frequency and mean amplitude, using a 1mm grid, were also visually explored. multi-taper.

3.4 Results

3.4.1 Estimates from multi-taper spectra

The mean values of induced amplitude and frequency across the different sampling grids can be seen in Table 3.1.

Table 3.1. Descriptives

| | 1mm | | 2mm | | 4mm | | 6mm | |
|------------------------|-------------|-----------|-------------|-----------|-------------|-----------|-------------|-----------|
| N=96 | Mean | SD | Mean | SD | Mean | SD | Mean | SD |
| Peak Amplitude (power) | 297 | 242 | 296 | 243 | 292 | 236 | 283 | 222 |
| Peak Frequency | 50 | 8 | 50 | 8 | 50 | 8 | 51 | 8 |
| Weighted Frequency | 52 | 4 | 52 | 3 | 52 | 4 | 52 | 4 |
| Mean Amplitude (power) | 103 | 67 | 103 | 67 | 101 | 66 | 100 | 64 |

ANOVAs

Peak amplitude values were significantly different ($F(1.463, 138.973) = 15.272$, $p < .001$), sphericity not assumed. Mean amplitude values were significantly different ($F(1.556, 148.806) = 38.651$, $p < .001$), sphericity not assumed. Amplitude pairwise comparisons are shown in Tables 3.2 & 3.3. Neither peak ($F(2.376, 225.715) = .809$, $p = .465$), or COM ($F(1.953, 185.507) = 1.648$, $p = .196$), frequency were significantly different, sphericity not assumed.

Table 3.2. Peak Amplitude ANOVA

| (I) GridSize | (J) GridSize | Mean Difference (I-J) | | | 95% Confidence Interval for Difference^b | |
|---------------------|---------------------|------------------------------|-------------------|-------------------------|---|--------------------|
| | | J | Std. Error | Sig.^b | Lower Bound | Upper Bound |
| 1 | 2 | 0.76 | 0.77 | 1.00 | -1.31 | 2.83 |
| | 4 | 4.438* | 1.44 | 0.02 | 0.57 | 8.30 |
| | 6 | 13.377* | 2.92 | 0.00 | 5.51 | 21.24 |
| 2 | 1 | -0.76 | 0.77 | 1.00 | -2.83 | 1.31 |
| | 4 | 3.68 | 1.75 | 0.23 | -1.04 | 8.39 |
| | 6 | 12.614* | 3.12 | 0.00 | 4.22 | 21.01 |
| 4 | 1 | -4.438* | 1.44 | 0.02 | -8.30 | -0.57 |
| | 2 | -3.68 | 1.75 | 0.23 | -8.39 | 1.04 |
| | 6 | 8.940* | 2.38 | 0.00 | 2.54 | 15.34 |

*. The mean difference is significant at the .05 level.

b. Adjustment for multiple comparisons: Bonferroni.

Table 3.3. Mean Amplitude ANOVA

| (I) GridSize | (J) GridSize | Mean | Std. Error | Sig. ^b | 95% Confidence Interval for | |
|--------------|--------------|------------------|------------|-------------------|-----------------------------|-------------|
| | | Difference (I-J) | | | Difference ^b | Lower Bound |
| 1 | 2 | 0.31 | 0.14 | 0.16 | -0.06 | 0.68 |
| | 4 | 1.924* | 0.36 | 0.00 | 0.96 | 2.89 |
| | 6 | 3.650* | 0.53 | 0.00 | 2.24 | 5.06 |
| 2 | 1 | -0.31 | 0.14 | 0.16 | -0.68 | 0.06 |
| | 4 | 1.614* | 0.29 | 0.00 | 0.82 | 2.41 |
| | 6 | 3.340* | 0.48 | 0.00 | 2.04 | 4.64 |
| 4 | 1 | -1.924* | 0.36 | 0.00 | -2.89 | -0.96 |
| | 2 | -1.614* | 0.29 | 0.00 | -2.41 | -0.82 |
| | 6 | 1.726* | 0.37 | 0.00 | 0.74 | 2.72 |

Based on estimated marginal means

*. The mean difference is significant at the .05 level.

b. Adjustment for multiple comparisons: Bonferroni.

There was no significant difference between power at 1mm and 2mm ($p > .05$). However, differences between metrics at 1mm and metrics at 4 & 6mm were significant ($p < .05$). Differences between power metrics a 6mm and all other grid sizes were significant ($p < .05$). No significant differences were found between peak frequency or centre of mass frequency metrics across grid sizes ($p > .05$). As a further check, amplitude (sqrt power) was compared across grid sizes and the same pattern of results were found.

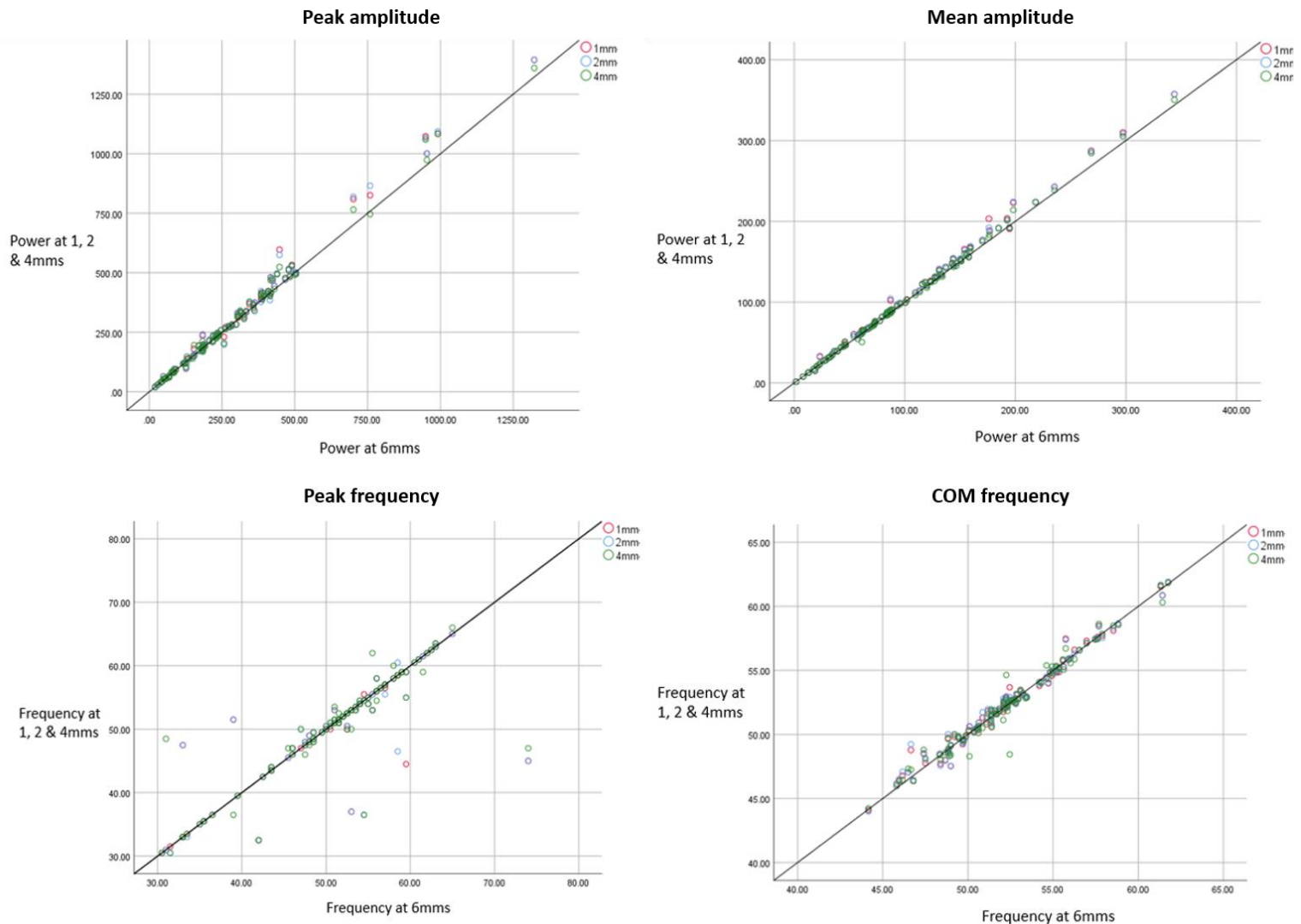


Figure 3.2. Shows the multispectra estimates of peak power (top left), mean power (top right), peak frequency (bottom left) and centre-of-mass frequency (bottom right), at 1mm, 2mm and 4mm resolution, plotted against 6mm output, with line of reference.

The figure above (3.2) shows a modest increase in power at 1mm & 2mm resolution.

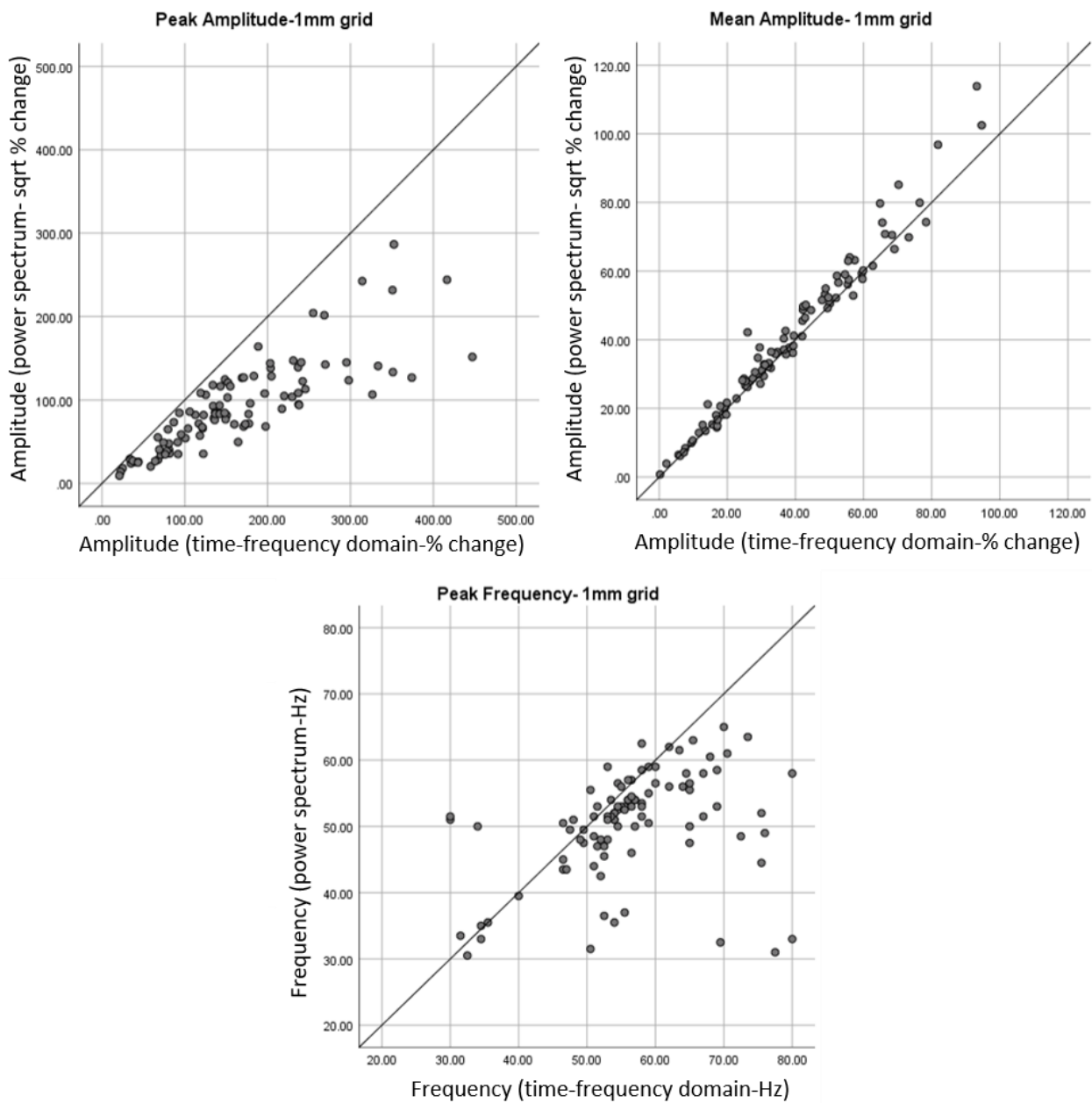


Figure 3.3. Peak amplitude, mean amplitude and peak frequency (multi-taper spectra) versus the analogous time-frequency metric, with line of reference.

There was a trend between all multi-taper spectra metrics and time-frequency metrics. Peak amplitude was higher in the time-frequency spectra compared to the multi-taper spectra. Power measures were naturally higher (~factor 3) than amplitude measures because power is directly proportional to amplitude squared. Peak frequency estimates were mostly higher in the time-

frequency domain compared to the multi-taper spectra. Peak frequency appears to be less consistent than amplitude over multi-taper spectra and time frequency domains.

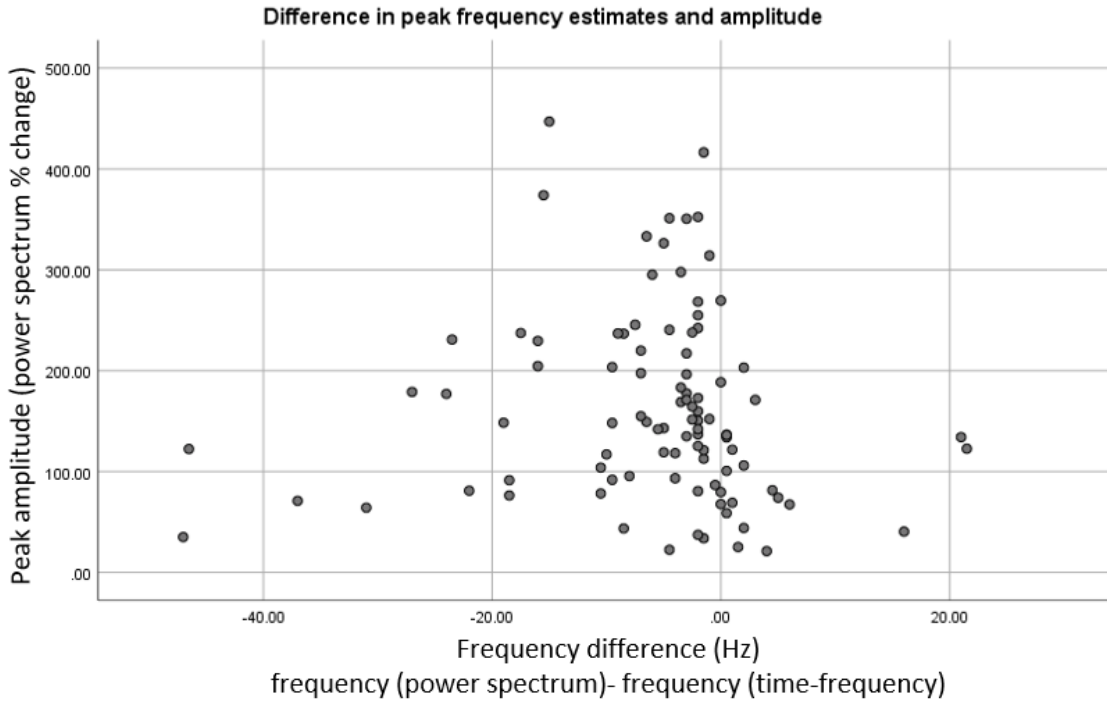


Figure 3.4. Peak amplitude against Difference in peak frequency (multi-taper spectra peak frequency minus time-frequency peak frequency). This plot shows how frequency estimates differed with amplitude.

The consistency of frequency metrics between the multi-taper and time-frequency estimates, in relation to amplitude, was explored in Figure 3.4. The more divergent peak frequency gamma estimates were obtained at lower gamma amplitude. Conversely, high amplitude estimates appear to have less different peak frequency values between the two methods of analysis.

3.5 Discussion

The aim of this chapter was to investigate the effect of the sampling resolution of LCMV beamforming on visual gamma (range 30-80Hz) estimates of amplitude and frequency. In summary the results showed sustained gamma amplitude significantly differed with grid size, with highest estimates at 1mm sampling resolution; 6mm estimates were significantly ‘poorer’ than all others. Consistent with the hypothesis, using a higher resolution sampling grid increased sustained visual gamma estimates (amplitude), albeit moderately, with a 1mm grid being optimal. This is an improvement because higher amplitude represents increased signal to noise. Frequency estimates did not significantly differ with grid size. Weighted frequency appears to be a more stable measure of frequency, than peak frequency. However, in support of conclusion made by Barnes and colleagues, frequency signals at lower amplitude, where signal to noise is lower, may be more uncertain (Barnes et al., 2004).

Obtaining optimal estimates of sustained visual gamma is important considering its role in local circuitry. For example, direct Local Field Potential (LFP) studies in cat and macaque have shown that gamma amplitude and/or frequency are sensitive to characteristics of visual stimuli, such as orientation and velocity (Friedman-Hill, 2000; Gray & Singer, 1989). In humans, studies have associated visual gamma frequency with both the BOLD response ($R = -0.64$) and MRS GABA concentration, a primary inhibitory neurotransmitter, ($R = 0.68$), in the visual cortex (Muthukumaraswamy et al., 2009). This work supports the Pyramidal Interneuron Gamma (PING) model of gamma oscillations which suggests that local cortical inhibition-excitation systems can be probed with visual gamma paradigms.

Visual gamma is disturbed in several clinical samples, for example in schizophrenia patients (Spencer, 2008) and in major depressive disorder (Fitzgerald & Watson, 2018). In schizophrenia, reductions in visual gamma have been considered a biomarker of the disorder (Shin, O’Donnell, Youn, & Kwon, 2011). Acquiring an optimal reconstruction of the gamma signal is therefore important for the identification of dysfunction and to give the biomarker potential for clinical use.

Dynamic Causal Modelling (DCM) suggests that visual gamma response is mediated by connections between superficial pyramidal cells (in layers 2/3- signal reflected in MEG) and interneurons (Shaw et al., 2017b; Sumner, Spriggs, & Shaw, 2021) in V1. Coupling strength between inhibitory neurons and layer 2/3 superficial pyramidal cells has also been shown to predict performance on the visual orientation task (Shaw et al., 2020). Recently, layer 4 stellate cells - superficial pyramidal (L4S->SP) connections have also been implicated (Sumner et al., 2021).

MEG recordings of the sustained component of the gamma response has an established electrophysiological basis as far as the sustained period is known to be oscillatory (Cohen, 2014). The evoked signal is short and phase-locked to the stimulus, while the sustained period is non-phase-locked, or induced, with a longer duration. Evoked responses are highly repeatable between participants, even when a sustained gamma signal barely exists, suggesting the evoked response is less subject to individual differences (Muthukumaraswamy et al., 2010). It is the sustained oscillatory period that is of interest in the upcoming analyses in this thesis.

In addition to a role in local circuitry (Buzsáki & Wang, 2012b; Donner & Siegel, 2011; Shaw et al., 2017), gamma oscillations have been associated with cognitive processes such as visual binding (Tallon-Baudry, 2009). Fundamentally, ability to infer such processes requires accurate source estimates. In resting-state data, the LCMV beamformer has been shown to perform well even in lower SNR/high sensor noise circumstances (Tait, Ozkan, Szul, & Zhang, 2020), which is often the case in clinical data. However, peak frequency estimates at low amplitude, i.e., lower signal to noise (SNR), appear to be more uncertain. Furthermore, the comparison of frequency estimates extracted with multi-taper spectra and time frequency methods show frequency estimates were more different at lower amplitude. The uncertainty in peak frequency may be mitigated with increased sampling resolution as amplitude estimates were significantly higher using a 1mm grid. Uncertainty in frequency estimates may also be mitigated by using the centre of mass frequency method, estimates from which appear to be more consistent over different spatial sampling resolutions and individuals.

Limitations

The study was subject to some limitations and subsequent points of further investigation. Although implementation of the LCMV with Fieldtrip, as compared with MNE-Python, FieldTrip, DAiSS (SPM12), and Brainstorm, has been shown to have adequate accuracy and sensitivity (Jaiswal et al., 2019), improvement in amplitude measures were not as large as expected. This could be for a couple of reasons, 1) a beamformer can reconstruct a strong gamma response, at high SNR, if sampling is conducted at the exact source location. However, even with a 1mm grid it is unlikely that a peak at that precise location will be reconstructed, so amplitude will usually be underestimated & 2) the strength of the sustained gamma response is limited, so the improvement is likely to also be modest.

Furthermore, interpretation of the statistical improvement in sustained amplitude should be made with some caution as the increased number of data points at 1mm due to the higher resolution could have led to statistical differences. Nonetheless, the nature of the beamformer necessitates an improvement to estimates with a finer grid and the purpose of this this chapter was to consider the nature of the difference in estimates with a finer grid in light of the following chapters in this thesis. Admittedly, the difference in estimates was not as large as anticipated, however estimates at 1mm are of greater amplitude, and therefore higher SNR, which is important for subsequent analyses. In fact, amplitude increases might be relatively larger with paradigms that do not induce such a strong gamma response and where several sources might exist. This is something that could be explored using a non-grating stimulus.

One unexpected finding was that amplitude and frequency estimates appeared to be higher in the time frequency spectra than multi-taper spectra. This might be attributed to differences the multi-taper and Hilbert transforms. For example, the generation of the time-frequency spectrograms involves smoothing each line by ~4Hz across frequencies which could enhance amplitude. However, this is beyond the scope of this chapter and could be further explored elsewhere.

Future directions/Uses

This work could be important to clinical studies which usually generate data at lower SNR and would benefit from improved source estimates. It should be noted that this is not a repeatability analysis as this would require an alternative dataset or analysis of a control region. However, this

could be completed elsewhere and would allow additional statistical probing. Furthermore, the centre-of-mass frequency measure provides more consistent estimates than peak frequency and future research would benefit from the inclusion of this metric. Peak frequency or mean frequency estimates are, however, most common in previous literature and therefore these measures were used in other chapters of this thesis. Uncertainty in peak frequency estimates at low SNR appears to be somewhat mitigated by using a high resolution (1mm) grid, nevertheless at lower sampling resolutions, a centre of mass approach is endorsed.

Overall, a 1mm grid allowed the highest estimates of amplitude to be reconstructed. A difference was not seen for frequency. While use of a 1mm grid appears to be optimal, it seems that if computation time has priority, reconstructions at 2mm or 4mm have no considerable disadvantage when considering sustained gamma.

Chapter 4. Extracting long-range networks from task data

4.1 Rationale

Optimising the utility of our experimental paradigms is also of considerable importance for the acquisition of quality MEG data. Previous findings suggest that similar long-range network patterns can be extracted in task and rest data. Where MEG scan sessions are long, or participants vulnerable to head-motion, i.e., in clinical cohorts, excluding a resting-state task (~10minutes), would be advantageous. Finding established oscillatory network characteristics in task data may lead to the question of whether a resting-state paradigm is required in certain scanning protocols.

4.2 Introduction

The dominant functional network patterns observed in so-called ‘at-rest states’ are well established (Sietzman et al., 2019). Resting-state networks (RSNs) represent synchronous activity across different neuronal populations in the absence of a task or stimulation. These have mostly been explored with fMRI, with its high spatial localisation and sensitivity to slow metabolic dynamics ($\approx 0.01\text{--}0.1$ Hz), revealing distant connectivity patterns across the brain. The default mode network, fronto-parietal network, fronto-temporal network and occipital network have subsequently become signatures of the brain at rest (Damoiseaux, Rombouts, Barkhof, Scheltens, Stam, Smith, Beckmann, et al., 2006; Seitzman, Snyder, Leuthardt, & Shimony, 2019). These areas have been implicated in several cognitive functions such as motor function, visual processing, executive functioning and auditory processing. Functional networks are now becoming better understood in the oscillatory and time domains and RSNs revealed with M/EEG have been shown to converge with fMRI findings (Brookes et al., 2011; Brookes et al., 2011).

An interesting question in this area, is to what extent RSNs are unique, i.e., as the brain is never truly at rest, how do these networks differ to those in stimulated circumstances? Despite a clear distinction in the literature between ‘rest’ and ‘task’ studies, numerous studies have shown a relationship between stimulus associated activity and RSNs (Northoff, Qin & Nakao, 2010). For example, when Smith and colleagues (2009), compared the resting fMRI networks of 36 subjects, to activation studies (ICA derived networks), in the BrainMap Database (~30,000

subjects). They found considerable overlap in visual, default mode, cerebellum, sensorimotor, auditory, executive control and fronto-parietal networks (Smith et al., 2009). Furthermore, Cole and colleagues (2014), also found high similarity between fMRI connectivity matrices from a 64-task paradigm and the resting-state (Pearson correlation coefficient $r=0.90$, $p<.00001$), which suggests the existence of intrinsic connectivity patterns. The multi-task paradigm comprised minimal changes in perceptual features across tasks, but targeted different cognitive domains: logic, sensory and motor, etc. (Cole, Bassett, Power, Braver, & Petersen, 2014).

Evidence from the time-resolved imaging and modelling literature suggests these intrinsic global within-frequency-band connectivity patterns are more likely to be observed in the lower frequency ranges, i.e., 8-13Hz, 13-30Hz (Cabral et al., 2011; de Pasquale et al., 2010; Samogin et al., 2020; Wang, Jiao, Tang, Wang, & Lu, 2013). One plausible reason is because alpha and beta oscillations have been considered to reflect connectivity, or synchronisation, between long-range populations of neurons (Pascal Fries, 2015). These networks are synaptically driven, however, the exact mechanism behind these findings is yet to be understood.

Interestingly, in a reliability MEG study of connectivity methods, Colclough and colleagues, found that the most repeatable and consistent static connectivity methods, at the individual and group level, were alpha and beta networks, extracted with amplitude envelope correlation (Colclough et al., 2016). These findings could support the existence of intrinsic oscillatory connectivity patterns in the alpha and beta bands, both within and across individuals. Moreover, intrinsic connectivity patterns should remain in the presence of high frequency activity (i.e., the gamma range $>30\text{Hz}$), as PET studies suggest that the brain's metabolic processes only require a minimal amount of additional energy, for mentally demanding tasks (Raichle, 2006; Raichle & Mintun, 2006).

In neuroimaging, it is well known that long scanning sessions comprising different tasks can lead to fatigue effects. Subsequent head motion effects, movement effects and 'off-taskness' have an impact on data quality, with the latter being a more discrete and worrisome problem in analysis and interpretation. This is particularly the case in clinical cohorts, where individuals may already be experiencing symptoms or discomfort. While wellbeing maintenance is paramount in research

and ensured via ethical procedures, reducing scan time can only be of benefit to both participants and data quality.

The quantification of connectivity networks is critical to clinical studies, particularly our understanding of neuropathology in schizophrenia. Experiences of individuals suffering with symptoms make scanning sessions prone to confounding factors. Therefore, it is essential that scanning sessions are as short as possible. Being able to dispense with the RSN paradigm and extract global networks from task data would help, not to mention improving the tolerability of sessions for participants.

4.2.1 Aims and hypotheses

The aim of this chapter is to compare static amplitude-amplitude connectivity networks extracted from visuomotor task (VM) or resting-state (RS) MEG data from the same individuals. The following research questions will be explored 1) how do the patterns of connectivity compare between RS and VM data, 2) how does the strength of connectivity compare between RS and VM data, 3) how do node activity and connectivity compare over RS and VM data, 4) how consistent are connectivity matrices across participants in RS and VM data, 5) how do NNMF-derived network weightings compare between RS and VM data?

The first hypothesis is that those connections that show strong connectivity (averaged across participants) in VM data would also show strong connectivity in RSN data. Considering the robustness of amplitude-amplitude functional connectivity in the alpha and beta bands (Colclough et al., 2016; Godfrey & Singh, 2020), it is also hypothesised that similar long-range connectivity networks can be extracted from both task and rest data in these frequency ranges. As the visuomotor (gamma) task induces local gamma oscillations (increases amplitude) in visual cortex (Muthukumaraswamy et al., 2010), it is not expected that occipital gamma connections will be consistent in task and rest data.

4.3 Method

4.3.1 Participants

The MEG-Partnership project was a large UK-wide multisite project. The data acquired at Cardiff University are included in this thesis. All participants were healthy individuals with no history of neurological or neuropsychiatric dysfunction. Participants were right-handed, with British-Caucasian ethnicity and English as their first language, of age 21-55 years.

Table 4.1. MEG-Partnership demographics

| | N 88 | Mean | SD |
|--------|-------------|--------------|-----------|
| Age | n 88 | 25.5 (years) | 6.73 |
| Gender | n 88 | 61f:27m | |

4.3.2 MEG Acquisition and Tasks

All data were acquired using the CTF-Omega axial gradiometer (275 channel) system, at CUBRIC. Participants were sat upright in the scanner, which is placed inside a magnetically shielded room. Data were sampled at 1200Hz, with a 300Hz lowpass antialiasing filter. For head localisation, electromagnetic coils were attached to the fiducial areas; nasion and right and left pre-auricular. Head localisation was completed at the beginning and the end of each scan. For noise cancellation, data were acquired with 29 reference channels and were analysed in third-order gradiometer mode as recommended by Vrba and Robinson (Vrba & Robinson, 2001).

Each participant completed a battery of tasks in the scanner, including a resting-state paradigm and a visuomotor task. The resting-state task comprised a 5-minute presentation of a central fixation cross. Participants were instructed to focus, with eyes open, at the cross for the duration of the scan. Resting-state data was acquired for 88 participants.

The visuomotor task comprised 100 trials in total, which lasted ~ 13 minutes. The visual stimulus presented in the lower left visual field was a stationary, vertical, maximum contrast, three cycles per minute, square-wave grating, subtended vertically and horizontally at a 4° angle. The stimulus was presented for 1.5-2 seconds, jittered, on a mean luminance background. The ITIs were either 4 seconds or 8 seconds and allocated to half of the trials, presented in random order. Participants were also required to perform a finger abduction with the index finger on the

right hand whenever the grating disappeared. This task can be referred to as visuomotor task and visual gamma task interchangeably, but will be referred to as VM in this chapter. The motor component was not analysed in this thesis. Visual data were acquired for 84 of the 88 participants with resting-state data, and it is this subset of 84 that was taken forward for comparative analysis.

Both paradigms were programmed in Matlab (2015) and presented at a refresh rate of 100Hz.

4.3.3 Pre-processing

Data analysis was performed in Matlab (version 2017) and with Fieldtrip (revision 20190219). The resting-state data were split into 2 second epochs and visually inspected for large blink muscle or movement artefacts in DataEditor. These epochs were removed from the data. VM data were split into 4 second epochs around the stimulus onset (-2, 2). Trials with large blink, muscle or movement artefacts were also manually removed from the data.

MRIs and co-registration

MRIs (1mm- isotropic, T1 weighted), were acquired on the 3 Tesla General Electric system at CUBRIC. Co-registration was completed with photographs taken of the fiducial coils (nasion, left and right pre-auricular) during the MEG scanning session. Fiduciary markers were placed at three anatomical landmarks identifiable in the subject's anatomical MR scan. Their locations were then manually marked in the MR image.

4.3.4 Resting-state Analysis

CUBRIC's in-house amplitude-amplitude functional connectivity pipeline (kAAL_ConnectKL) was applied to both the resting-state and VM data. In summary, data were read in as continuous data, down-sampled to 600 Hz, and filtered with a 1 Hz high-pass and a 150 Hz low-pass filter. Data were split into 2 second trials and filtered into canonical frequency bands. A covariance matrix was generated for each of the following bands: Delta 1-4Hz, Theta 4-8Hz, Alpha 8-13Hz, Beta 13-30Hz, Low Gamma 30-60Hz and High Gamma 60-90Hz. Source localisation was achieved with a LCMV beamformer, a 6 mm sampling grid and a single-shell forward model (Nolte, 2003).

Virtual sensor data for each trial was created and concatenated per voxel. A representative timecourse for each AAL region, i.e., the virtual sensor with the largest temporal standard deviation was then selected and orthogonalisation applied to reduce source leakage (Colclough, Brookes, Smith, & Woolrich, 2015). Matlab's *hilbert* function was then used to generate the analytic signal for each of these 90 orthogonalized timeseries – the absolute amplitude of this yields the time-varying amplitude envelope of the band-passed signal, here called the *Hilbert envelope*. This envelope was then temporally downsampled (1Hz) and conditioned (despiked to remove artefactual temporal transients using a median filter and trimmed to avoid edge effects; removing the first 2 and last three samples). Pairwise correlations were calculated between the 90 Hilbert envelopes, providing connectivity matrices comprised of 4005 unique correlations (connections) per frequency band for each participant.

Finally, global effects can arise from experimental factors such as head size, head movement and head position within the MEG dewar. In this case, after the correlation matrices were generated, the global normalisation procedure applied involved subtracting a Gaussian of the weakest connections considered to be noise, per participant, (i.e., a null mean and standard deviation) from all connections for that participant (see appendix A). This resulted in a normalised 90x90 connectivity matrix for each subject, where each value represents the strength of connectivity between two regions.

The corresponding 84 VM and resting-state (RS/N) matrices were carried forward for further analysis.

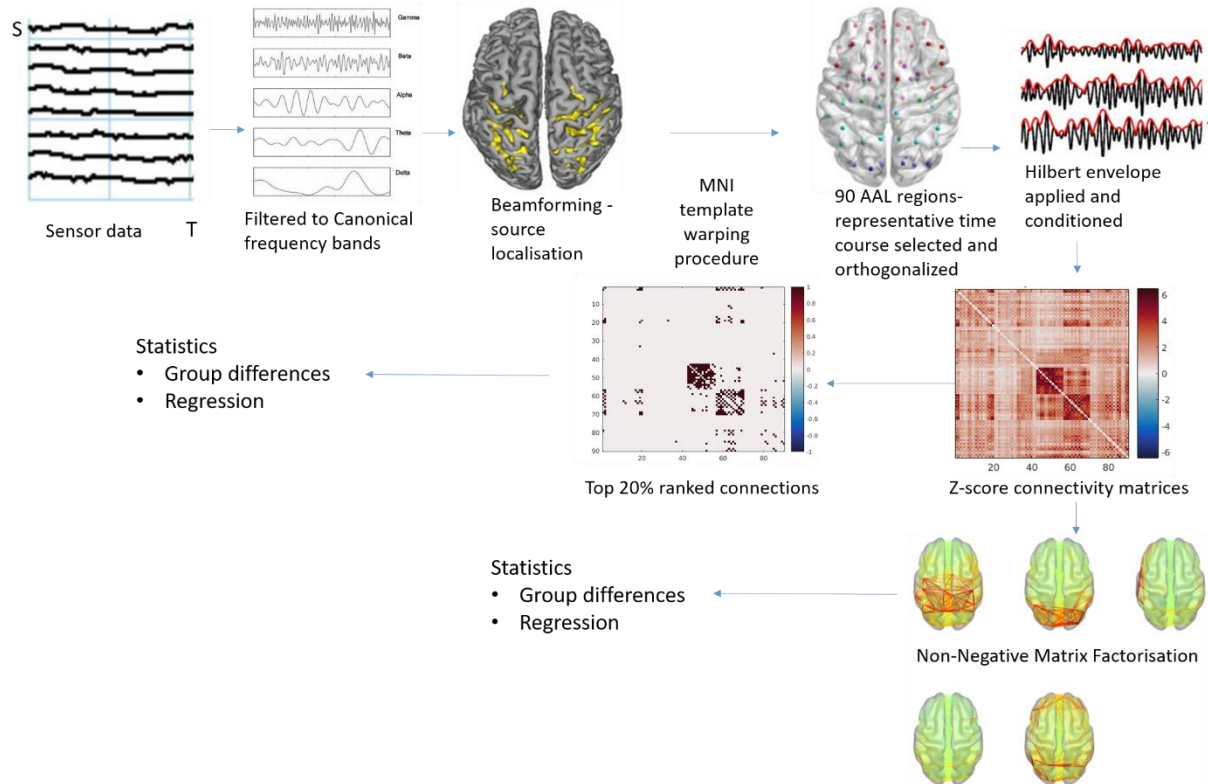


Figure 4.1. A schematic of the amplitude-amplitude connectivity pipeline³.

4.3.5 Non-Negative Matrix Factorization (NNMF)

Whole brain connectivity data is complex, with many node-node connections. It has previously been shown that many of these individual connections can be grouped into functionally relevant sub-networks, using data-driven reduction methods such as Principal Components Analysis (PCA) or Independent Components Analysis (ICA) (Brookes et al., 2011; Smith, Hyvärinen, Varoquaux, Miller, & Beckmann, 2014; Smith et al., 2012). Analyses such as these allow the consistency of networks across participants to be observed.

³ Note: images of sensor data, source localisation template brain and the Hilbert envelope are adapted from Koelewijn, L., Lancaster, T. M., Linden, D., Dima, D. C., Routley, B. C., Magazzini, L., ... & Singh, K. (2019). Oscillatory hyperactivity and hyperconnectivity in young APOE- ϵ 4 carriers and hypoconnectivity in Alzheimer's disease. *Elife*, 8, e36011. The brain template depicting 90 AAL nodes is adapted from Pang, E. W., & Snead Iii, O. C. (2016). From structure to circuits: the contribution of MEG connectivity studies to functional neurosurgery. *Frontiers in neuroanatomy*, 10, 67.

In the specific case we have here, namely amplitude-amplitude connectivity matrices, all of the significant connectivity values tend to be positive (Koelewijn et al., 2017) and conceptually it makes sense for each participant to have positive-only loadings on to each sub-network. Therefore, a specific algorithm, similar to PCA, was used, which constrains both the sub-networks and their loadings to be positive, namely Non-Negative Matrix Factorization (NNMF, Lee & Seung, 1999; Phalen, Coffman, Ghuman, Sejdić, & Salisbury, 2019; Doherty et al., 2021; Messaritaki et al., 2021a). Each component comprises a linear combination of the original data points. In this case, a number of network components are generated which co-vary across participants. Each participant has one component weighting per component in each frequency band (Delta 1-4Hz, Theta 4-8Hz, Alpha 8-13Hz, Beta 13-30Hz, Low Gamma 30-60Hz and High Gamma 60-90Hz).

A specific challenge with NNMF is choosing how many sub-network components in which to decompose the original network matrices. Conventional methods of looking at the explained variance do not tend to work well, as NNMF will increasingly use components which only load on to very few participants. In this way, increased components always lead to a better fit. So, a rule for iteratively assessing the fit was chosen, but with a set of stopping rules based on how many participants have non-zero component weightings. Namely, in each frequency band, there were a maximum of 20 components allowed; every component need to have a non-zero value in at least 50% of participants and, averaging across all components, the mean number of non-zero weightings needed to be greater than 70% of participants, in order for the algorithm to continue.

4.3.6 Planned Comparisons

From the connectivity matrices the following measures were derived and used for dataset comparisons across 3 levels (separately for each frequency band): across connections (i.e., the 90 AAL regions/nodes), by participant (across subjects' comparisons) and by NNMF components.

Node measures

a) Mean effect activity at each node is a measure of temporal variation in the Hilbert-derived envelope. It is generated by, first, taking the Hilbert envelope of each virtual time series at each node. Then, summarising how variable this envelope is over the entire data run by

calculating the coefficient-of-variation (i.e., temporal SD/temporal Mean). This results in a temporal activity measure at each of 90 AAL regions for each participant (Doherty et al., 2021; Koelewijn et al., 2019).

b) Node strength connectivity is how connected each of the 90 AAL nodes is to every other node, i.e., the sum of weights (connection strength) of links connected to the node.

Participant consistency measures

The datasets were also assessed with two participant consistency measures. This was to explore whether the within-group network estimates were more or less variable in the VM data than the resting-state data.

a) Mean rank, in this case, is a measure of the consistency of magnitude of connections, across participants. Connections are first ranked in order of magnitude, with the strongest connection being given the value 1 and the weakest given value 0. The mean rank is then found across participants for each connection (Godfrey & Singh, 2021). If the connectivity matrices are all randomly dissimilar across participants, then the sorted mean rank would be flat, around 0.5.

b) Spatial correlation is a measure of how similar each person's connectivity profile is to the mean connectivity map across participants. A vector of the mean z-score connectivity values is calculated across participants. A vector of mean connectivity scores is also generated for each participant and correlated with the mean across participants. A high pattern correlation represents robust networks across participants, whereas low pattern correlations represent networks that are variable between participants.

Non-Negative Matrix Factorization

To compare the component weightings between the resting-state and VM datasets, connectivity matrices from both the VM and RSN datasets were concatenated. This was to ensure that the same spatial sub-networks were extracted. If the analyses were run separately the networks would not be guaranteed to be identical. The NNMF algorithm was then run over the combined 168 datasets. This resulted in two component weighting values, per network, per frequency band for each subject and allowed a direct comparison, in the same spatial sub-networks, of the network weightings from the VM and RSN experiments.

Results were explored visually, with Pearson's correlation, repeated measures T-tests and simple linear regression methods.

4.4 Results

4.4.1 Connection comparisons

The datasets were first compared across connections in each frequency band (Figure 4.2).

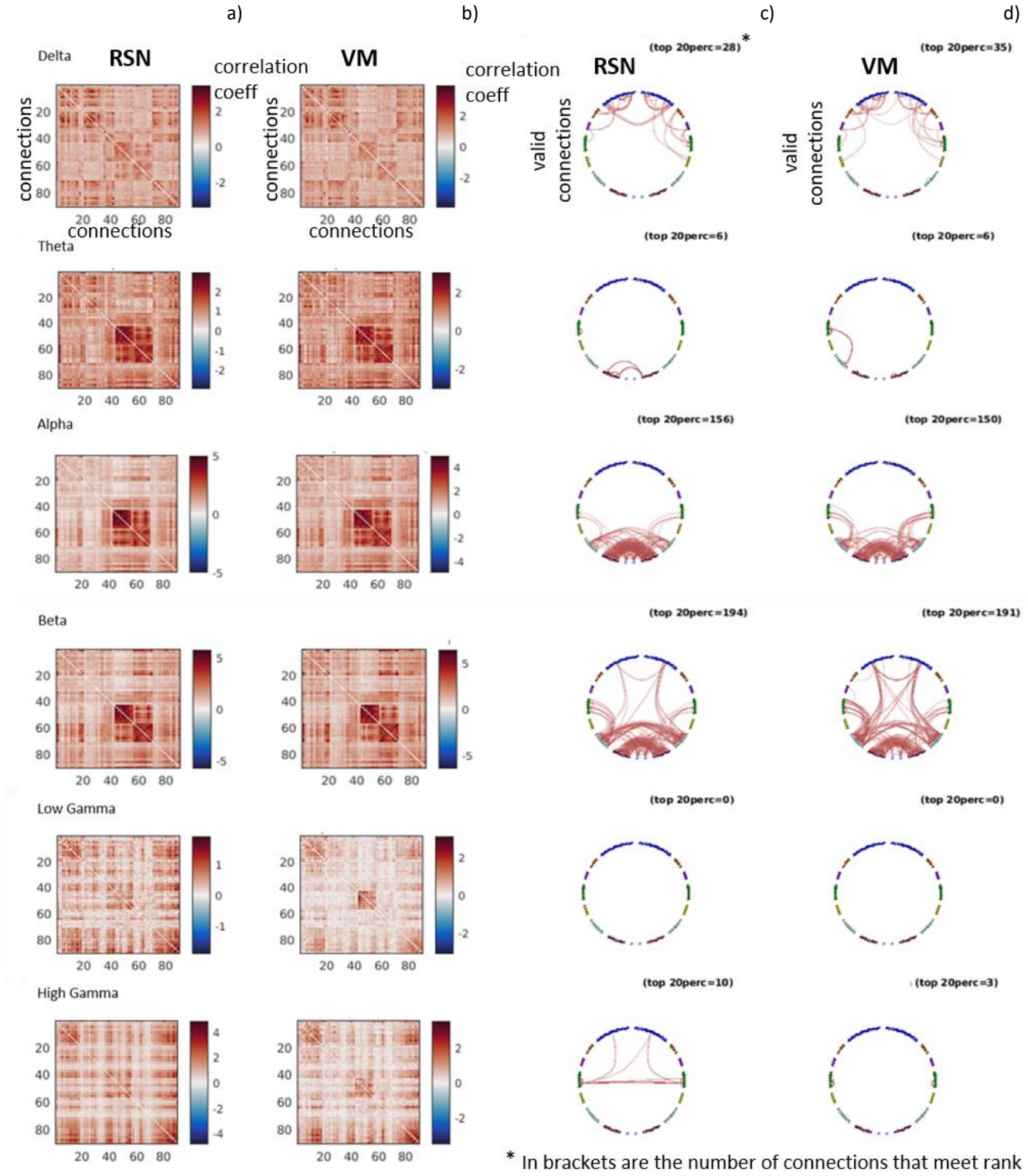


Figure 4.2. Patterns of connectivity in RS and VM data. For each frequency band (one per row), the figure shows a) a correlation matrix showing the mean connectivity between the 90 AAL regions across participants extracted from the resting-state data (colour-scale represents the corrected Z-scores for each correlation), b) a correlation matrix showing the mean connectivity between the 90 AAL regions across participants extracted from the VM data, c) a circular network plot showing connections in which the mean rank is $>.8$ in the resting-state data, and d) a circle plot showing connections in which the mean rank is $>.8$ in the VM data.

Mean connectivity and the connections which fall in mean ranks $>.8$ appeared to be very similar across the datasets in the alpha and beta bands. The same number of connections met the ranking threshold in theta, but these connections were between different areas in each of the two datasets. Connectivity strength was also similar in delta, although a slightly different pattern of connections met the ranking threshold across datasets. Patterns of connectivity in the high- and low-gamma bands differed considerably between the two datasets. No connections met the $>.8$ threshold in the lower gamma band, suggesting these connections were inconsistent across participants, perhaps due to low SNR or a lack of genuine connectivity in this band.

Differences and similarities in the strength of connectivity between the datasets were further explored (Figure 4.3).

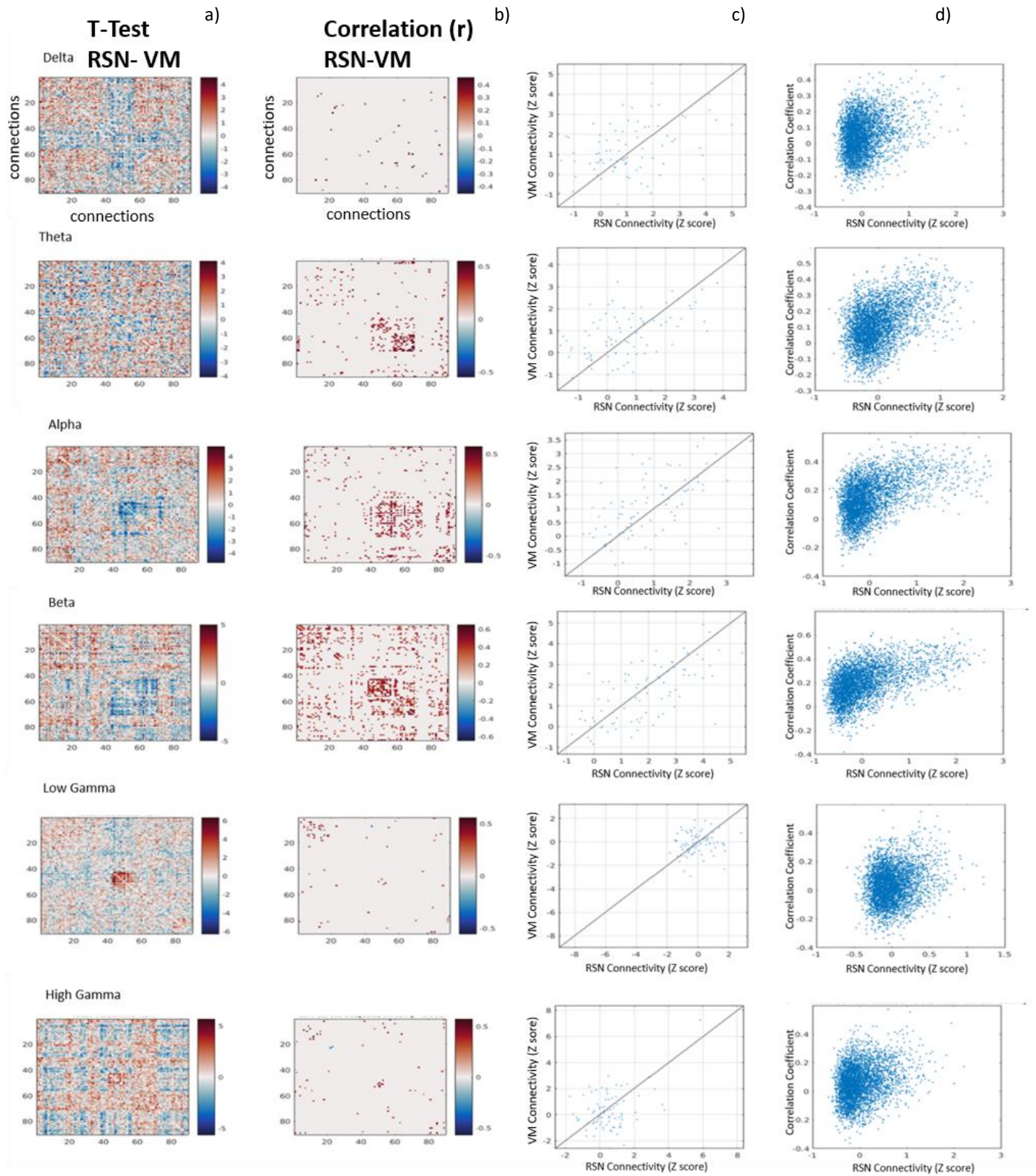


Figure 4.3. Differences and similarities in strength of connectivity in RS and VM datasets. For each frequency bands (one per row), the figure shows, a) connectivity differences – a matrix showing the paired t-statistic for each connection when comparing the resting-state data to the VM data (VM-RSN). Red pixels represent positive t-statistics (i.e., VM values are larger than RSN values) and blue represent negative t-statistics (i.e., RSN values are larger than VM values). The magnitude of the effect is shown by depth of colour, b) connectivity similarities- a matrix showing pairwise correlations across participants ($p > 0.001$) between connectivity (z-score measure) in the resting-state data and connectivity in the VM data, c) A scatter graph showing the connectivity magnitude from the VM data plotted against the connectivity magnitude from the RSN data, for the connection with the highest correlation between these two datasets for each frequency band – each dot represents one participant and d) the correlation between RSN and VM datasets for each connection (Y axis), plotted against the RSN mean connectivity strength, for each connection (X axis).

As might be expected, connections were stronger in the visual cortex in the gamma range in the VM data. Consistent with evidence showing a suppression of alpha during visual stimulation in posterior cortex (Brookes et al., 2005; Hämäläinen, Hari, Ilmoniemi, Knuutila, & Lounasmaa, 1993; Singh, Barnes, & Hillebrand, 2003), connections were weaker in the visual cortex in the alpha band in the VM data. Connections were also reduced in the beta occipital-parietal areas, in the VM data. Visual connections also appeared to be reduced in the VM data in the delta and theta bands. Differences between RS and VM connections, outside of these areas, were of mixed direction. Notably, positive and negative differences in gamma connections exist outside of the visual cortex.

Column (b) shows that connection magnitude is most correlated, between datasets and across participants, in the theta, alpha and beta bands. Connections appear to be most correlated in the visual areas in alpha and theta. In beta, correlations were high over widespread areas, with the strongest connection being between the left and right precuneus. Column (d) shows that stronger RS connections (i.e., at higher SNR), for example in alpha and beta, have a higher correlation with connections in the VM dataset.

To consider patterns of the strength of connectivity at each node in each frequency band, average node strength was compared between the RSN and VM data and plotted in Figure 4.4, below.

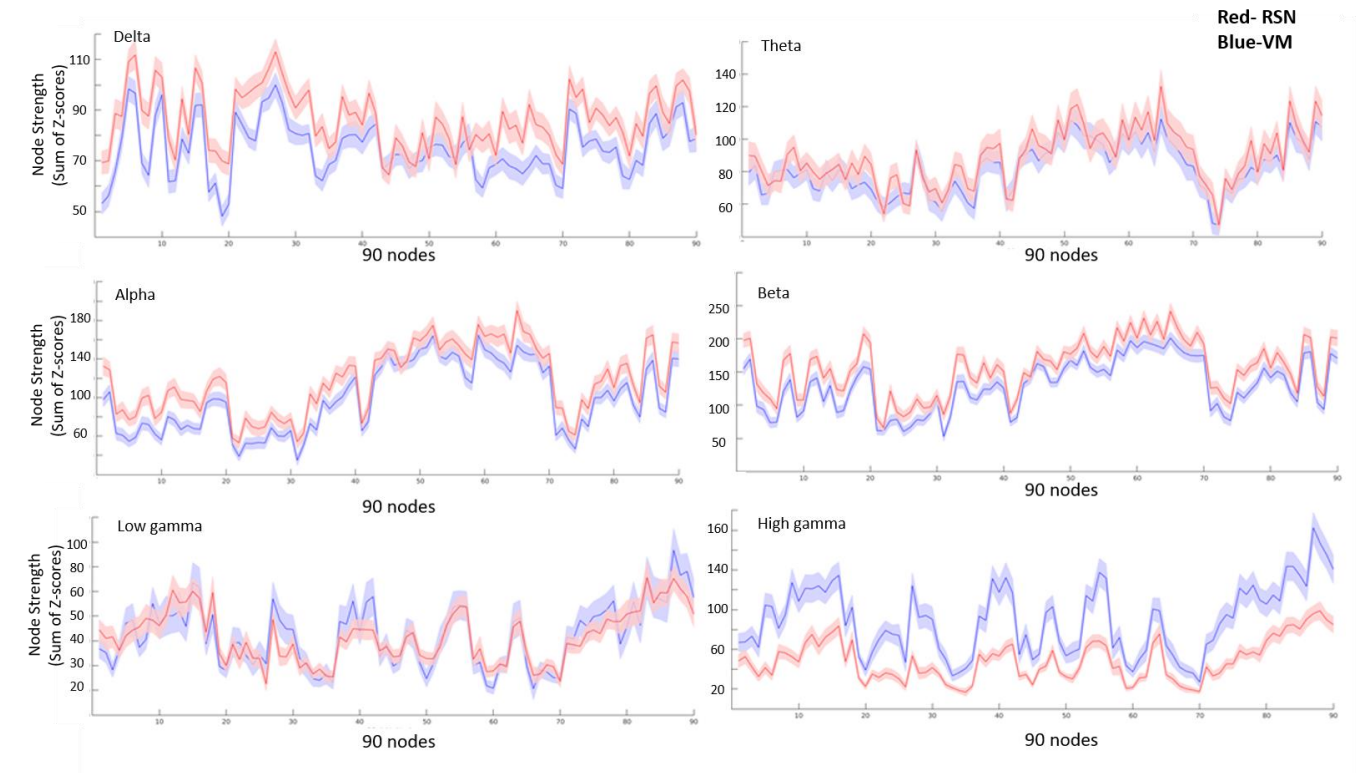


Figure 4.4. Node Strength (Sum of Z-scores) at each node per frequency band for each of the datasets. RS data is in blue. VM data is in red.

Node strength values were highly similar, both in terms of their magnitude and distribution within nodes, across datasets. The largest global difference in node values between datasets was in the delta and high gamma range. However, the across node trend in connectivity strength remained similar.

Activity at each node was also compared between the RSN and VM data and plotted in the Figure 4.5, below.

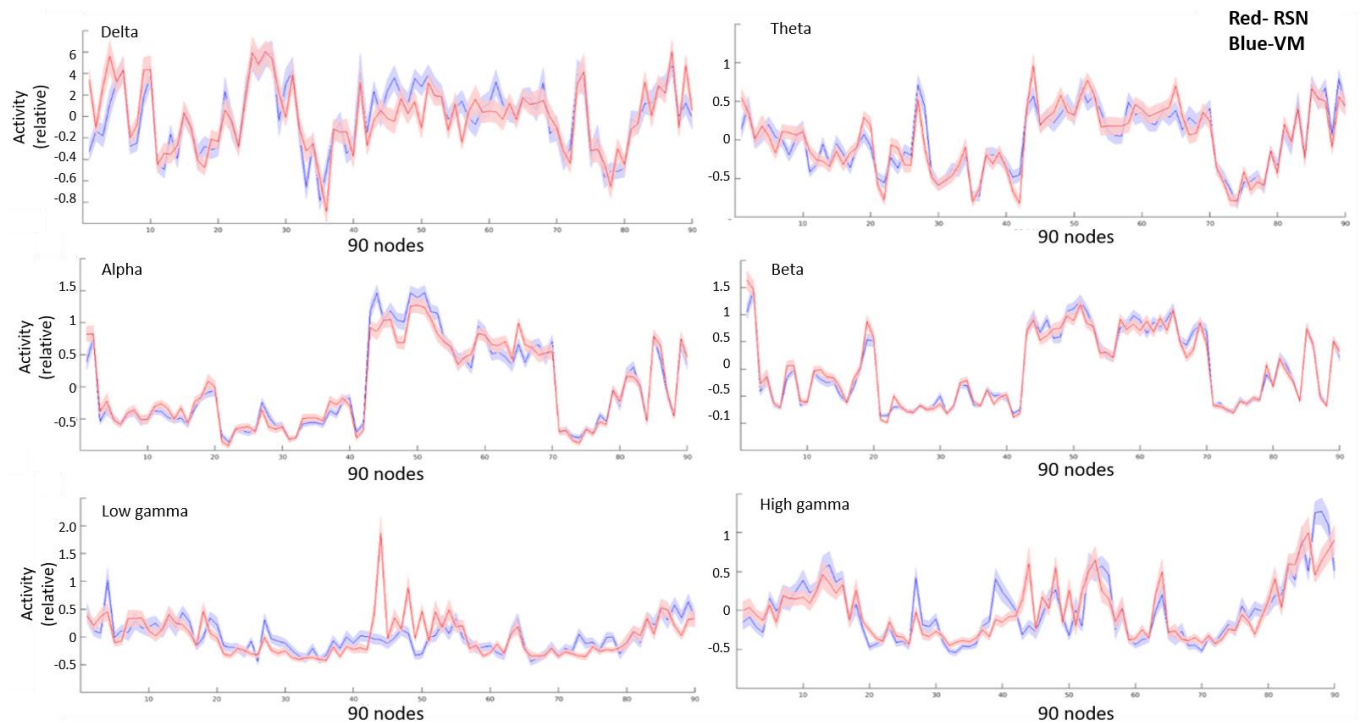


Figure 4.5. Activity at each node, for each dataset, per frequency band. RS data is in blue. VM data is in red.

Activity values were highly similar between datasets across all frequency ranges. Interestingly, a spike in activity can be seen in areas of the visual cortex (nodes 43 and 44), in the low gamma VM data. Nodes 43 and 44 are V1 (left calcarine, right calcarine). Peak gamma activity appears in the right calcarine which is encouraging considering the task stimulus was presented in the left visual field and is therefore what we would expect due to the lateralisation of the brain. Alpha activity also appeared to be slightly reduced in the VM data, in the same nodes.

For each frequency band the node strength and activity correlation coefficients, are plotted in Figures 4.6 and 4.7; that is, correlations between the VM data and the RS data at each node across participants. The figures demonstrate the magnitude of similarity between the data at any given area. Any correlations below the grey line are negative at those nodes.

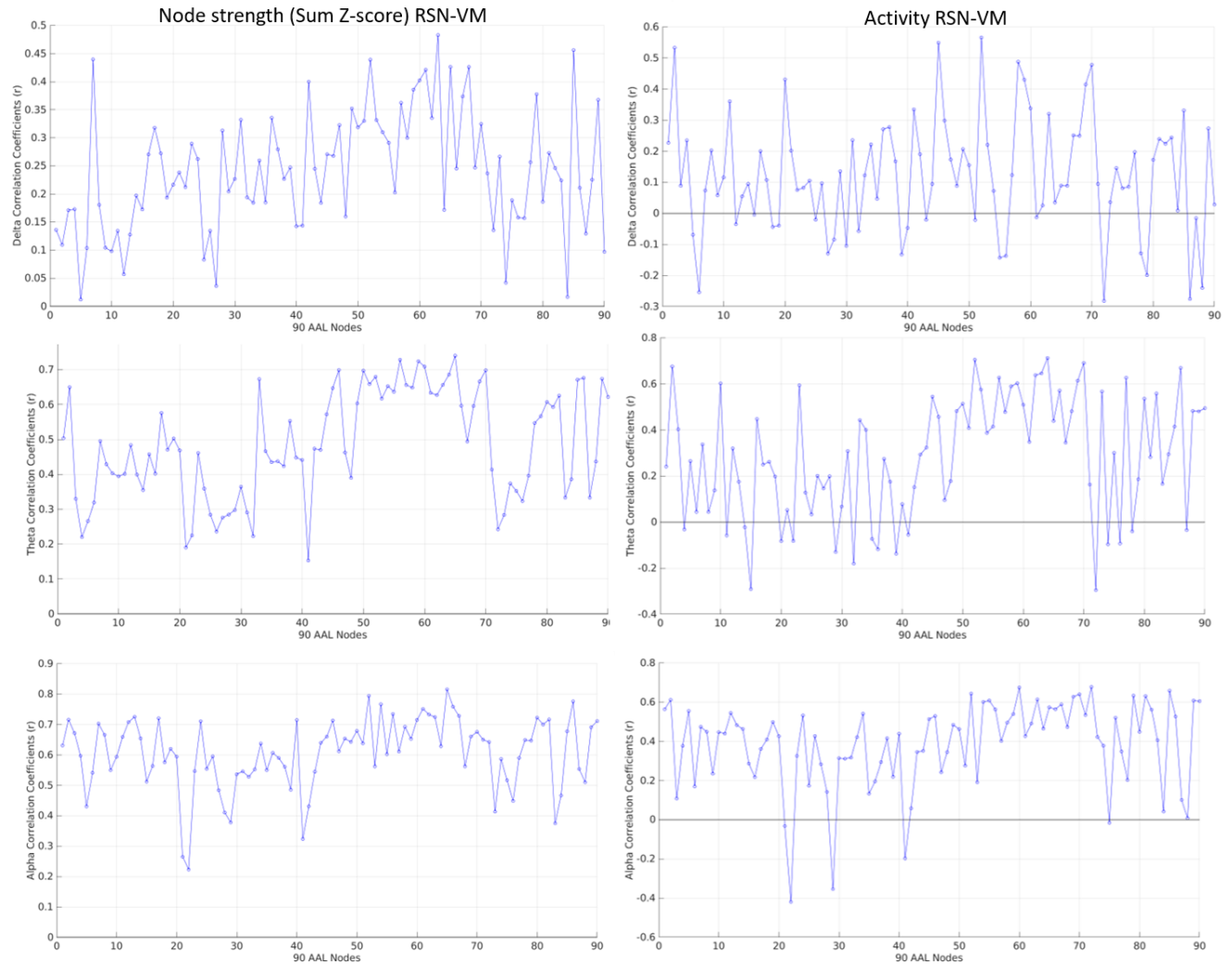


Figure 4.6. For frequency bands delta, theta and alpha, the figure shows, left) the node strength correlation coefficient (between RSN and VM data) per node, and right) the Activity correlation coefficient (between RSN and VM data, per node. A horizontal line is shown at 0. Where a 0 line is not visible correlation values are all positive (>0).

Correlations of the node strength measure between runs were particularly high in the alpha and beta bands, with most nodes correlated at $r=0.4-0.8$. The activity measures were also correlated at between $0.2-0.8$, in most nodes in alpha and beta. Correlations between gamma node strength measures, were weaker ($r=0-0.4$). Similarly, correlations between activity measures, in gamma, centred around the zero line, with maximum node correlations of $r=0.4-0.6$. Node strength measures in the theta band were moderately correlated, across nodes, at $r=0.2-0.7$. The activity

measures were less correlated in the theta band. Most nodes were correlated at $r < 0.4$, in the delta band, across both the node strength and activity measures.

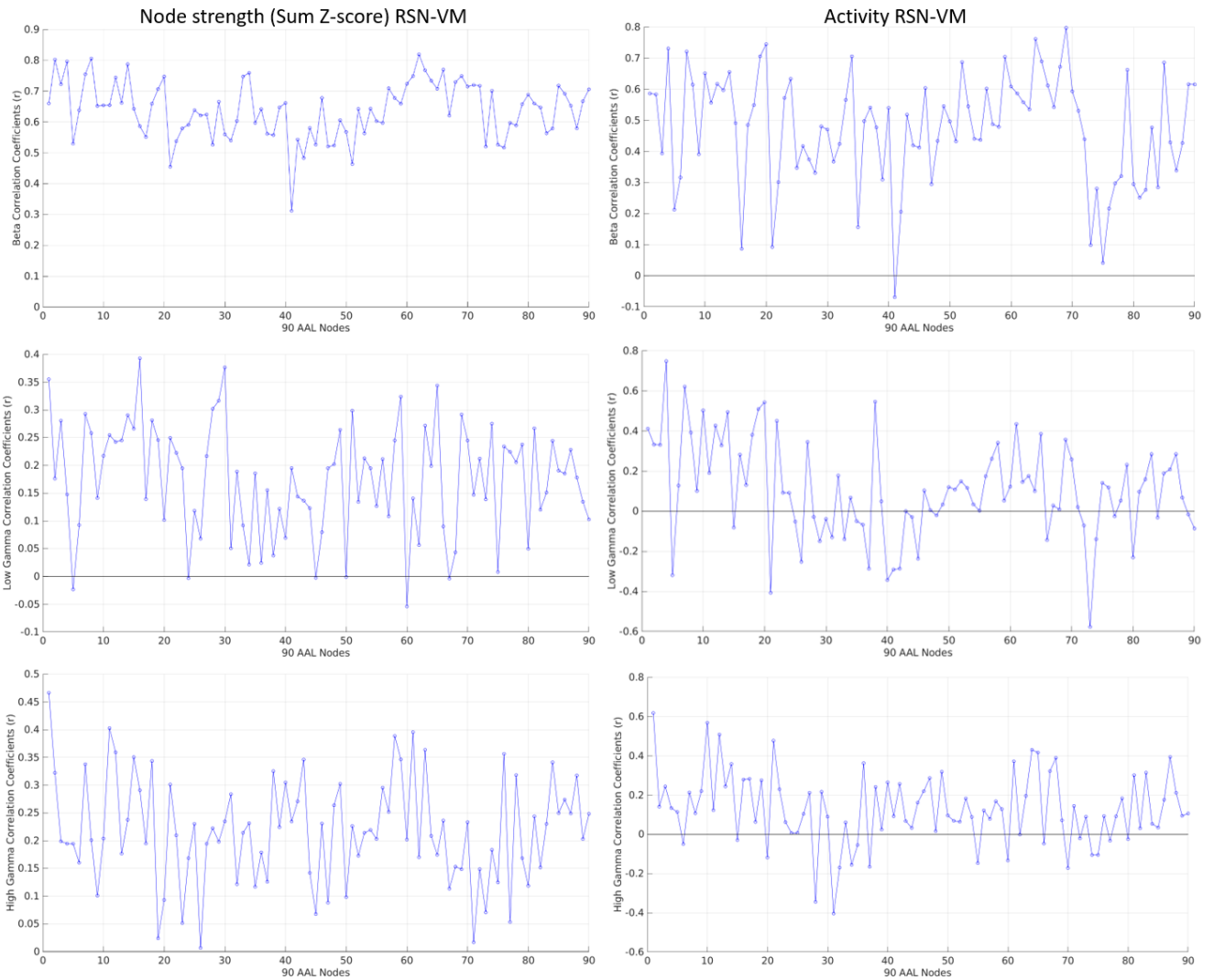


Figure 4.7. For frequency bands beta, low gamma and high gamma the figure shows, left) the node strength correlation coefficient (between RSN and VM data) per node, and right) the Activity correlation coefficient (between RSN and VM data, per node. A horizontal line is shown at 0. Where a 0 line is not visible correlation values are all positive (>0).

The least correlated effect activity and node strength areas in alpha and beta, are nodes 21 and 41; these comprise the olfactory bulb and amygdala, which are not well imaged with MEG due to their depth. Generally, areas 71-90 were also not well correlated between datasets. These comprise the caudate, thalamus and temporal areas.

Node strength and activity measures were further explored in the alpha and beta bands, where consistent and reliable network effects have previously been shown (Colclough et al., 2016; Godfrey & Singh, 2021)

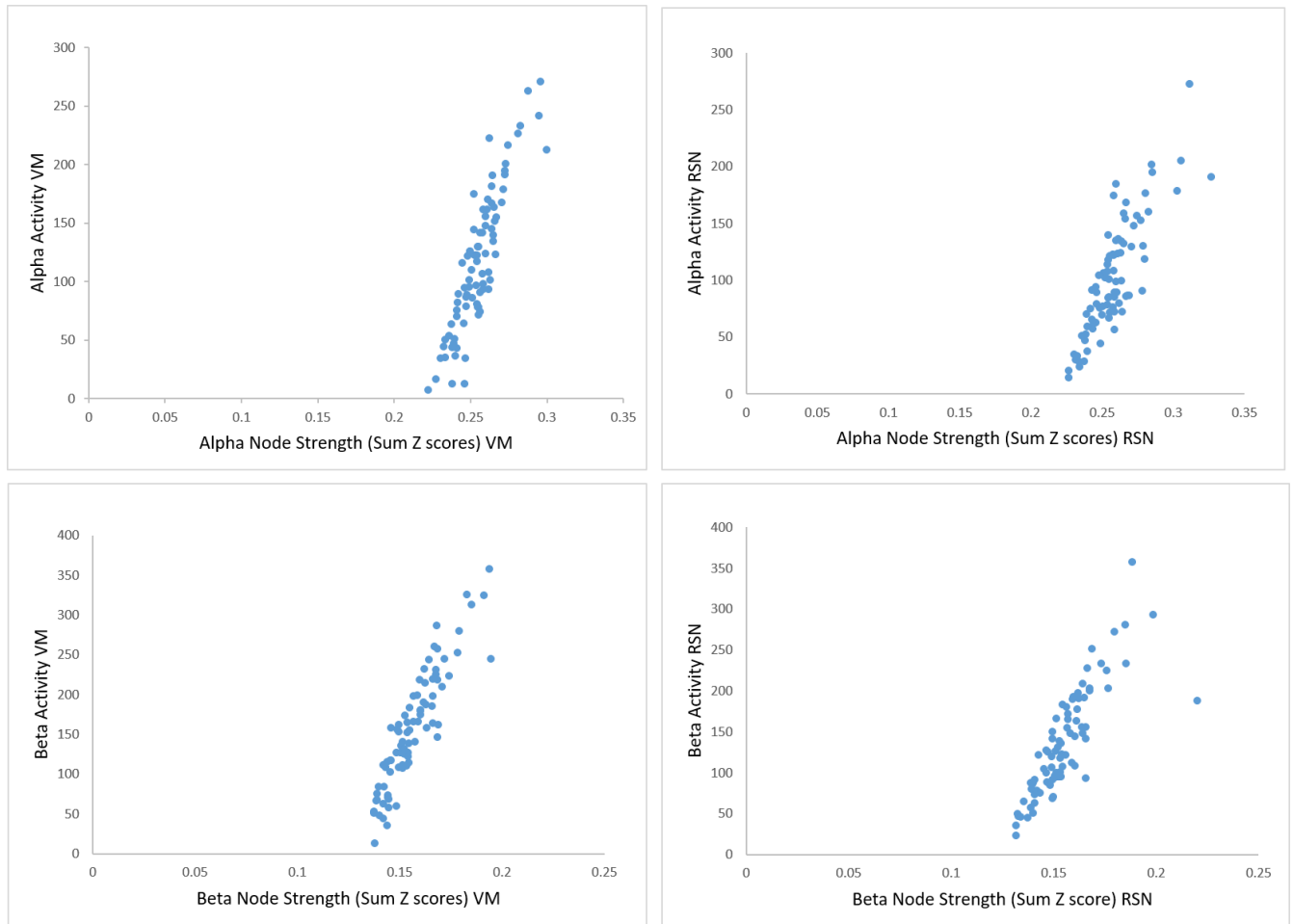


Figure 4.8. The relationship between node strength and activity measures at the 90 nodes, averaged over participants, in the alpha and beta bands.

For both the VM and RSN datasets, a positive relationship can be seen between node strength and activity measures suggesting that nodes which have the highest amount of activity were also the most functionally connected and suggesting both node strength and activity measures were capturing the same variance.

Together, results in this section suggest both node connectivity and activity are reproducible across paradigms in the alpha and beta bands.

4.4.2 Consistency across participants' comparisons

Next, the consistency of network estimates were considered across participants. This was to assess the variability of estimates between individuals in the VM and RS and data. Large differences in within-group variability could have implications for significance testing differences in networks extracted from task and rest data , i.e., under the assumption of equality of variances.

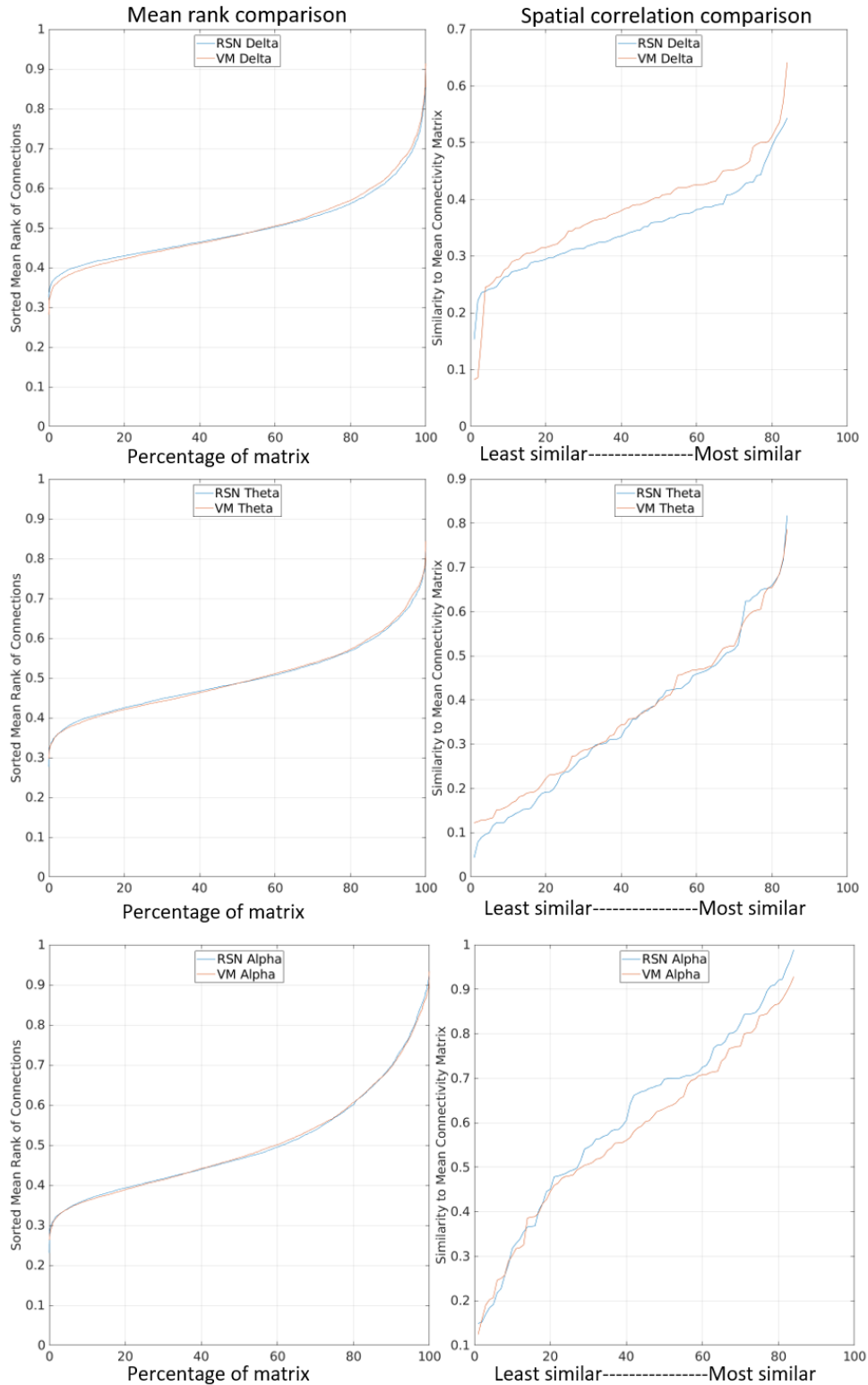


Figure 4.9. Shows the ranked connectivity matrices across participants (1st column), where the flatter the line around mean rank 0.5, the more dissimilar participant's matrices are, and correlations, by participant, with the mean connectivity matrix across participants (2nd column).

Both plots show RS (blue) and VM (orange) data. Result in the delta, theta and alpha bands are shown here.

Both RS and VM datasets followed a similar trend of across participants' connectivity, even in the gamma range. Across participants' connectivity was most similar in VM and RS data in the theta, alpha and beta bands. Participant's datasets in the gamma range were most dissimilar to each other.

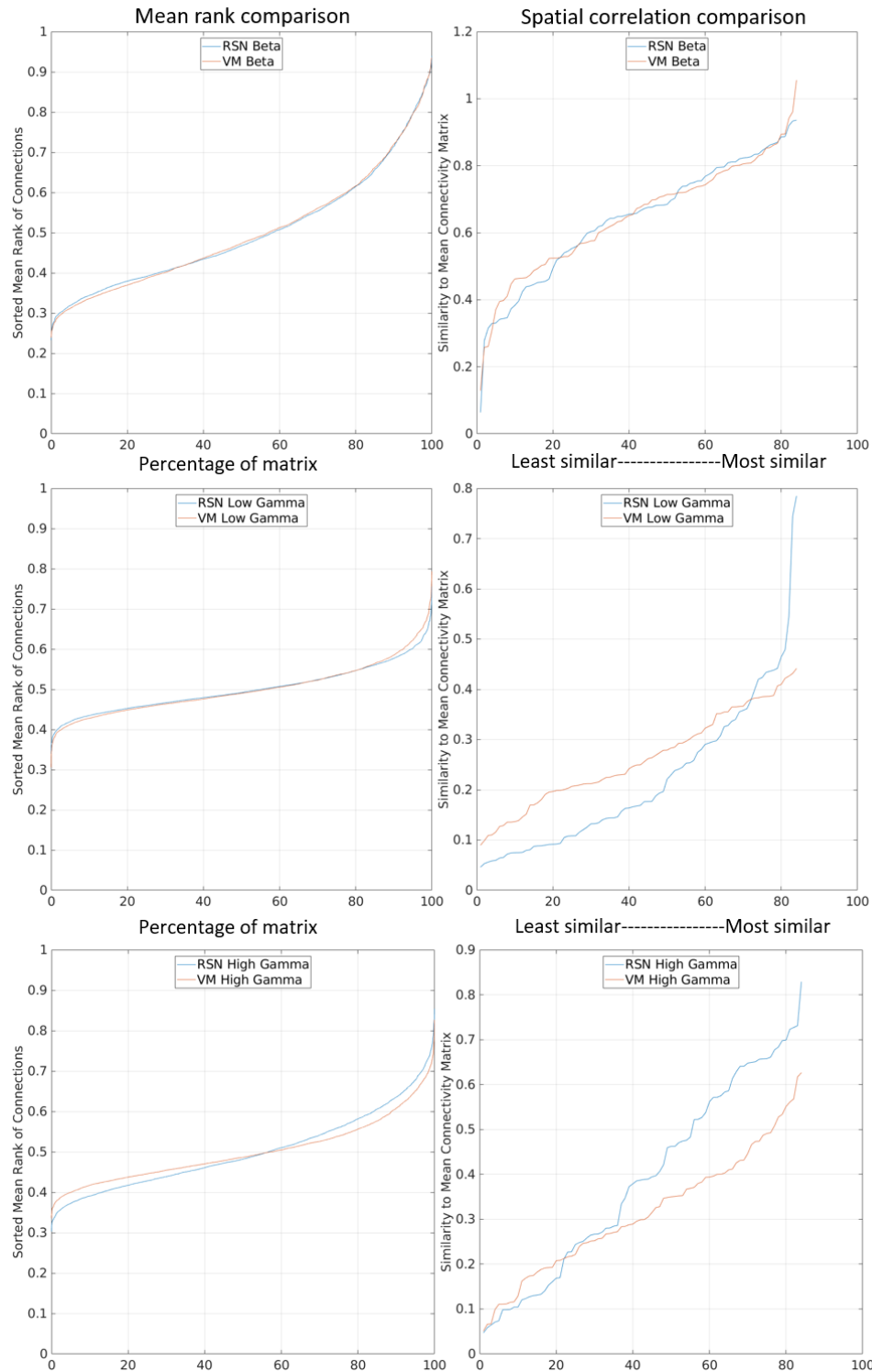


Figure 4.10. Shows the ranked connectivity matrices across participants (1st column), where the flatter the line around mean rank 0.5, the more dissimilar participant's matrices are, and correlations, by participant, with the mean connectivity matrix across participants (2nd column).

Both plots show RS (blue) and VM (orange) data. Results in the beta, low gamma and high gamma bands are shown here.

4.4.3 NNMF sub-network decomposition

To explore similarities between sub-networks derived with NNMF, a comparison was made between network weightings for each dataset in a repeated measures design. In the delta, theta and high gamma frequency bands 10 sub-network components were derived. Alpha, beta and low gamma frequency matrices were more densely populated with connections and 11 sub-network components were derived.

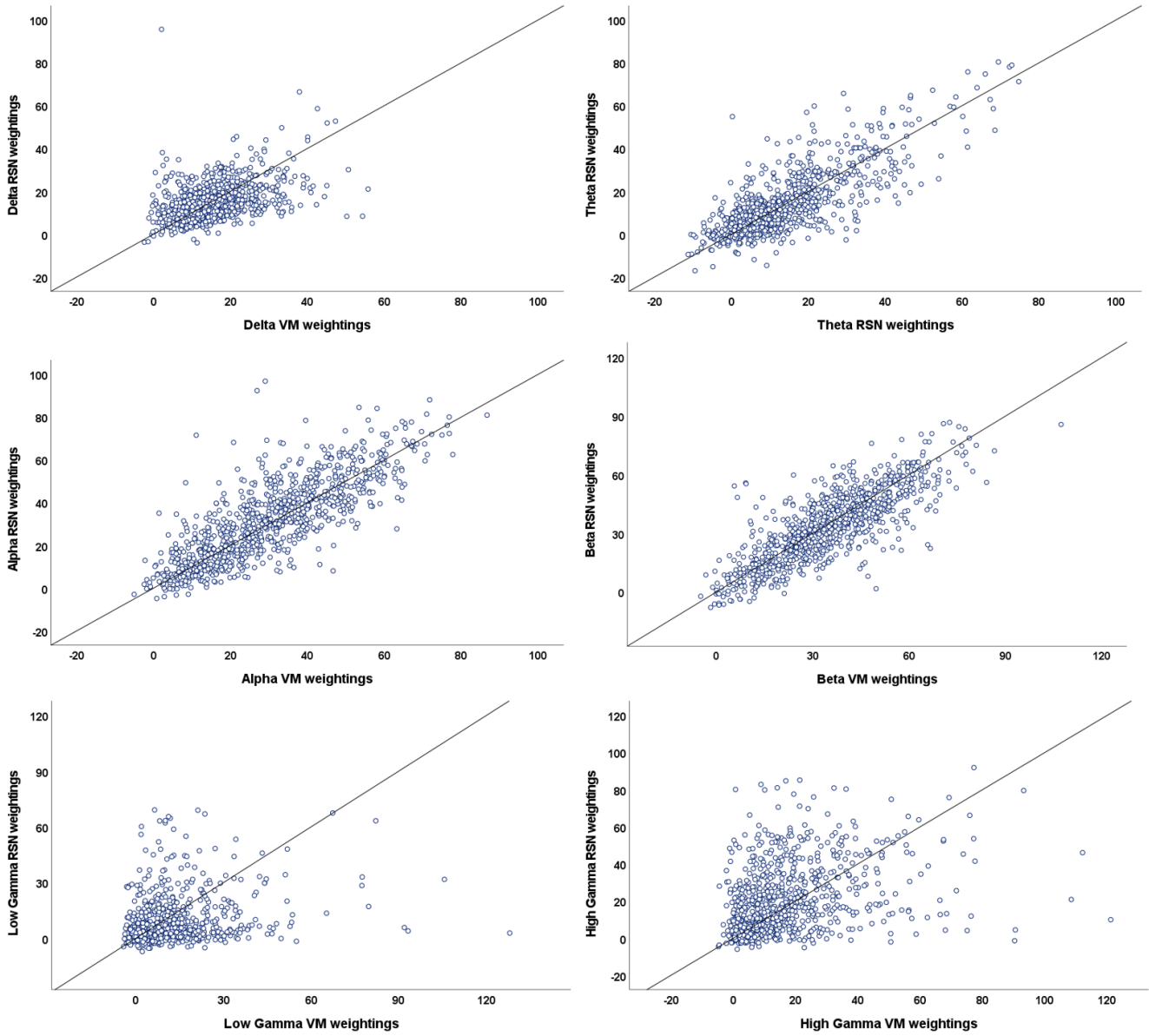


Figure 4.11. Shows resting-state weightings plotted against VM weightings (Z-scores) for the different frequency bands. The reference line is an equality line. Each dot represents one of the NNMF components for participant; delta, theta and high gamma-84*10 values, alpha, beta and low gamma-84*11 values.

The delta weightings were unevenly dispersed around the equality line, with some having much higher RS values and others having much higher VM values. Theta weightings were, overall, evenly dispersed around the equality line. Alpha and beta weightings were, overall, evenly

dispersed around the equality line, with a few values being higher in the alpha resting-state. Neither low nor high gamma weightings were tightly distributed across the line, suggesting values differ in the resting and VM data.

Paired correlation between the VM and RSN paradigms, across participants, was conducted for each component weighting separately, and plotted across the frequency bands (Figure 4.12).

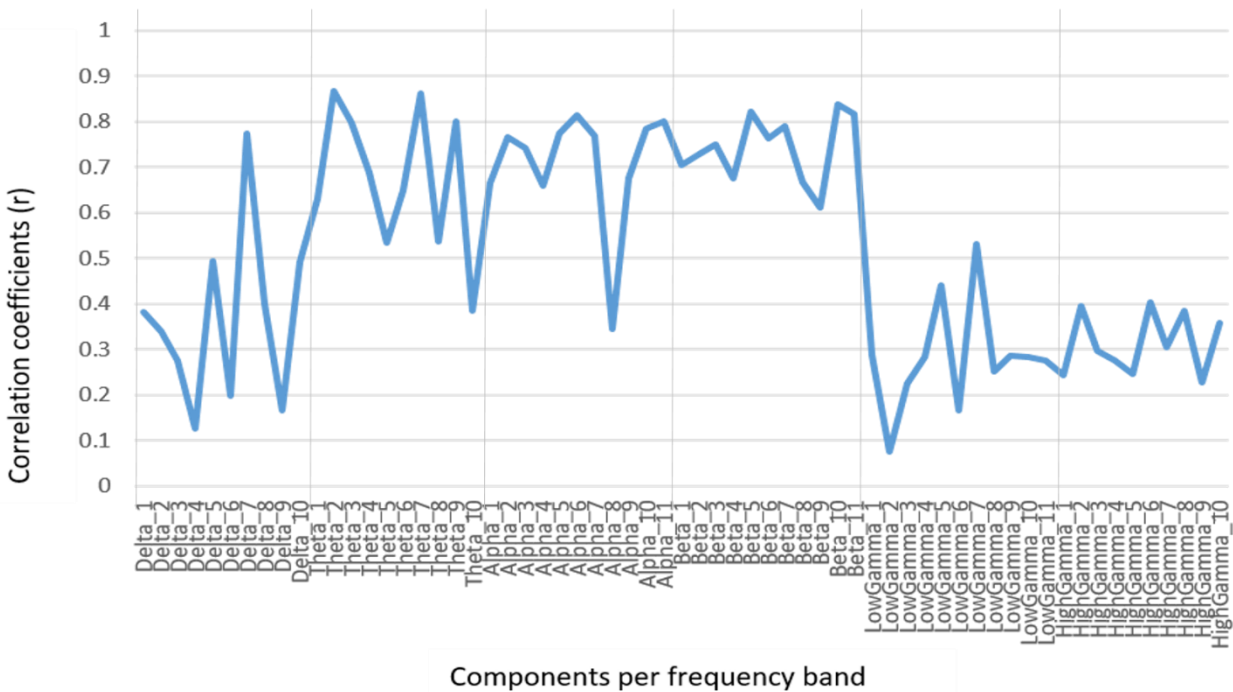


Figure 4.12. Shows the paired correlation coefficients between resting-state and VM NMF weightings, across components (63 components total).

Network weightings were highly correlated in the theta, alpha and beta bands ($r=0.35-0.85$). Correlations between network weightings in the delta and gamma ranges were, overall, weaker; the majority between 0.2 and 0.4. Two delta components did reach a moderate to high correlation ($r>0.6$).

4.4.4 Additional analyses

A clear gamma peak can be seen in the VM connectivity analyses in visual cortex (Figure 4.5). This finding was further explored in relation to metrics derived with conventional visual gamma analysis (described in full in Chapter 3). Being able to extract both long-range alpha and beta connectivity as well as the induced gamma signal from task-based connectivity analysis could considerably reduce the amount of time that would otherwise be needed for pre-processing and analysis of two different datasets.

Extracting gamma from the gamma RSN connectivity analysis

The spike in low gamma activity can be seen at node 44, which is the right calcarine. Two gamma measures were extracted for each participant: 1) the difference in RSN gamma activity and VM connectivity activity at node 44, and 2) the percentage change in gamma activity at node 44, with the resting value as baseline.

Traditional visual gamma analysis

To summarise, visual gamma data was sampled at 1200Hz, with a 300Hz lowpass antialiasing filter and then epoched in 4 second trials around the stimulus onset. Data were manually co-registered to the participant's MRI (isotropic T1-weighted). LCMV beamformer source localisation was conducted on the 12 visual AAL regions, based on the data covariance between 30-80 Hz. Source power was projected separately for baseline (-1.2-0s) and stimulus periods. The sustained period of the response was of interest and the oscillatory period was selected at 0.3s- 1.2s after stimulus onset. A virtual sensor was inserted at the point of the peak source. Estimates of peak amplitude and peak frequency in the power domain were considered here.

Gamma measures

Gamma activity in the VM connectivity analysis: 1) differences between resting and gamma values and 2) the percentage change between resting and gamma values.

Sustained gamma in the traditional visual gamma analysis: 3) amplitude at the point of peak source, and 4) frequency at the point of peak source.

Pearson correlation did not reveal any significant relationships between gamma extracted with conventional visual gamma analysis and the VM connectivity analysis, as shown in Table 4.2.

Table 4.2. Results of correlations between gamma measures

| | | Peak Amplitude | Peak Frequency | Gamma Difference (node 44) | Gamma Difference (node 44) |
|--------------------------------------|-----------|---------------------------|---------------------------|---|---|
| Peak Amplitude | Pearson r | 1 | -.114 | -.124 | .082 |
| | p value | | .302 | .260 | .457 |
| Peak Frequency | Pearson r | -.114 | 1 | .009 | .145 |
| | p value | .302 | | .933 | .188 |
| Gamma Percentage Change (node 44) | Pearson r | -.124 | .009 | 1 | .091 |
| | p value | .260 | .933 | | .413 |
| Gamma Difference (node 44) | Pearson r | .082 | .145 | .091 | 1 |
| | p value | .457 | .188 | .413 | |

4.5 Discussion

In this chapter, networks extracted from the resting-state and VM task data have been compared across 3 levels: across connections, across participants and across NNMF derived network components. As previously mentioned, fMRI studies have found the default mode network, fronto-parietal network, fronto-temporal networks and occipital networks to be signatures of the brain at rest (Damoiseaux, Rombouts, Barkhof, Scheltens, Stam, Smith, Beckmann, et al., 2006; Seitzman et al., 2019). This chapter provides evidence that intrinsic network connections can be revealed, using amplitude- amplitude coupling analysis, in both MEG rest and task data.

An exploration of *connection patterns*, across the 90 AAL regions, found the pattern of connections to be highly similar in the alpha and beta bands across datasets. The datasets had some consistency in delta and theta connections, though connections meeting the mean rank (>.8) threshold (connection strength) differ, especially in theta. As expected, the stronger connections in the gamma-range differed noticeably between the datasets.

Notably, in the visual cortex (VC), connections were stronger in the gamma band and reduced in the alpha band, in the VM data. Beta was also reduced in the visual-parietal areas in the VM data. This is unsurprising considering previous literature on frequency coupling in the visual cortex (Bastos et al., 2015b; Bonnefond & Jensen, 2015; Kerkoerle et al., 2014b; Lozano-Soldevilla et al., 2014a). A discussion of the possible underpinnings of these findings is beyond the purpose of this chapter, particularly as there has been some recent evidence suggesting gamma-alpha oscillations are not directly coupled in VC, as previously thought (Zhigalov & Jensen, 2020). However, it does suggest that caution should be applied to comparisons of connections in the VC.

Regarding *magnitude of connectivity*, across the datasets the strongest connections were in the alpha and beta bands. These were also the most correlated between the datasets (<.65, moderate correlation), which makes sense considering that these are the connections at highest SNR. This is consistent with the hypothesis that those with strong oscillatory RSN connectivity will also have strong oscillatory connectivity during a task paradigm. Connection strength also was fairly well correlated in the theta band, with the strongest correlations located in the visual-parietal

areas. Connection magnitude was weakly correlated across the 90 AAL regions between datasets in delta and gamma. The limited magnitude of connectivity in the delta and gamma bands suggests these correlations could be spurious.

Connectivity and activity at *each node* were, subsequently, explored across the frequency bands. The node connectivity values were found to be strikingly similar across the resting-state and VM datasets (reaching high correlations, $r > .8$). These node correlation values were like those found by Cole and colleagues with fMRI (Cole et al., 2014). Small global differences in node connectivity were found in delta and high gamma. Activity at each node was also highly similar between datasets in the delta, alpha and beta bands. Interestingly, a spike in activity was observed in the visual cortex in the low gamma activity band (VM data) due to the grating stimulus.

It is noted, however, that neither the difference, nor the percentage change in gamma between VM connectivity and resting-state connectivity correlated with traditional gamma amplitude or frequency metrics. One reason could be that in the connectivity analysis, concatenated data are downsampled to 1Hz, meaning temporal information (i.e., changes in the envelope greater than 1Hz) is lost. The translations between visual stimulation and baseline would, therefore, have been smoothed out by the RSN analyses pipeline. Furthermore, more variation exists in the baseline, i.e., the resting-state, in the connectivity measures, with some RSN values being higher than their VM counterpart. This was an ad hoc exploration. It is also possible that the difference/percentage change metrics were not sensitive enough to extract gamma from the connectivity analysis. Measures were also obtained at different beamformer sampling resolutions (RSN 6mm, Gamma 1mm). In view of Chapter 3, it is expected that the beamforming at 1mm would have given more precise estimates of gamma. Until this is further explored, the conventional method for extracting gamma metrics remains the recommended approach.

The *Non-Negative Matrix Factorization* signal processing method has become increasingly popular in neuroimaging methods because complex patterns of connections can be simplified and presented as coherent sub-networks. The pipeline used in this thesis generates 4005 unique connections (e.g. $((90 \times 90) - 90) / 2$), so reducing these to fundamental components with NNMF

aids interpretability of functionally relevant sub-networks, as well as reducing the issue of multiple comparisons. The results here show that NNMF component weightings, while not identical, are highly comparable in the alpha, beta and theta frequency bands in both resting-state and VM task data. This was not the case for delta and gamma weightings which was to be expected considering 1) that one of the paradigms is known to induced gamma oscillations and 2) artefacts such as eye movement affect connectivity in the lower frequencies (Godfrey & Singh, 2021).

Lastly, connectivity was also variable *across participants* in a way that was expected considering previous work (Godfrey & Singh, 2020). Matrices were most dissimilar in the gamma range and most similar in the beta range. However importantly here, the *trends* of similarity were highly comparable between the resting-state and VM data, across the frequency bands.

In summary, therefore, alpha and beta connections had a high level of consistency between resting-state and VM data. This was demonstrated across the different modes of analysis here. However, connections in the VC differed and caution would be urged in comparing connections in this area. Connectivity and activity were also surprisingly well correlated between the datasets in the theta band, across many nodes. Correlations between theta NNMF components were also high. However, connectivity patterns (strongest connections) did appear to differ in theta. The idea that theta connectivity is more variable than alpha and beta connectivity, is supported by recent work which found considerable fluctuations in measures of network organisation in theta (Zink, Mückschel, & Beste, 2021), i.e., measures of local (small-worldness), and global network properties. This could limit the comparability of rest and task data in this frequency band.

Limitations and future directions

This chapter is subject to some limitations. For example, a reliability comparison was not possible, as this would have required additional resting-state data in the same cohort. This, in fact, has been undertaken elsewhere (Colclough et al., 2016; Dimitriadis, Routley, Linden, & Singh, 2018). The primary aim of this chapter was to explore the extraction of intrinsic networks in task and rest data, which has been achieved. However, it is unclear how these findings apply to other MEG network extraction methods, for example, phase measures, such as the phase lag

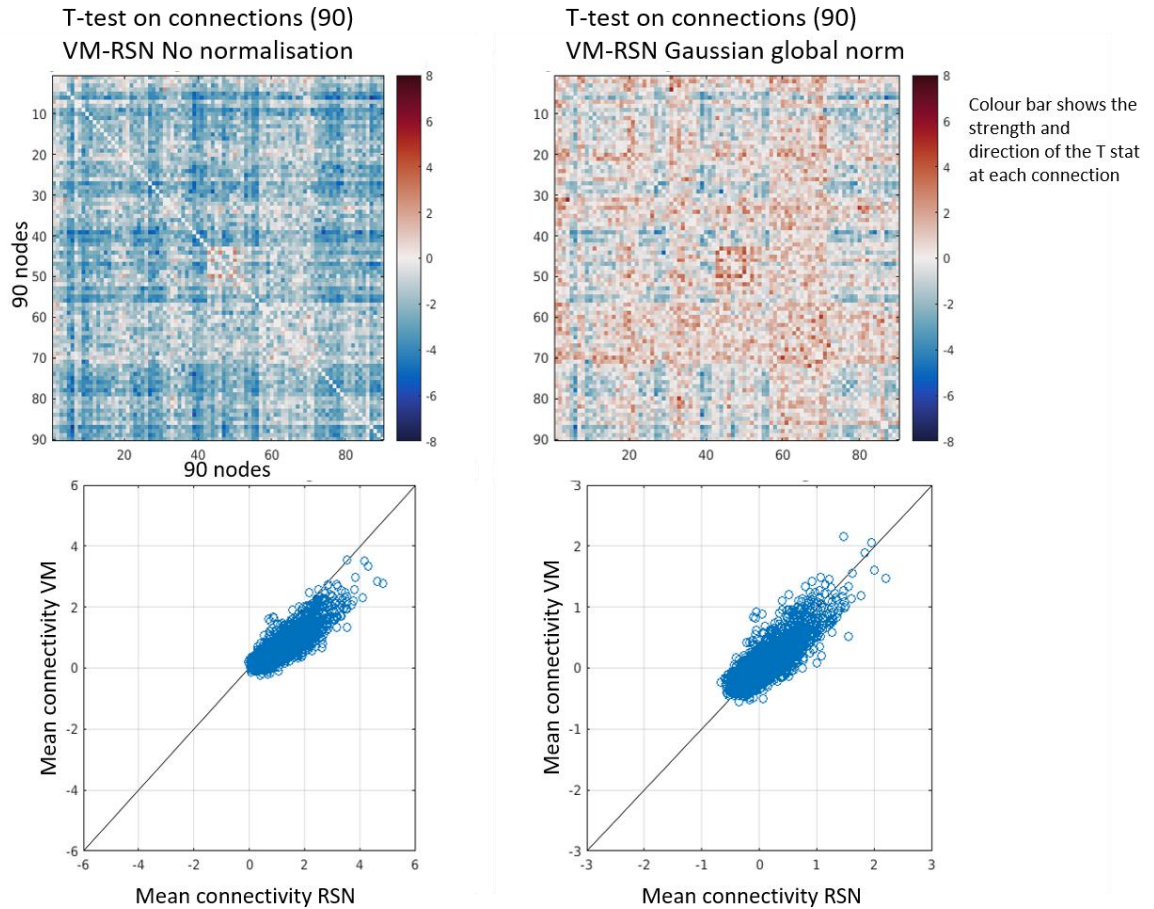
index (PLI), which has been shown to have poor test-retest reliability (Colclough et al., 2016). Also, no comments can be made about task data where paradigms stimulate modalities outside of the VC. In future, multi-modality task data collected in the same session might be compared in an analogous way.

Furthermore, it would also be interesting to explore whether clinical factors, for example diagnosis status, or genetic risk, are sensitive to the same connections in task and rest data. If the same connections were predicted, it would suggest a resting-state paradigm could be superfluous to requirement, in some studies. This the next step for this research.

In conclusion, this chapter has provided comparisons between functional networks extracted from resting and visual task MEG data. Patterns of connectivity were different in the visual cortex across frequency bands. Gamma band connectivity was also non-comparable. However, alpha, beta and theta connectivity, outside of the visual cortex, was comparable. This calls into question the use of a resting-state paradigm in some studies, particularly in challenging populations who can less tolerate long experimental sessions. It may be that long-range static connectivity measures can be extracted from other task-based scans. Task-based paradigms have the additional advantage of helping to maintain alertness and compliance.

4.6 Appendix A

1. An example of the normalisation procedure applied to connectivity matrices.



Each participant's connectivity matrix was corrected for global effects caused by head size, head motion and position within the MEG helmet. The null mean and standard deviation of connectivity was estimated by selecting the weakest connections, considered noise, and fitting a Gaussian to the peak (± 1 standard deviation) of the distribution. This mean and SD was then applied as a z score to the strength of connectivity (z) values for the respective person. See Messaritaki et al., (2021).

The images on the left show a global (mean) shift in gamma connectivity in the RSN data prior to the normalisation procedure (images on the right). This may have been due to increased participant head motion during the resting-state scans.

Chapter 5. Identifying sub-networks with Non-Negative Matrix Factorization: Initial results

5.1 Rationale

The following experimental chapters include MEG resting-state data and structural data obtained in ~ 183 subjects, collected as part of the 100-Brains and MEG-Partnership projects. To probe global functional and structural sub-networks a Non-Negative Matrix Factorization (NNMF) procedure was applied to the data. Results are presented on template brain plots here, so that the spatial organisations of the sub-networks can be visually explored. Identifying subnetworks is useful because 1) they summarise biologically-relevant functional sub-units, and 2) they allow more efficient statistics i.e., tens of tests instead of 100s or 1000s and therefore reduce the innate multiple comparisons problem in neuroimaging research. Relationships between these networks and predictors of interest are explored in subsequent chapters.

5.2 Non-Negative Matrix Factorization

NNMF is a mathematical approach (Lee & Seung, 1999) whereby matrices can be reduced into fundamental networks, in a method akin to Principal Components Analysis (PCA). In this respect components reflect consistency of networks across participants, with the first component being most present and so on. The component networks are generated across individuals. Individuals are then assigned a weighting value for each component which represents the extent to which their data contributes to that component. In this respect, the network weightings represent the consistency of any given network across participants. Functional connectivity analysis in the resting-state using Hilbert envelope correlation lends itself well to NNMF as 1) amplitude-amplitude correlations are usually positive, and 2) unlike methods such as PCA which can result in both positive and negative network weightings, NNMF produces only positive weightings, which is helpful for understanding the contribution of each person's data to any given network.

The number of components for investigation are selected apriori meaning this requires caution, as components which are variable in only a few participants could be included. Conversely, a cut off that is too stringent could lead to information being missed. In this thesis, NNMF was

performed on the 90x90 Automated Anatomical Labelling connectivity matrices (AAL Tzourio-Mazoyer et al., 2002), weighted by different functional and structural measures.

Data were analysed in MATLAB (version 2019) using in-house scripts. To prevent overfitting, components were selected for further analysis until one of the following stopping criteria was met: 1) a maximum of 20 components, 2) the percentage of people who have a non-zero score for each component must be more than 50%, and 3) the average score (percentage) of non-zero scores across all the components must be greater than 70%. If all of these conditions were satisfied the algorithm moved on to the next component.

The NNMF algorithm, as used in this thesis, uses the variance across participants to identify a set of spatial components. Then for each of these components there is an associated weight, one per person in this case, that represents how strongly that person's data contributes to any given network. The weights were then statistically analysed in relation to predictors of interest with regression and T-test analyses in subsequent chapters.

5.3 Functional components

The functional NNMF components were derived, separately per frequency band, across the 183 resting-state datasets in the 100-Brains and MEG-Partnership cohorts (described in Chapters 3 & 4). Alpha (8-12Hz) and beta (13-30Hz) components are considered in this thesis; 11 and 9 components were derived, respectively. Components were projected onto an AAL atlas (Tzourio-Mazoyer et al., 2002) which comprised 90 anatomical areas (nodes) and are presented in Figures 5.1 and 5.2 below.

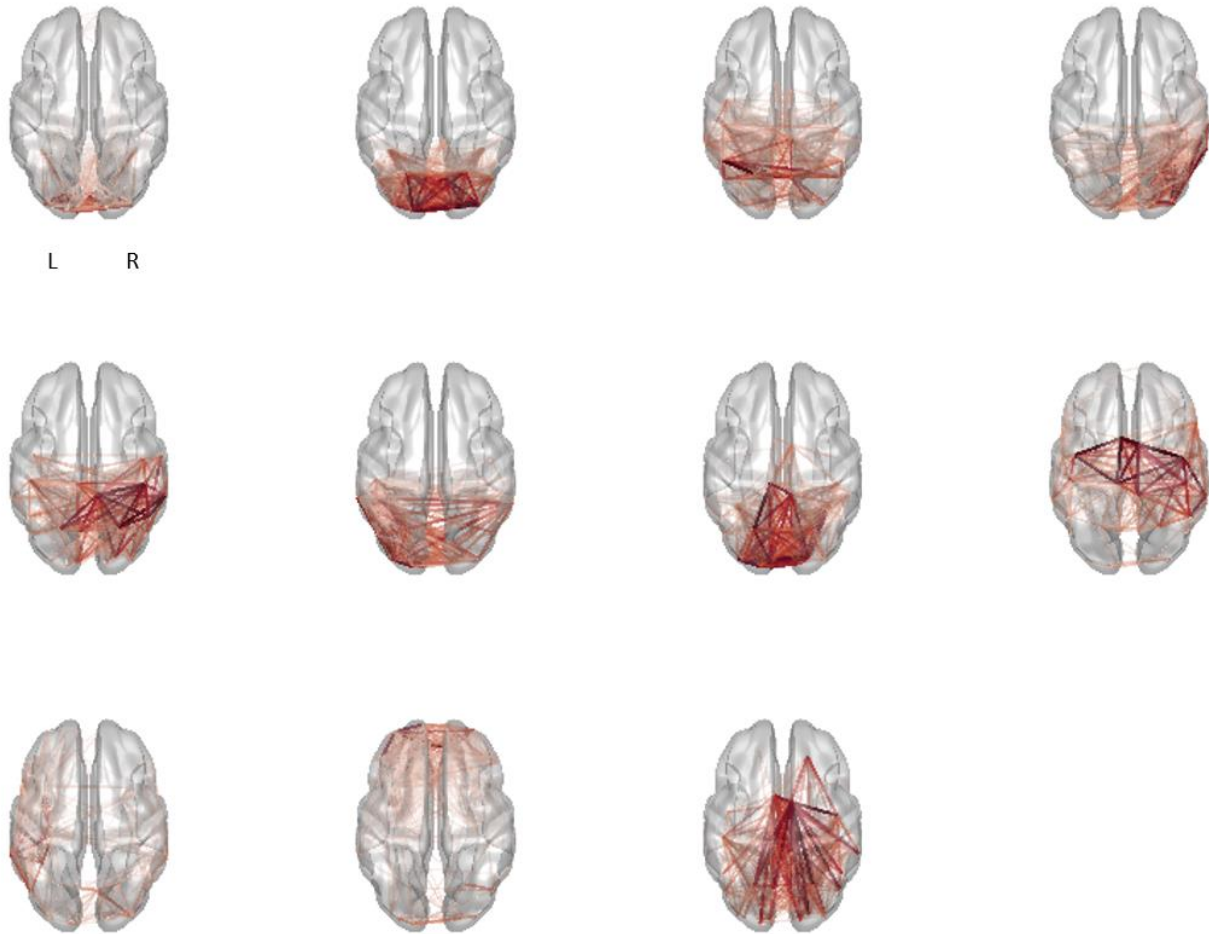


Figure 5.1. 11 Alpha components, axial view from overhead. Top 10% of non-zero connections are plotted on an MNI template brain surface. Note, scaling applied so the boldness of edges indicates the strength of connection, with weaker connections less visible.

The networks shown in Figure 5.1 appear to be consistent with known resting-state networks (Brookes, Woolrich, et al., 2011; Damoiseaux, Rombouts, Barkhof, Scheltens, Stam, Smith, & Beckmann, 2006). The implicated anatomical areas are shown in Table 5.1.

Table 5.1. Shows the anatomical labels for the top 10% of nodes in each of the alpha components

| | | | |
|----------------------|---------------------|----------------------|----------------------|
| 1 | 2 | 3 | 4 |
| Calcarine_R | Occipital_Sup_L | Parietal_Inf_L | Temporal_Inf_R |
| Calcarine_L | Occipital_Mid_R | Precuneus_R | Temporal_Mid_R |
| Lingual_L | Precuneus_R | Angular_R | Fusiform_R |
| Lingual_R | Cuneus_R | Angular_L | Temporal_Sup_R |
| Occipital_Inf_R | Occipital_Sup_R | SupraMarginal_L | Occipital_Mid_R |
| Occipital_Inf_L | Occipital_Mid_L | Heschl_L | Angular_R |
| Cuneus_L | Cuneus_L | Precuneus_L | Occipital_Inf_R |
| Cuneus_R | Occipital_Inf_R | Parietal_Inf_R | Hippocampus_R |
| Occipital_Sup_L | Parietal_Sup_R | Paracentral_Lobule_R | Occipital_Sup_R |
| 5 | 6 | 7 | 8 |
| SupraMarginal_R | Temporal_Mid_L | Paracentral_Lobule_L | Precentral_R |
| Postcentral_R | Temporal_Mid_R | Occipital_Mid_L | Supp_Motor_Area_L |
| Paracentral_Lobule_R | Occipital_Mid_L | Parietal_Sup_L | Parietal_Inf_R |
| Parietal_Inf_R | Temporal_Inf_L | Paracentral_Lobule_R | Supp_Motor_Area_R |
| Rolandic_Oper_R | Fusiform_L | Cuneus_L | Postcentral_R |
| Precuneus_L | Lingual_L | Occipital_Sup_R | Precentral_L |
| Paracentral_Lobule_L | Occipital_Inf_L | Calcarine_L | SupraMarginal_R |
| Parietal_Sup_R | Postcentral_L | Fusiform_R | Paracentral_Lobule_L |
| Postcentral_L | Parietal_Sup_L | Precuneus_L | Postcentral_L |
| 9 | 10 | 11 | |
| Hippocampus_L | Frontal_Mid_Orb_L | Supp_Motor_Area_R | |
| Temporal_Inf_L | Frontal_Inf_Orb_L | Cingulum_Mid_L | |
| Temporal_Pole_Mid_L | Rectus_L | Supp_Motor_Area_L | |
| Temporal_Mid_L | Frontal_Med_Orb_L | Precentral_R | |
| SupraMarginal_L | Temporal_Pole_Mid_L | Paracentral_Lobule_L | |
| Temporal_Pole_Sup_L | Rectus_R | Postcentral_L | |
| Heschl_L | Frontal_Mid_Orb_R | Frontal_Sup_R | |
| ParaHippocampal_L | Frontal_Sup_Orb_R | Parietal_Sup_R | |
| Temporal_Sup_L | Caudate_L | Lingual_L | |

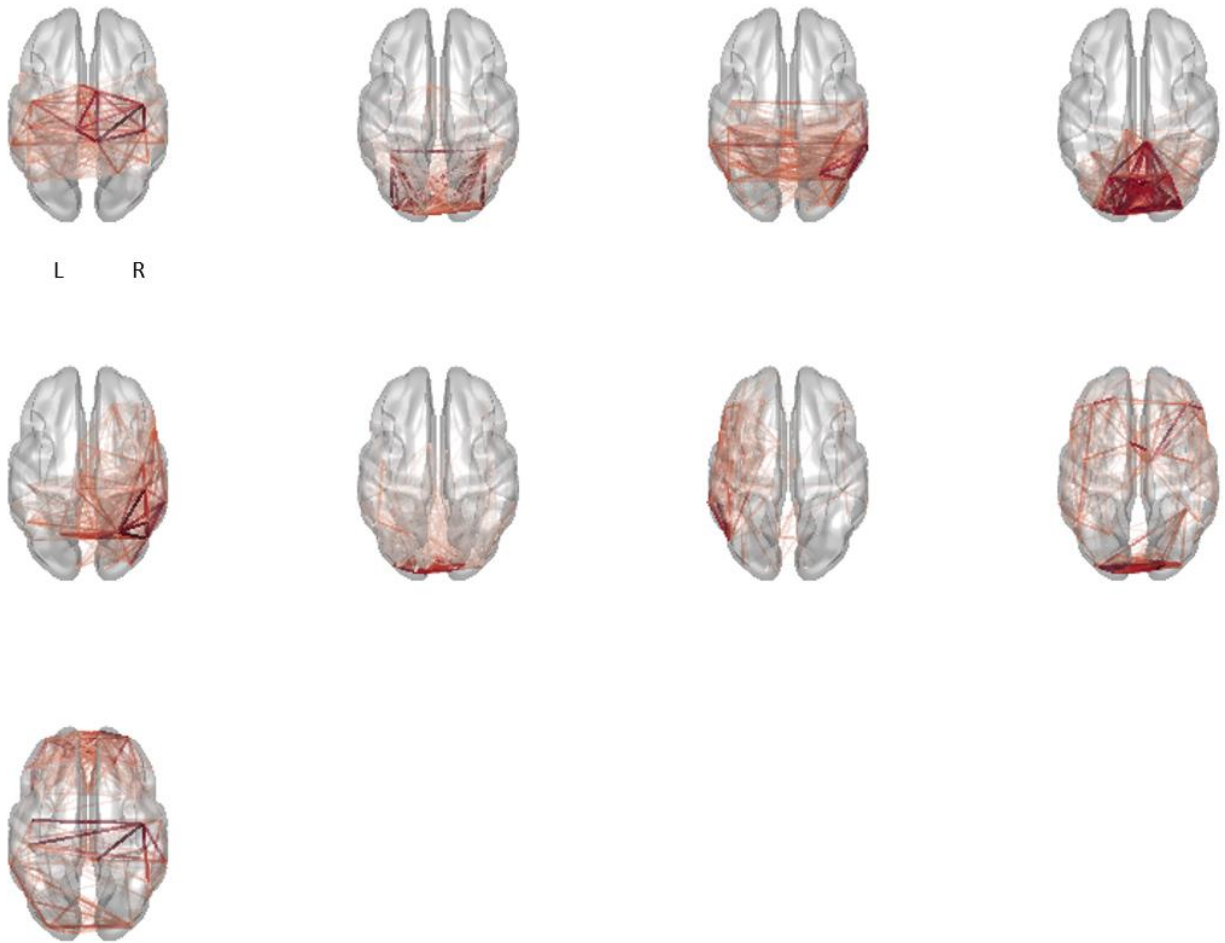


Figure 5.2. 9 Beta components, axial view from overhead. Top 10% of non-zero connections are plotted on an MNI template brain surface. Note, scaling applied so the boldness of edges indicates the strength of connection, with weaker connections less visible.

Again, the networks shown in Figure 5.2 appear to be consistent with known resting-state networks (Brookes, Woolrich, et al., 2011; Damoiseaux, Rombouts, Barkhof, Scheltens, Stam, Smith, & Beckmann, 2006). The corresponding AAL labels for each component (top 10% of implicated nodes) are shown in Table 5.2.

Table 5.2. Shows the anatomical labels for the top 10% of nodes in each of the beta components

| 1 | 2 | 3 | 4 |
|----------------------|-----------------|---------------------|----------------------|
| Paracentral_Lobule_R | Fusiform_R | SupraMarginal_R | Occipital_Mid_R |
| Postcentral_R | Occipital_Inf_L | Temporal_Mid_R | Paracentral_Lobule_R |
| Supp_Motor_Area_R | Fusiform_L | Angular_R | Precuneus_L |
| Postcentral_L | Occipital_Inf_R | Parietal_Inf_R | Cuneus_L |
| Precentral_R | Lingual_L | Temporal_Inf_R | Occipital_Mid_L |
| Precentral_L | Calcarine_L | Temporal_Sup_R | Precuneus_R |
| SupraMarginal_L | Lingual_R | Parietal_Sup_R | Occipital_Sup_L |
| Paracentral_Lobule_L | Calcarine_R | SupraMarginal_L | Parietal_Sup_L |
| Cingulum_Mid_L | Cuneus_R | Heschl_R | Cuneus_R |
| 5 | 6 | 7 | 8 |
| Angular_R | Occipital_Sup_R | Temporal_Inf_L | Cingulum_Mid_R |
| Parietal_Sup_R | Cuneus_R | Angular_L | Frontal_Mid_R |
| Parietal_Inf_R | Lingual_R | Temporal_Pole_Sup_L | Frontal_Inf_Tri_R |
| Postcentral_R | Cuneus_L | Temporal_Sup_L | Frontal_Sup_L |
| Precuneus_R | Calcarine_R | Temporal_Mid_L | Frontal_Mid_L |
| SupraMarginal_R | Occipital_Sup_L | Frontal_Inf_Tri_L | Supp_Motor_Area_L |
| Frontal_Inf_Oper_R | Occipital_Inf_L | Heschl_L | Parietal_Inf_L |
| Rolandic_Oper_R | Occipital_Mid_L | ParaHippocampal_L | Caudate_R |
| Cingulum_Mid_L | Calcarine_L | SupraMarginal_L | Frontal_Inf_Oper_R |
| 9 | | | |
| Rectus_L | | | |
| Frontal_Mid_Orb_R | | | |
| Rectus_R | | | |
| Frontal_Med_Orb_R | | | |
| Frontal_Inf_Orb_L | | | |
| Frontal_Mid_Orb_L | | | |
| Temporal_Pole_Mid_L | | | |
| Frontal_Sup_Orb_L | | | |
| Frontal_Sup_Orb_R | | | |

5.4 Structural components (DTI measures)

The same NNMF algorithm was applied to the structural connectivity matrices (comprising 4005 undirected connections). Identical thresholding parameters, to those described above, were applied to avoid overfitting. This resulted in between 10-18 components for each of the structural measures: 4 Streamline measures, Fractional Anisotropy (FA), Radial Diffusivity (RD), Axial Diffusivity (AD), Mean Diffusivity (MD) & myelin content. The structural measures will be described in detail in the experimental chapters. In short, streamlines result from tractography analysis and represent reconstructed white matter tracts. There are four measures because the analysis can be conducted in different ways (and with different thresholds) and this work provides an opportunity to compare them. FA is a measure of anisotropy of water diffusion within white matter tracts. RD and AD are measures of water diffusion in the perpendicular and parallel directions, respectively, and MD is the mean of diffusivity in the tract over 3 directions. Myelin content is a measure of diffusivity within myelin and is an indirect measure of myelin density.

The structural measures were derived by Eirini Messaritaki (Messaritaki et al., 2021a). The streamline components were generated over both the 100-Brains and MEG-Partnership cohorts (N=161). The diffusivity and myelin measures were available for the 100-Brains cohort (N=90). The structural components were also projected onto the AAL atlas and the first 10 were plotted on template brains, as seen in Figures 5.3-5.11. The top 5% of non-zero connections were plotted on the same scale in each case.

5.4.1 *The streamline measures*

Generally, the minimum number of streamlines that would allow us to assume that a tract has been reliably reconstructed has been selected somewhat arbitrarily, limiting the quantitative nature of streamline measures (Daducci, Palù, Lemkaddem, & Thiran, 2015). The COMMIT method (Daducci et al., 2015) is a data-driven alternative. Instead of rejecting tracts reconstructed with a number of streamlines lower than an arbitrary threshold, it rejects any streamlines that are not consistent with the overall diffusion signal in the diffusion-weighted images. This is done by fitting a linear combination of restricted and/or hindered contributions of candidate tracts and selecting those which result in the best global fit of the signal in each voxel.

To assess networks generated with the COMMIT method of streamline selection, the traditional method of streamline selection was also conducted with a minimum threshold of 18; that is, with the same sparsity of tracts selected with the COMMIT method. NNMF analyses were conducted on connectivity matrices weighted by streamlines selected with the COMMIT and the traditional approach and can be seen in Figures 5.3-5.6.

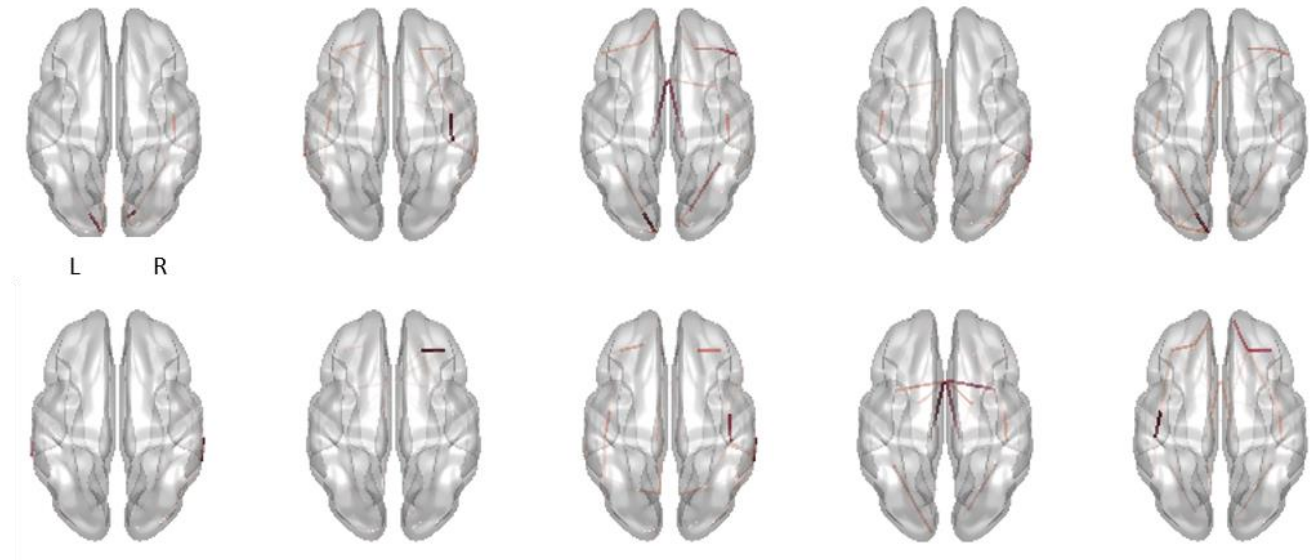


Figure 5.3. Number of streamlines derived with the COMMIT method, axial view from overhead. Component matrices are plotted on a template brain. Top 5% of non-zero connections are plotted. The boldness of edges indicates the strength of connections.

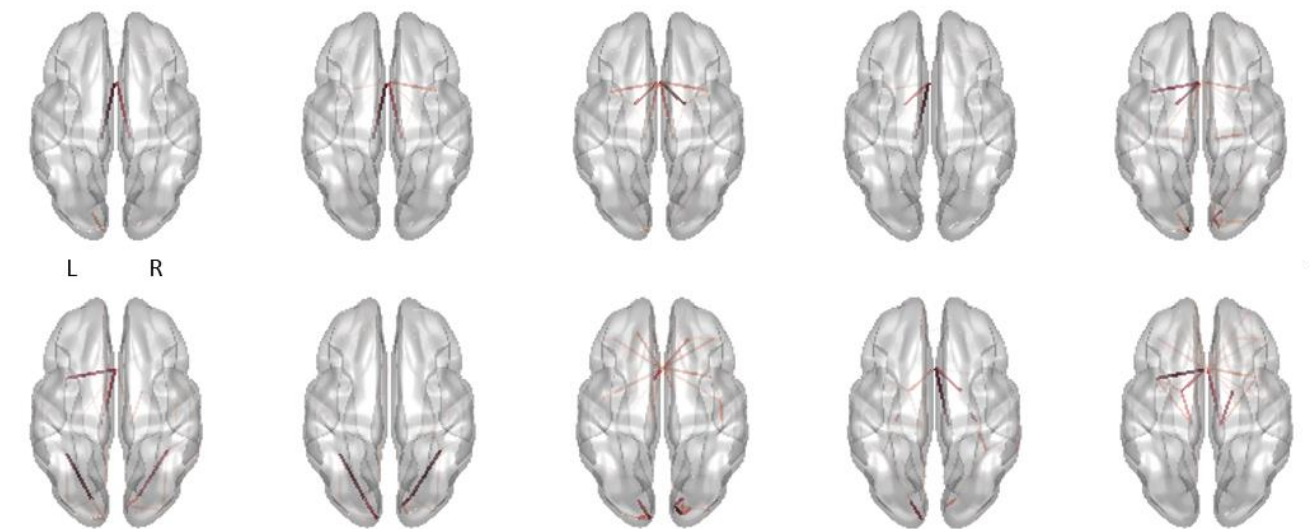


Figure 5.4. Standardised streamlines components derived with the COMMIT method, axial view from overhead. Component matrices are plotted on a template brain. Top 5% of non-zero connections are plotted. The boldness of edges indicates the strength of connections.

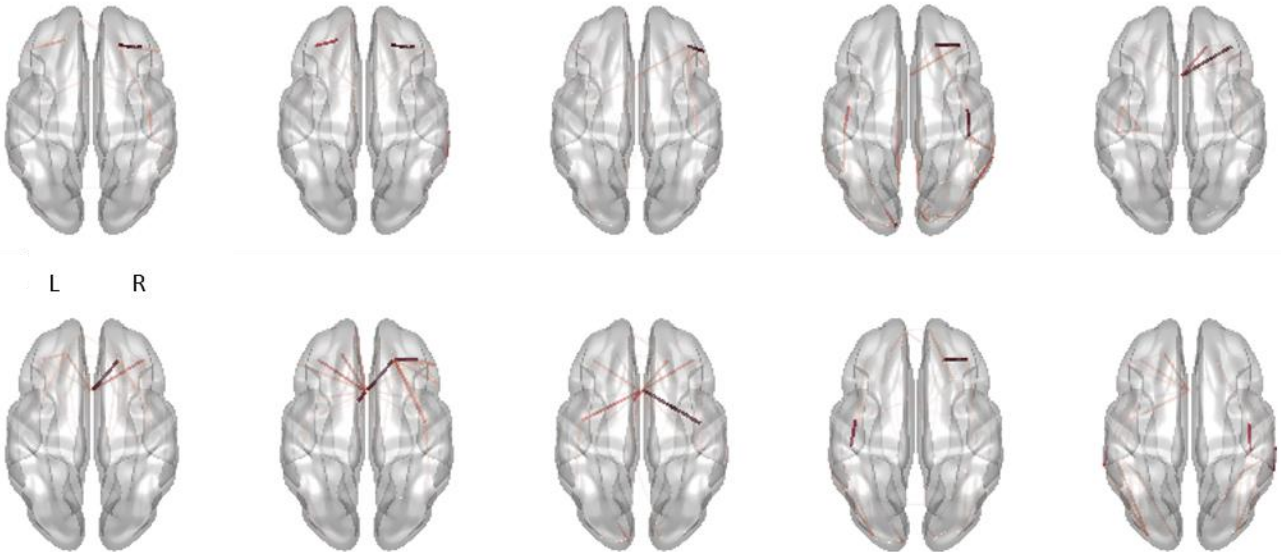


Figure 5.5. Number of streamlines derived with a minimum threshold of 18, axial view from overhead. Component matrices are plotted on a template brain. Top 5% of non-zero connections are plotted. The boldness of edges indicates the strength of connections.

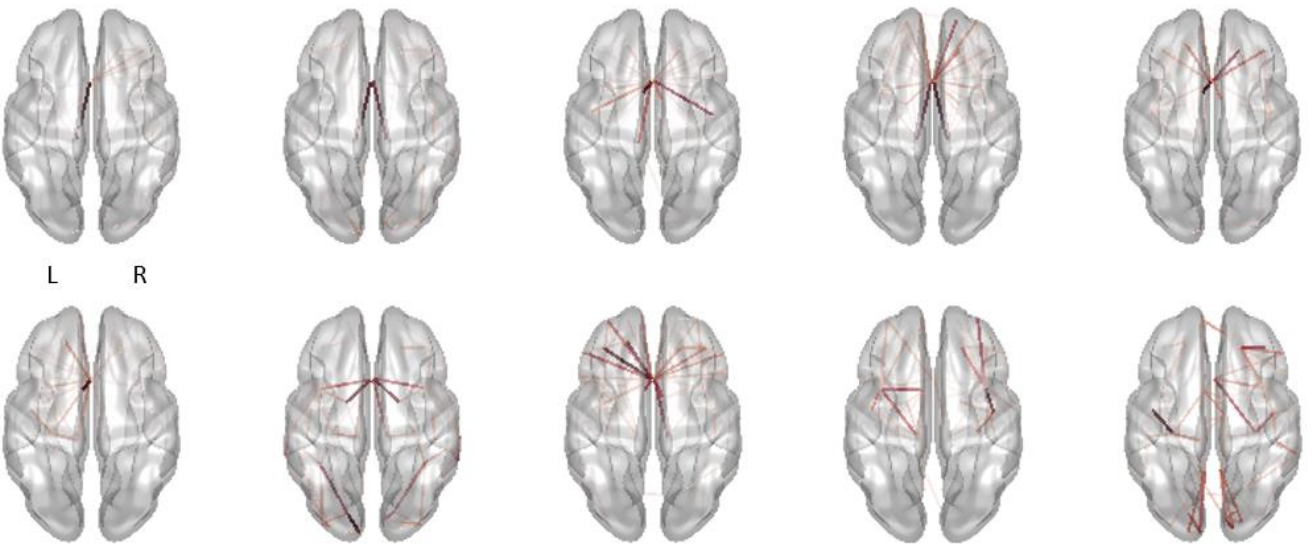


Figure 5.6. Standardised streamlines components derived with a minimum threshold of 18, axial view from overhead. Component matrices are plotted on a template brain. Top 5% of non- zero connections are plotted. The boldness of edges indicates the strength of connections.

5.4.2 Diffusivity measures

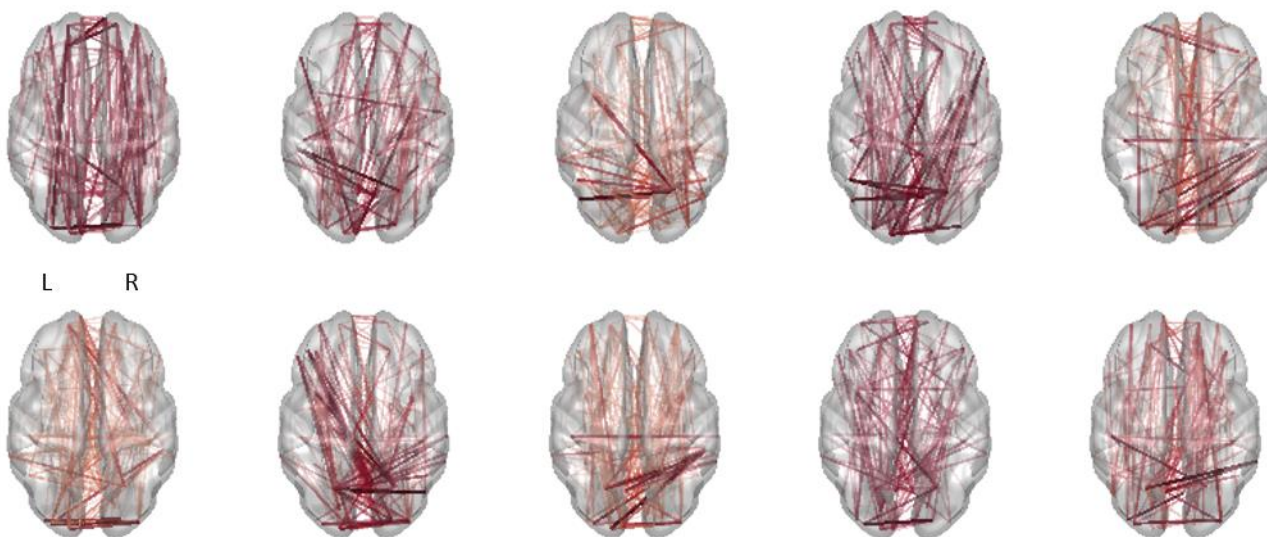


Figure 5.7. FA components, axial view from overhead. Component matrices are plotted on a template brain. Top 5% of non- zero connections are plotted. The boldness of edges indicates the strength of connections.

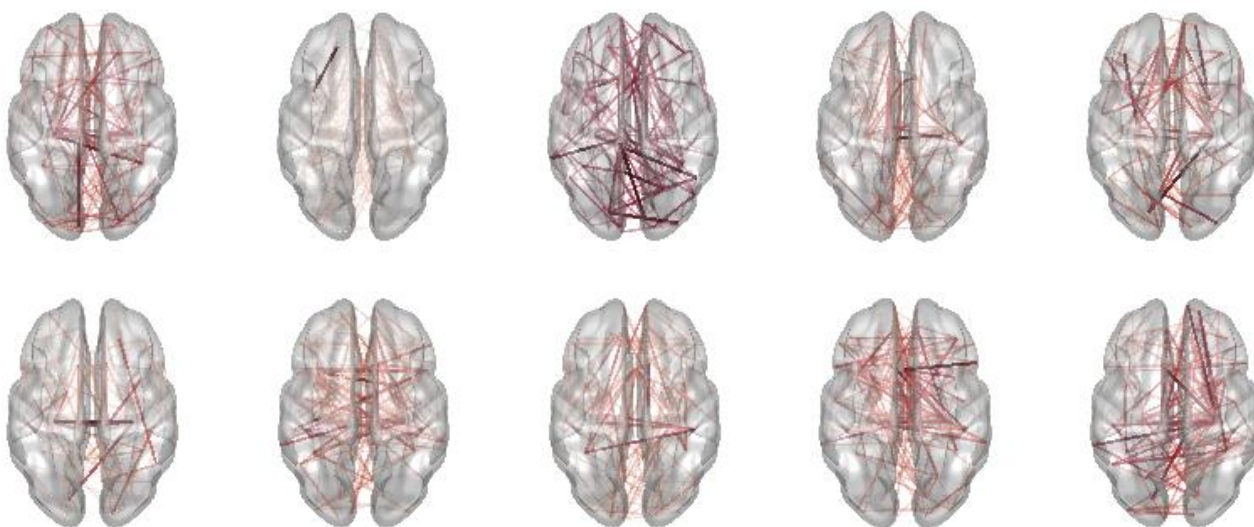


Figure 5.8. RD components, axial view from overhead. Component matrices are plotted on a template brain. Top 5% of non- zero connections are plotted. The boldness of edges indicates the

strength of connections.

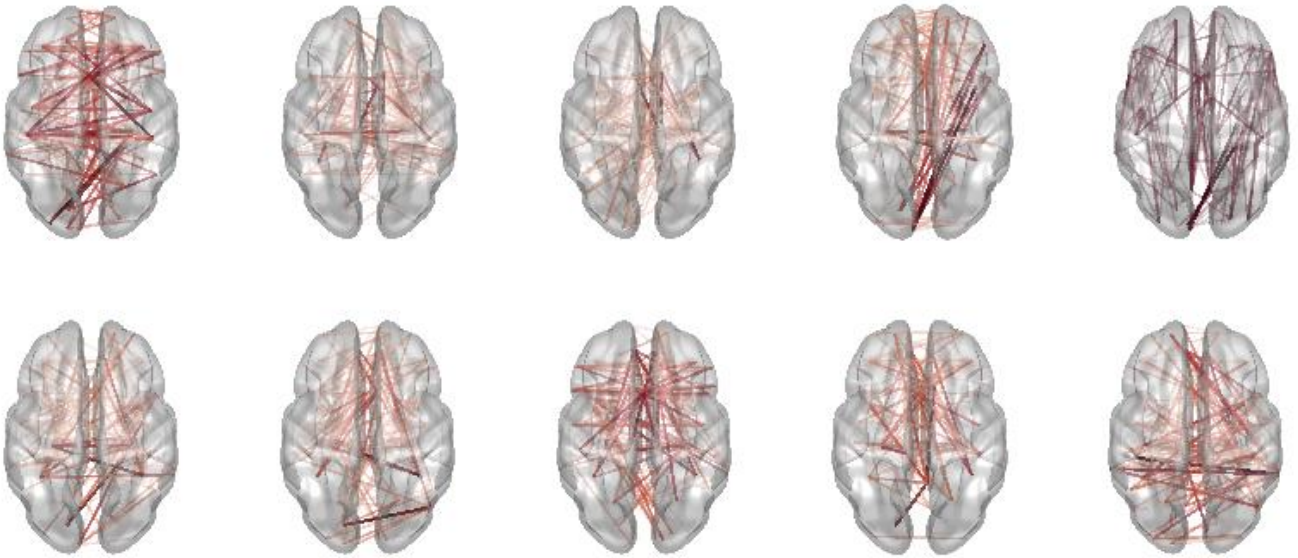


Figure 5.9. AD components, axial view from overhead. Component matrices are plotted on a template brain. Top 5% of non- zero connections are plotted. The boldness of edges indicates the strength of connections.

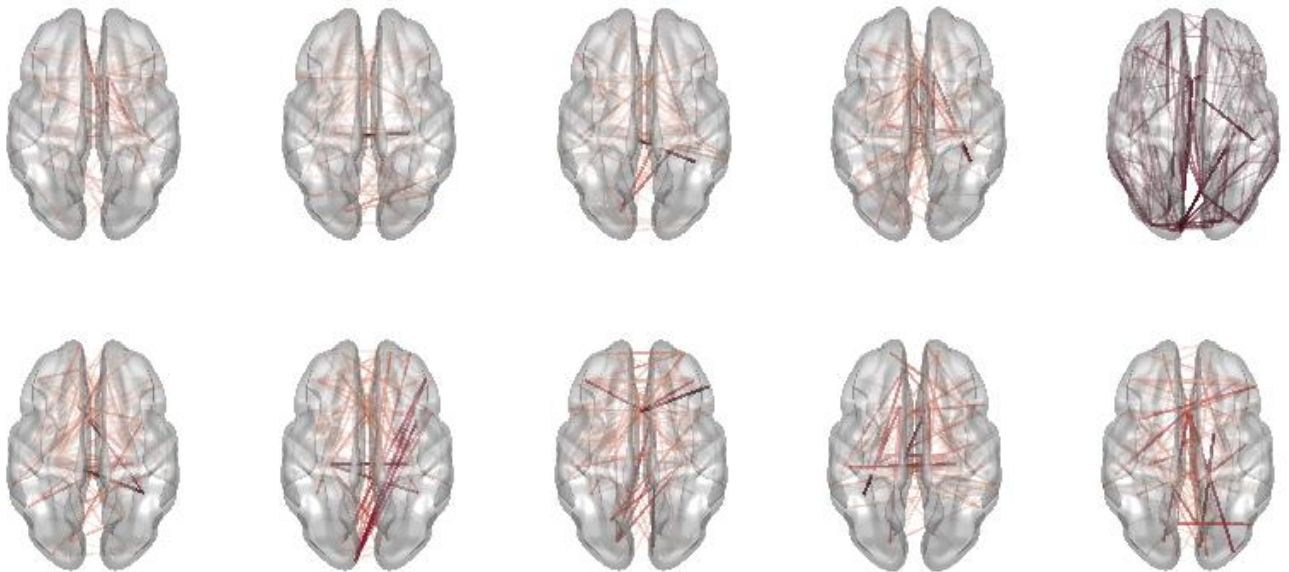


Figure 5.10. MD components, axial view from overhead. Component matrices are plotted on a template brain. Top 5% of non- zero connections are plotted. The boldness of edges indicates the strength of connections.

5.4.3 Myelin content

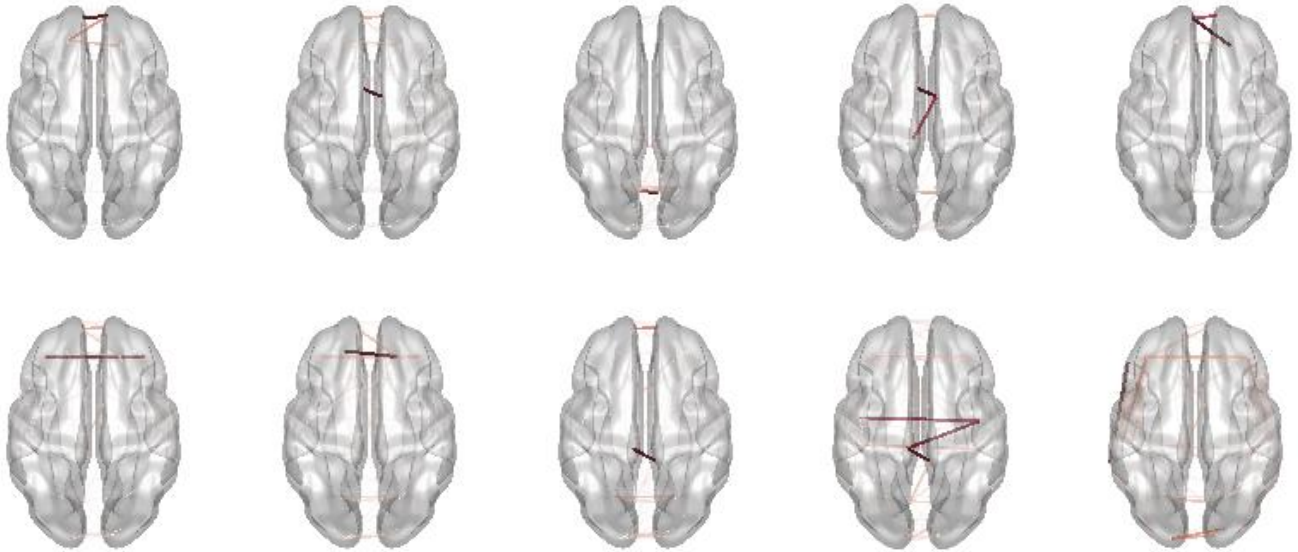


Figure 5.11. Myelin components, axial view from overhead. Component matrices are plotted on a template brain. Top 5% of non- zero connections are plotted. The boldness of edges indicates the strength of connections.

This is the first time that the NNMF algorithm has been applied to structural connectivity matrices. In the main, the structural sub-networks do not map onto the alpha and beta functional networks shown in Figures 5.1 and 5.2. This is consistent with recent work by Messaritaki et al. who used different structural connectivity metrics (number of streamlines, fractional anisotropy, myelination, radial diffusivity, and a binary weighting) and function predicting algorithms to predict NNMF components derived from functional MEG resting-state data (Messaritaki et al., 2021). The structural connectivity measures were assessed on how well they could predict the observed MEG functional connectivity data. Mostly, only weak correlations ($r < .45$) between predicted and observed functional connectivity were shown. Number of streamlines and myelination were the measures that had the highest correlations between the predicted and the observed functional connectivity. In general, the structural components shown here are either sparse or diffuse. Structural connectivity may, therefore, be necessary but not sufficient for functional connectivity. As mentioned, the weightings generated from the NNMF procedure were carried forward for further analysis, as the outcome variables, in the next chapters.

Chapter 6. Relationships between local and global oscillatory measures of connectivity and structural connectivity in the healthy population

6.1 Rationale

Understanding relationships between the brain's local and long-range, or global, networks is important in both health and disease and required for the attribution of cognitive functioning. As seen in chapters 3 and 4, MEG allows us to quantify local functional connectivity, reflected in high frequency oscillations, and global functional connectivity processes, reflected in the lower frequencies. Previous literature suggests that individuals with strong local gamma connectivity also have strong global connectivity, such that the amplitude of local and global oscillatory measures is correlated. Relationships between the brain's structure and function are also of considerable interest. Therefore, how individual variability in the structural connectome is related to individual variability in local and global connectivity will also be assessed.

The aim of this chapter is to 1) further define physiologically-informed inter- intra-areal oscillatory relationships by investigating relationships between local and global MEG measures, and 2) to explore how functional connectivity relates to the underlying structural connectome by investigating local connectivity and its relationship to a variety of structural connectivity measures. An improved understanding of these relationships will provide a perspective from which to better explore neural markers of disease.

6.2 Introduction

A healthy brain requires organised structural and functional networks (Bowyer, 2016; Buzsáki & Schomburg, 2015b; Collin & Keshavan, 2018; Damoiseaux, Rombouts, Barkhof, Scheltens, Stam, Smith, Beckmann, et al., 2006; Sadaghiani & Wirsich, 2020; Schreiner et al., 2017; Zink et al., 2021). Numerous studies have shown that clinical cohorts, for example those with schizophrenia, have functional and structural impairments at both the local and global level (Brookes et al., 2016; Gonzalez-Burgos, Cho, & Lewis, 2015; Kelly et al., 2017; Shaw et al., 2020; Uhlhaas & Singer, 2010). Understanding the characteristics of connectivity and associated

interactions across frequency bands and modalities, in the normative population, is a primary concern and will facilitate our understanding of clinical impairments.

In the functional literature, gamma oscillations are taken to reflect local circuitry (Buzsáki & Wang, 2012; Donner & Siegel, 2011; Fries, Schröder, Roelfsema, Singer, & Engel, 2002; Shaw et al., 2017), particularly in visual cortex (VC), with several lines of evidence in support. For example, in cat, the insertion of an electrode directly into V1 reveals increased gamma amplitude in response to visual stimuli (Gray et al., 1989b). In mice, the genetic knock out of local pyramidal- interneuron connections, fundamental to local circuitry, also causes a reduction in gamma amplitude (Fuchs et al., 2007). In humans, gamma oscillations induced with a visual grating paradigm are tightly coupled with the haemodynamic BOLD response in V1 (Muthukumaraswamy et al., 2009). Furthermore, with Dynamic Causal Modelling, it has been shown that connectivity between the superficial layers (2/3) of the cortex is associated with the amplitude and frequency of the induced visual gamma response (Shaw et al., 2017; Shaw et al., 2020). While the gamma signal has several forms, the induced or oscillatory or non-phase locked part, is suggested to have a higher order role, beyond primary sensory processing (Cohen, 2014; Fries, 2005; Tallon-Baudry, 2009). Extracting the gamma power spectrum can be viewed as taking a static snapshot of these processes (Donner & Siegel, 2011). Local connectivity therefore refers to connectivity at the microcircuit level i.e., parameters around pyramidal<>interneuron coupling (PING model, Wang & Buzsáki, 1996).

At the global functional level, though large-scale networks have most frequently been studied with functional Magnetic Resonance Imaging (fMRI), advancements in electrophysiological source localisation techniques have encouraged a surge in MEG/EGG connectivity studies. Subsequent comparisons with fMRI data have shown that MEG has the required sensitivity to detect network effects (Brookes et al., 2011; Brookes, et al., 2011; de Pasquale et al., 2010; Lui et al., 2010). Specifically, oscillatory connectivity in the alpha and beta ranges has been shown to, most closely, reflect established functional MRI networks, for example the default mode network (DMN), and in this instance represent a static snapshot of global functional processes (Brookes et al., 2011; Damoiseaux, Rombouts, Barkhof, Scheltens, Stam, Smith, & Beckmann, 2006; Siegel, Donner, & Engel, 2012). Furthermore, regarding static resting-state networks,

improved reliability of amplitude envelope correlations, as compared with phase measures, has been shown (Colclough et al., 2016; Dimitriadis et al., 2018). Amplitude-amplitude networks have been implicated in healthy brain functioning and found to be disrupted in diseases such as schizophrenia (Friston et al., 2016; Manzano et al., 2017), and Alzheimers disease (Koelewijn et al., 2017).

Alpha oscillations are generated via thalamo-cortical loops (Vijayan et al., 2013), though there is also some evidence that the cortex may also have an independent contribution (Lopes Da Silva, Pijn, Velis, & Nijssen, 1997). Nonetheless, the functionality of alpha oscillations is diverse. In the VC for example, increased alpha oscillations are strongly associated with reduced attention and also have an active role in dynamic temporally tuned perception (Clayton, Yeung, & Cohen Kadosh, 2015; Clayton, Yeung, & Kadosh, 2018). The latter finding led to the suggestion that alpha has a modulatory effect on cortical excitability (Keitel et al., 2019; Romei et al., 2008). In more recent years, it has been shown that while the 8-13Hz oscillation may not have a direct role in modulating cortical excitability in V1 (Zhigalov, Herring, Herpers, Bergmann, & Jensen, 2019; Zhigalov & Jensen, 2020), it could have a feedback role in updating prediction errors, in accordance with Prediction Theory (Alamia & VanRullen, 2019; Clayton, Yeung, & Kadosh, 2018; Michalareas et al., 2016a). In this case, alpha-band oscillations may facilitate the transmission of top-down representations to VC. The final function of alpha, which is of relevance to this chapter, is that alpha synchronisations or coherence is found across widespread areas of the brain, including frontal to posterior areas (Clayton, Yeung, & Kadosh, 2018). These synchronisations between areas result in alpha networks, which are considered to support intra-areal communication (Palva & Palva, 2007; Uhlhaas, Haenschel, Nikolić, & Singer, 2008).

The origins of beta oscillations are yet to be established. However, it is known that beta oscillations are sensitive to GABA-drug manipulations with Tiagabine and benzodiazepines (Jensen et al., 2005; Shaw et al., 2020). While the motor cortex and basal ganglia have been implicated as generators of beta oscillations (Jensen et al., 2005; Mirzaei et al., 2017), it is unclear whether they form part of a cortical – basal ganglia network or are independent. Similarly, there is current debate over whether beta does occur as a rhythmic oscillation or rather brief bursting activity over time (Barone & Rossiter, 2021). Changes in beta amplitude are

predominantly seen in the sensorimotor cortex and have a proposed role in movement preparation and cessation (Barone & Rossiter, 2021; Gascoyne et al., 2021; Jurkiewicz, Gaetz, Bostan, & Cheyne, 2006). That being said, in oscillatory connectivity measures, beta synchronisations occur in widespread networks (Baillet, 2017; Brookes, Woolrich, & Barnes, 2012; Doesburg et al., 2010; Godfrey & Singh, 2020; Pasquale et al., 2010; Tewarie et al., 2019), beyond the somatosensory cortex, and have therefore been implicated in long distance communication, which facilitates processes such as decision making, working memory and semantic processing (Hirvonen et al., 2017; Siegel et al., 2012, 2011; Spitzer & Haegens, 2017).

Without the assumption that oscillations act as cognitive operators, higher and lower frequency oscillations may simply harmonise local and global processing in the brain (see introductory section ‘The oscillatory local-global story’). Certainly, oscillatory coupling has been shown both within (Bonfond & Jensen, 2015), and between brain regions (Siegel et al., 2012).

Furthermore, Hidden Markov Modelling has previously shown a relationship between induced gamma amplitude and connectivity in the resting-state (Hirschmann et al., 2020a). Additional research on the interactions between these phenomena might facilitate understanding of GABAergic and glutamatergic mechanisms both in local excitation-inhibition and in dispersed systems.

In recent years there has also been increasing interest into relationships between structural and functional features of the brain: in particular, the overlap between structural networks and functional networks. On one hand, considerable overlap has been shown. For example, the Default Mode Network revealed with fMRI has significant spatial consistency with the hubs of the structural connectome (Power et al., 2010). Furthermore, with bifurcation analysis, it has been shown that the excitation of relevant structural network eigenmodes allows the specific prediction of alpha and beta functional resting-state networks (Tewarie et al., 2019). On the other hand, however, structure –function relations have been shown to be sensitive to the structural measures employed. For example, a MEG – DTI paper found that the ability to predict MEG resting-state functional connectivity networks generated with Non-negative Matrix Factorization (NNMF), from the structural connectome, depended highly on the structural parameters involved (Messaritaki et al., 2021b).

Such studies fall under the bracket of *Connectomics* (Charvet, 2020; Sadaghiani, Brookes, & Baillet, 2021a; Tewarie et al., 2020) which has become a popular mode of neuroscience. However, exploring structure-function relationship over the global functional connectome is not trivial. Functional resting-state networks represent averaged dynamic activity acquired over a time frame and over the whole brain, at rest. The study of structural and functional connectomics has, therefore, become associated with the use of increasingly complex modelling techniques (Cabral, Kringelbach, & Deco, 2017; Kopell, Gritton, Whittington, & Kramer, 2014).

As local connectivity in the VC is better understood (at least at the physiological/ mechanistic level) than global functional networks, exploring relationships between local functional connectivity and the connectome might be fruitful. Slower oscillatory fluctuations may have a role in connecting local oscillatory units via the structural connectome, for example, considering modelling work that has shown, with a structurally informed model, that the generation of local gamma oscillators is associated with widespread slower oscillatory fluctuations in BOLD activity in healthy individuals (Cabral et al., 2011). As mentioned, BOLD connectivity has been correlated with alpha and beta connectivity networks (Brookes et al., 2011).

Relationships between local micro-circuitry and long-range oscillatory connectivity are particularly interesting in the context of the clinical literature. Individuals with schizophrenia, for example, have been shown to have both reduced local visual connectivity (Grützner et al., 2013; Rutter et al., 2009; Shaw et al., 2020; Uhlhaas & Singer, 2013; Vierling-Claassen, Siekmeier, Stufflebeam, & Kopell, 2008) and reduced long-range connectivity (Alamian et al., 2017b; Karbasforoushan & Woodward, 2013; Pettersson-Yeo, Allen, Benetti, McGuire, & Mechelli, 2010), so that the amplitude of visual gamma might be correlated with the amplitude of long-range connections. Elucidating relationships between local and global connectivity in the healthy population, first, would be useful.

6. 2. 1 Aim and hypotheses

The aim of this chapter is two-fold. First, is to investigate the relationship between local oscillatory connectivity and long-range oscillatory connectivity, across participants, using MEG.

Based on previous modelling findings, it is hypothesised that increased gamma amplitude will be associated with increased alpha and beta connectivity, such that healthy individuals with stronger connectivity in VC with also have stronger global functional connectivity. In the process, whether these static-snapshot measures of connectivity capture the same or distinct aspects of covariance in connectivity, might be better understood⁴. The relationship between visual gamma frequency and global functional connectivity is also to be explored.

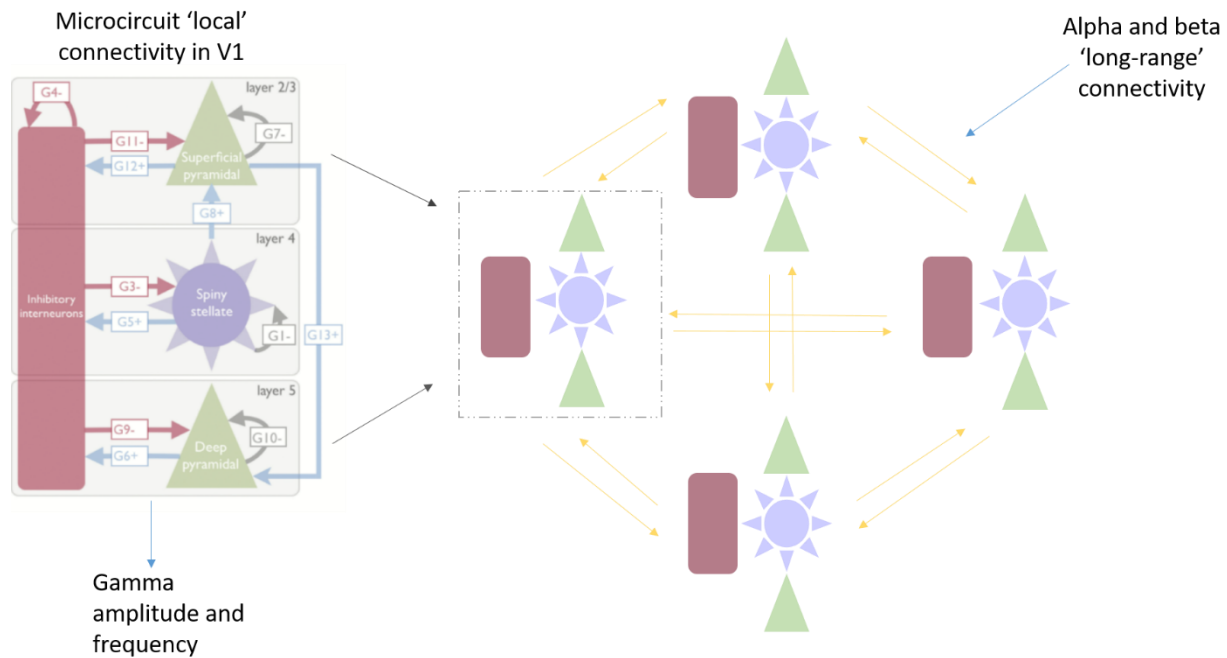


Figure 6.1. A model of high frequency 'local' and lower frequency 'global' interactions⁵.

Second, is to explore relationships between local functional connectivity in VC and global structural networks. As an exploratory analysis no formal hypotheses are provided, however, using simple regression analysis it is hoped that further insight into structure- function

⁴ At the time no other studies had investigated the relationship between these task and resting oscillatory measures.

⁵ Note: The schematic of the canonical microcircuit in visual cortex, on the left, adapted from Shaw, A. D., Knight, L., Freeman, T. C., Williams, G. M., Moran, R. J., Friston, K. J., ... & Singh, K. D. (2020). Oscillatory, computational, and behavioral evidence for impaired GABAergic inhibition in schizophrenia. *Schizophrenia bulletin*, 46(2), 345-353

relationships might be gained. Both functional and structural data will be reduced to fundamental networks using Non- Negative Matrix Factorization (NNMF). This method has been used previously to investigate structural and functional correlates (Messaritaki et al., 2021a; Phalen et al., 2019).

6.3 Method

6.3.1 Participants

100-Brains

The 100-Brains project was a large genetic and multimodal imaging study conducted in the normative population. There were 100 participants recruited of which 97 had MEG data. Participants were all right-handed (Edinburgh Inventory-Oldfield, 1971), absent of neuropsychiatric conditions (General Health Questionnaire, Goldberg & Williams, 1988), and of Caucasian ethnicity. Participants were university students and, as such, similar in education level and age. None of the participants had a history of drug or alcohol abuse. Ethics was granted by the School of Psychology Ethics Committee at Cardiff University.

Table 6.1. 100-Brains demographics

| 100-Brains | N 97 | Mean | SD |
|-------------------|-------------|-------------|-----------|
| Age | n 97 | 24 | 3.5 |
| Gender | n 97 | 63f:34m | |

Participants completed a battery of tasks in the MEG scanner including a resting-state and visual gamma paradigm.

MEG-Partnership

The MEG-Partnership project was a collaboration between MEG sites across the UK. Data collected at Cardiff University Brain Research Imaging Centre (CUBRIC), is included in this thesis. All participants were healthy individuals with no history of neurological or neuropsychiatric dysfunction. Participants were right-handed, with British-Caucasian ethnicity and English as their first language and of similar age. Ethics was granted by the School of Psychology Ethics Committee at Cardiff University.

Table 6.2. MEG-Partnership demographics

| MEG-Partnership | N 88 | Mean | SD |
|------------------------|-------------|-------------|-----------|
| Age | n 88 | 25.5 | 6.73 |
| Gender | n 88 | 61f:27m | |

Each participant completed a battery of tasks in the scanner, including a resting-state paradigm and a visuomotor task. Consistency in task paradigms and demographics allowed data from the two cohorts to be compiled in this chapter.

6.3.2 Tasks and data acquisition

Visual gamma tasks differed slightly between cohorts. The 100-Brains paradigm involved 100 trials and lasted ~ 10 minutes. The stimulus comprised a visual grating presented centrally. The grating was a vertical, stationary, maximum contrast square-wave grating with a spatial frequency of 3 cycles per degree ($8^\circ \times 8^\circ$ visual angle). The background was of mean luminescence. Stimuli were jittered between 1.5-2 seconds and followed by an inter-stimulus interval (ITI) of 2 seconds. Participants were required to push a button with their right hand every time the grating disappeared. Participants were notified if no response was detected after 750ms.

The MEG-Partnership visuomotor task also had 100 trials in total and lasted ~ 13 minutes. The visual stimulus presented in the lower left visual field was a stationary, vertical, maximum contrast, three cycles per minute, square-wave grating, subtended vertically and horizontally at a 4° angle. The stimulus was presented for 1.5-2 seconds, jittered, on a mean luminance background. The ITIs were either 4 seconds or 8 seconds and allocated to half of the trials, presented in random order. Participants were also required to perform a finger abduction with the index finger on the right hand whenever the grating disappeared. This task has been referred to as the visuomotor task (Gascoyne et al., 2021), though the motor component was not analysed and not of primary interest to the research questions addressed in this thesis.

The resting-state paradigm used in each cohort was identical. It comprised a 5-minute presentation of a central fixation cross. Participants were instructed to focus, with eyes open, on

the cross at the centre of the screen. Both paradigms were programmed in Matlab (2015) and presented at a refresh rate of 100Hz.

All data were collected on a 275-channel axial gradiometer CTF system at Cardiff University. Participants sat upright in the scanner. For head localisation, electromagnetic coils were attached to the fiducial areas; nasion and right and left pre-auricular. Head localisation was completed at the beginning and the end of each scan.

6.3.3 Visual gamma analysis

Pre-processing and co-registration

Third-order gradient mode was applied, transforming the primary sensors for environmental noise reduction. Data were sampled at 1200Hz, with a 300Hz lowpass antialiasing filter. Data were then epoched into 4 second trials (-2, 2) around the stimulus onset, before being manually inspected for artefacts in DataEditor. Any trials that contained movement, muscular or ocular artefacts were discarded. MRIs (1mm- isotropic, T1 weighted), were acquired on the 3 Tesla General Electric system at CUBRIC. Participant's data was manually co-registered to their MRI by localising the fiducial markers, using photographs taken in the MEG scanning session, in CTF space.

Visual gamma analysis

Visual gamma metrics were extracted with the method described in Chapter 3, which will be summarised here. LCMV beamforming was completed on 6 bilateral visual areas: Calcarine, Cuneus, Lingual, Superior Occipital, Mid Occipital and Inferior Occipital. The leadfield was constructed using a 1mm MNI sampling grid. The beamformer weights were based on the global data covariance between 30-80 Hz. Source power was constructed separately for baseline (-1.2-0s) and stimulus periods. The sustained period of the response was of interest and the oscillatory period was selected at 0.3s- 1.2s after stimulus onset. A virtual sensor was inserted at the point of the peak source amplitude. That is, at the coordinates of the source with the maximal percentage change in gamma power. Estimates of peak amplitude and peak frequency of the virtual sensor, estimated from the power spectrum, were carried forward for further analysis.

6.3.4 Functional Resting-state Analyses

Pre-processing and co-registration

Data was pre-processed in DataEditor software. After downsampling to 600Hz and band-pass filtering (1-150 Hz), data were split into 2 second intervals. Intervals including large muscle artefacts, cardiac artefacts, eye movements or environmental artefacts were discarded. Individual anatomical MRIs (1mm- isotropic, T1 weighted), were collected on a 3 Tesla General Electric system at Cardiff University. Data was manually co-registered to the MRIs by localising the fiducial markers, using photographs taken in the MEG scanning session, in CTF space.

Amplitude- amplitude connectivity analysis

The same LCMV beamforming approach, as described above, was applied for source localisation. Due to the computational demand of considering all the cortical areas, a coarser 6mm sampling grid was employed. The MNI inverse-warping procedure was adopted to ensure source grid consistency across participants. Data were band filtered into the canonical frequency bands (Delta 1-4Hz, Theta 4-8Hz, Alpha 8-13Hz, Beta 13-30Hz, Low Gamma 30-60Hz and High Gamma 60-90Hz) and analysed continuously. A virtual time series was constructed in each brain area according to the AAL atlas (90 regions in total). Data were orthogonalized to minimise source leakage (Colclough et al., 2015) and a Hilbert transform applied to give an estimate of amplitude and phase per region. Amplitude envelope covariance across regions was then calculated to assess the strength of connectivity between regions. Connections across the frequency bands were also inspected by combining band specific data in the following way:

Combined $ij = \text{sqrt}(\text{Delta } ij^2 + \text{Theta } ij^2 + \text{Alpha } ij^2 + \text{Beta } ij^2 + \text{LowGamma } ij^2 + \text{HighGamma } ij^2)$ (Koelewijn, 2017).

To account for potential between participant sources of variance arisen in data collection, and for interpretation, raw covariance matrices were standardised (z-scored) by subtracting the grand mean from each connectivity score and dividing the difference by the overall standard deviation. Therefore, each connection value represents the strength of connectivity (z- score correlation), in relation to the mean.

6.3.4 Statistical analysis – Functional connectivity

Edge level

To investigate the relationship between visual gamma metrics and resting-state networks a regression model using visual gamma amplitude (and frequency), gender⁶ and age as regressors, was constructed. To control for the slight difference in visual gamma paradigms used in the 100-Brains and MEG-Partnership cohorts, paradigm type was also included as a regressor. Results therefore show to what extent visual gamma amplitude and frequency predict strength of connectivity across the frequency bands. Over both cohorts 179 participants had both visual gamma and RSN datasets.

Statistical analyses were completed at 4 stages for each of the 6 frequency bands and for the combined frequency band, in the connectivity analysis.

- 1) Owing to the shape of the undirected, and hence symmetrical, connectivity matrices (90 x 90), 4005 unique connection values were generated. Self-connections were set to 0. All z-scored connections were ranked to a strength between 0-1 for each participant. Ranked connections were then averaged across participants and those connections with a mean rank of greater than 0.8 (i.e., mean rank in top 20%) were selected as valid connections.
- 2) Univariate linear regression, with visual gamma as the main predictor, was conducted on valid connections ($p < .05$).
- 3) A further 1000 iteration randomisation test with omnibus thresholding was conducted to assign significance to each edge connection while correcting for multiple comparisons. Omnibus testing finds the absolute maximum null r value across all connections and tests against it. This method reveals connections adjusted for multiple comparisons. All other connections were set to 0.

⁶ Note: Gender is the primary descriptive of choice in this thesis as responses were self-reported and at least half of the overall cohort (MEG-Partnership) were explicitly asked to state their gender. Participants in the 100-Brains cohort were asked to select a 'male' or 'female' option. As the data were pooled there are some instances where 'gender' and 'sex' are used interchangeably, though it is acknowledged that they are not the same and it is possible some differences could exist. This statement applies to Chapters 6-9.

- 4) To consider the generalisability of results, a 95% confidence interval was generated on the regression slope for each connection in the univariate analyses. In subsequent circular plots connections were plotted in the direction of the effect if its corresponding confidence interval did not include 0.

Non-Negative Matrix Factorization – Functional connectivity

Non-Negative Matrix Factorization was performed on the functional resting-state data, as described in Chapter 5. NMF is a mathematical approach (Lee & Seung, 1999) whereby matrices can be reduced into fundamental networks, in a method akin to Principal Components Analysis (PCA). NMF components were derived separately per frequency band. Alpha and beta components are considered here; 11 and 9 components were derived, respectively.

Statistical analyses were based on the General Linear Model (GLM), implemented in Fieldtrip (2019). Separate GLMs were constructed with peak amplitude and peak frequency as the main predictors; covariates, age, gender and visual gamma task, were included. Cook's distance was set to 3. Cook's distance is the scaled change in the coefficients due to the deletion of an observation (subject in this case). Thus, Cook's distance is useful for identifying high-leverage outliers in observations for predictor variables. Individuals with a Cook's distance of greater than $3 \times \text{mean}$, were rejected from the analysis. Subjects were also rejected if they have a Cook's distance of >0.5 , which is considered large.

6.3.5 Structural analysis

Structural connectivity measures were derived by Dr Eirini Messaritaki (Messaritaki et al., 2021a). Structural regions were defined with an AAL labeling atlas (90 cortical and subcortical regions). Structural networks were then also represented as 90×90 symmetrical matrices, for each participant.

MRI data acquisition and pre-processing

All MRI data were acquired on a GE Signa HDx 3T scanner (GE Healthcare, Milwaukee, WI). T1 images were acquired with a three-dimensional fast spoiled gradient and downsampled to 1.5-mm isotropic resolution.

Diffusion weighted MRI data were acquired with a peripherally cardiac-gated sequence with $b = 1,200 \text{ s/mm}^2$, $TR = 20 \text{ s}$, $TE = 90 \text{ ms}$, isotropic resolution of 2.4 mm , zero slice gap, $FOV = 230 \text{ mm}$. Diffusion data were co-registered to the T1. Corrections for head movement and eddy current distortions were made. Free-water correction was also conducted.

mcDESPOT data (which can provide myelin measures) were acquired using multicomponent-driven equilibrium single pulse observation of T1 and T2 (Deoni, Rutt, Arun, Pierpaoli, & Jones, 2008). Images for each participant were linearly coregistered to a spoiled gradient recall (SPGR) image, to correct for subject motion. Nonbrain tissue was removed using a mask computed with the BET algorithm (Smith, 2002). Registration and brain masking were conducted with FSL (Jenkinson, M, Beckmann, CF, Behrens, Woolrich, & Smith, 2012).

Tractography analysis

White matter tracts can be represented as connections, or edges, in a structural network. Tractography was performed on the DTI data, using the streamline algorithm in MRtrix 3.0 (Dhollander, Raffelt, & Connelly, 2016). White matter tracts were localised using a WM mask generated from the T1-weighted images using FSL fast (Jenkinson et al., 2012). The minimum and maximum tract lengths were 30 and 250 mm, respectively.

Streamline selection

As mentioned in Chapter 5, the minimum number of streamlines that would allow us to assume that a tract has been reliably reconstructed has been selected arbitrarily, limiting the quantitative nature of streamline measures (Daducci et al., 2015). The COMMIT method (Daducci et al., 2015) is a data-driven alternative. Instead of rejecting tracts reconstructed with a number of streamlines lower than an arbitrary threshold, it rejects any streamlines that are not consistent with the overall diffusion signal in the diffusion-weighted images. This is done by fitting a linear combination of restricted and/or hindered contributions of candidate tracts and selecting those which result in the best global fit of the signal in each voxel.

mcDESPOT analysis

A mcDESPOT algorithm was used to detect the fast (water constrained by myelin), and slow (free-moving water in intra- and extracellular space), elements of the T1 and T2 times, and a nonexchanging free-water component (Deoni et al., 2013). The fast volume fraction was taken as a map of the myelin water fraction. The ratio of myelin-bound water to total water was calculated, which is the myelin volume fraction (MVF). A MRtrix function (tcksample), was used to assign a proportion of the MVF to each streamline, in each tract. This measure was averaged over its streamlines, providing a myelin-weighted value (MM), for each tract.

The matrices that resulted from these procedures were normalised by dividing by the largest value of each matrix, so that, within any given matrix, the values range from 0 to 1. Self-connections (diagonals) were set to zero.

The structural measures that resulted are:

White matter tractography DTI measures

The following measures are of interest because 1) the streamlines measures index the reconstruction of any given tract and 2) the subsequent diffusivity measures give values for the diffusion of water within any given tract and provide information, indirectly, on the tract's microstructural properties.

- Number of streamlines (NSC) is number of streamlines in the tracts as selected by the COMMIT method described above.
- Standardised number of streamlines (SSC), is number of streamlines within a tract divided by the length of the tract, selected by the COMMIT method.
- Fractional Anisotropy (FA) is a measure of the anisotropy in the diffusivity of water molecules calculated from three eigenvectors. An isotropic tensor would have equal eigenvectors.
- Radial Diffusivity (RD λ_{\perp}) is a measure of water diffusion perpendicular to the direction of the tracts.
- Axial Diffusivity (AD λ_{\parallel}) is a measure of water diffusion parallel to the direction of the tracts.
- Mean Diffusivity (overall diffusivity) is the mean of the three eigenvalues ($(\lambda_1 + \lambda_2 + \lambda_3)/3$) of the diffusion tensor.

mcDESPOT measures

- Myelin Water Fraction (MM), measures water diffusivity within the myelin giving an indirect measure of myelin density in the voxels including tracts.

Number of streamlines connectivity measures were available for the 100-Brains and MEG-Partnership cohorts (N=161). The other structural connectivity metrics were only available for the 100-Brains cohort (n=90). The MEG-Partnership cohort underwent only some of microstructural scans that were completed in the 100-Brains cohort and had not been analysed.

Non-Negative matrix Factorization

The same NNMF algorithm was applied to the structural connectivity matrices. For undirected correlations, there were 4005 unique connections which are taken forward for analysis. Self-connections were set to 0. Identical thresholding parameters were applied to avoid overfitting. This resulted in between 10-18 components for each of the structural measures; NST, SST, NSC, SSC, FA, RD, AD, MD & MM.

6.3.5 Statistical analysis- Structural connectivity

The structural components were analysed with regression analysis. Visual gamma response (amplitude and frequency) was the main predictor and age and gender were covariates. Bonferroni correction was applied to adjust for the number of components within each regression model.

6.4 Results

6.4.1 *Functional edge level connectivity*

First, analyses at the edge level were conducted to explore any relationships between gamma and individual connections. In each frequency band ‘valid’ connections were selected based on the mean rank $>.8$ criteria (shown in column 1 of subsequent aggregate circle plots). Two levels of regression analysis were performed. First, univariate regression was performed where each connection is considered separately in relation to the predictors of interest (shown in column 2 of subsequent circle plots). Second, the regressors were randomised and tested against an omnibus threshold, revealing connections that withstood multiple comparison correction. No connection met this this threshold and are not therefore plotted in subsequent circle plots. A 95% confidence interval was generated for each connection in the univariate regression which indicates the generalisability of associated connections in the population. Connections were plotted if their associated CI did not include zero (shown in column 3 of subsequent circle plots). Visual gamma amplitude (Figure 6.2) and frequency (Figure 6.3) were investigated as main predictors.

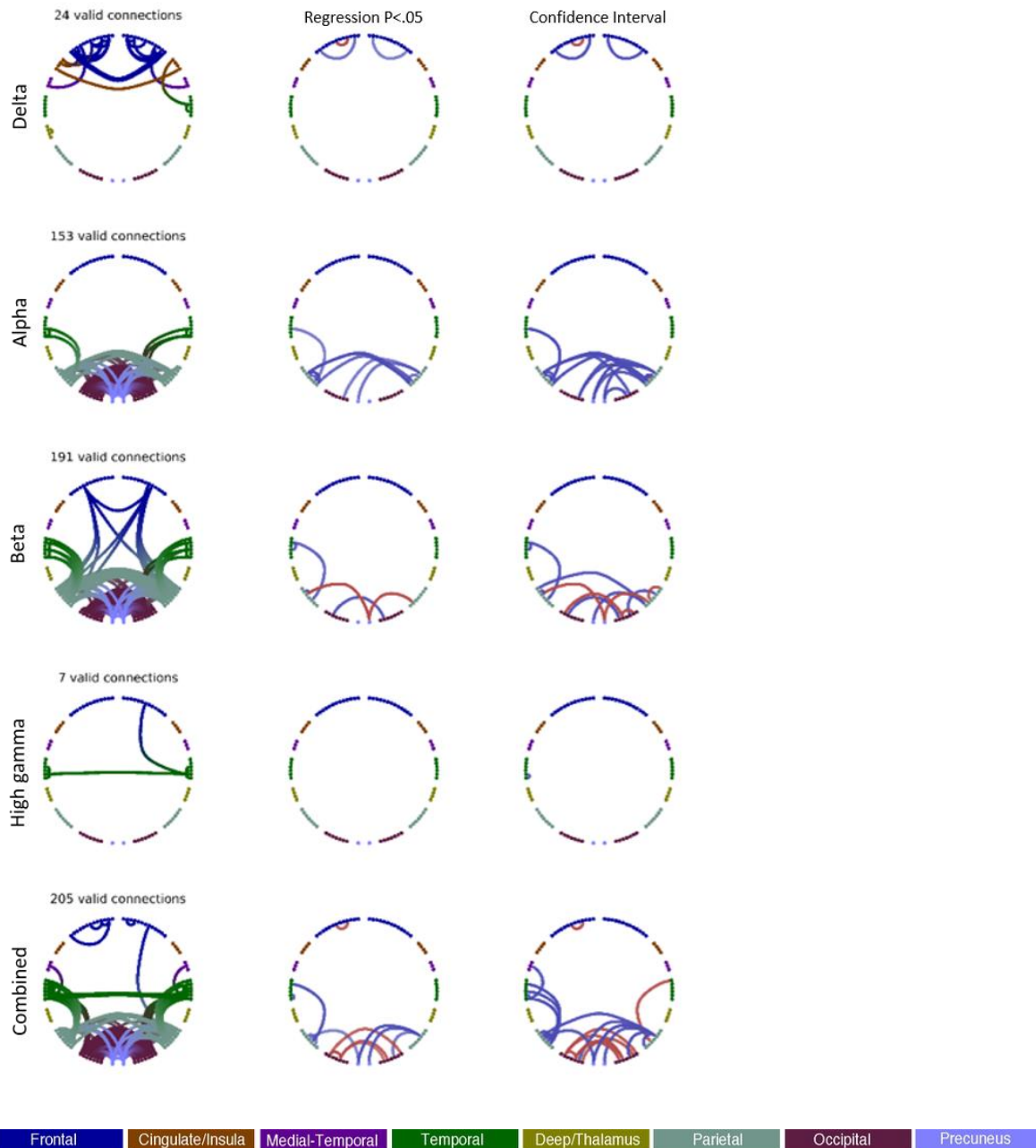


Figure 6.2. Connectivity maps showing functional connections predicted by peak gamma amplitude in the combined 100-Brains & MEG-Partnership cohorts, when controlling for age, gender and cohort. The first column, valid connections, shows the connections at mean rank >0.8 , per frequency band and across the combined frequencies. The second column shows connections significantly associated with gamma amplitude ($p < 0.05$) at the uncorrected level (univariate regression). To consider the generalisability of associated connections, the third column shows univariate connections where the confidence interval (95%) on the regression

slope did not include zero. In column 2 and 3, positive correlations, i.e., increased connectivity, are represented with red lines whereas negative correlations, i.e., decreased connectivity are represented with blue lines.

Gamma amplitude was significantly negatively associated with posterior alpha connectivity (lateral parietal and parietal-temporal). Some increased posterior beta connectivity was also shown along with one parietal- temporal and one occipital hypoconnection. The combined analyses show increased lateral occipital connectivity with reduced parietal temporal connectivity in the left hemisphere. One frontal delta hyper-connection withstood multiple comparison testing, however, is acknowledged with caution as MEG amplitude-amplitude frontal delta connections have been related to ocular artefacts (Godfrey, 2021).

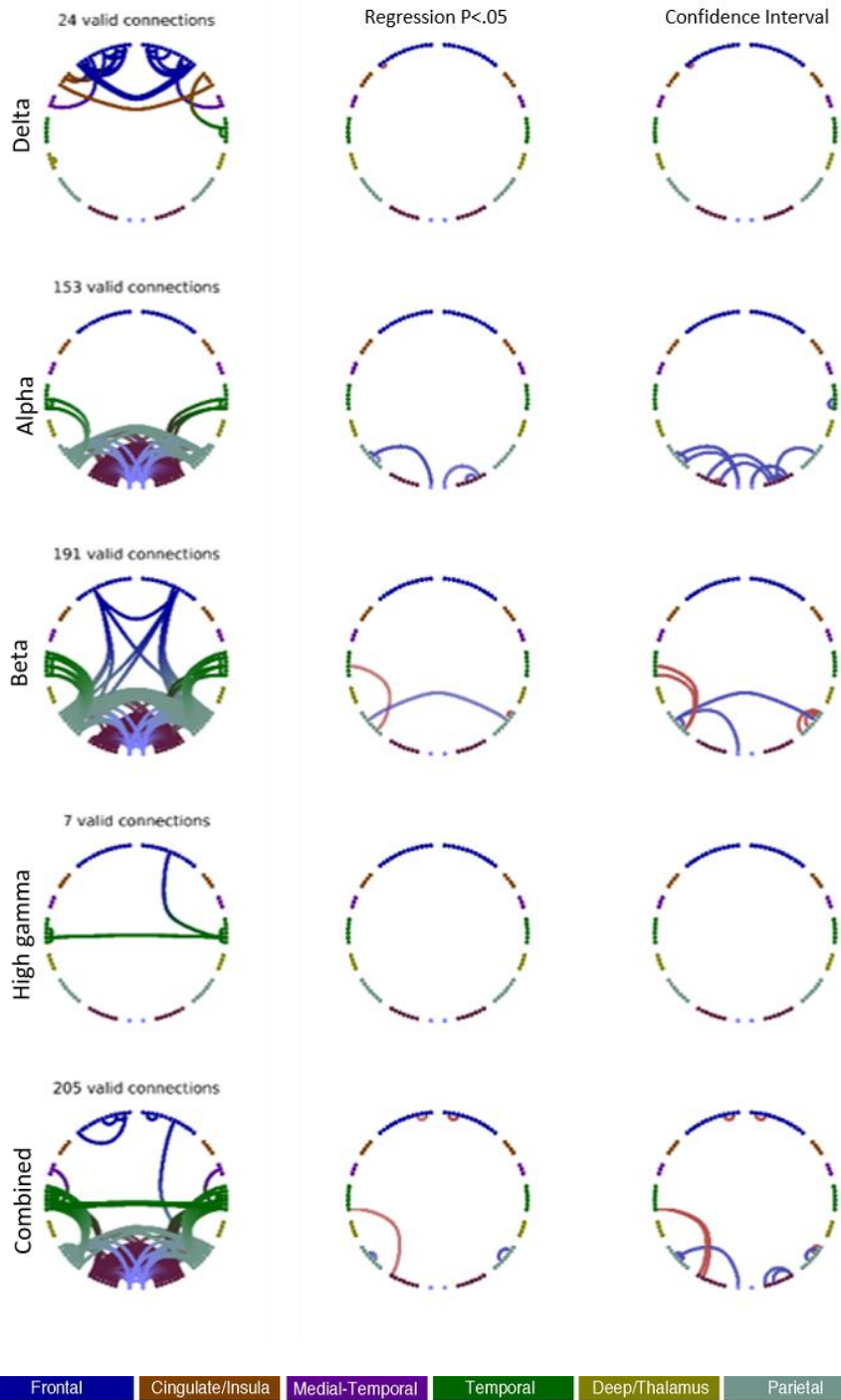


Figure 6.3. Connectivity maps showing functional connections predicted by peak gamma frequency in the combined 100-Brains & MEG-Partnership cohorts, when controlling and age gender and visual gamma paradigm. The first column, valid connections, shows the connections at mean rank >0.8 , per frequency band and across the combined frequencies. The second column shows connections significantly associated with gamma frequency ($p < 0.05$) at the

uncorrected level (univariate regression). To consider the generalisability of associated connections, the third column shows univariate connections where the confidence interval (95%) on the regression slope did not include zero. In column 2 and 3, positive correlations, i.e., increased connectivity, are represented with red lines whereas negative correlations, i.e., decreased connectivity are represented with blue lines.

Gamma frequency was negatively associated with a few reduced occipital, parietal and precuneus connections in the alpha band, although not significantly. One reduced connection in the beta band (lateral parietal), was observed. The combined analyses showed some hyperconnectivity in the left hemisphere and posterior dysconnectivity.

6.4.2 Non-Negative Matrix Factorization – Functional Networks

Functional sub-networks were revealed in the alpha and beta bands with NNMF of the resting-state networks and investigated in relation to the gamma metrics. As the visual gamma paradigms differed slightly between the two grouped cohorts a visual gamma task covariate was also included.

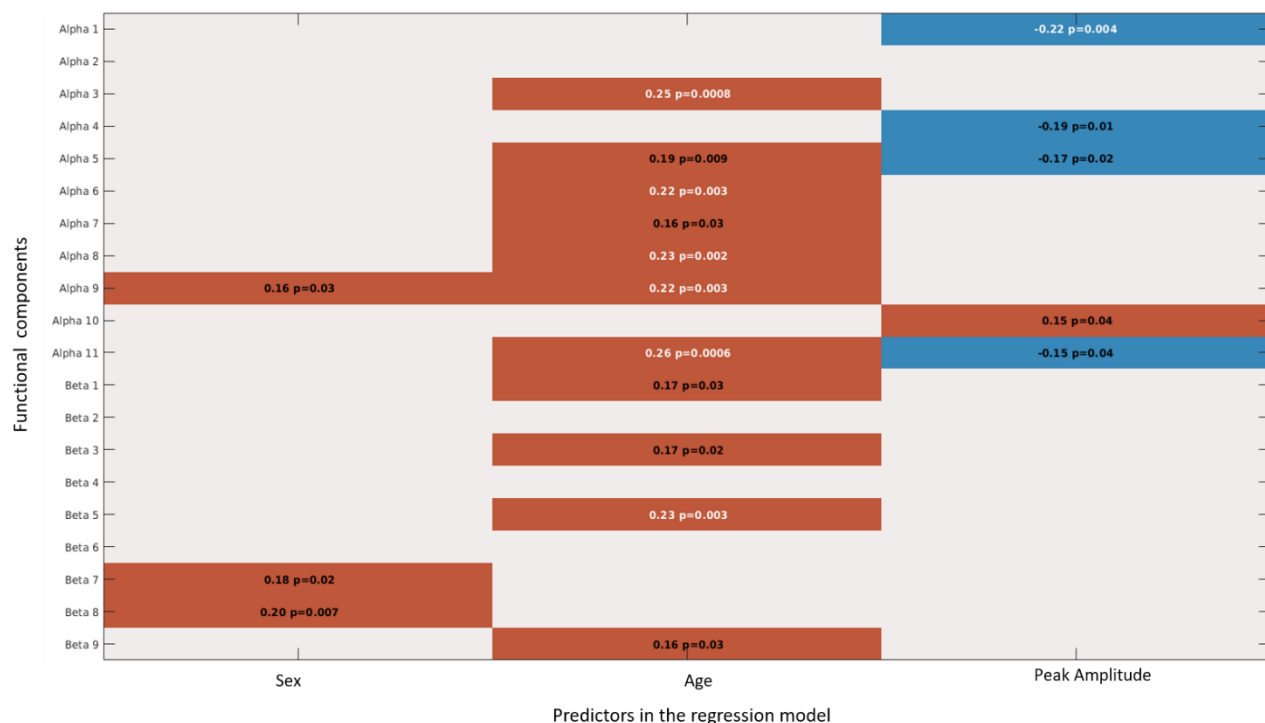


Figure 6.4. Functional NMF connectivity components in alpha and beta, across gender, age, peak amplitude and peak frequency. The within component text shown the effect size (beta) and the p-value. Red boxes represent positive relationships. Blue boxes represent negative relationships. Text in white shows relationships which meet multiple comparison adjustment ($p < .05$), whereas text in black shows relationships significant at the uncorrected level ($p < .05$).

Peak amplitude negatively predicted 4 alpha components and positively predicted 1 alpha component. One of the negative relationships met multiple comparison adjustment suggesting gamma amplitude is associated with reduced alpha weightings in this network (plotted below in Figure 6.5) i.e., those participants with greater induced visual gamma magnitude had less alpha connectivity within this posterior network component. No beta components were predicted by peak gamma amplitude.

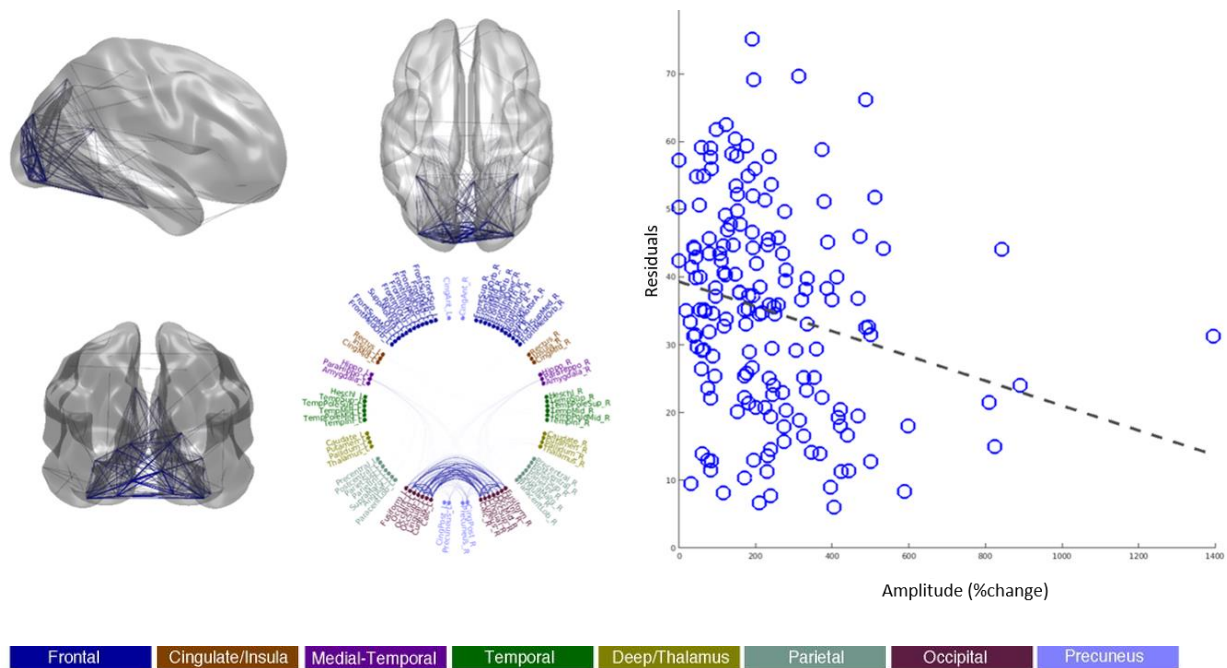


Figure 6.5. Left, shows alpha component 1 plotted on a template brain and circular plot. The blue edges represent the negative correlation with gamma amplitude. Right, shows the regression residuals plotted against peak amplitude.

This finding is interesting in consideration of previous work which has shown coupling between posterior gamma and alpha oscillations (Bastos et al., 2015; Jensen & Colgin, 2007; Lozano-Soldevilla, Ter Huurne, Cools, & Jensen, 2014).

Peak frequency did not significantly predict any alpha or beta NMF components ($p > .05$). Both age and gender had a positive relationship with some alpha and beta components, demonstrating the importance of including these variables as covariates in the gamma-network models. Age was associated with 5 alpha components and 1 beta component after multiple comparisons adjustment.

Within-task relationships

To investigate whether this effect was detectable in data acquired in the exact same session, within paradigm local gamma and global connectivity relationships were also explored in a sub-cohort of participants using resting-state analysis of the visual gamma data (as detailed in Chapter 4).

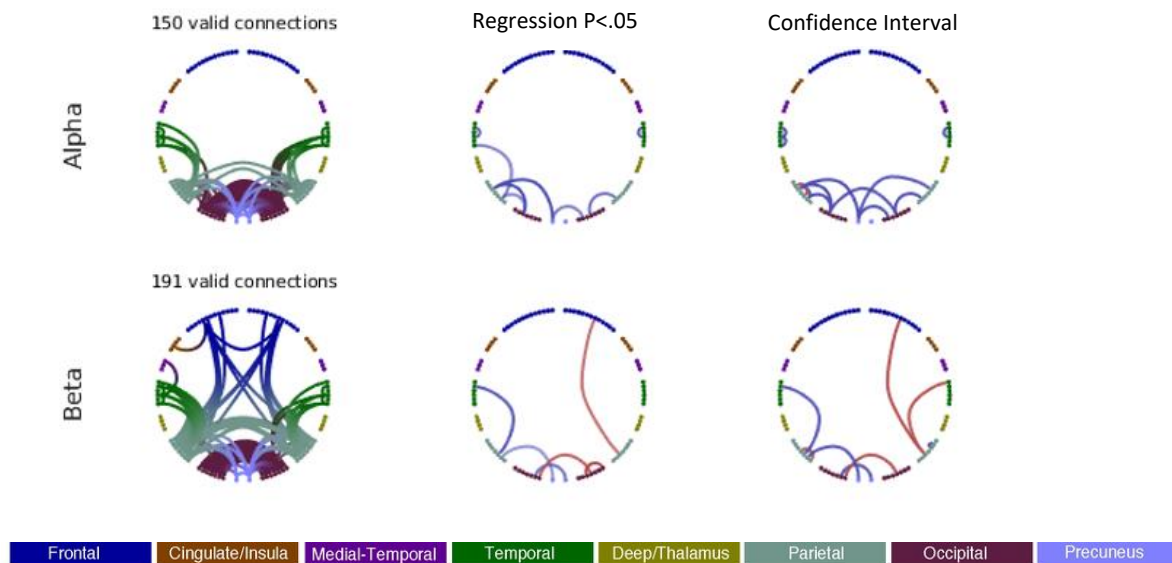


Figure 6.6. Connectivity maps showing functional connections associated with peak gamma amplitude in the MEG-Partnership cohort, when controlling age and gender. The first column, valid connections, shows the connections at mean rank >0.8 , per frequency band and across the combined frequencies. The second column shows significant connections ($p < 0.05$) at the uncorrected level (univariate regression). To consider the generalisability of associated connections, the third column shows univariate connections where the confidence interval (95%) on the regression slope did not include zero. In column 2 and 3, positive correlations, i.e., increased connectivity, are represented with red lines whereas negative correlations, i.e.,

decreased connectivity are represented with blue lines. No connections withstood multiple connection testing with omnibus thresholding.

At the edge level, as with the analysis shown in Figure 6.6, peak amplitude negatively predicted posterior connections in the alpha band, but these did not meet multiple comparisons adjustment. Peak frequency, activity at node 44 (v1) and percentage change in gamma activity at node 44 ((Gamma-RSN)/RSN), were also investigated as predictors of gamma connectivity (within paradigm). Few associated connections were found, and these also did not meet multiple comparison adjustment.

Covariate relationships

Regarding the covariates, peak amplitude differed with visual gamma task ($p < .05$). Peak amplitude was higher in the 100-Brains cohort (M 295, SD 245.63) where the stimuli was presented centrally, as opposed to the MEG-Partnership cohort (M 204, SD 156.78) where the stimulus was presented subtended vertically and horizontally at a 4° angle.

Males had significantly higher peak frequency than females (Male= M 53Hz, SD 6.44, Female=M 51Hz, SD 8.44). However, due to the gender differential in the sample this is interpreted with caution. Age differed with visual gamma task which represents a cohort effect. This difference was negligible (Brains M 23.6, SD 3.51, Meg-P M 25.5, SD 6.73).

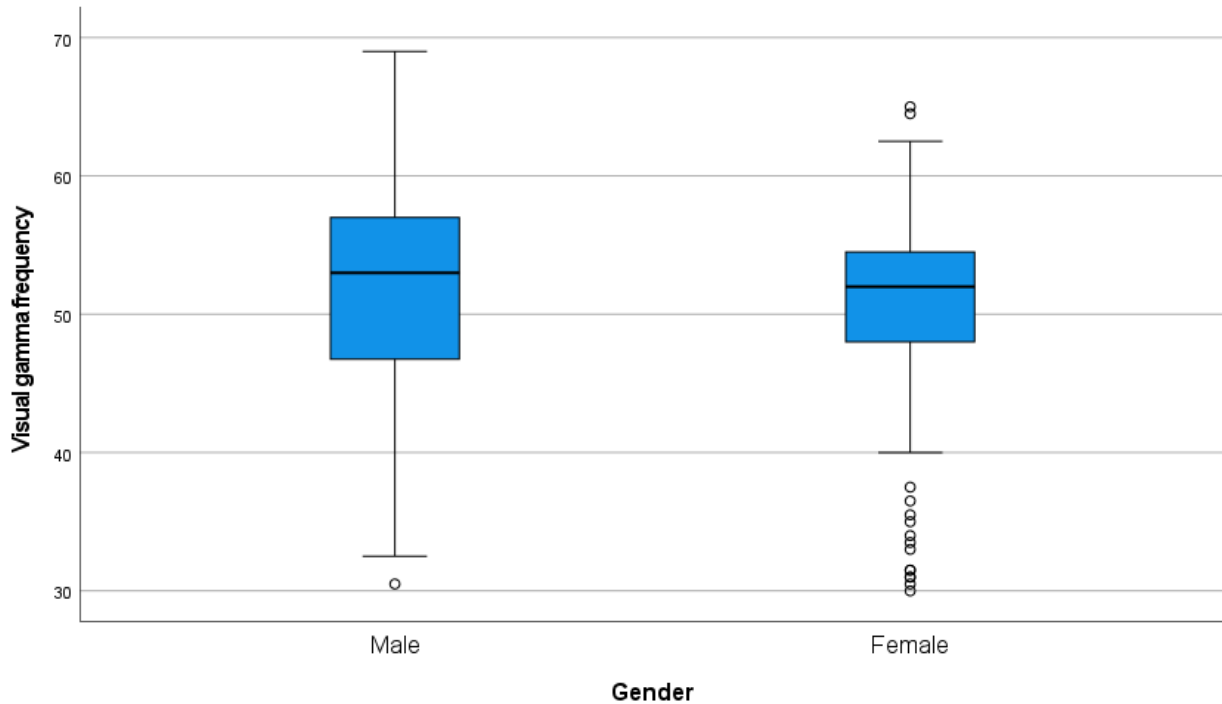


Figure 6.7. Boxplot showing the distribution of gamma frequency (Hz) scores for men and women. The horizontal lines represent the distribution quartiles, with the blue area representing the interquartile range.

6.4.3 Non-Negative Matrix Factorization-structural networks

Functional sub-networks have been successfully revealed here and in previous research using NNMF (Doherty et al., 2021; Messaritaki et al., 2021a; Phalen et al., 2019). Both functional and structural connectivity matrices projected in AAL space were available in the 100-Brains cohort. Structural connectivity matrices are more densely populated with connections than functional matrices. Therefore, part of the work in this thesis is to explore the application of NNMF to microstructural connectivity with the aim of revealing dominant microstructural sub-networks across participants, and also their relationships with the correlates of interest. In this chapter, to explore structure-local function relationships, gamma amplitude and frequency were investigated as predictors of a variety of structural NNMF components. Age and gender (and where appropriate Cohort) were included in the gamma models as covariates.

Streamline measures

The results of the regression models where amplitude and frequency were main predictors (with age, gender and cohort covariates) can be seen in Figure 6.8.

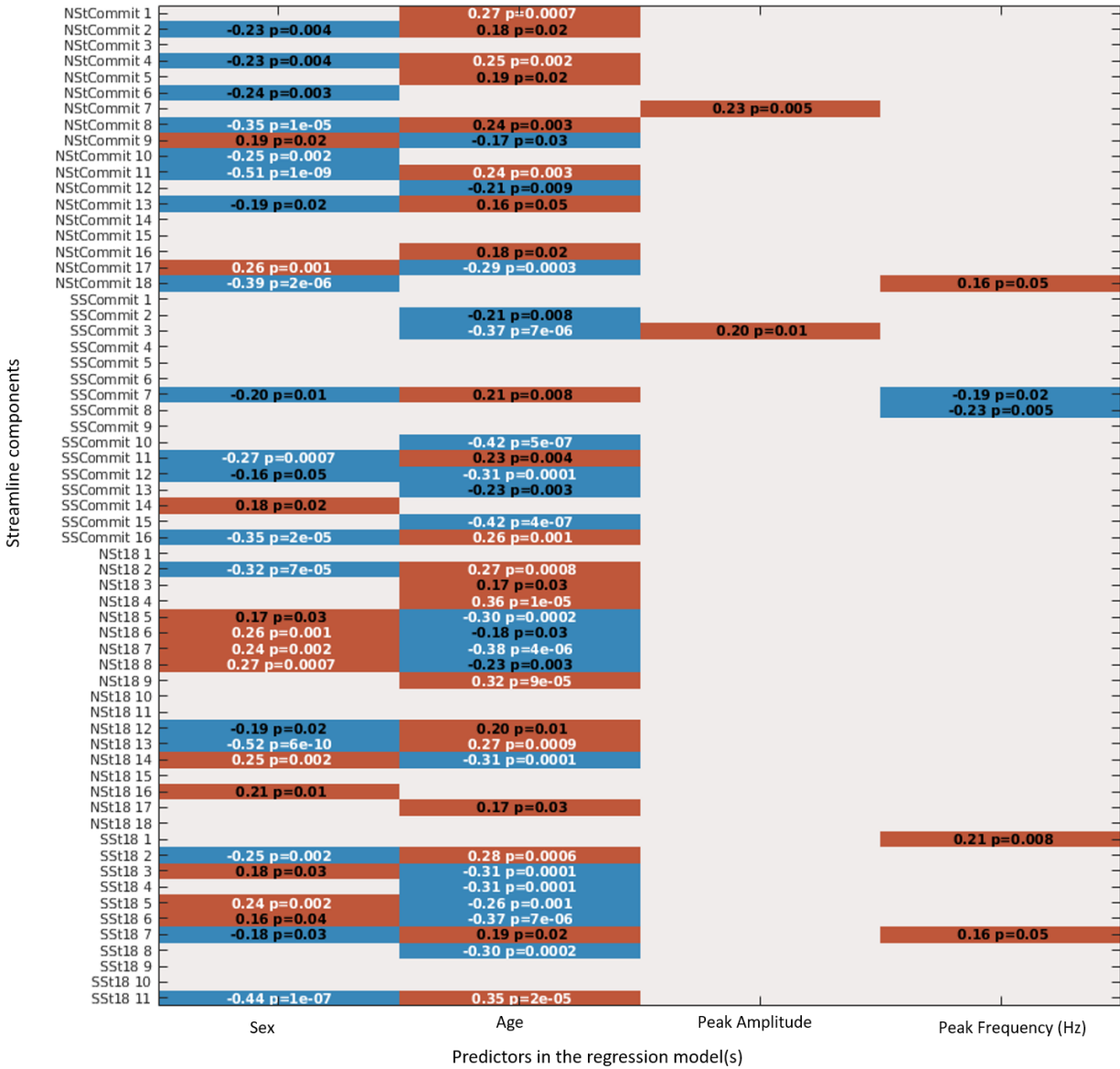


Figure 6.8. Streamlines NNMF connectivity relationships across gender, age, peak amplitude and peak frequency. The within component text shown the effect size (beta) and the p-value. Red boxes represent positive relationships. Blue boxes represent negative relationships. Text in white shows relationships which meet multiple comparison adjustment ($p < .05$), whereas text in black shows relationships significant at the uncorrected level ($p < .05$).

Peak gamma amplitude positively predicted two streamlines components, however these did not survive multiple comparisons adjustment. Peak gamma frequency positively predicted 3 streamlines components and negative predicted 2 others, but these also did not meet multiple comparisons adjustment. Both age and gender positively and negatively predicted many streamlines components. However, no clear patterns between measures derived with the standard thresholding approach or the COMMIT approach, can be seen.

Structural measures

NNMF was also applied to structural connectivity measures derived from the tractography and McDespot analyses. These were explored in regard to peak amplitude and peak frequency. Age and gender were included in the regression models.

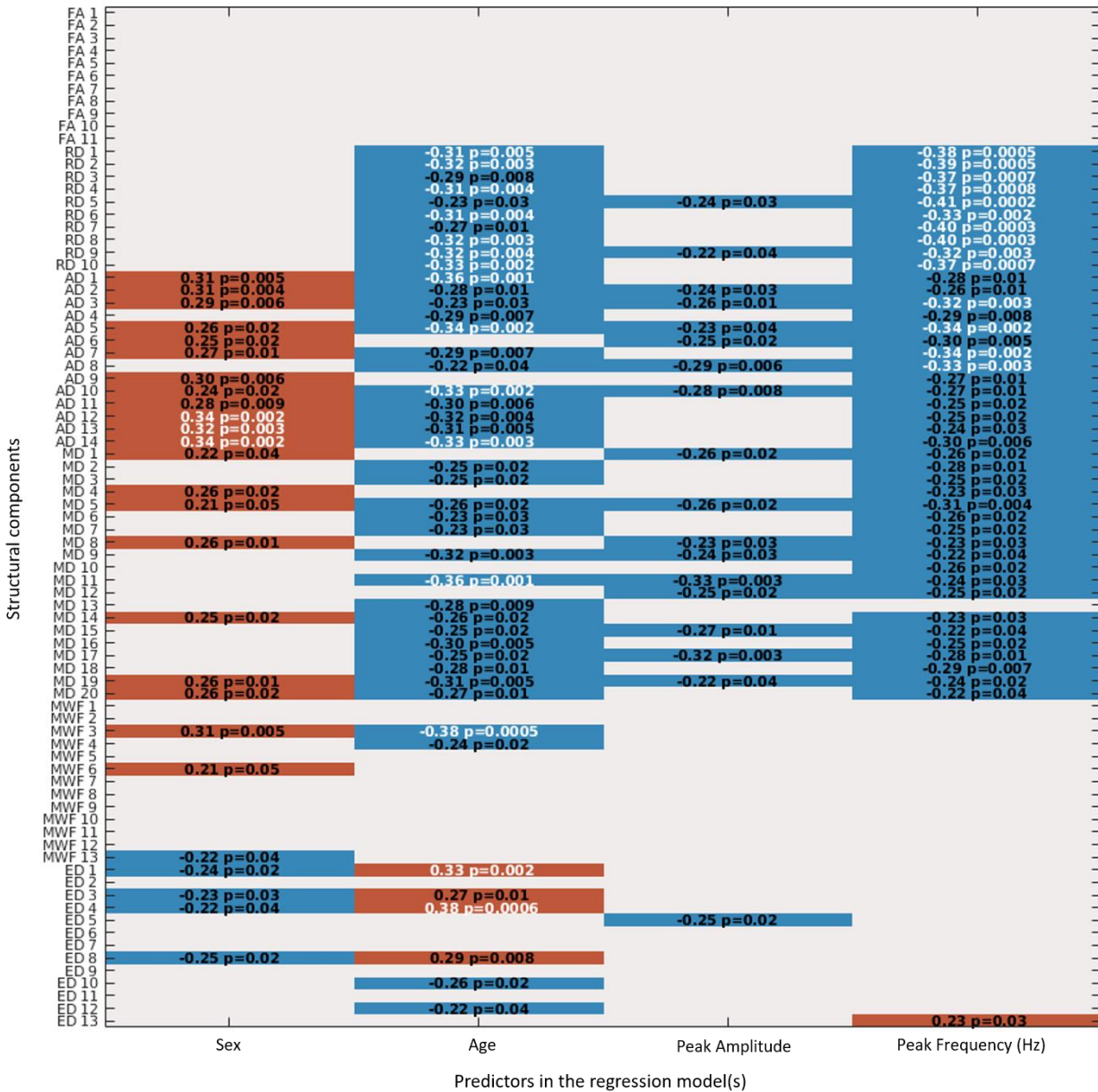


Figure 6.9. Top to bottom: FA, RD, AD, MD, MWF & ED NNMF connectivity components explored across gender, age, peak amplitude and peak frequency. The within component text shows the effect size (beta) and the p-value. Red boxes represent positive relationships. Blue boxes represent negative relationships. Text in white shows relationships which meet multiple

comparison adjustment ($p < .05$), whereas text in black shows relationships significant at the uncorrected level ($p < .05$).

Peak amplitude was negatively associated with different structural NMF components, though none of these relationships survived multiple comparisons adjustment. Peak frequency, however, was negatively associated with 10 RD components and 4 AD components, after adjustment. Peak frequency had no association with FA. In fact, none of the predictors had a relationship with FA.

Consistent with previous research suggesting that an effect of aging on diffusivity (Kumar, Chavez, Macey, Woo, & Harper, 2013a), age was negatively associated with AD, RD, MD and myelin component weightings. That both peak frequency and age significantly negative predict similar components could implicate a modulation effect between these variables. However, age was included as a covariate in the frequency regression model to account for variation in RD and AD associated with age. RD and AD components predicted by gamma frequency are plotted in Figures 6.10 and 6.11, respectively.

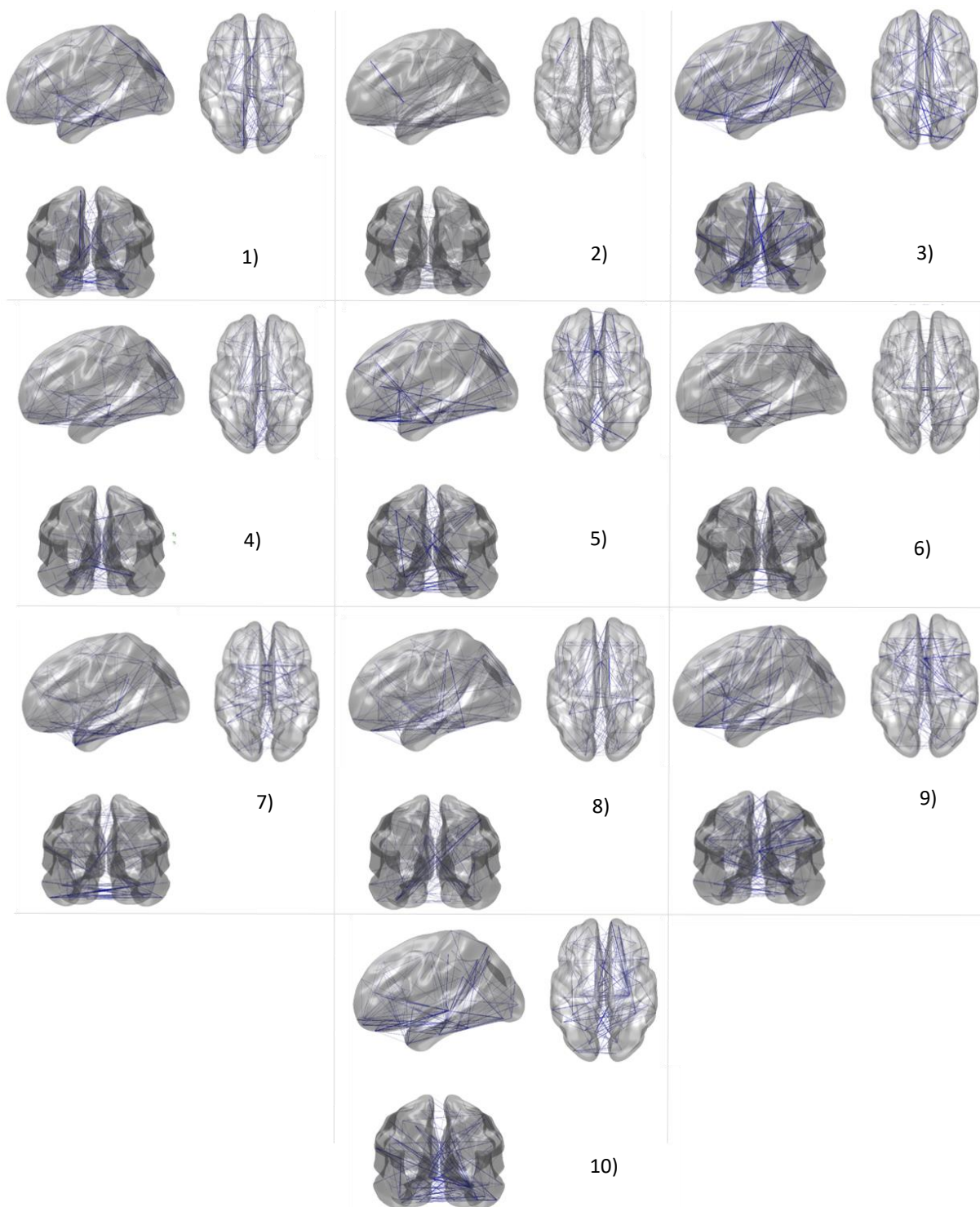


Figure 6.10. Shows the significant RD network components predicted by visual gamma frequency (right to left, 1-10). Blue lines represent a negative relationship between frequency and the network weightings.

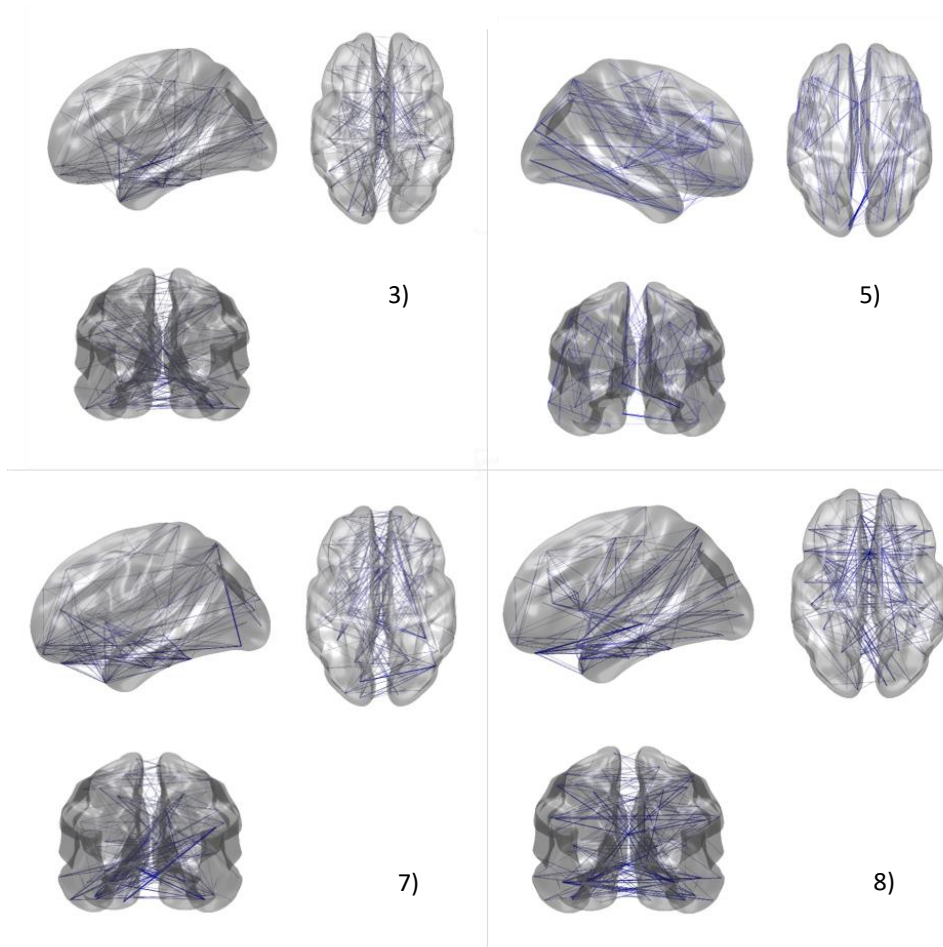


Figure 6.11. Axial diffusivity (AD) network components predicted by visual gamma frequency. Blue lines represent a negative relationship between frequency and the network weightings.

Gender significantly predicted 3 AD components after adjustment, however these results are interpreted with caution due to the gender differential in the sample.

Additional exploration of structure-function relationships

To further explore the gamma frequency relationships, node strength of connections in the VC was extracted (12 AAL areas). A regression model was built with gamma frequency, age and gender as predictors and visual node strength (summed), as the outcome variable, for both RD and AD visual connections. Gamma frequency did not significantly predict strength of visual RD connections ($b=3.482e-05$, $p=0.57$), nor strength of AD connections ($b= 4.867e-05$, $p=0.57$), suggesting the NNMF relationships were not driven by connections to or from the VC.

The spatial distribution of significant components, shown in Figure 6.10 and Figure 6.11, were widespread across the brain. To explore, therefore, whether the relationships between gamma frequency and RD, AD and MD components were driven by a global factor(s), the mean RD, AD and MD values were calculated across the structural 90 AAL nodes, per person, and used as the outcome in a regression model with gamma frequency and gender predictors. Gamma frequency did not predict global RD ($b=5.401e-07$, $p=0.06$), though this relationship was at trend, and did not predict global AD ($b=1.323e-07$, $p=0.61$), nor MD ($b=3.875e-07$, $p=0.13$), suggesting it was not a global effect driving the gamma frequency NNMF relationships. The RD relationship at trend could warrant further exploration.

Finally, to briefly explore relationships between global RSN functional connectivity and the structural NNMF components, average node strength across the AAL regions was calculated for each person in the alpha and beta bands and correlated with the RD and AD NNMF components. No relationships were found between alpha RSN connectivity and the structural components ($p>.05$). Average node strength in the beta band significantly positively predicted 10 RD components ($p<.05$), but these relationships did not meet multiple comparison correction. Average node strength in the RSN beta band also predicted 7 AD components ($p<.05$), but these also did not meet multiple comparison adjustment. These results suggest there might be a global RSN functional connectivity relationship, but further investigation is needed.

6.5. Discussion

In this chapter, the extent to which local and global functional oscillatory measures, extracted with MEG, are related, was investigated. At the edge level, no significant relationships were found between local visual gamma amplitude and alpha and beta connectivity measures in the resting-state, nor between visual gamma frequency and alpha and beta connectivity measures. However, when exploring resting-state subnetworks derived with NNMF, visual gamma amplitude was found to negatively predict one bilateral occipital alpha network. To explore whether this effect could also be observed in within-task data visual gamma amplitude was correlated with edge level connectivity derived from the visual gamma data. In the same direction, gamma amplitude was negatively correlated with alpha connectivity, but connections did not survive multiple comparisons correction.

The gamma-alpha finding is contra-prediction in as far as increased gamma was correlated with *suppressed* long-range alpha. However, it supports recent work by Hirschmann and colleagues who found a relationship between induced gamma activity in VC and brain states in the resting-state below 35Hz, using HMM (Hirschmann et al., 2020a). Previously, phase and amplitude coupling of gamma and lower frequency oscillations has been shown both within (Bonfond & Jensen, 2015; Michalareas et al., 2016a) and between brain regions (Bowyer, 2016; Siegel et al., 2012). Results such as these suggest there is an interaction between visual gamma and long-range connectivity which might support local-global communication in the healthy brain, however providing a mechanistic explanation for such findings is non-trivial.

Bonfond and Jensen (2015) found coupling between gamma amplitude and the phase of alpha, and that higher alpha amplitude was associated with lower gamma amplitude in the alpha trough. These observations were interpreted as a gating mechanism whereby alpha modulates cortical excitability in V1 (Bonfond & Jensen, 2015). The relationship between V1, probed with the gamma paradigm, and occipital alpha connectivity, could provide support for this theory as the correlational design means no directionality can be assumed. That being said, recent research using a frequency tagging paradigm has suggested that alpha oscillations do not modulate V1 but have a downstream role, localised in the occipito-parietal sulcus (Zhigalov & Jensen, 2020).

In other research, gamma has a role in encoding local information in a feedforward fashion (Donner & Siegel, 2011; Fries et al., 2002; Shaw et al., 2020), whereas slower alpha and beta oscillatory connectivity is thought to have a role in feedback and large-scale integrative processes (Bastos et al., 2015b; Michalareas et al., 2016a; Siegel et al., 2012). In this regard, alpha and gamma oscillations have distinct, but interlinked roles in visual circuitry, that facilitate perception via the updating of prediction errors (Alamia & VanRullen, 2019; Michalareas et al., 2016a) and could be reflected in the association between local gamma amplitude and long-range alpha suppression shown here.

Beyond the driving mechanism, this is an important finding considering clinical cohorts show disturbances in both induced visual gamma and amplitude connectivity MEG measures (Friston, Brown, Siemerikus, & Stephan, 2016; Grent-'t-Jong et al., 2016; Koelewijn et al., 2017; Phalen et al., 2019; Shaw et al., 2020). The relationship between alpha and gamma oscillations in the occipital lobe might then be a good target for investigation in clinical groups.

Relationships between visual gamma amplitude and frequency and structural networks, derived with NNMF, were also explored. No notable relationships between gamma amplitude and any structural measures were found. Interestingly, however, visual gamma frequency was negatively associated with several RD and AD network components. These relationships were robust to multiple comparisons adjustment.

Further exploration of the structure-function relationships suggests the gamma frequency relationships were not driven by a global effect. This is reassuring, particularly regarding AD, which has been previously shown to change with age (Kumar et al., 2013a). For that reason, both age and gender were included as covariates in the regression models reported here. Tangentially, a relationship between global functional connectivity in the resting-state and structural connectivity NNMF components may also exist in a positive direction. However, due to the aims of this chapter this was a limited exploratory step, which could be pursued elsewhere.

Interpretation of white matter measures requires some caution because diffusivity parameters are based on tractography performed at the voxel level (Jones, Knösche, & Turner, 2013). One

problem, for example, is values based on the diffusion tensor can be compromised by crossing of white matter fibres. However, despite this, increased RD and reduced AD values are commonly taken to reflect demyelination and reduced axonal integrity, respectively, in light of a series of microstructural studies which induced ischemia and demyelination in animals (Song et al., 2003; Sun et al., 2006). In this view, a reduction in RD could reflect improved myelin integrity, which could support the healthy excitability of the cortex.

Work using PING informed Dynamic Causal Modelling (Shaw et al., 2017a; Sumner, Spriggs, & Shaw, 2021), has shown that the amplitude of the MEG induced gamma response is associated with coupling strength between inhibitory neurons and layer 2/3 superficial pyramidal cells, supporting the idea that gamma oscillations reflect local inhibitory processes (Muthukumaraswamy et al., 2015b). Theoretically, the frequency of the oscillation is under the control of the interneurons, within the cortical laminae, and recorded from superficial pyramidal cells. Therefore, connections between superficial interneurons (SI) and superficial pyramidal cells (SP), in directions SI->SP, SI->SI and SP->SI, are implicated in local gamma circuitry (Sumner et al., 2021). The superficial pyramidal to superficial pyramidal (SP->SP) connection is also inhibitory and adds to the frequency response. While gamma is, therefore, an excellent probe of intrinsic local connectivity, exploring specific DCM parameters in relation to alpha connectivity would be particularly interesting in future.

Pharmacological studies also suggest that gamma frequency is under the control of local GABAergic circuitry, as the administration of substances, such as tiagabine (a GABA reuptake inhibitor), reduce amplitude and increase gamma frequency (Shaw et al., 2017b). This is interesting in the context of the structural findings in this chapter. In taking gamma frequency as a proxy for cortical excitability in VC, whereby altered gamma frequency represents altered GABAergic inhibition, the following postulations may be made, bearing in mind AD reflects axonal integrity and RD reflects myelin density (Winklewski et al., 2018) :

- 1) Altered inhibition in local circuitry in VC (increased frequency) is related to reduced global axonal integrity (AD↓) in white matter networks.

2) Altered inhibition in local visual gamma circuitry (increased frequency) is related to increased myelin integrity (RD↓) in white matter networks.

While it must be emphasised that these are postulations, the potential structure-function relationships are interesting in the context of existing Transcranial Magnetic Stimulation (TMS) research, which has shown an association between cortical excitability and structural connectivity in stroke patients (Guder et al., 2020).

The second postulation is less intuitive as increased myelination supports the transmission of neural signals, which might be expected to support balanced Excitatory-Inhibitory functioning. Considering the at-trend relationship between gamma frequency and average RD values, a global effect could be at play and further exploration is warranted. A final comment on the gamma and diffusivity findings is that gamma frequency was also negatively correlated with MD components, which suggests there may be general a diffusivity effect. The extent to which mean diffusivity is physiologically informative, however, remains to be established.

Regarding the covariates, an unexpected finding was that men had a significantly higher peak frequency than women, suggesting men and women may exhibit differences in local processing in VC. A previous study, which used the same paradigm to induce gamma oscillations, failed to find any gender differences in amplitude or frequency (Muthukumaraswamy et al., 2010). Evoked studies, conversely, have shown higher amplitude of Event-Related Potential responses (ERPs), in women (Guillem & Mograss, 2005; Orozco & Ehlers, 1998). To the authors knowledge this a novel finding, however any conclusions are made with caution, as there was a much higher proportion of women to men in the sample and thus the response distributions differed by group.

Limitations and future directions

There were some additional considerations and limitations in this chapter. While both the visual gamma paradigm and the resting-state connectivity are considered to capture oscillatory connectivity at the local and global level, these measures provide a static snapshot of dynamic

processes. In view of the recent work by Hirschmann and colleagues these relationships might be further explored with a dynamic approach.

Moreover, the visual gamma response is variable between individuals (Muthukumaraswamy et al., 2010). The analyses presented here were across participants with the loss of some information associated with the error term in the General Linear Model. However, these differences could be exploited in future work which might involve investigating local – global relationships on a participant level, to better explore individual differences in connectivity. Additionally, within-gamma task local-global relationships might also be further explored with NNMF, in view of the relationship found in the resting-state.

In view of the attention literature, a measure of alertness might have also been useful in this analysis. Alertness is associated with alpha-band suppression (Clayton et al., 2015; Clayton, Yeung, & Cohen Kadosh, 2018) and naturally some participants will be more engaged than others. It is feasible, therefore, that those who were more alert in the resting paradigm were also more compliant in the gamma task. Spatial attention has been shown to have a gamma boosting effect (Magazzini & Singh, 2018) which may contribute to the alpha-gamma relationship seen in this chapter. Collecting a simultaneous measure of attention in future would provide a means for delineating these effects.

Furthermore, structural measures were projected onto an AAL map to make structure-function comparisons in the same atlas space, as has been conducted in previous research (Messaritaki et al., 2021a). However, by representing white matter connections in this way it is acknowledged that some spatial tractography information is lost. Furthermore, structural connectivity matrices, being static white matter measures, are densely populated with connections in comparison to the dynamic functional connectivity matrices. Thus, applying the NNMF algorithm with the same thresholding procedures to both structural and functional data, resulted in less constrained structural networks than functional networks, making the spatial characteristics of the components challenging to interpret. In future, it would be interesting to mask the structural connectivity matrices with the functional NNMF networks prior to investigating the correlates of interest. This would provide a spatial constraint to the structural networks.

In conclusion, this chapter has investigated the relationship between local visual gamma oscillations and global functional alpha and beta connectivity in 183 healthy individuals. At the functional level, visual gamma amplitude was negatively associated with an occipital resting-state network. This is interesting considering gamma-alpha coupling phenomena previously observed. Structural connectivity, in the same participants, was also explored in relation to the local oscillatory measures, which revealed a negative relationship between visual gamma frequency and AD and RD network components. Postulations are made about these findings; however, additional research is required.

Chapter 7. Schizotypy and global functional and structural networks

7.1 Rationale

Schizophrenia can be thought of as a disorder of dysconnectivity (Friston & Frith, 1995; Friston, Brown, Siemerkus, & Stephan, 2016). Identifying dysconnectivity markers in those at-high-risk and prior the onset of acute psychosis has fundamental implications for our understanding of the continuity between health and schizophrenia as well as the prevention of schizophrenia disorders. Individuals with Schizotypal Personality Disorder (SPD) and those who score highly on schizotypy traits measures, have ‘schizophrenia-like’ experiences, albeit to a far lesser degree. Individuals with high schizotypy, though clinically normal, are more likely to develop schizophrenia (Barrantes-Vidal, Grant, & Kwapil, 2015). Therefore, schizotypy makes an excellent candidate for studying clinical risk and brain connectivity in the healthy population.

7.2 Introduction

Schizophrenia is a multifaceted and debilitating disorder, facets of which remain poorly understood and treated. Nevertheless, the view of schizophrenia as a disorder of functional and structural dysconnectivity has become well established (Friston & Frith, 1995; Friston, Brown, Siemerkus, & Stephan, 2016). A recent meta-analysis of fMRI resting-state studies (patients and controls, $N < 2,500$, seed based) found hypoconnectivity in the auditory network (left insula), core network (right superior temporal cortex), default mode network (right medial prefrontal cortex, and left precuneus and anterior cingulate cortices), self-referential network (right superior temporal cortex), and somatomotor network (right precentral gyrus) in patients (Li et al., 2019). Frontal and occipital reductions and altered network characteristics, investigated with graph theory, have also commonly been reported (Karbasforoushan & Woodward, 2013).

Patterns of aberrant functional connectivity differ with disease stage (Anticevic et al., 2014; Grent-'t-jong et al., 2018), genetics (Kirov, Grozeva, et al., 2009; Purcell et al., 2009) and imaging analysis (Karbasforoushan & Woodward, 2013; Yu et al., 2013). An example of the latter is that more long-range reduced connectivity is found with seed-based fMRI methods, compared with ICA methods (Yu et al., 2012).

Characterisation of neural oscillations, using MEG, affords a rich electrophysiological picture of connectivity differences in schizophrenia (Bowyer et al., 2015; Cetin et al 2016; Hinkley et al., 2011; Houck et al., 2017; Kim et al., 2014; Robinson & Mandell, 2015; Sanfratello, Houck, & Calhoun, 2018; Zhang et al., 2015). Relative to MRI, MEG research remains in its infancy, with hypo- and hyper-connectivity being revealed in patients (Alamian et al., 2017a).

Several studies have investigated oscillatory coherence; a frequency domain measure that quantifies coupling in terms of amplitude and phase (Bowyer et al., 2015, Kim et al., 2014, Hinkley et al., 2011). Hinkley and colleagues (2011), for example, found decreased connectivity in left PFC and right superior temporal cortex, whereas increased connectivity was observed in left extrastriate cortex and the right inferior PFC in the alpha band. Moreover, Bowyer and colleagues (2015) found increased amplitude connectivity in patients with schizophrenia in the right inferior frontal lobe, left superior frontal lobe, right middle frontal lobe and right cingulate, whereas Kim and colleagues (2014) found decreased coherence in patients between the posterior cingulate cortex and medial PFC in the gamma band.

In patients, oscillatory disruptions across the frequency bands have been related to positive, negative, and cognitive symptoms, with both positive and negative trends being found (e.g., Chen et al., 2016; Fehr et al., 2001, 2003; Kim et al., 2014; Spencer et al., 2008; Sperling et al., 2002; Sperling et al., 2003). Importantly the study of oscillatory activity may provide a window into the underpinnings of persistent cognitive and negative impairment in psychosis which is, at present, unclear.

In addition to the aforementioned functional cortical impairments, numerous studies have shown individuals with schizophrenia have structural white matter abnormalities, revealed with Diffusion Tensor Imaging (DTI) methods. The consistency and clarity of these findings, however, is limited. One finding, that does seem to be consistent, is that patients have increased Radial Diffusivity (RD), within white matter tracts (Joo et al., 2018; Parnanzone et al., 2017). RD is a measure of diffusion perpendicular to the direction of tracts, and has been considered a marker for myelin density (Winklewski et al., 2018), with increased RD representing

demyelination. Due to the difficulty of co-registering histology to DTI findings, however, this theory is yet to be fully verified (Winklewski et al., 2018). Nonetheless, a recent paper by Joo and colleagues (2018), found increased RD in the left thalamo-occipital tract, right uncinate fascicle, the right middle longitudinal fascicle (MDLF), and the right superior longitudinal fascicle, in patients (Joo et al., 2018).

Other commonly reviewed white matter metrics are Fractional Anisotropy (FA), of the diffusion tensor, which is a measure representing directionality of water diffusion (with values varying from 0 for isotropic diffusion to 1 for anisotropic diffusion), and Axial Diffusivity (AD), which represents the magnitude of water diffusion parallel to white matter tracts. Both have been considered to reflect axonal integrity (Leow et al., 2009; Winklewski et al., 2018), however, the aforementioned measures should be interpreted with caution because they are measured at voxel-level and are not specific to one type of change in the white matter tracts (Jones et al., 2013). In schizophrenia, numerous patient groups have been shown to have decreased FA values (Parnanzone et al., 2017), whereas increased FA has also been found locally (De Erausquin & Alba-Ferrara, 2013), and in early onset patients (Canu, Agosta, & Filippi, 2015). In 22q.11 deletion carriers, who have significant increased risk of developing schizophrenia, both reductions in FA and AD have been found (Kikinis et al., 2012).

As with functional impairments, white matter abnormalities appear to worsen with disease stage (Biase et al., 2017a; Canu et al., 2015), with chronic patients displaying more widespread network disruptions than recent onset patients; where, for example, reductions in connectivity have been shown in the anterior corpus callosum (Biase et al., 2017b). The extent to which structural and functional dysconnectivity in schizophrenia are related is also an increasingly popular question (Cabral et al., 2013; Pettersson-Yeo et al., 2010). Intuitively, functional dysconnectivity could be the result of impairments in the forming of white matter hubs or tracts during development (Fornito & Bullmore, 2015). In general, however, research has failed to establish a link between functional alterations and structural typology in patients (Cabral et al., 2013; Pettersson-Yeo et al., 2011), suggesting functional and structural techniques reveal different neuropathology in schizophrenia.

Notably, long-range oscillatory functional connectivity is reliant on excitatory-inhibitory (E-I) synaptic balance, via neurotransmitters (Alamian et al., 2017b; Uhlhaas, 2013). Therefore, even subtle changes in the temporal measures, including Long-Range Temporal Correlations (LRTCs) within the brain could be associated with significant cognitive impairments, even if there are no visible structural changes.

Beyond diagnosis status, abnormal connectivity is also found in those at clinical high risk (CHR) of psychosis. For example, with fMRI, Du and colleagues (2018) found both CHR and early onset schizophrenia groups showed significant differences, primarily in DMN, salience, auditory-related, visuospatial, sensory-motor, and parietal resting-state networks, compared with controls. CHR individuals usually show some attenuated positive symptoms and may score highly on other risk areas such as lifestyle and genetics. Identifying neural markers in individuals before the onset of acute psychosis could be fundamental to the prevention of disease progression and highlights the importance of studying ‘at-risk’ individuals.

In the dimensional approach (Claridge & Beech, 2010; Eysenck & Peck, 1962; Liddle, 1987), schizophrenia symptomology is viewed as a continuum, from asymptotology or rare symptoms in the normal population, through schizotypy traits, to acute psychosis (Esterberg & Compton, 2009). Schizotypy is associated with proneness to schizophrenia (Barrantes-Vidal, Grant, & Kwapil, 2015), and refers to the presence of schizophrenia-like personality characteristics and experiences, such as non-delusional ideas of reference, magical thinking, and odd perceptual experiences. Given that family members of those with schizophrenia have been shown to have high schizotypy traits (Vollema, Sitskoorn, Appels, & Kahn, 2002; Yarialian et al., 2000), the genetic contribution and underlying aetiology between schizophrenia and schizotypy is thought to be similar.

One advantage of studying schizotypy is that participants are usually drug-naïve due to the trait being distributed in the healthy population. Thus, investigations are free from confounds such as anti-psychotic medication exposure and medical co-morbidities known in affected individuals, while still providing important insight into Schizophrenia Disorders (Vollema et al., 2002).

Evidence suggests that connectivity deficits found in schizophrenia extend to high schizotypy individuals. A recent fMRI study found resting-state connectivity to be impaired in high-schizotypy individuals across temporal-occipital-striatal networks (Waltmann et al., 2019). Zhu and colleagues also found reduced connectivity between the bilateral precuneus and parahippocampal gyrus in Schizotypal Personality Disorder (SPD), with a negative association between connectivity and schizotypy scores (Zhu et al., 2017). In a task-based MEG study, oscillatory phase-locking-factor in the gamma and beta band has also been shown to be reduced in fronto-central and fronto-occipital areas, during working memory (Koychev, Deakin, Haenschel, & El-Dereby, 2011a). Moreover, in line with the reduced motor-sensory beta rebound effect in schizophrenia (Gascoyne et al., 2021; Robson et al., 2016), Hunt (2018), found a negative correlation between schizotypy scores and MEG beta rebound on a visuomotor task in a sample of 160 participants. Variance in this study was driven by scores on the disorganisation and interpersonal factors which are known to severely impact quality of life (Pinikahana, Happell, Hope, & Keks, 2002).

Until recently, few DTI studies have investigated schizotypy, *per se*. SPD individuals have been shown to have white matter abnormalities in the temporal lobe (Hazlett, Goldstein, & Kolaitis, 2011), and lower FA in the corpus callosum (Lener et al., 2015). Studies, specifically looking at schizotypy, have found increased white matter connectivity probability between the right insula and the right middle frontal gyrus, between the left precuneus and the left angular gyrus (the DMN) (Wang et al., 2020), reduced FA in the anterior corona radiata, (Wang et al., 2020), increased FA in the in the left arcuate fasciculus (Volpe et al., 2008), and FA reductions in fronto-temporal white matter tracts (Nelson et al., 2011). Additional research could further clarify these findings.

7.2.1 Aims and hypotheses

The aim of this chapter was to explore how schizotypy, as a clinical risk factor for schizophrenia, affects functional resting-state connectivity and structural white matter connectivity. At the time of the analysis no other studies have investigated schizotypy and MEG amplitude-amplitude

connectivity⁷, alongside structural connectivity measures, in a large sample covarying for age and gender.

A linear regression model, employed in the analysis here, is a powerful tool for analysis of continuous data, as all subjects can be included (subject to outliers etc.). Based on previous findings (Koychev, Deakin, Haenschel, & El-Deredy, 2011b; Williams, 2018), it is expected that schizotypy will predict reduced functional connectivity in the alpha and beta band across parietal- precuneal and occipital areas.

Furthermore, it is expected that schizotypy will be associated with white matter abnormalities. In view of papers by Parnanzone, Joo and colleagues, it is expected that schizotypy will negatively predict FA connectivity and positively predict RD (Joo et al., 2018; Parnanzone et al., 2017). Regarding the other WM measures, due to the mixed nature of previous findings in schizophrenia and schizotypy, the directionality of abnormalities is to be explored.

¹ A subset of the functional data (MEG-Partnership & 100-Brains, N=183), has been previously analysed using a between groups method without covariates, by Dr Gemma Williams. High and low schizotypy groups were formed by taking the top and bottom 20% of schizotypy values (H n=33, L n=33). Resting-state connections that met the signal to noise threshold (top 20%), were compared between groups. The analysis revealed significantly reduced left precuneus -paracentral lobule alpha connectivity in high schizotypy individuals. Reduced parieto-parietal beta connectivity was also suggested but did not reach significance.

7.3 Method

7.3.1 Participants

Participants were recruited as part of the '100-Brains' and 'MEG-Partnership' studies. Participants were screened and excluded based on psychiatric illness history and use of psychoactive drugs. Of the 183 recruited, 168 had completed the Schizotypal Personality Questionnaire (SPQ-Raine & Raine, 1991), and were included in the analysis. The SPQ is a self-rated questionnaire consisting of 74 items that fall under nine sub-scales: ideas of reference, social anxiety, odd beliefs/magical thinking, unusual perceptual experiences, eccentric/odd behaviour and appearance, no close friends, odd speech, constricted affect and suspiciousness/paranoid ideation.

Table 7.1. Demographics

| | N | Mean(SD) | Range | Ratio |
|------------|-------------------|-----------------|--------------|--------------|
| Schizotypy | 168 | 12.04(9.83) | 43(0-43) | - |
| Age | 183 | 24.5(5.38) | 37(18-55) | - |
| Gender | 183 (123F/60M) | - | - | 0.48 M:F |

Schizotypy is naturally a left skewed measure as in the normal population individuals will often report no schizotypy traits. Logged schizotypy scores were also considered with no notable difference to the subsequent analyses' outputs.

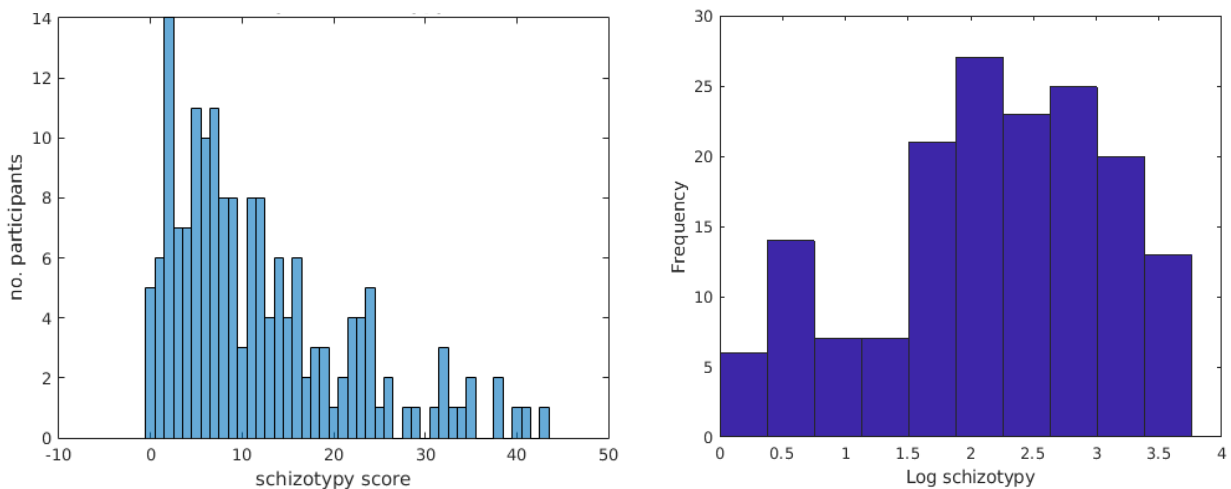


Figure 7.1. Left shows a histogram of the schizotypy scores. Right shows a histogram of logged schizotypy scores.

7.3.2 *Resting-state analysis*

MEG connectivity analyses were the same as those described in Chapter 4, but are summarised here. Resting-state MEG recordings were collected at 1200Hz using a CTF275 MEG system. Synthetic third-order noise cancellation was applied. Participants were oriented upright and completed a 5-minute eyes open paradigm, where they were asked to fixate on a red fixation point. MRI, T1-weighted anatomical images were collected on a 3T GE scanner and used for co-registration.

Pre-processing steps were completed in DataEditor. After down sampling to 600Hz, datasets were epoched into 2-second trials and then visually inspected for ocular and muscular artefacts. Any trials containing artefacts were discarded. Manual co-registration was completed on the MR image using photographs of the fiducial marks made on the participants during the MEG recording.

Whole-brain connectivity analysis was performed in Fieldtrip (2019), using LCMV beamforming source localisation and amplitude - amplitude coupling pipelines (Koelewijn et al., 2017; Routley, Singh, Hamandi, & Muthukumaraswamy, 2017) providing connectivity measures across six frequency bands (delta 1-4Hz, theta3-8Hz, alpha8-13Hz, beta 13-30Hz, low gamma 40-60Hz and high gamma 60-90Hz). Based on the Automatic Labelling Atlas (AAL) (Tzourio-Mazoyer et al., 2002) 90 nodes were selected for analysis. Beamforming was completed using a 6mm grid and single shell forward model (Nolte, 2003); a vector norm normalisation was applied to weights in each frequency band separately (Hillebrand et al., 2012), and a MNI inverse-warping procedure was adopted to ensure source grid consistency across participants. A virtual time course for each region was selected. This involved keeping the time-courses with the greatest temporal standard-deviation in each of the 90 AAL regions.

To adjust for potential spurious correlations between virtual sensor data, the 90 time-series were orthogonalized (Colclough et al., 2015). Amplitude envelopes were calculated using a Hilbert transform. A median filter and edge trimming were applied to account for any transient spiking and edge effects (first 2 and last 3 samples removed).

Finally, within-frequency band correlations between amplitude envelopes, across the AAL regions, were calculated and a Fisher transform applied, generating a connectivity matrix of variance-normalised Z-scores for each frequency band. An across-frequency band connectivity matrix was also created by taking the square root of the summed, squared connectivity matrices in each frequency band.

7.3.3 Statistical analysis

Functional edge-level measures

Connectivity matrices were z-scored by participant (demeaned, unit variance) to account for possible across-group sources of variance such as differences in data quality between recordings. As a result, the value of each connection is a strength of connectivity (Z-scored correlation) in relation to the mean. Valid connections were selected by ranking each of the connections by strength for each participant and then discarding the poorest 80% of consistently ranked connections across the whole group.

A linear regression ($p < 0.05$, uncorrected) was then performed on the valid connections in each frequency band and the combined map using schizotypy score as the main predictor and age and gender as covariates. To adjust for multiple comparisons a 10,000 iteration randomisation test with omnibus thresholding was also performed ($p < 0.05$). To assess generalisability a 5000-iteration resampling procedure was performed to construct a 95% confidence interval for connections per frequency band. Mean connection strength is a measure of the strength of amplitude- amplitude connectivity at each of the 90 AAL nodes, averaged across nodes per subject and was also visually explored.

Non-Negative Matrix Factorization- Functional

Consistent sub-network patterns were derived from resting-state data using a Non-Negative Matrix Factorization procedure (NNMF method and results as described in Chapter 5). Variance across connections, across subjects, is captured in a method like Principal Components Analysis (PCA), revealing independent connectivity patterns (components) at improved signal-to-noise ratio. As long-range alpha and beta connections are of interest in this thesis, focus was given to alpha and beta connectivity, thereby reducing the chance of revealing spurious relationships.

Alpha and beta MEG connectivity has been shown to be more robust over subjects than connectivity in other frequency bands (Colclough et al., 2017; Godfrey & Singh, 2021). 11 components were derived in the alpha band and 9 in the beta band.

Statistical analysis-NNMF

NNMF generates spatial components which together comprise the observed functional connectivity (strength of connectivity) for the group of participants. Component weightings represent the contribution of that participant to a given network for that individual. Different components were generated for each frequency band. A regression model with schizotypy as the main predictor and age and gender covariates, was generated for each of the components. A Bonferroni adjustment was used to control for multiple comparisons in each regression model. The Cooks distance outlier rejection procedure, which rejects observations, in this case participants, from the regression model on the basis of residuals, was applied (set to $3 \times \text{mean}$).

7.3.4 Structural analysis

Structural connectivity measures were derived by Dr Eirini Messaritaki (Messaritaki et al., 2021a), details of which are summarised here. The same AAL labeling atlas (90 cortical and subcortical regions) was used to define structural regions. This allowed the structural network to also be represented as 90×90 symmetrical matrices, for each participant.

MRI data acquisition and pre-processing

All MRI data were acquired on a GE Signa HDx 3T scanner (GE Healthcare, Milwaukee, WI). T1 images were acquired with a three-dimensional fast spoiled gradient and downsampled to 1.5-mm isotropic resolution.

Diffusion weighted MRI data were acquired with a peripherally cardiac-gated sequence with $b = 1,200 \text{ s/mm}^2$, $TR = 20 \text{ s}$, $TE = 90 \text{ ms}$, isotropic resolution of 2.4 mm, zero slice gap, $FOV = 230 \text{ mm}$. Diffusion data were co-registered to the T1. Corrections for head movement and eddy current distortions were made. Free-water correction was also conducted.

mcDESPOT data (which can provide myelin measures) were acquired using multicomponent-driven equilibrium single pulse observation of T1 and T2 (Deoni, Rutt, Arun, Pierpaoli, & Jones, 2008). Images for each participant were linearly coregistered to a spoiled gradient recall (SPGR) image, to correct for subject motion. Nonbrain tissue was removed using a mask computed with the BET algorithm (Smith, 2002). Registration and brain masking were conducted with FSL (Jenkinson et al., 2012).

Tractography analysis

White matter tracts can be represented as connections, or edges, in a structural network. Tractography was performed on the DTI data, using the streamline algorithm in MRtrix 3.0 (Dhollander et al., 2016). White matter tracts were localised using a WM mask generated from the T1-weighted images using FSL fast (Jenkinson et al., 2012). The minimum and maximum tract lengths were 30 and 250 mm, respectively.

Streamline selection- Threshold Vs COMMIT methods

Historically, the minimum number of streamlines that would allow us to assume that a tract has been reliably reconstructed has been selected arbitrarily, limiting the quantitative nature of streamline measures (Daducci et al., 2015). The COMMIT method (Daducci et al., 2015) is a data-driven alternative. Instead of rejecting tracts reconstructed with a number of streamlines lower than an arbitrary threshold, it rejects any streamlines that are not consistent with the overall diffusion signal in the diffusion-weighted images, as described in Chapter 5. For that reason, in addition to connectivity matrices derived using the COMMIT method, a standard thresholding approach was also followed. For that, any tracts reconstructed with fewer than 18 streamlines were discarded. The threshold of 18 was chosen so that the thresholded matrices had the same sparsity as the COMMIT-derived matrices, to avoid the sparsity of the matrices being a confound in our analysis.

mcDESPOT analysis

A mcDESPOT algorithm was used to detect the fast (water constrained by myelin), and slow (free-moving water in intra- and extracellular space), elements of the T1 and T2 times, and a nonexchanging free-water component (Deoni et al., 2013). The fast volume fraction was taken as

a map of the myelin water fraction. The ratio of myelin-bound water to total water was calculated, which is the myelin volume fraction (MVF). A MRtrix function (tcksample), was used to assign a proportion of the MVF to each streamline, in each tract. This measure was averaged over its streamlines, providing a myelin-weighted value (MM), for each tract.

The matrices that resulted from these procedures were normalised by dividing by the largest value of each matrix, so that, within any given matrix, the values range from 0 to 1. Self-connections (diagonals) were set to zero.

As described in Chapter 6, the structural measures that resulted are:

White matter tractography DTI measures

- Number of streamlines (NST), is the number of reconstructed streamlines, subject to the threshold of 18.
- Standardised number of streamlines (SST), is the number of reconstructed streamlines at threshold 18, divided by the length of the tract.
- Number of streamlines (NSC), is number of streamlines in the tracts as selected by the COMMIT method described above.
- Standardised number of streamlines (SSC), is number of streamlines within a tract divided by the length of the tract, selected by the COMMIT method.
- Fractional Anisotropy (FA), is a measure of the anisotropy in the diffusivity of water molecules calculated from three eigenvectors. An isotropic tensor would have equal eigenvectors.
- Radial Diffusivity (RD λ_{\perp}) is a measure of water diffusion perpendicular to the direction of the tracts.
- Axial Diffusivity (AD λ_{\parallel}) is a measure of water diffusion parallel to the direction of the tracts.

mcDESPOT measures

- Myelin Water Fraction (MM), measures water diffusivity within the myelin giving an indirect measure of myelin density in the voxels including tracts.

Number of streamlines connectivity measures were available for the 100-Brains and MEG-Partnership cohorts (N=161). Diffusivity and myelin measures were analysed in a sub-cohort of 90 participants.

Non-Negative matrix Factorization- Structural networks

The same NNMF algorithm was applied to the structural connectivity matrices. As with the functional analysis, there were 4005 unique undirected connections carried forward for NNMF analysis. Identical thresholding parameters were applied to avoid overfitting. This resulted in between 10-18 components for each of the structural measures; NST, SST, NSC, SSC, FA, RD, AD & MM.

7.3.5 Statistical analysis- Structural networks

The structural components were analysed with regression analysis. Schizotypy was the main predictor, and age and gender were covariates. Bonferroni correction was applied in each regression model to adjust for the number of components.

7.4 Results

7.4.1 Functional connectivity

Valid edge connections were present in frontal areas in the delta band but did not survive any significance testing. Decreased posterior connectivity was found in the alpha band (occ-occ, par-par, occ-parietal, $p < 0.01$, uncorrected). More widespread decreased (R precuneus- par, par-occ, par-par) connectivity and few increased (R occ-par, R occ-temp) connections were found in the beta band ($p < 0.05$, uncorrected).

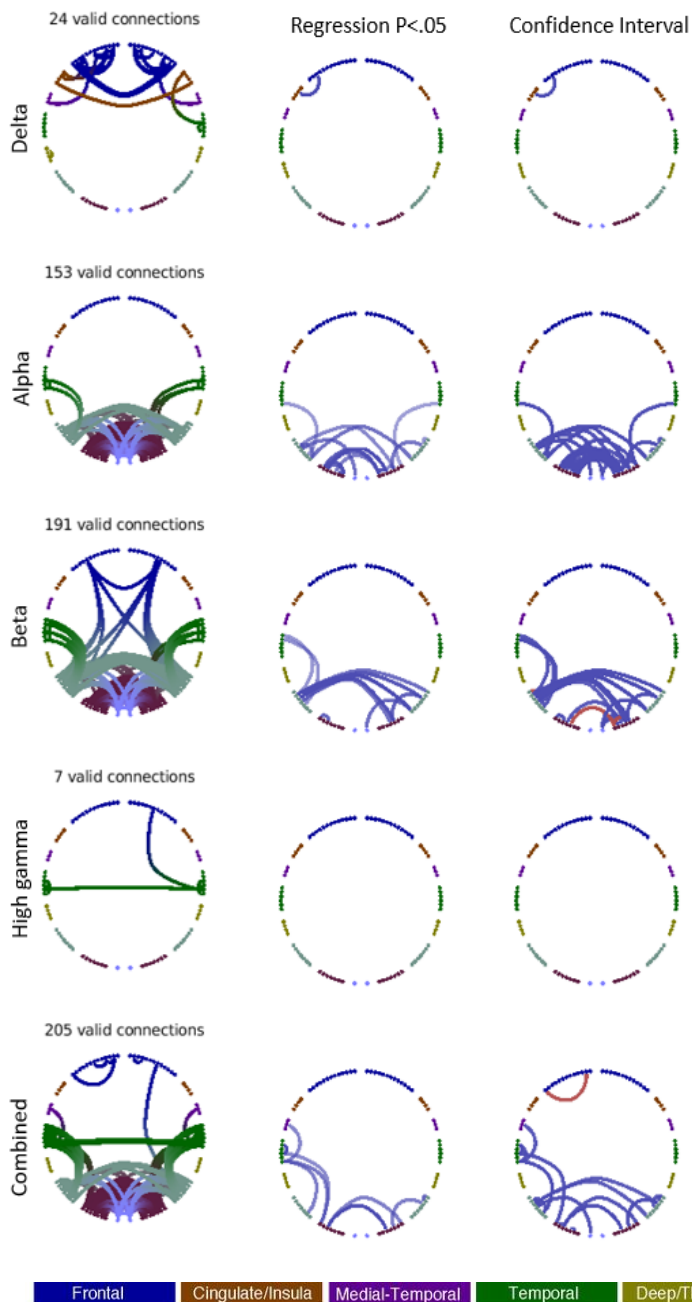


Figure 7.2. Connectivity analysis: Each row shows oscillatory amplitude correlations for the four frequency ranges where valid edges were found, and the combined map. The first column, valid connections, shows the connections at mean rank > 0.8 , per frequency band and across the combined frequencies. The second column shows connections significantly associated with schizotypy ($p < 0.05$) at the uncorrected level (univariate regression). To consider the generalisability of associated connections, the third column shows univariate connections where the confidence interval (95%) on the regression slope did not include zero. In column 2 and 3, positive correlations, i.e., increased connectivity, are represented with red lines whereas negative correlations are represented with blue lines.

The prominent observation is that schizotypy predicted reductions in alpha and beta connectivity in posterior areas of the brain at the uncorrected level.

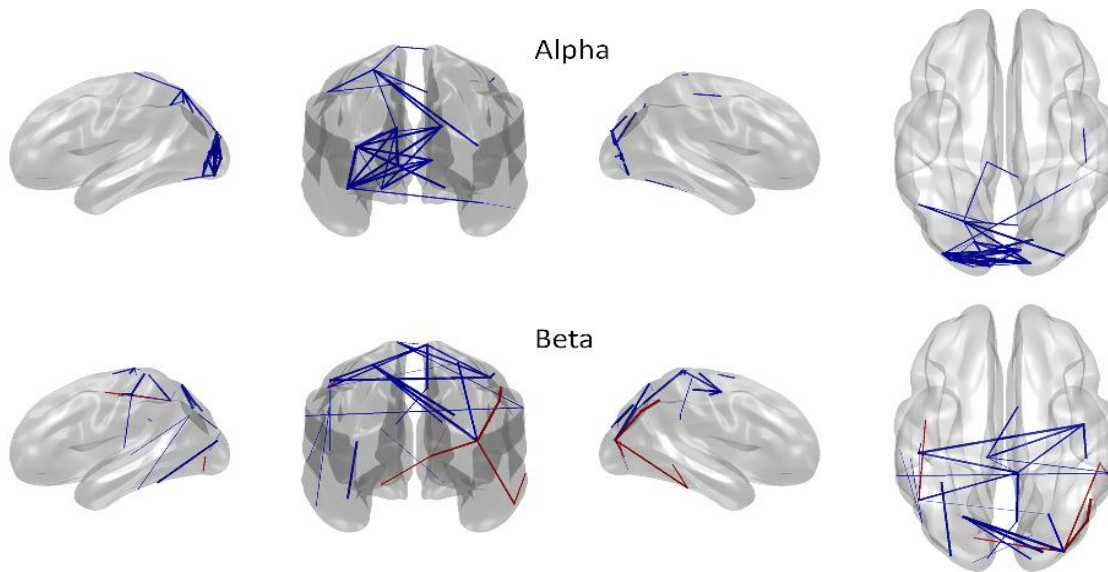


Figure 7.3. Alpha and beta connectivity (resampling confidence interval, 95%, 5000 iterations) depicted on a template brain. Blue lines represent robust decreases in connectivity for participants with high schizotypy scores, red lines represent increases.

As shown in Figures 7.2 and 7.3, connections in the alpha band are predominantly between bilateral occipital areas, occipital-parietal and parietal-temporal areas. Connections in the beta band were more widespread between parietal, occipital and temporal areas.

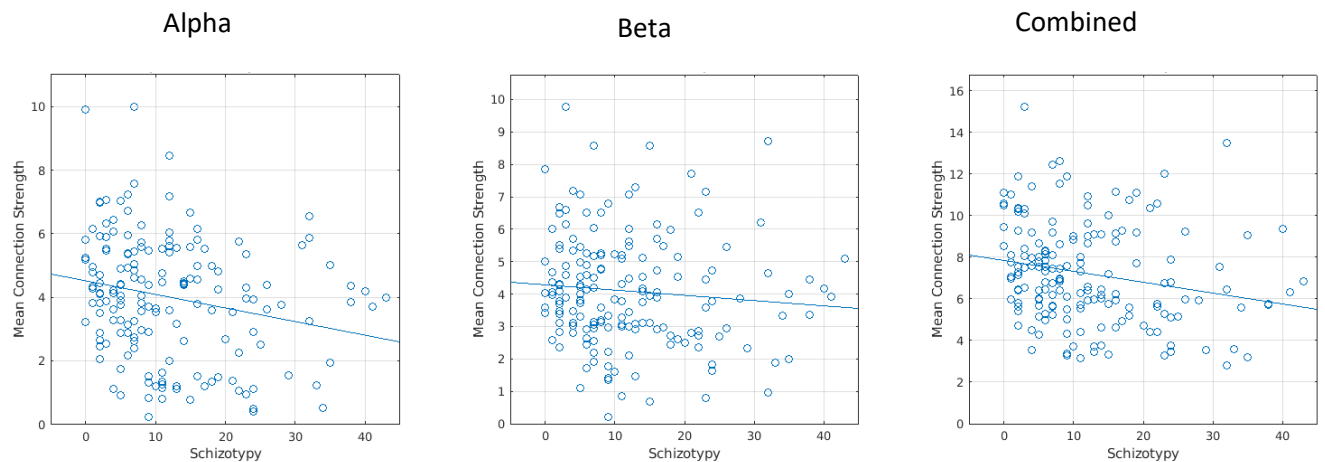


Figure 7.4. Scatter plots of mean strength of significant connections ($p < 0.05$) versus schizotypy (raw scores) in the alpha, beta and combined frequency bands.

Figure 7.4 shows a negative trend in mean connectivity in the alpha and combined bands.

7.4.2 Non-Negative Matrix Factorization- Functional networks

NNMF was applied to the functional connectivity matrices to reveal common functional sub-networks across participants.

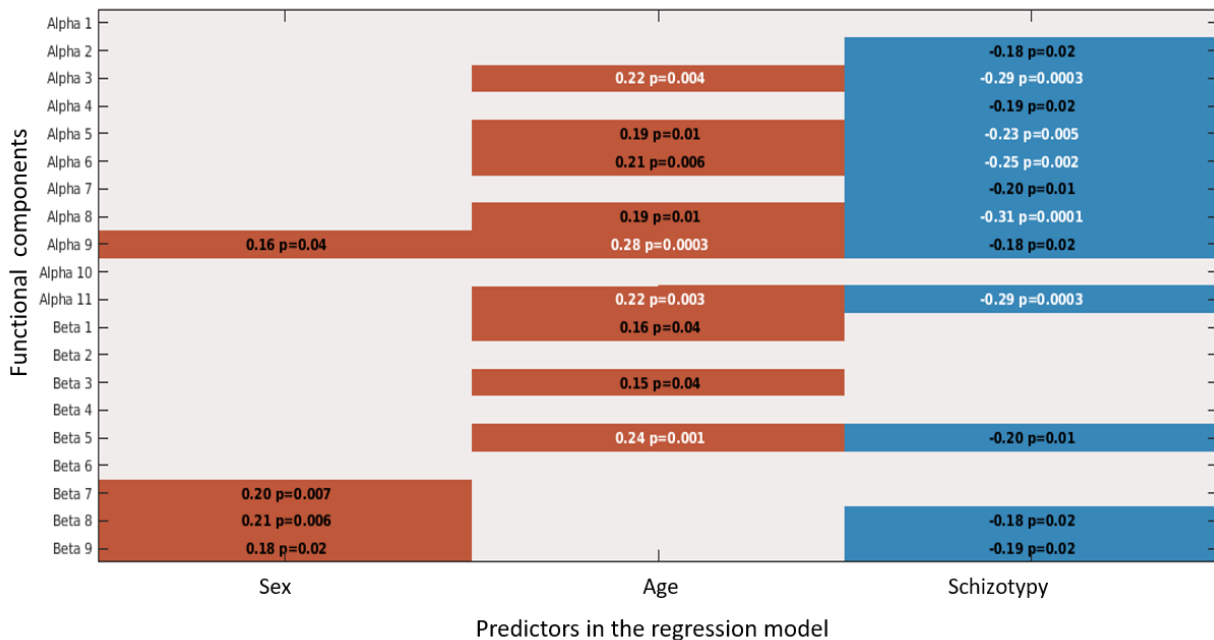


Figure 7.5. Functional NNMF connectivity components in alpha and beta, across gender, age and schizotypy. The within box text shows the effect size (beta) and the p -value for that component. Red boxes represent positive relationships. Blue boxes represent negative relationships. Text in white shows relationships which meet multiple comparison adjustment ($p < .05$), whereas text in black shows relationships significant at the uncorrected level ($p < .05$).

Schizotypy negatively predicted 5 alpha components after Bonferroni correction ($p < .05$), as shown in Figure 7.5, suggesting high schizotypy individuals have reduced alpha connectivity.

The 5 significant networks are plotted on template brains in Figure 7.6 below.

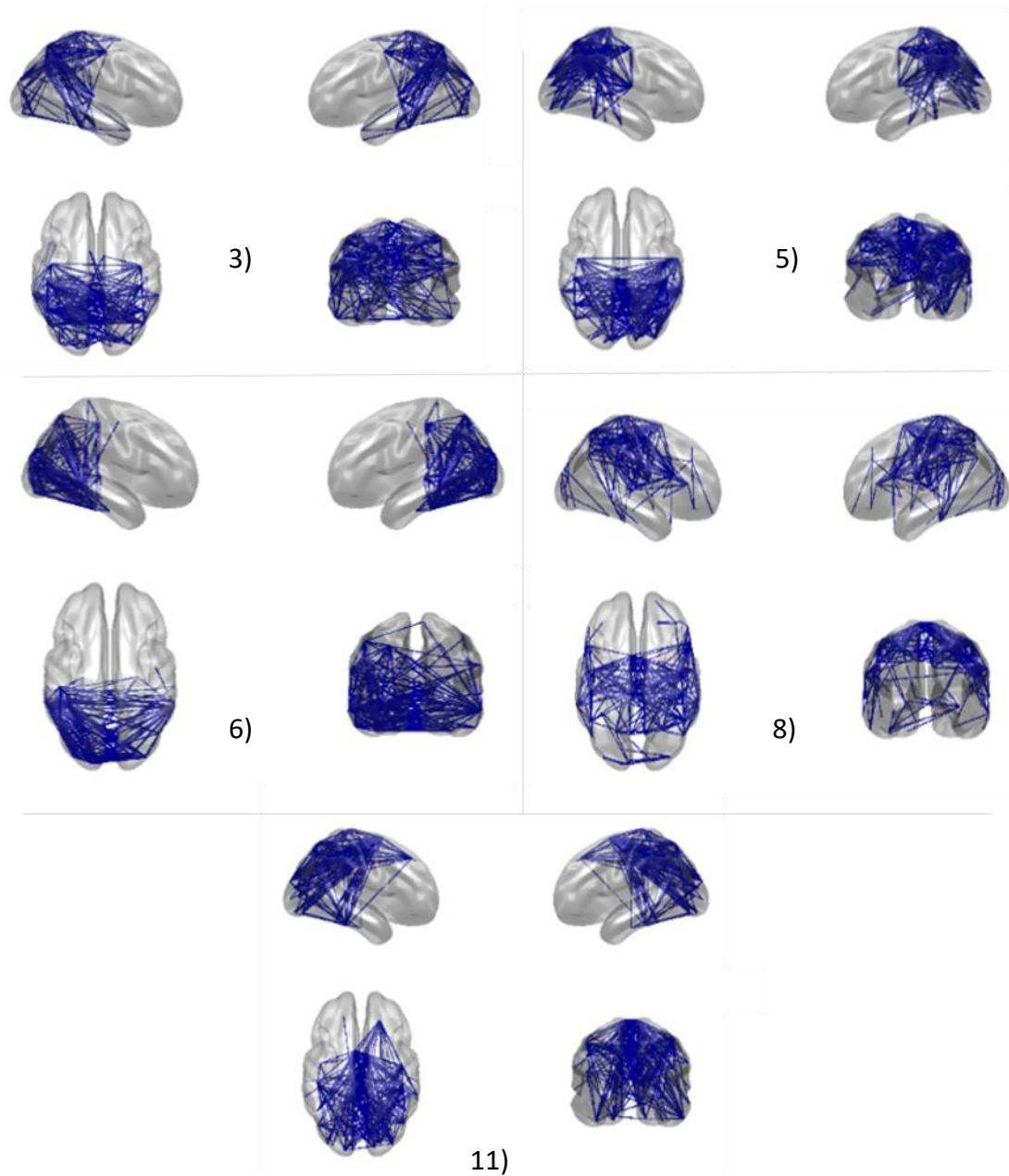


Figure 7.6. The 5 Alpha network components significantly predicted by schizotypy. Blue lines represent a negative relationship with schizotypy.

Alpha network reductions associated with schizotypy mostly spanned posterior areas of the brain. The predominant spatial distributions of the reduced networks were as follows:

Network 3 – bilateral occipital-parietal network with some temporal connections

Network 5- bilateral parietal and right occipital connections

Network 6- occipital and parietal network with dense left parietal connections

Network 8- parietal and temporal connections with few frontal and occipital edges

Network 11- bilateral occipital-parietal network with some left frontal connections

Schizotypy was not associated with age or gender. Despite there being negative relationships with 3 beta components (shown in Figure 7.5), schizotypy did not significantly predict any beta components after multiple comparisons correction.

7.4.3 Structural connectivity

NNMF was also applied to structural matrices in order to explore any possible structural sub-network relationships with schizotypy.

Streamlines measures

Schizotypy was negatively associated with 10 streamlines components, however, only 2 components withstood multiple comparison adjustment. Differences in schizotypy relationships can be observed depending on the streamlines measures used.

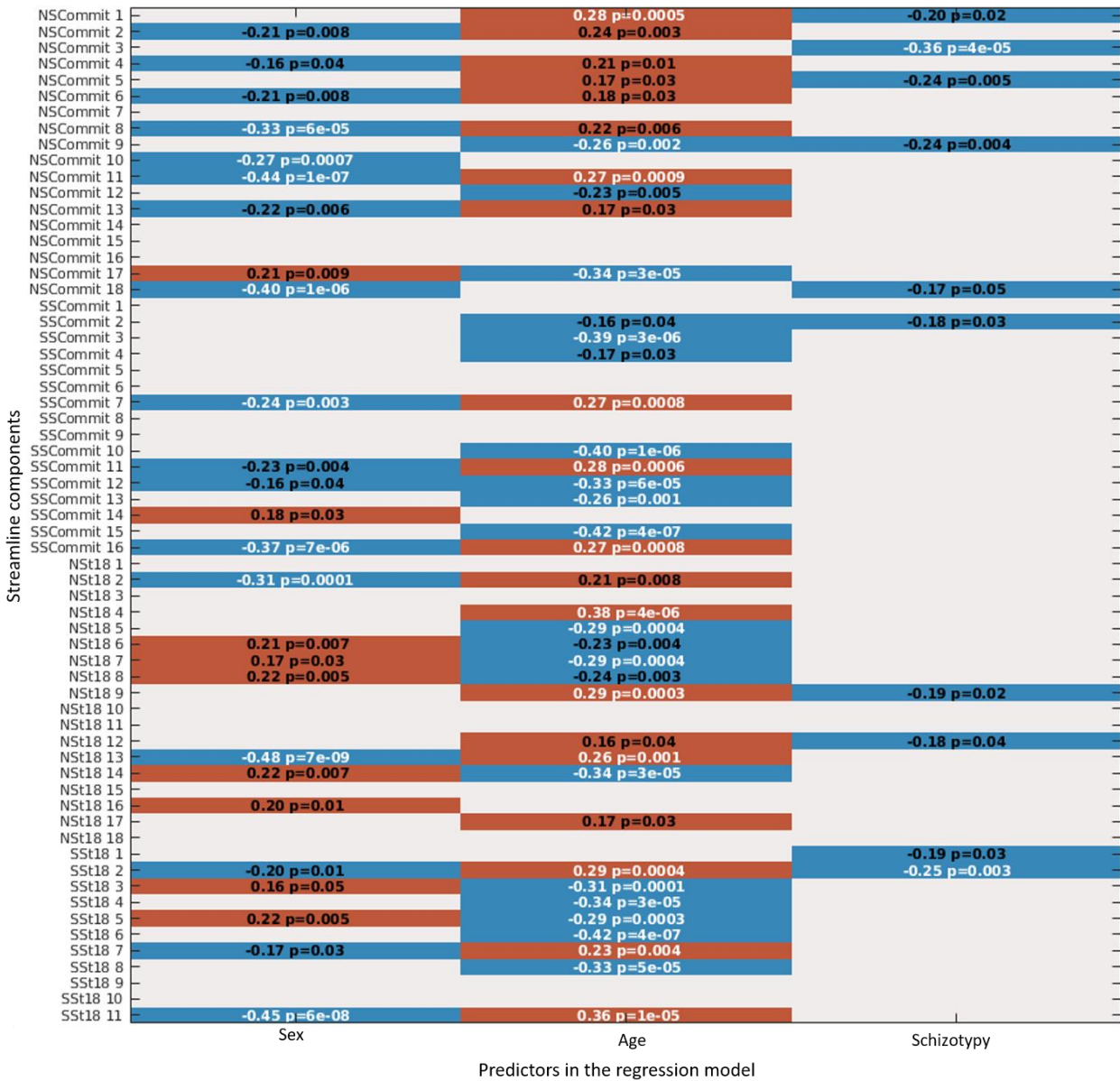


Figure 7.7. Streamlines NNMF connectivity components across gender, age and schizotypy. The within component text shows the effect size (beta) and the p-value. Red boxes represent positive relationships. Blue boxes represent negative relationships. Text in white shows relationships which meet multiple comparison adjustment ($p < .05$), whereas text in black shows relationships significant at the uncorrected level ($p < .05$).

Regarding the covariates, age was highly correlated with the streamlines components, however in no clear pattern. Gender was also related to different streamlines components, with significant differences comprising reductions in women.

The two network components that had significant relationships with schizotypy, after correction, are plotted in Figure 7.8 below.

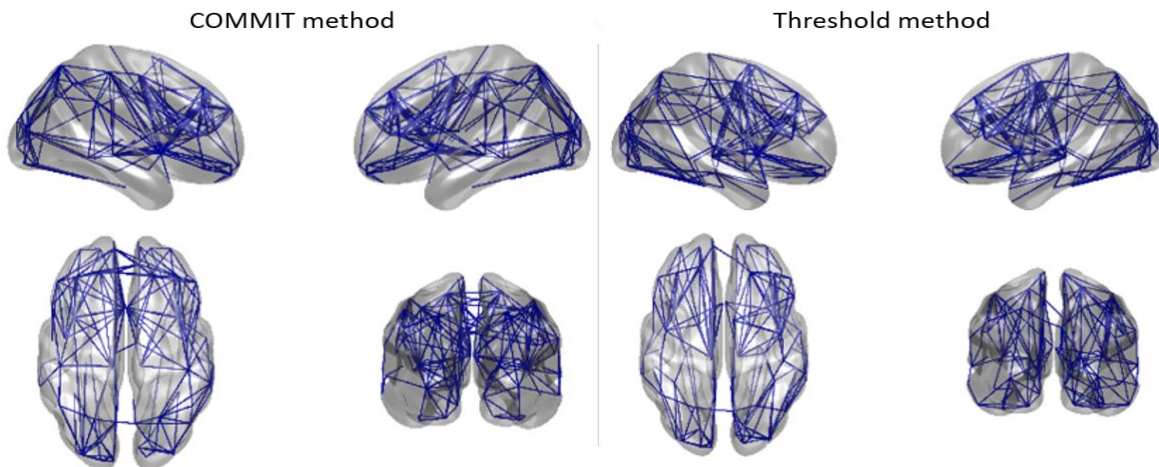


Figure 7.8. Streamlines networks predicted by schizotypy plotted on template brains. Left, is the number of streamlines (COMMIT) network predicted by schizotypy. Right, is standardised streamlines (thresholded) network predicted by schizotypy. Blue lines represent negative correlations.

Two measures, number of streamlines (COMMIT) and standardised streamlines (thresholded), had significant components that were negatively predicted by schizotypy. Some overlap can be observed in these networks in Figure 7.8, suggesting that the method of streamline selection is less important than sparsity in capturing variance associated with schizotypy. Both networks comprise widespread lateral connections and few frontal and posterior bilateral connections.

Structural measures

Schizotypy was negatively associated with 6 Euclidean distance components and 1 myelin component, but none of these relationships met correction for multiple comparisons. Euclidean distance connectivity was explored considering a paper by Messaritaki and colleagues, who found that the strength of MEG functional resting-state connectivity depended on the Euclidean distance between brain regions (Messaritaki et al., 2021b); a finding previously shown elsewhere (Tewarie et al., 2019). This suggests that areas that structurally closer together, exhibit stronger functional connectivity.

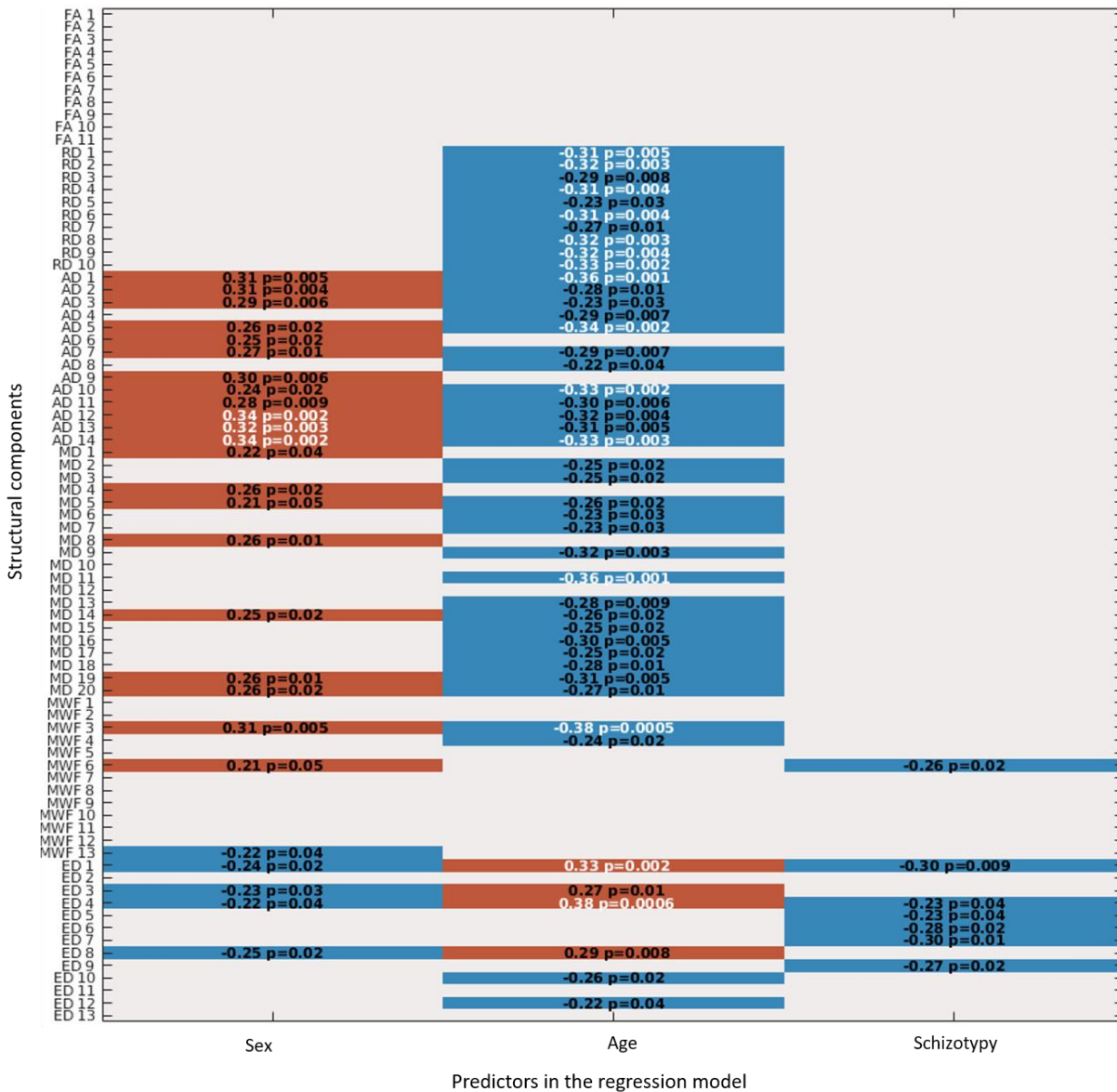


Figure 7.9. Structural NMF connectivity components across gender, age and schizotypy. The within component text shows the effect size (beta) and the p-value. Red boxes represent positive relationships. Blue boxes represent negative relationships. Text in white shows relationships which meet multiple comparison adjustment ($p < .05$), whereas text in black shows relationships significant at the uncorrected level ($p < .05$).

Regarding age and gender, increased age was negatively associated with most structural components except Euclidean distance. Women generally had higher component weightings than men, apart from the Euclidean distance relationships where men had higher weightings than women. No other relationships were found.

7.5 Discussion

This chapter has investigated schizotypy as a predictor of functional and structural connectivity. The findings are consistent with the disconnection hypothesis of schizophrenia (Friston et al., 2016). From the functional imaging, a relationship between schizotypy and reduced oscillatory connectivity, across posterior regions in the alpha and beta bands, was suggested by examination of amplitude-amplitude connectivity across 90 AAL nodes, though not convincingly. However, by extracting networks using non-negative matrix factorization, thereby improving signal to noise, schizotypy was found to significantly predict connectivity in 5 alpha networks. Some negative relationships with 3 beta NNMF networks were also suggested, but these relationships were not robust to multiple comparison correction. These analyses support and go beyond the previous results showing reduced left precuneus -paracentral lobule alpha connectivity in high schizotypy individuals (Williams, 2018).

Schizotypy was associated with *reduced* amplitude-amplitude oscillatory coupling in all of the associated networks. This is interesting in the context of previous work by Phalen and colleagues, who found a reduction in phase locking connectivity in 4 alpha networks, using NNMF, in first episode schizophrenia patients (Phalen et al., 2019). The networks comprised the bilateral anterior and posterior cingulate; left auditory, medial temporal, and cingulate cortex; right inferior frontal gyrus - widespread areas; and right posterior parietal cortex - widespread areas. Positive and Negative Syndrome Scale total and thought disorder factors were also correlated with the first three (reduced) networks in patients. The left posterior temporal network was associated with positive and negative factors, and the right inferior frontal network was associated with the positive factor suggesting networks revealed with NNMF could have symptom specificity.

Alpha oscillations are important in several cognitive and perceptual tasks involving the sensory modalities (Uhlhaas & Singer, 2010a); particularly attention, many facets of which have shown to be disturbed in schizophrenia (Hoonakker, Doignon-Camus, & Bonnefond, 2017; Nuechterlein et al., 2015). More broadly, alpha oscillations seem to have a role in functional coupling across brain regions (Nunez et al., 1997; Palva & Palva, 2007), which comes from a thalamo-cortical drive (Roux et al., 2013; Vijayan et al., 2013).

While the mechanisms underpinning alpha oscillations are yet to be fully understood, due to the well-established effect of attention on alpha oscillations in the visual cortex, alpha oscillations have been thought to have a role in feedforward and feedback processes (Baillet, 2017; Bastos et al., 2012; Bastos et al., 2015; Michalareas et al., 2016), and a modulatory effect on cortical excitability (Bonfond & Jensen, 2015; Popov et al., 2017; Roux et al., 2013). Findings such as these complement Predictive Coding theory of schizophrenia, where positive symptoms such as hallucination and delusion result from a faulty ability to update prior beliefs with incoming sensory information (Friston et al., 2016; Sterzer et al., 2018). Theoretically, these processes are underpinned by alpha and gamma oscillatory dynamics.

Considering the continuum view of schizophrenia (Claridge & Beech, 2010), the alpha dysconnectivity shown in this chapter may also relate to cognitive and perceptual experiences reported in high schizotypy individuals. However, this has not been directly shown. It is to be noted that, in the healthy population, a recent frequency tagging (V1) paper found simultaneous alpha oscillations to be sourced outside of V1, around the parieto-occipital sulcus (Zhigalov, Herring, Herpers, Bergmann, & Jensen, 2019), suggesting alpha is not a modulator of V1 excitability, or at least not directly. Furthermore, an investigation by Humpston, Tüefel and colleagues did not find altered prediction error responses, on 3 different tasks, in >100 high schizotypy individuals (Humpston, Evans, Teufel, Ihssen, & Linden, 2017). Therefore, while like schizophrenia, alpha dysconnectivity is associated with schizotypy, further work is needed to unpick the underlying mechanisms in the schizotypy population.

Of the 5 alpha networks that had significant relationships with schizotypy, 3 were heavily occipital and parietal and the other 2 comprised predominantly occipital/parietal to frontal connections. This is consistent with previous studies showing resting-state alpha occipital and frontal EEG connectivity related to schizotypy using a phase lag index measure (PLI) (Hu, Li, Lopour, & Martin, 2020). Interestingly, the paper by Hu et al., also found that individuals scoring highly on the positive schizotypy dimensions showed reduced occipital and frontal connectivity, compared to controls, while those scoring highly on the negative dimension showed increased alpha concentration in the occipital lobe, compared to controls.

On this note, the dimensionality of schizotypy appears to be important in regard to connectivity. For example, Wang and colleagues, found that schizotypy scores in the positive dimension were positively correlated with ventral striatum and frontal cortex fMRI connectivity and negatively associated with connections between the dorsal striatum and posterior cingulate, while no associations were found with the negative schizotypy dimension (Wang, Ettinger, Meindl, & Chan, 2018). Similarly, Waltman found fMRI differences between the ventral striatum and ventromedial prefrontal cortex, and dorsal striatum and temporo-occipital regions, in high (total) schizotypy individuals, but these all comprised hypo-connectivity (Waltmann et al., 2019).

Moreover, the structural findings were not as predicted as no relationships were found between schizotypy and FA and RD. There was some evidence for a relationship between schizotypy and reduced widespread network integrity, based on the streamlines measures. However, these relationships differed considerably depending on the thresholding and standardisation approach taken in deriving the measures, suggesting these findings should be interpreted with caution.

Schizotypy was associated with Euclidean Distance, however not after adjustment. Euclidean distance is fundamentally the straight-line distance between two points. However, interestingly, Messaritaki et al., (2021a), made a link between MEG and DTI measures of connectivity, by showing white matter Euclidean distance to be highly correlated with functional MEG connections. The interpretation of the negative relationship between schizotypy and Euclidean distance found here, however, would be that functional connectivity is increased between fronto-occipital regions. While possible, this postulation does not coincide with the functional results in this chapter.

This is not the first simultaneous structure-function investigation of schizotypy. Using a DTI measure of white matter structural connectivity, and static and dynamic fMRI (~200 subjects), Wang and colleagues found high schizotypy individuals (n=87) showed, 1) increased structural connectivity probability within a task control network (right insula and the right middle frontal gyrus) and within the default mode network (DMN), 2) increased variability and decreased stability of functional connectivity within DMN and between the auditory network and the

subcortical network, and, 3) decreased static mean functional connectivity strength in the sensorimotor network, the DMN and the task control network (Cai, Zhang, & Zhou, 2021). Thus, such an approach appears to be informative. This is, to the authors knowledge, the first simultaneous investigation of schizotypy with MEG and DTI.

Finally, on a broader note, whether the disconnection hypotheses can be extended to traits distributed in the normal population is an ongoing question. While the continuum view of schizotypy is controversial, with some scholars now placing schizotypy in the context of affective and social functioning rather than schizophrenia per se (Cohen, Mohr, Ettinger, Chan, & Park, 2015), there is also research to suggest considerable genetic, cognitive and neurobiological overlap with schizophrenia (Ettinger, Meyhöfer, Steffens, Wagner, & Koutsouleris, 2014). Our finding that individuals with high schizotypy have reduced alpha connectivity supports the dimensional approach to schizophrenia

Tangentially, an interesting line of recent research involves the classification of individuals into high and low schizotypy groups, which can be completed successfully using neuroimaging data and machine learning (Madsen, Krohne, Cai, Wang, & Chan, 2018). Because individuals with high schizotypy traits are more likely to develop schizophrenia (Barrantes-Vidal et al., 2015) and the identification of pre-clinical tools is crucial to psychosis prevention, continued research on schizotypy is important. This will allow further elucidation of schizotypy on a construct level and alpha connectivity as an endotype for high schizotypy traits and schizophrenia.

Limitations and future directions

This chapter was subject to some limitations. The main limitation was that the raw schizotypy scores, which would have allowed values to be assigned to the different dimensions of schizotypy, were unavailable. Many of the papers discussed show different connectivity results based on, at least, positive and negative dimensions, suggesting both schizophrenia and schizotypy are heterogeneous. This should be considered in future. Furthermore, in the functional analysis, due to the scope of this thesis, only alpha and beta NNMF networks were inspected. Network relationships in other frequency bands may exist and should be investigated.

To conclude, there appears to be a robust relationship between increased schizotypy and reduced functional connectivity in the alpha band. These findings are noteworthy considering the alpha dysconnectivity shown in people with schizophrenia and adds to the growing body of neuroimaging literature showing functional continuity between health and diagnosis.

Relationships between increased schizotypy and white matter connectivity were less clear. One explanation is that schizophrenia-traits result from the disruption of synaptic properties, via excitatory-inhibitory neurotransmitter systems, that specifically affect the efficacy of dynamic signals, such as those in the alpha band, and hence structural connectivity may only be minimally implicated.

Undertaking a dimensional separation of schizotypy constructs in future analysis is also encouraged.

Chapter 8. Polygenic Risk Score for Schizophrenia and structural and functional connectivity

8.1 Rationale

Genetic variation is highly implicated in schizophrenia (Friston, Brown, Siemerkus, & Stephan, 2016; Hall et al., 2015a; Kirov et al., 2012; Kong et al., 2012; Nakazawa et al., 2012; Walton et al., 2013). As the disorder significantly affects the quality of life of the individual (Bobes, Garcia-Portilla, Bascaran, Saiz, & Bousoño, 2007) and those around them (Ribé et al., 2018), considerable attention has been given to researching the genetic underpinnings. The combination of modern genetic analysis tools and MEG provides an opportunity to explore genetic-electrophysiological correlates as well as genetic continuity between health and disease. Furthermore, as the assumption is that functional connectivity subject to the integrity of structural pathways, and genetics play a critical role in connectome development (Akarca, Vértes, Bullmore, & Astle, 2021; Domen et al., 2017; Greicius, Supekar, Menon, & Dougherty, 2009), the genetic contribution to white matter pathology is also of considerable interest.

8.2 Introduction

A body of studies have shown that large-scale functional networks are impaired in schizophrenia (Bowyer, 2016; Hinkley et al., 2011; Houck et al., 2017; Kim et al., 2014; Sanfratello, Houck, & Calhoun, 2018; Uhlhaas & Singer, 2010a; Yang et al., 2014; Zhang et al., 2015) but the drivers of such network impairments at a mechanistic and genetic level are not fully clear. Large meta-analytic studies, such as the ENIGMA project (~2000 patients), have also solidified the evidence of widespread white matter abnormalities, specifically reduced anisotropy, in these individuals, where consistent structural dysconnections had previously been difficult to identify (Kelly et al., 2017a). Schizophrenia is a highly heritable disorder and while about 1 percent of the population are diagnosed with schizophrenia, risk to family members is increased by at least 10 percent (Hilker et al., 2018). Thus, increasing interest is being given to its genetic contributors.

To differentiate subclinical and clinical connectivity differences from a genetic basis *in vivo*, studies have investigated connectivity differences in patients and close family members (Cho et

al., 2019; de Leeuw et al., 2016; Edmiston et al., 2020; Goghari, Sanford, Spilka, & Woodward, 2017; Ou et al., 2016). For example, in a resting-state fMRI study, Edmiston and colleagues (2020), found both patients and unaffected family members to have reduced connectivity between the hippocampus and striatum, which was associated with poorer performance on the Wisconsin Card Sort Task (WCST), a measure of frontal lobe function, in both groups. As with patients, family members exhibit reduced Fractional Anisotropy (FA), suggesting white matter abnormalities extend to offspring and siblings (Cho et al., 2019; Domen et al., 2017; Ou et al., 2016).

In the functional literature, family members show dysconnectivity in the Default Mode Network and networks involved in emotion processing (Goghari, 2017). Individuals with schizophrenia show impaired emotion recognition and attribute negative affect to neutral faces (Bell, Bryson, & Lysaker, 1997; Pinkham, Brelsinger, Kohler, Gur, & Gur, 2011). Hence, false attribution features as an endotype in prominent theories of schizophrenia, such as the Dysconnection hypothesis (Friston, 2016) and aberrant salience theory (Kapur, 2003). Interestingly, in the study by Goghari and colleagues, family members showed intermediate connectivity effects in the aforementioned networks but unlike patients, did not show disturbances of the visual areas, suggesting some networks are subject to genetic liability.

Oscillatory disturbances in schizophrenia are seen across the frequency bands (Uhlhaas, 2013; Uhlhaas & Singer, 2010a). Connectivity in the alpha and beta bands appears to be robustly estimated and have a highly heritable basis (Colclough et al., 2017) and slower frequency oscillations are considered to have a fundamental role in long distance neural communication and integration of information, via widespread synchronisations (Siegel, Donner, & Engel, 2012; Traub, Whittington, Stanford, & Jefferys, 1996). Disturbances of such activity likely contribute to the persisting cognitive and negative symptoms seen in some patients (Uhlhaas & Singer, 2010a) and therefore understanding the genetic contribution to dysconnectivity has connotations for the development of better treatments.

Beyond familial studies, researchers have attempted to identify the building blocks of schizophrenia in the form of 'risk genes'. Both common and rare differences in genetics

contribute to schizophrenia susceptibility (Rees, O'Donovan, & Owen, 2015). Studies of genomic copy number variation (CNVs) have established the role of rare variants in the aetiology of schizophrenia. CNVs can be either duplications or deletions of a stretch of DNA (Purcell et al., 2009). For example, the 22q 11 deletion variant is associated with schizophrenia proneness (Bassett et al., 2008) and has subsequently been associated with long-range and local connectivity (Dima et al., 2020; Doherty et al., 2021; Scariati et al., 2014) as well as white matter deficits (Olszewski et al., 2017; Roalf et al., 2017). Consistent with the view that dysconnectivity is underpinned by faulty NMDAR function, many duplication and deletion CNVs on NMDA related genes have also been found to be highly associated with schizophrenia (Marshall et al., 2017).

Some mutations are inherited while others arise de novo; because of a new mutational event. Patients have far more de novo mutations than their healthy counterparts (Rees, Kirov, O'donovan, & Owen, 2012). Such mutations have been strongly related to environmental factors such as paternal age at conception (Kong et al., 2012) and, to a lesser extent, maternal age also (Acuna-Hidalgo, Veltman, & Hoischen, 2016; Goldmann et al., 2016). The increased presence of these mutations can partly explain why the disorder persists in the population under the pressure of natural selection.

Other genetic studies have investigated Single Nucleotide Polymorphisms (SNPs), which comprise small common variations in the genome, many of which have been associated with schizophrenia. Large genome wide association studies (GWAS) have made this possible, with over 100 loci being found (Working Group of the Psychiatric Genomics Consortium, 2014). It is now widely recognised that genetic susceptibility is not underpinned by large effects of individual variants, but by several SNPs which collectively contribute a great amount to genetic risk and heritability of schizophrenia and may relate to functional connectivity differences. For example, Walton (2013) found a positive relationship between a genetic risk score, generated by the cumulative effect of 41 SNPs from 34 putative schizophrenia risk genes, and left dorsal lateral prefrontal cortex (DLPFC) network inefficiency, during a fMRI working memory task.

While attempts to relate individual SNPs to functional connectivity are redundant, a wealth of information comes from studies relating genes to synaptic functioning. A key feature of the dysconnection hypothesis is that dysconnectivity is underpinned by faulty synaptic transmission, dysregulated synaptic gain of synchronous pyramidal cells and an imbalance of excitatory-inhibitory processes. Genetic support for faulty glutamatergic NMDA receptors in schizophrenia comes from the 2014 GWAS study that found a number of genes associated with schizophrenia have a role in NMDAR function, plasticity or modulation; for example, the NMDAR/GRIN2A subunit and GRM3 receptor (Friston et al., 2016; Working Group of the Psychiatric Genomics Consortium, 2014).

The aforementioned studies demonstrate the complexity of schizophrenia's genetic forms. Over the last 10 years, attention has turned to studying the aggregate effect of associated genes. The Polygenic Risk Score for Schizophrenia (PRS-SZ) is calculated by summing the logged odds ratios of alleles (SNPs) associated with schizophrenia diagnosis (Purcell et al., 2009). PRS is a valuable measure of genetic risk in so far as it considered to predict at least 20% of heritability and ~10% of liability in schizophrenia (Pardiñas et al., 2018; Ripke et al., 2014).

Subsequently, researchers have investigated PRS and its imaging correlates, particularly in large databases such as ENIGMA and BioBank (Alloza et al., 2020, 2018; Hall et al., 2015a; Lancaster et al., 2019; Stauffer et al., 2021). For example, polygenic risk has been associated with structural features, namely cortical thickness of the salience, default mode, and central-executive networks, in a large sample (UK Biobank, $N=3875$) of healthy subjects (Alloza et al., 2020). Investigations of white matter connectivity specifically, however, in UK Biobank, have mostly yielded null results (Reus et al., 2017). Two other studies have also failed to find a relationship between PRS and whole brain FA (Bolhuis et al., 2019; Jansen et al., 2019).

However, in the largest Biobank study to date ($N=69,369$ cases and $N=236,642$ healthy controls), Stauffer and colleagues found PRS to be negatively associated with FA in 63 regions and positively associated in 2 regions. The most strongly associated (FA) regions were all areas of temporal, cingulate, frontal, and insular cortex (Stauffer et al., 2021). An association with increased Mean Diffusivity (MD), i.e., an overall measure of diffusivity in the white matter

tracts, was also found in areas which overlapped with those showing a negative association between PRS and FA. Furthermore, a study of older adults (Alloza et al., 2018), found a relationship between PRS and age-linked decline in graph theory metrics calculated on FA network data. Those with higher PRS scores also showed longitudinal increases in mean diffusivity (MD), suggesting age, or PRS, could have a mediating effect on white matter dysconnectivity.

Little work has been undertaken with PRS and oscillatory connectivity measures, particularly using MEG. In fact, to the best of the author's knowledge no study has, thus far, investigated the relationship between PRS and global MEG oscillatory connectivity. However, several f/MRI studies have been conducted by a group at Cardiff University Brain Research Imaging Centre (CUBRIC), finding PRS to be associated with reward processing and reversal learning pathways, particularly in the ventral striatum, in adolescents and adults respectively (Lancaster et al., 2019; Lancaster, Ihssen, et al., 2016; Lancaster, Linden, et al., 2016). fMRI studies (n=12) conducted elsewhere, have been reviewed by Dezhina and Colleagues (2019). Most studies included were task-based and results differed considerably with both hyper- and hypo-connectivity across different cortical areas being found. Of the studies included, only one related PRS for schizophrenia to resting-state connectivity, finding increased connectivity between the bilateral insula and the left angular gyrus and reduced connectivity between the bilateral insula and the left DLPFC (Wang et al., 2017).

Interestingly, Anderson and colleagues (2018), found evidence suggesting polygenic risk is enriched among interneuron genes involved in parvalbumin expression. Parvalbumin interneurons are inhibitory GABAergic cells involved in local excitation – inhibition circuitry. FMRI resting-state amplitude was negatively predicted by PRS in a pattern spatially congruent with parvalbumin interneuron density; namely posteriorly. This finding is consistent with the increasing body of evidence which suggests that glutamatergic NMDA receptors on interneurons are disturbed in schizophrenia (Balu, 2016; Belforte et al., 2010).

Finally, electrophysiological PRS studies are largely missing, however with EEG, Narayanan and colleagues (2015) found multivariate genetic variants, associated with schizophrenia, were

related to alpha, delta and theta oscillations, when looking at activity derived with ICA. In adolescents, higher PRS scores have also been associated with elevated theta (3–7 Hz) and alpha (7–12 Hz) EEG connectivity (Meyers et al., 2021).

Alpha and beta oscillations have been associated with numerous neurocognitive functions. Clayton and colleagues (Clayton, Yeung, & Kadosh, 2018) suggest alpha functions can be categorised as: inhibitory, perceptual, predictive, communicative and perceptually stabilising. With such widespread potential functionality, evidence for these oscillatory ‘characters’ is both complementary and conflicting and research to elucidate such theories is ongoing. Furthermore, in addition to communication in large scale networks (Buzsaki & Draguhn, 2004), beta oscillations appear to have a role in decision making (Siegel et al., 2012; Siegel, Engel, & Donner, 2011; Spitzer & Haegens, 2017), and are most frequently studied in the motor cortex (Jurkiewicz, Gaetz, Bostan, & Cheyne, 2006; Robson et al., 2016), though mechanisms underpinning beta oscillations remain unclear. Nonetheless, as schizophrenia patients show oscillatory disturbances across the frequency ranges (Uhlhaas & Singer, 2010b), and alpha and beta oscillatory connectivity has been shown to have a heritable basis through the study of twins (Colclough et al., 2017), potential relationships between band specific connectivity and PRS, ought to be explored.

8.2.1 Aim and hypothesis

Polygenic risk score provides a means to study schizophrenia risk in the healthy population. In this chapter I sought to investigate genetic liability (PRS 30%), for schizophrenia and structural and functional connectivity. Though the sample available is smaller than recent Biobank and ENIGMA studies (Alloza et al., 2020; Kelly et al., 2017a), functional correlates have previously been identified in the cohort with fMRI (Chandler et al., 2019; Lancaster, Ihssen, et al., 2016). Analyses investigating the relationship between polygenic risk and global oscillatory connectivity measures will be conducted using MEG for the first time to the authors knowledge. PRS as a predictor of structural white matter connectivity will also be investigated as functional connectivity might, at least partly, be assumed to rely on the integrity and length of white matter pathways (Amico & Goñi, 2018; Coronel-Oliveros, Castro, Cofré, & Orio, 2021; Messaritaki et

al., 2021). Age and gender will be controlled for, which is important considering the possible mediating effect of age on white matter abnormalities in schizophrenia (Alloza et al., 2018).

Previous studies suggest schizophrenia and PRS are both associated with reduced FA and increased MD (Alloza et al., 2018; Canu, Agosta, & Filippi, 2015; Stauffer et al., 2021), thus it is hypothesised that that PRS will predict reduced FA and increased MD. Other structural measures will be explored. Furthermore, though MEG studies have revealed both hyper and hypo-connectivity (Alamian et al., 2017) in patients, the majority of Blood Oxygen Level Dependent (BOLD) studies show reduced connectivity in schizophrenia (Pettersson-Yeo, Allen, Benetti, McGuire, & Mechelli, 2010). As consistency has been shown between fMRI connectivity and alpha and beta connectivity (Brookes et al., 2011), a reduction in alpha and beta MEG connectivity associated with genetic load for schizophrenia is also expected.

8.3 Method

8.3.1 Participants

Participants were recruited as part of the 100-Brains and MEG-Partnership studies (N=183), at Cardiff University. Participants were screened and excluded based on psychiatric illness history and use of psychoactive drugs. Participants were all right-handed and university students. There were a higher proportion of females (67%) than males (33%), in this cohort. Of the 183 subjects some failures to generate polygenic risk score occurred, leaving 158 values.

8.3.2 Genotyping and extraction of DNA

DNA was collected using Oragene saliva kits. Genotyping was completed using genotyping arrays which contain approximately 500,000 common genetic variants (Illumina). Participants were subjected to the following quality control exclusions 1) ambiguous sex, 2) cryptic relatedness up to third-degree relatives, 3) less than 98% genotyping completeness, 4) non-European ethnicity admixture, and 5) autosomal heterozygosity outliers. SNPs were excluded where major allele frequencies were dominant (minor alleles less than 1%), if the call rate was less than 98%, or if the χ^2 test for Hardy-Weinberg equilibrium (population evolution) had a p value less than $1e-6$. Principal component analysis was used for population stratification. A total of 233054 SNPs remained after quality control. Autosomal chromosomes were imputed using the reference panel HRCv1.1 (hrc. r1.1.2016) using a mixed population panel. A total of 7545595 SNPs were imputed. Imputed data was converted to best-guess genotypes. The SNPs with multi-allelic sites, a minor allele frequency <0.01 , or significant departure from Hardy-Weinberg Equilibrium ($P < 0.0001$) were removed.

8.3.3 Creation of polygenic scores

Calculations were performed according to the procedure described by the International Schizophrenia Consortium (2009). Training data were from the most recent schizophrenia GWAS using results from the Psychiatric Genomics Consortium (PGC) schizophrenia genome-wide association studies (GWAS). SNPs were removed from all analyses if they had a low minor allele frequency ($P < 0.01$). Subsequently, the data were pruned for linkage disequilibrium using the clumping function (`-clump`), removing SNPs within 500 kilobase (`-clump-kb`) and $R^2 > 0.1$ (`-clump-r2`) with a more significantly associated SNP. The '`-score`' command in PLINK (version

1.07) software was used to calculate polygenic score. Individual scores were created by summing the number of risk alleles present for each SNP (0, 1, or 2) weighted by the logarithm of each SNP's odd ratio for schizophrenia from the PGC summary statistics. SNPs associated with SZ that surpassed three GWAS thresholds (PT 0.5, 0.1 & 0.05), were considered. These thresholds represent the approximate percentage of associated SNPs in the training dataset. For example, a $P \leq 0.05$ threshold, approximately includes 5% of all imputed SNPs.

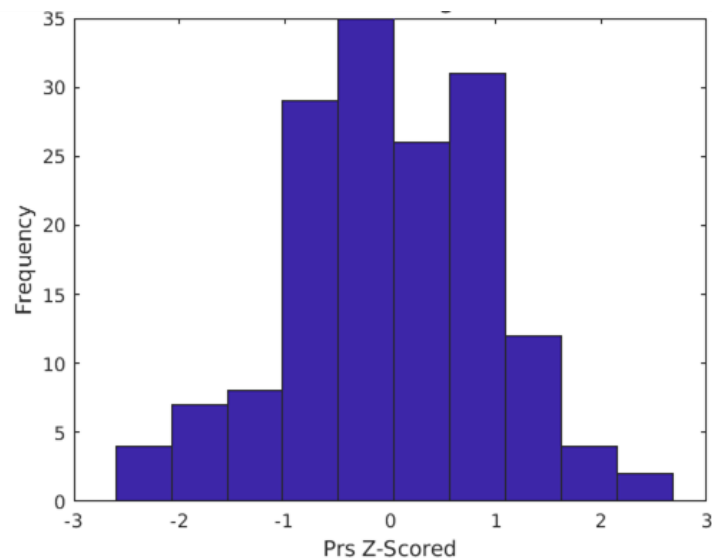


Figure 8.1. Frequency distribution of Z-scored PRS scores at threshold .05 ($n=158$)

8.3.4 Functional resting-state analysis

Amplitude-amplitude coupling connectivity parameters were estimated, using the methods described in Chapter 4. For each participant, a 5-minute resting-state scan was collected on a CTF275 MEG system at 1200Hz. Synthetic third-order noise cancellation was applied. Participants fixated on a red fixation point and were oriented upright. MRI, T1-weighted anatomical images were collected on a 3T GE scanner and used for co-registration.

Pre-processing steps were completed in DataEditor. After down sampling to 600Hz datasets were epoched into two second trials and then visually inspected eye and muscle artefacts. Any trials containing artefacts were discarded. Co-registration was performed manually, marking the fiducial points in CTF space using photographs of participants nasion and pre-auricular areas.

Whole-brain connectivity analysis was performed in Fieldtrip, using LCMV beamforming source localisation and amplitude and amplitude coupling pipelines (Koelewijn et al., 2017; Routley, Singh, Hamandi, & Muthukumaraswamy, 2017). This generated connectivity measures across six frequency bands (delta 1-4Hz, theta 3-8Hz, alpha 8-13Hz, beta 13-30Hz, low gamma 40-60 Hz and high gamma 60-90Hz). Data were projected onto a 90 node Automatic Labelling Atlas (AAL) (Tzourio-Mazoyer et al., 2002). Beamforming was completed using a 6mm grid and single shell forward model (Nolte, 2003). A vector norm normalisation was applied to weights in each frequency band separately (Hillebrand, Barnes, Bosboom, Berendse, & Stam, 2012), and a MNI inverse-warping procedure was adopted to ensure source grid consistency across participants. Selection of the 90 AAL nodes was based on the computation of virtual sensor time-courses, where the beamformer voxel with the greatest temporal variance was chosen as the representative time-course for each of the 90 AAL regions.

The resulting 90 time-series were orthogonalized to adjust for potential spurious correlations between virtual sensor data (Colclough et al., 2015). Amplitude envelopes were calculated using a Hilbert transform (the Hilbert function in MATLAB). The amplitude envelopes were also downsampled to a temporal resolution of 1s to study connectivity mediated by slow amplitude envelope changes (Colclough et al., 2015). Correlations between the amplitude envelopes (across the 90 AAL regions) in each frequency band were calculated and a Fisher z-transform applied. This resulted in 4005 connectivity correlations that were adjusted for differences in the length of time series between participants. An across-frequency band connectivity matrix was also created by taking the square root of the summed, squared connectivity matrices in each frequency band.

8.3.5 Functional statistical analysis

The value of each connection is, therefore, a strength of connectivity (z-scored correlation). Connections were selected as ‘valid connections’ by ranking each of the connections by strength, for each participant, and discarding the poorest 80% of consistently ranked connections across the whole group. Valid connections were carried forward for further statistical analysis.

Consistent with the schizophrenia literature, risk scores at the 0.05 threshold level were used in the subsequent regression analyses, the results of which are reported here. At this level, there is

enough SNPs included for sufficient statistical power while strength of associations between SNPs and schizophrenia diagnosis is maintained (Purcell et al., 2009). PRS scores were Z-scored to account for any group differences across participants. A linear regression ($p < 0.05$, uncorrected) was performed on the valid connections in each frequency band and the combined map, with the main predictor of PRS, and age and gender as covariates, at the three PRS thresholds (0.05, 0.1, 0.5). To adjust for multiple comparisons a 10,000-iteration randomisation test with omnibus thresholding was also performed ($p < 0.05$). To assess generalisability, a 5000-iteration resampling procedure (sign test) was performed to construct a 95% confidence interval for connections per frequency band.

Non-Negative Matrix Factorization

A Non-Negative Matrix Factorization procedure (NNMF as described in Chapter 5) was applied to the resting-state data to summarise connections across the 90 AAL regions into a limited set of consistent network patterns across participants. As resting-state patterns of MEG connectivity in the alpha and beta bands are most consistent with fMRI resting-state networks (Houck et al., 2016), focus was given to alpha and beta connectivity; 11 components were derived in the alpha band and 9 in the beta band. A regression model was built including the main predictor PRS, at the .05 threshold (z-scores), and age and gender covariates. The outcome variables were the component weightings, which represent the contribution from each participant to the component network (univariate testing). A Bonferroni adjustment was used to control for multiple comparisons within each regression model. To exclude outliers, the Cook's distance method was used and set to $3 * \text{mean weighting value}$.

8.3.6 Structural analysis

Structural connectivity measures were initially derived by Dr Eirini Messaritaki (Messaritaki et al., 2021) and are summarised here. The same AAL labeling atlas that was used for the MEG functional connectivity analysis (90 cortical and subcortical regions) was used to summarise structural measures. This allowed the structural network to also be represented as 90×90 symmetrical matrices, for each participant.

MRI data acquisition and pre-processing

All MRI data were acquired on a GE Signa HDx 3T scanner (GE Healthcare, Milwaukee, WI). T1 images were acquired with a three-dimensional fast spoiled gradient and downsampled to 1.5-mm isotropic resolution.

A standard diffusion weighted MRI sequence (isotropic resolution of 2.4 mm) was used. Diffusion MRI data were co-registered to the T1 and corrections for head movement and eddy current distortions were made. Free-water correction was also conducted. A mcDESPOT sequence (which can provide myelin measures), was also implemented (Deoni, Rutt, Arun, Pierpaoli, & Jones, 2008). Images for each participant were linearly coregistered to a spoiled gradient recall (SPGR) image, to correct for subject motion. Non-brain tissue was removed using a mask computed with the BET algorithm (Smith, 2002).

Tractography analysis

Tractography was performed on the DTI data, using the streamline algorithm in MRtrix 3.0 (Dhollander, Raffelt, & Connelly, 2016). White matter tracts were localised using a WM mask generated from the T1-weighted images using FSL fast (Jenkinson et al., 2012). The minimum and maximum tract lengths were 30 and 250 mm, respectively. Structural networks (connectivity matrices) were generated with connections or edges representing white matter tracts.

Streamline selection- Threshold Vs COMMIT methods

Previously, the minimum number of streamlines taken to suggest that a tract has been reliably reconstructed has been selected arbitrarily, limiting the quantitative nature of streamline measures (Daducci, Palù, Lemkaddem, & Thiran, 2015). The COMMIT method (Daducci et al., 2015) is a data driven alternative and rejects any streamlines that are not consistent with the overall diffusion signal in the diffusion-weighted images. This is done by fitting a linear combination of restricted and/or hindered contributions of candidate tracts and selecting those which result in the best global fit of the signal in each voxel. This research provides an opportunity to compare the traditional and COMMIT methods. The number of streamlines was also generated in the conventional approach with a threshold of 18 streamlines which was found

to give the same sparsity of connections produced by the COMMIT method. That is, that tracts with fewer than 18 streamlines were discarded.

mcDESPOT analysis

A mcDESPOT algorithm was used to detect the fast (water constrained by myelin), and slow (free-moving water in intra- and extracellular space), elements of the T1 and T2 times, and a non-exchanging free-water component (Deoni, Matthews, & Kolind, 2013). The fast volume fraction was taken as a map of the myelin water fraction. The ratio of myelin-bound water to total water was calculated, which is the myelin volume fraction (MVF). A MRtrix function (tcksample), was used to assign a proportion of the MVF to each streamline, in each tract. This measure was averaged over its streamlines, providing a myelin-weighted value (MM), for each tract.

The matrices that resulted from these procedures were normalised by dividing by the largest value of each matrix, so that, within any given matrix, the values range from 0 to 1. Self-connections (diagonals) were set to zero so that 4005 unique connections were carried forward for further analysis.

As described in Chapters 6 and 7 of this thesis, the structural measures that resulted are:

White matter tractography DTI measures

- Number of streamlines (NST) is the number of reconstructed streamlines, subject to the threshold of 18.
- Standardised number of streamlines (SST) is the number of reconstructed streamlines at threshold 18, divided by the length of the tract.
- Number of streamlines (NSC) is number of streamlines in the tracts as selected by the COMMIT method described above.
- Standardised number of streamlines (SSC) is number of streamlines within a tract divided by the length of the tract, selected by the COMMIT method.
- Fractional Anisotropy (FA) is a measure of the anisotropy in the diffusivity of water molecules calculated from three eigenvectors. An isotropic tensor would have equal eigenvectors.

- Radial Diffusivity (RD λ_{\perp}) is a measure of water diffusion perpendicular to the direction of the tracts.
- Axial Diffusivity (AD λ_{\parallel}) is a measure of water diffusion parallel to the direction of the tracts.
- Mean Diffusivity (overall diffusivity) is the mean of the three eigenvalues ($(\lambda_1 + \lambda_2 + \lambda_3)/3$) of the diffusion tensor.

mcDESPOT measures

- Myelin Water Fraction (MM), measures water diffusivity within the myelin giving an indirect measure of myelin density in the voxels including tracts.

As stated in earlier chapters, the number of streamlines connectivity measures were available for the 100-Brains and MEG-Partnership cohorts (N=161). The other structural connectivity metrics were only available for the 100-Brains cohort (n=90).

Non-Negative Matrix Factorization- Structural

The NNMF algorithm was also applied to the structural connectivity matrices. The same thresholding parameters, used in the functional NNMF procedure, were applied to avoid overfitting. This resulted in between 10-18 components for each of the structural measures; NST, SST, NSC, SSC, FA, RD, AD, MD & MM.

8.3.7 Structural statistical analysis

The structural components were analysed with regression analysis. PRS was the main predictor, and age and gender were covariates. Bonferroni correction was applied to adjust for the number of components.

8.4 Results

8.4.1 Functional Connectivity - Edge level

Associated edge level connectivity is shown in Figure 8.2. Reduced frontal connectivity in the delta band (two edge connections) was found ($P < 0.05$, uncorrected). Few connections were found in the alpha band ($p < 0.05$, uncorrected). Increased connectivity was found between the occipital lobes whereas decreased connectivity was found in the left occipital and left parietal areas. Changes in connectivity associated with PRS in the beta band were more widespread with reduced connectivity across occipital, parietal, temporal areas ($p < 0.05$, uncorrected). Two increased edge connections were also found (occipital, parietal). Valid connections were found in the high gamma range but did not survive significance testing. No connections withstood testing for multiple comparisons with a 1000 iteration permutation testing.

When the frequency bands were combined left occipital-temporal connectivity was reduced (see Figure 8.2, where strength of associated edge connections is represented by the colour intensity of red or blue lines). A decreased connection edge was also found between occipital areas in the combined map ($p < 0.05$, uncorrected). No valid connections were found in the theta and low gamma bands. Analysis at the 95% confidence interval found reduced and increase posterior alpha connectivity and more widespread reduced beta connectivity (into temporal and frontal areas- see Figure 8.3).

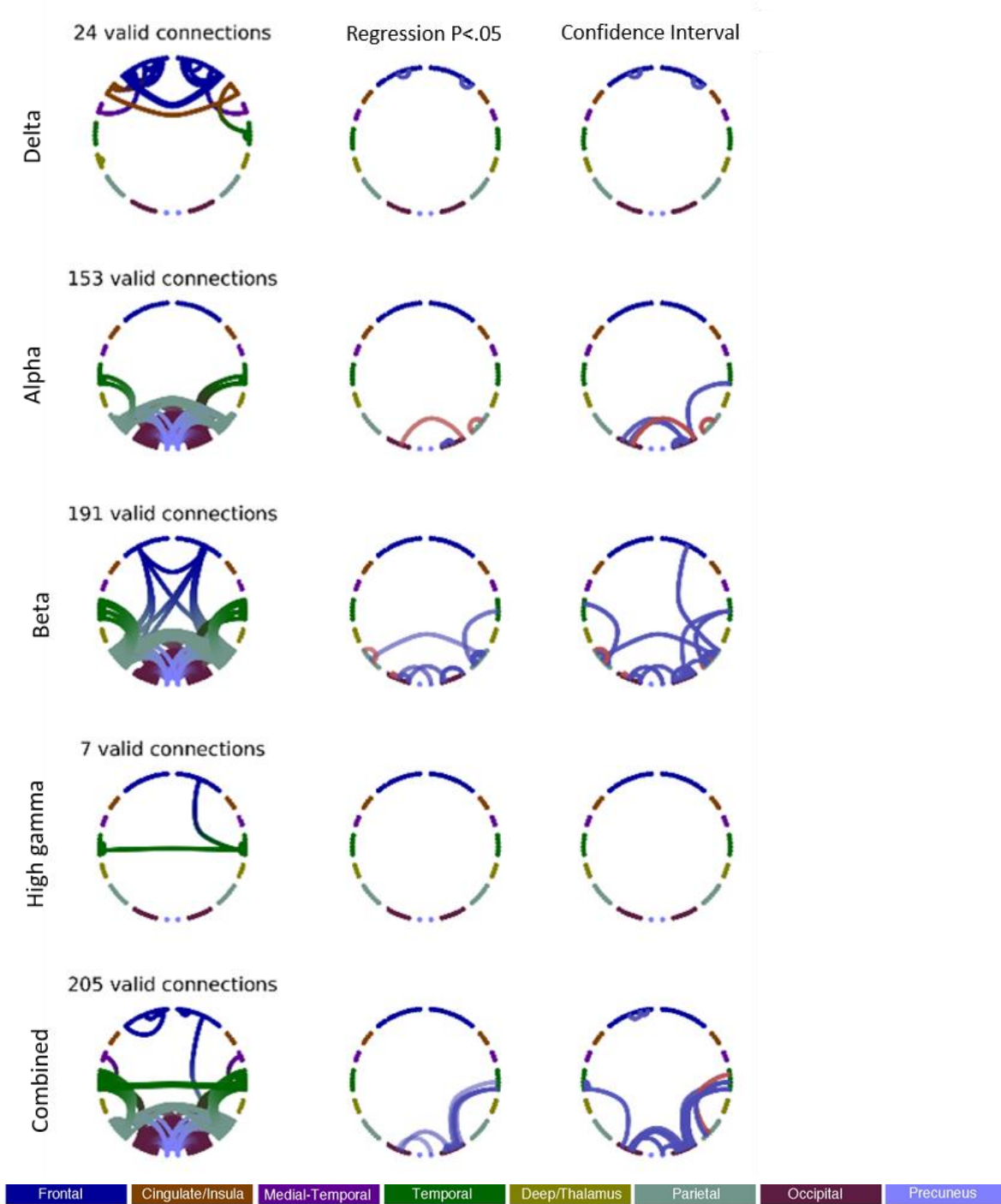


Figure 8.2. Connectivity analysis, circle plots: Each row shows across subjects' oscillatory amplitude correlations for the four frequency ranges where valid edges were found and the combined map. The first column, valid connections, shows the connections at mean rank >0.8 , per frequency band and across the combined frequencies. The second column shows connections significantly associated with PRS 0.05 at the uncorrected level (univariate regression, $p < 0.05$).

To consider the generalisability of associated connections, the third column shows univariate connections where the confidence interval (95%) on the regression slope did not include zero. In column 2 and 3, positive correlations, i.e., increased connectivity, are represented with red lines whereas negative correlations, i.e., decreased connectivity are represented with blue lines.

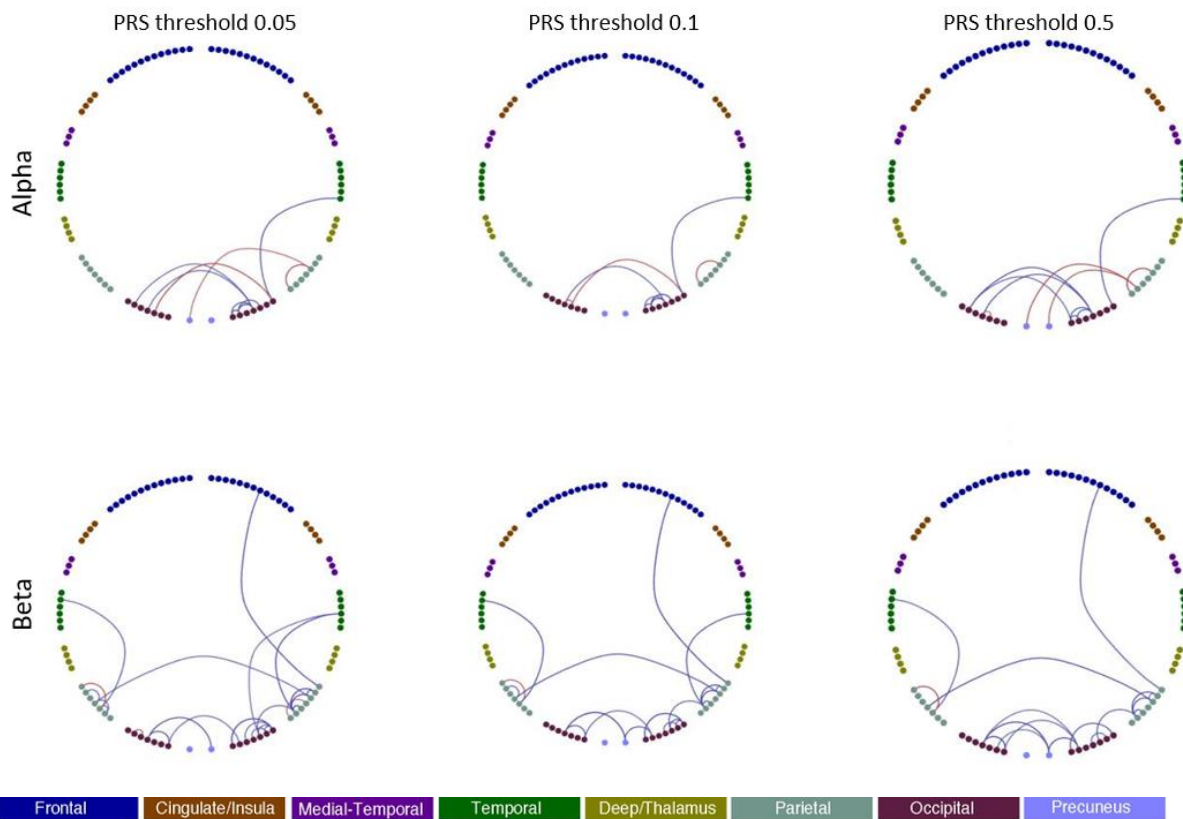


Figure 8.3. Alpha and beta connectivity (resampling confidence interval, 95%, 5000 iterations) across the three risk score thresholds, from left to right: 0.05, 0.1, 0.5. Blue lines represent decreases in connectivity, whereas red lines represent increases.

8.4.2 Non-Negative Matrix Factorization- Functional

PRS was not significantly associated with any functional NNMF components, even at the uncorrected level, nor any covariates.

8.4.3 Non-Negative Matrix Factorization- Structural

NNMF was applied to the structural matrices, across participants, to explore whether PRS is associated with any structural sub-networks.

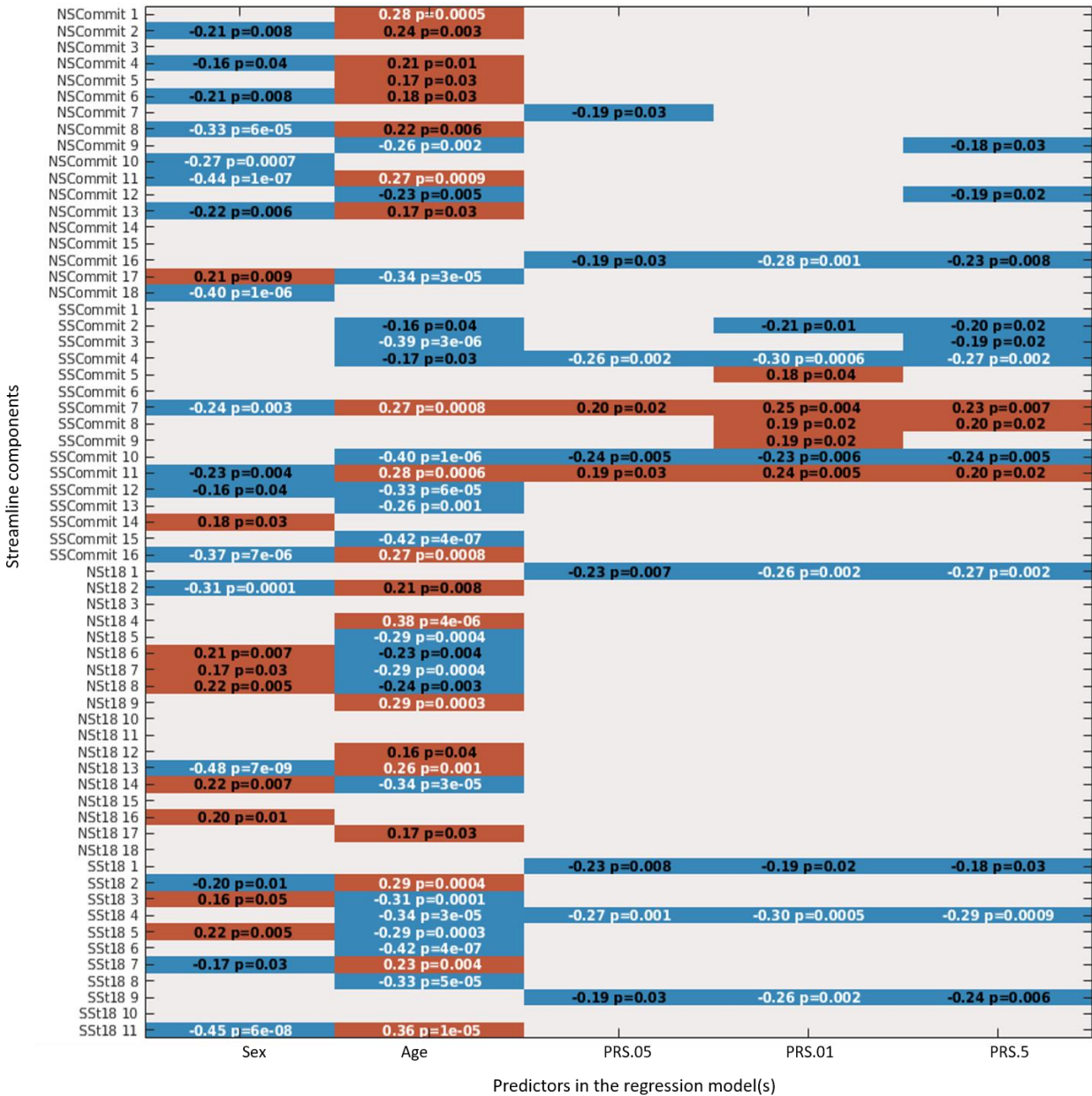


Figure 8.4. Streamlines NNMF connectivity components across gender, age, and PRS score across the three thresholds. The text shows the effect size (beta) and the p-value for each component. Red boxes represent positive relationships. Blue boxes represent negative relationships. Text in white shows relationships which meet multiple comparison adjustment ($p < .05$), whereas text in black shows relationships significant at the uncorrected level ($p < .05$).

PRS was overall negatively associated with the streamlines components, as can be seen in Figure 8.4. Two components, derived from standardised streamlines measures, survived adjustment across the different PRS thresholds, which is good evidence towards an effect. These components can be seen in Figure 8.5.

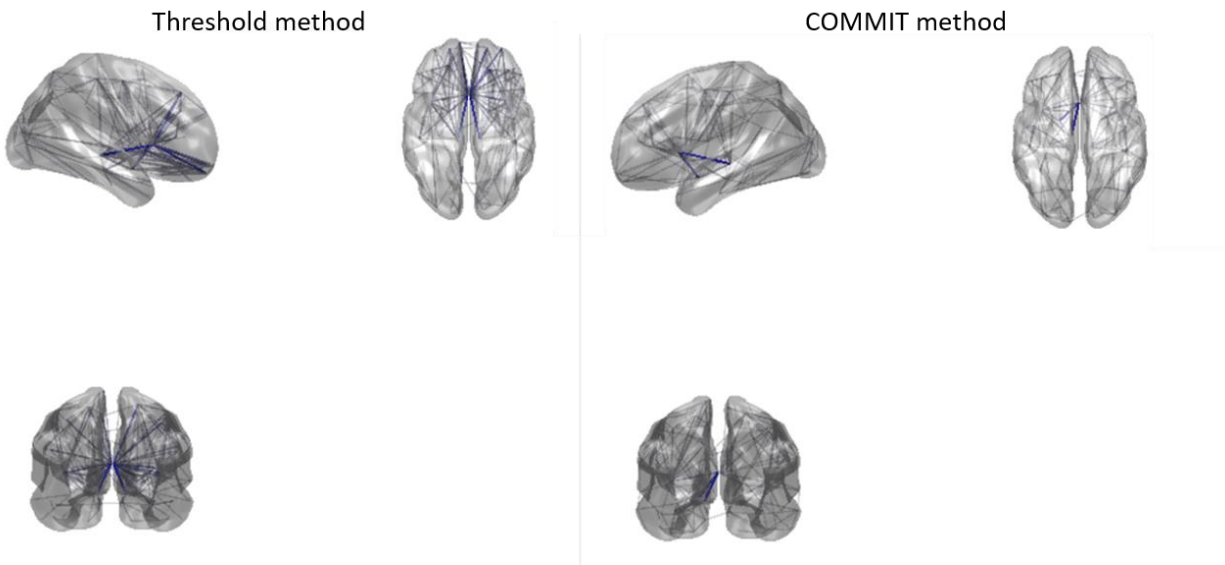


Figure 8.5. Standardised streamline components consistently predicted by PRS across the three PRS thresholds. Left: SS component 4 (Thresh18). Right: SS component 4 (COMMIT). The blue line shows that PRS predicted reductions in these networks.

Some overlap can be seen in the significant streamlines component networks suggesting PRS is correlated with reductions in these networks, suggesting that the methods is less important that sparsity in streamline selection and capturing variance associated with PRS. The network on the left comprised caudate-frontal connections whereas the network on the right comprises primarily caudate connections.

Structural measures

The correlations between PRS and the structural measures can be seen in Figure 8.6.

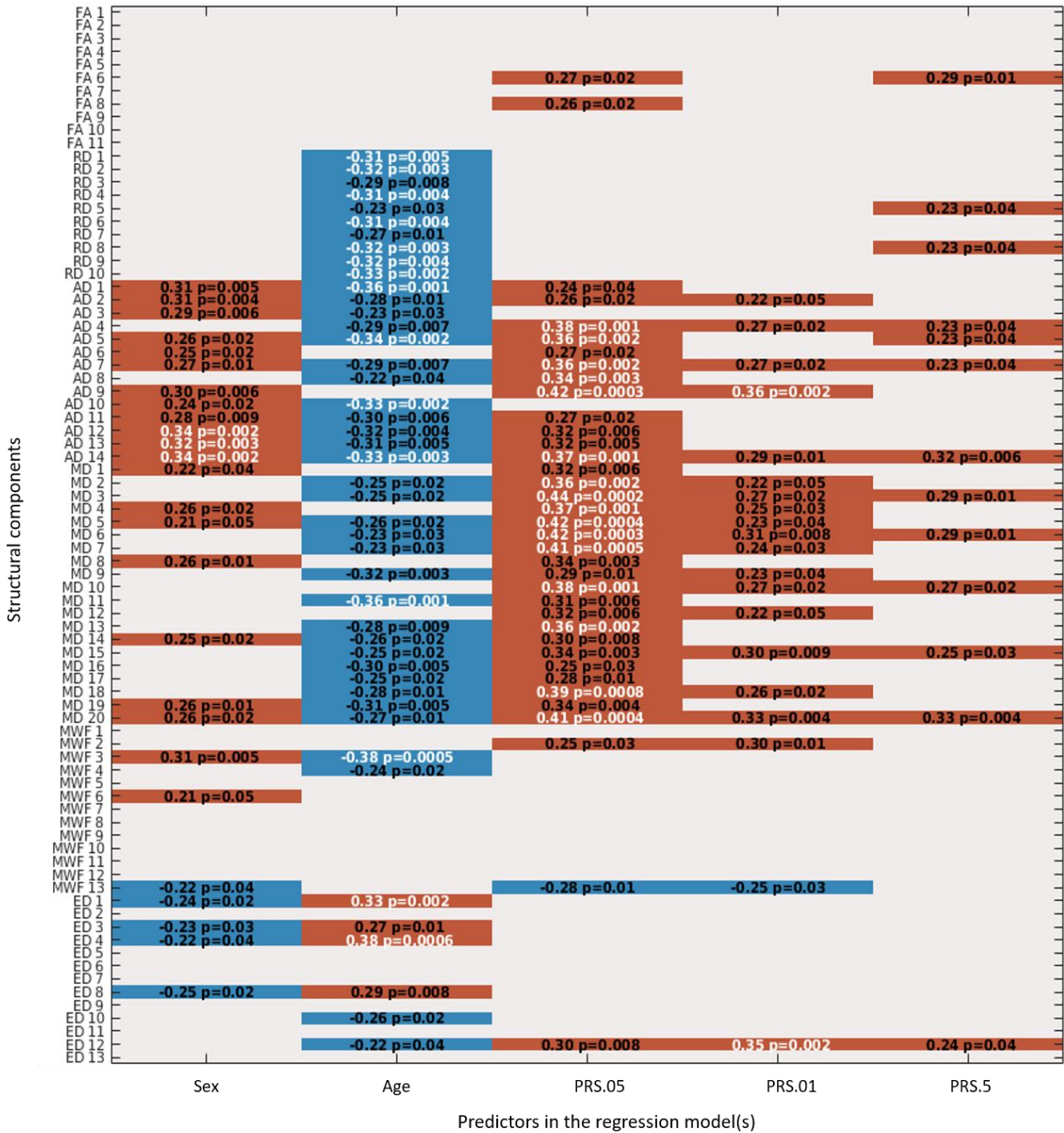


Figure 8.6. Structural NMF connectivity components across gender, age, and PRS score across the three thresholds. The within component text shows the effect size (beta) and the p-value. Red boxes represent positive relationships. Blue boxes represent negative relationships. Text in white shows relationships which meet multiple comparison adjustment ($p < .05$), whereas text in black shows relationships significant at the uncorrected level ($p < .05$).

Consistent with findings by Stauffer and colleagues (2021), PRS positively predicted all the MD components, with 10 surviving adjustment for multiple comparisons (shown in Figure 8.7).



Figure 8.7. The 10 MD network components significantly predicted by PRS. The red lines show that PRS was positively correlated with these networks.

There were also 6 axial diffusivity components predicted by PRS which survived multiple comparisons adjustment. Another six components were positively correlated but did not survive multiple comparison adjustment. These findings suggest that higher PRS scores are associated with increased Axial Diffusivity (AD) components. Significant AD component networks are plotted below in Figure 8.8.

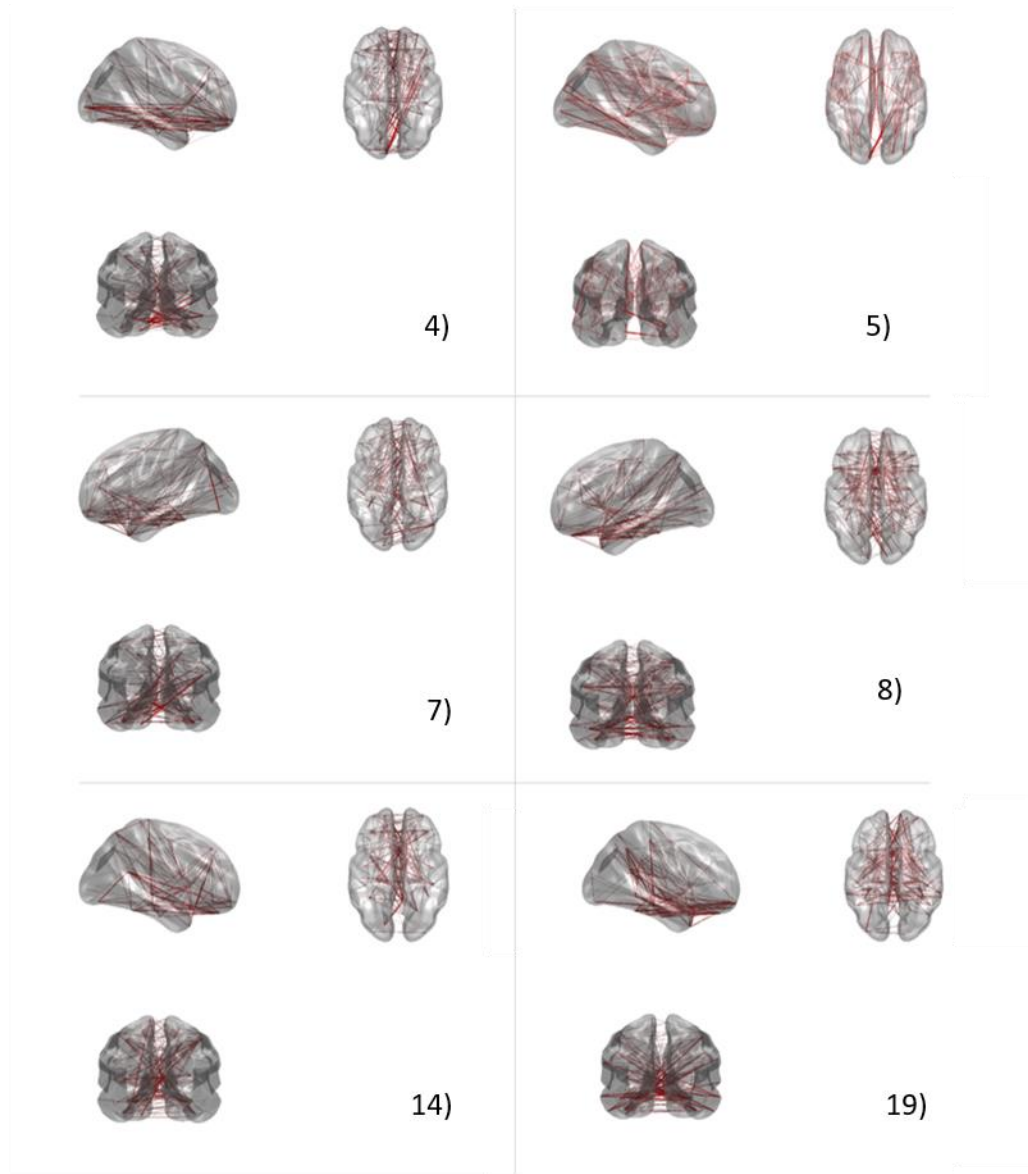


Figure 8.8. The six AD networks significantly predicted by PRS. Networks span widespread areas. The red lines show that PRS was positively correlated with these networks

Contra-prediction, no significant relationships were found with FA components. A significant positive relationship between PRS score and one Euclidean distance component was found at the PRS.01 threshold only. No other significant relationships were found with the structural measures after adjustment.

Additional analyses

To further explore whether any global effects could be responsible for the relationship between PRS and AD and PRS and MD, the global mean of non-zero connection across each participant's 90x90 connectivity matrices was calculated. Two regression models were built with global AD and MD as the outcome variables and PRS, age and gender as predictors. The results are shown in Tables 8.1 and 8.2.

Table 8.1. Regression output for a global AD outcome

| | beta estimate | SE | T stat | P value | |
|-----------|----------------------|-----------|---------------|----------------|-------|
| Intercept | 0.001 | | 1.766 | 66.303 | 0.000 |
| Prs_05 | 0.000 | | 0.000 | -1.020 | 0.311 |
| Age | 0.000 | | 0.000 | 2.549 | 0.013 |
| Gender | 0.000 | | 0.000 | -3.793 | 0.000 |

Table 8.2. Regression output for a global MD outcome

| | beta estimate | SE | T stat | P value | |
|-----------|----------------------|-----------|---------------|----------------|-------|
| Intercept | 0.001 | | 0.000 | 45.531 | 0.000 |
| Prs_05 | 0.000 | | 0.000 | -0.174 | 0.862 |
| Age | 0.000 | | 0.000 | 1.610 | 0.111 |
| Gender | 0.000 | | 0.000 | -1.744 | 0.085 |

Interestingly, both age ($p < .05$) and gender ($p < .01$) were significantly associated with global AD, however PRS was not ($p > .05$), suggesting the relationship between PRS and AD is not driven by a global effect. PRS was also not associated with global MD suggesting the PRS–MD relationships found in this chapter were also not the result of a global effect.

The covariate relationships support previous research showing a relationship between age and AD (Kumar, Chavez, Macey, Woo, & Harper, 2013b; Kumar, Nguyen, Macey, Woo, & Harper, 2012). Gender differences in AD have also been shown in putamen, thalamic, hypothalamic, cerebellar, limbic, temporal, and other cortical sites (Kumar et al., 2013a, 2012), highlighting the importance of including these factors as covariates.

8.5 Discussion

In this chapter, polygenic risk score for schizophrenia, as a predictor of global MEG resting-state connectivity, was explored for the first time to the author's knowledge. Regarding functional oscillatory connectivity, at the edge level, while no connections withstood multiple comparisons, some posterior alpha and beta connections were suggested at the uncorrected level and 95% confidence interval. However, further exploration of networks derived by Non-Negative Factorization across subjects, did not reveal any significant functional relationships, despite the reduced number of outcomes. While previously some large-scale studies have failed to reveal a relationship between PRS and white matter connectivity (Bolhuis et al., 2019; Jansen et al., 2019), a robust relationship was found between PRS and structural connectivity measures, namely increases in axial diffusivity (AD) and mean diffusivity (MD) NNMF measures. Reductions in NNMF networks generated from standardised streamline measures were also predicted by PRS.

AD describes the mean diffusion value (mm^2/s) of water molecules diffusing parallel to the tract within a voxel of interest (Winklewski et al., 2018). AD values have been taken as an index of axonal injury on account of animal findings by Song, Sun and colleagues (Song et al., 2003; Sun et al., 2006). MD refers to the average value of diffusivity in 3 tangential directions and is therefore considered a measure of overall diffusivity in white matter tracts. Both are unspecific, like other measures taken at the voxel level (FA, RD & MD), and may also reflect axonal calibre, or coherence in the orientation of axons within a given voxel, so interpretations of findings are made with caution.

The widespread positive AD effect suggests that individuals with high genetic load for schizophrenia have stronger axial diffusivity network components. Increased AD would suggest that water is less constrained in the direction of the white matter tracts. The opposite effect has been suggested in previous research showing patients (Kelly et al., 2017b), 22.q.11 carriers (Kikinis et al., 2012), and those with increased PRS scores (Stauffer et al., 2021), have widespread reduced FA. Although, broadly, AD and FA measure water movement parallel to white matter tracts, the different effects in AD and FA correlates suggest these measures could be capturing distinct aspects of diffusivity along the direction of the tract.

Regardless of the physiological mechanisms, the finding adds to the body of research showing white matter alterations in schizophrenia genetic risk, where AD findings have been mixed. For example, a recent study (2359 controls & 1963 patients), did not find any AD differences between patients and controls (Kelly et al., 2017b), whereas the largest recent Biobank study to date (Stauffer et al., 2021), found patients to have significantly higher AD in the fornix in comparison with controls. Although in healthy participants, the present investigation supports the work Stauffer and colleagues and suggests AD could be a marker of pathogenetic continuity between the healthy and patient populations.

PRS was also positively associated with half of the MD components. This result is also consistent with the Biobank study by Stauffer and colleagues (2021), who found PRS associated with increased MD, within callosal fibers, projection fibers, association fibers, limbic system fibers, and brainstem tracts. These findings are interesting for two reasons, 1) that PRS might be associated with some overall diffusivity effect in the brain and 2) that applying NNMF to structural data might generate structural subnetworks that are sensitive to changes associated with PRS. Unlike AD and RD, MD has not been associated with specific physiological properties, limiting the interpretation of the results. However, if future research establishes a consistent relationship between PRS and increased MD, MD will provide an important target for future genetic and clinical studies. Importantly, neither the AD nor MD relationships were driven by a global mean effect.

Regarding the other structural measures, PRS was associated with reduction in standardised streamline components. Interestingly, the associated components derived from streamlines at threshold 18 and with the COMMIT method, were highly similar. This is reassuring as it suggests that the method of thresholding might be of less importance than sparsity, in capturing network variance associated with PRS.

Together therefore, structural results suggest PRS is associated with a reduction in the integrity of the white matter tracts based on the streamlines reconstruction, and an increase in diffusivity within white matter tracts.

While there is no significant evidence for an association between oscillatory connectivity and PRS given in this chapter, there are some reasons why these findings might not extend to the clinical population. Numerous studies have now shown patients with schizophrenia to have oscillatory dysconnectivity in networks involving occipital, parietal, frontal and temporal areas (Bowyer, 2016; Goghari et al., 2017; Hinkley et al., 2011; Houck et al., 2017; Kim et al., 2014; Sanfratello et al., 2018; Uhlhaas & Singer, 2010a; Yang et al., 2014; Zhang et al., 2015). Alpha and beta oscillations appear to be fundamental to cortical networks (Bastos et al., 2015; Bowyer et al., 2015; Brovelli et al., 2004; Buzsaki & Draguhn, 2004) and have been shown to have a heritable basis (Colclough et al., 2017).

On one hand, the reduced alpha and beta occipital- parietal connections found at the edge level are consistent with the aforementioned findings and could be further explored. On the other hand, however, findings in this chapter may well show that an increased genetic profile of SNPs associated with schizophrenia is correlated with structural but not functional dysconnectivity. It is possible that structural differences exist in those with high PRS and that functional changes develop later or are associated with a different facet of schizophrenia, for example the presentation of schizophrenia symptomology, as shown in the previous chapter. Support comes from studies which have shown that functional dysconnectivity is more widespread in chronic schizophrenia than in at-risk and first-episode groups (Grent-'t-Jong et al., 2018; T. Li et al., 2017; Pettersson-Yeo et al., 2011; Satterthwaite & Baker, 2015).

Limitations and future directions

Recent research associating PRS with fMRI/MRI phenotypes have utilised particularly large samples because of the availability of resources such as UK Biobank. By comparison, the sample size here was small/moderate, however at present, an equivalent MEG database has not been established. The largest electrophysiological PRS study to date was conducted by Hall and colleagues (2015), which investigated relationships with several event-related potentials (ERP), including P3, sensory gating (P50), and gamma oscillations (n=271 patients). The comparatively small sample size combined with the limited variability in PRS score, could mean the functional

analyses are underpowered, despite the published fMRI findings in the same group. Conducting PRS analysis in clinical populations, where scores are more likely to vary, is also important.

In general, PRS, as compared to family status, might be a more sensitive measure of disease proneness (Goghari et al., 2017). Specifically, PRS score incorporates a large number of variants, even at small effect, that contribute to manifestation; variants which family members may lack. Current thinking among researchers and clinicians is that PRS has the potential for use in clinical differentiation (Lewis & Vassos, 2020), however this would require standardisation of the methods and procedures used to generate the PRS scores.

Moreover, there is still much to be understood about genetic-electrophysiological mechanisms. Anderson and colleagues (2018) found resting-state fMRI amplitude to be associated with PRS in posterior areas congruous with increased inhibitory parvalbumin interneuron density, which is suggestive of a relationship between PRS and E-I balance. As MEG signal reflects the magnetic fields generated by thousands of synchronous pyramidal cells and is thus considered a direct measure of excitatory- inhibitory balance (Vrba & Robinson, 2001), MEG continues to be a valuable tool for considering PRS network relationships.

One of the aims of this research was to investigate global sub-networks from structural and functional data, however, in future, it would be interesting to investigate the relationship between PRS and AD/MD in specific white matter tracts. For example, as schizophrenia is associated with abnormalities of the anterior cingulate (Adam & David, 2007; Bowyer et al., 2015), and that PRS is associated with MD in the cingulate gyrus association fibres (Stauffer, 2021), these tracts might be a good target for investigation. Furthermore, as mentioned the participants in this cohort were healthy, so the effects found may be different in the patient population and could be explored further.

In conclusion, this chapter has shown a robust relationship between PRS and AD and MD diffusivity components derived using Non-Negative Matrix Factorization. However, no significant relationships were found between PRS and functional alpha and beta networks. The modest variability in PRS and factors discussed imply further larger studies are warranted. Such

research will facilitate our understanding of genetic contributions to structural and oscillatory disturbances in schizophrenia.

Chapter 9. Schizophrenia risk factors and local visual gamma

9.1 Rationale

Relationships between genetic and clinical risk and long-range connectivity have been shown in Chapters 7 and 9. However, to what extent these risk factors are correlated with local circuitry is still to be established. High frequency oscillations are thought to reflect local circuitry in the visual cortex (VC) and gamma abnormalities have consistently been shown in people with schizophrenia (Moran & Hong, 2011; Rutter et al., 2009; Shaw et al., 2020; Tsuchimoto et al., 2011; Williams & Boksa, 2010), to the extent that gamma reductions have been considered an endophenotype for schizophrenia disorders. Gamma reductions in the VC have also been associated with visual disturbance, perceptual abnormalities and delusional thought (Grent-‘t-Jong et al., 2016; Robson et al., 2016). This chapter explores risk factors for schizophrenia and their relationship to properties of the sustained visual gamma response, as a proxy for local circuitry in the VC.

9.2 Background

Schizophrenia has been proposed as a disorder of dysconnectivity, both within and between brain regions, with an abundance of research in support (Friston & Frith, 1995; Friston, Brown, Siemerikus, & Stephan, 2016). Individuals with schizophrenia have difficulties with clear perceptual thought, otherwise underpinned by coordinated cortical activity, making neural circuits prime candidates for investigation. The synaptic mechanisms involved in dysconnectivity remain under discussion. Theories include 1) impaired GABAergic modulation 2) NMDA receptor (Glu) hypofunction onto GABAergic interneurons and 3) dopamine dysregulation downstream from D2 receptors. Theories 1 & 2 implicate a disturbance of the aforementioned excitation- inhibition balance (see introductory section on gamma oscillations), where interactions between glutamatergic pyramidal cells and GABAergic interneurons are dysregulated.

Data from animal studies, post-mortem studies and genetic studies indicate altered GABAergic functioning in schizophrenia (Guidotti et al., 2005; Hashimoto et al., 2003; Pocklington et al.,

2015). GABA dysfunction is thought to lead to the disinhibition of glutamatergic pyramidal neurons and a loss of synchronous cortical activity (Lewis, Curley, Glausier, & Volk, 2012; Lisman et al., 2008). Certainly, in post-mortem brains there is a reduction in the GABA-synthesizing enzyme, GAD67 mRNA and protein which is responsible for the majority of GABA production (Hashimoto et al., 2003; Volk, Austin, Pierri, Sampson, & Lewis, 2000). Recent large scale genetic studies have also provided support for direct involvement of both common and rare genetic variations in primary GABAergic dysfunction (Pardiñas et al., 2018; Pocklington et al., 2015).

Studies in vivo however have provided mixed results. In a review of 16 Positron Emission Spectroscopy (GABA H-MRS) and 7 GABA_A Positron Emission Tomography (PET) and Single Photon Emission Computed Tomography (SPECT) neuroimaging studies in the prefrontal cortex and striatum, Egerton and colleagues did not find significant differences, though studies were observed to have considerable heterogeneity (Egerton, Modinos, Ferrera, & McGuire, 2017).

The association between gamma-eliciting visual orientation tasks and GABA concentrations makes these tasks a useful probe of GABA inhibitory processes (Edden, Muthukumaraswamy, Freeman, & Singh, 2009; Muthukumaraswamy et al., 2009). Gamma oscillations are generally reduced in schizophrenia, in both early onset and chronic groups, independent of antipsychotic medication treatment (Tillman et al., 2008; Spencer, Niznikiewicz, Shenton, & McCarley, 2008; Uhlhaas & Singer, 2010). The primary action of antipsychotics is targeting dopaminergic systems by D2 receptor antagonism. Thus, considering the PING model, gamma alterations appear at least in part due to impaired GABAergic functioning.

In support, a recent paper (Shaw et al., 2020) investigated occipital gamma oscillations and GABA in schizophrenia using a PING informed Dynamic Causal Modelling approach. Induced gamma oscillations, performance on the visual-orientation task and GABA levels were reduced in the clinical group. Interestingly, coupling strength between inhibitory neurons and layer 2/3 superficial pyramidal cells predicted performance on the visual orientation task, supporting the finding that gamma oscillations reflect local inhibitory processes (Muthukumaraswamy et al., 2015b). Furthermore, interneuron-interneuron effective connectivity was significantly reduced in

the schizophrenia group and was associated with reduced gamma frequency and severity of negative symptoms (Shaw, Knight, et al., 2020). Superficial pyramidal connections and deep pyramidal -interneuron projections (layers 4, 5/6) were also reduced at trend. No relationship was found between MRS measures and behavioural performance.

The extent to which characteristics of gamma oscillations elicited in this way relate to connections between the cortical laminae in VC has been established through Dynamic Causal Modelling (DCM). DCM has shown that the amplitude of the gamma signal is under the control of interneurons and pyramidal cells in the superficial layers (Shaw et al., 2017). Furthermore, if amplitude is relative to the strength of the postsynaptic current (synaptic gain) layer 4 stellate cells - superficial pyramidal (L4S->SP) connections could also be important, but multiple connections are feasible (Shaw, Muthukumaraswamy, et al., 2020a). Pharmacological studies should be informative. For example, it has been shown the tiagabine (GABA reuptake inhibitor) led to reduced amplitude and increased frequency of the visual gamma response (Shaw et al., 2017).

In theory, the frequency of the oscillation is under the control of the interneurons and recorded from superficial pyramidal cells (signal reflected in M/EEG). Thus, connections between superficial interneurons (SI) and superficial pyramidal cells (SP), in directions SI->SP, SI->SI and SP->SI, are implicated (Sumner et al., 2021). The superficial pyramidal to superficial pyramidal (SP->SP) connection is also inhibitory and may also contribute. In general, finding the same or similar connections predicting both gamma frequency and gamma amplitude is likely.

In schizophrenia, the failure of studies to find consistent effects for MRS GABA and behavioural measures lends support to the synaptic theory 2) that glutamatergic NMDA receptor hypofunction leads to aberrant GABAergic interneuron inhibition which then causes pyramidal cell dysfunction (Cohen, Tsien, Goff, & Halassa, 2015). Valuable insight comes from pharmacology studies with NMDAR agonists such as ketamine and phencyclidine (PCP), which have long been shown to produce an array of schizophrenia -like symptoms in healthy individuals (Cohen et al., 2015; Li & Vlisides, 2016; Luby, Cohen, Rosenbaum, Gottlieb, & Kelley, 1959). Notably, while dopamine agonists also produce a subset of psychotic symptoms,

sub-anaesthetic doses of ketamine produce the full syndrome, including by withdrawal, blunted affect, psychomotor retardation, delusions, and cognitive impairment (Krystal et al., 1994).

A number of putative risk genes for schizophrenia have also been found to be involved in NMDA regulation. For example, the expression of neuregulin 1 and ErbB4 genes is increased in the disorder (Harrison & Weinberger, 2005); an increase that has been associated with suppressed NMDAR regulation (Pitcher et al., 2011). Moreover, genetic ablation of NMDARs reduces the expression of cortical and hippocampal glutamic acid decarboxylase 67 (GAD67) and parvalbumin, in mouse, and leads to schizophrenia-like behaviours such as novelty-induced hyperlocomotion and impaired prepulse inhibition (Belforte et al., 2010). In humans, similar impairments result from *dysfunction* of NMDARs rather than a reduction in number (Kantrowitz & Javitt, 2010).

As with GABA, researchers have sought to explore dysregulation of the excitatory side of the E-I balance in schizophrenia using MRS. Establishing in vivo evidence for altered glutamate levels would provide additional, though indirect, support for the NMDAR hypothesis. At present, review studies show increased glutamate-related metabolites (basal ganglia, thalamus & medial temporal lobe) (Merritt, Egerton, Kempton, Taylor, & McGuire, 2016), increased cortical Glx (glutamate & glutamine combined) (Salavati et al., 2015) and no changes (Iwata et al., 2018). Unlike GABA, glutamate binds with other receptors such as AMPAR and kainite receptors, is involved in several processes outside of neurotransmission and is tightly coupled with glutamine (Tani et al., 2014) and glutathione (Sedlak et al., 2019) challenging the acquisition of reliable estimates. Separation of glutamate metabolites, e.g., glutamate and glutathione, via 3 Tesla MRS has also been controversial and generally considered to be difficult, due to in-sufficient peak resolution in the frequency domain. With the increasing availability of ultra-high field (e.g., 7T) MR scanners, allowing a clearer separation of metabolite peaks, the status of glutamate in schizophrenia will likely be elucidated in future.

The nature of gamma alterations in schizophrenia may also contribute some information about the mechanisms at play. A reduction of amplitude has been found consistently in patients

(Williams & Boksa, 2010). Reductions in frequency have also been found (Shaw et al., 2020; Spencer et al., 2004) but the directionality of the alteration has been more variable.

Alterations in gamma in schizophrenia have been associated with several cognitive, behaviour and symptom factors. For example, reduced task induced gamma amplitude found in the VC is accompanied by poorer visual task performance (Shaw et al., 2020; Uhlhaas & Singer, 2010). Oscillations are also associated with both positive (Spencer et al., 2008) and negative symptoms (Shaw et al., 2020) with one of the prominent positive symptoms in schizophrenia being visual disturbance and hallucinations. As regulated gamma oscillations are fundamental in perceptual binding (Tallon-Baudry et al., 1996), visual gamma oscillations seem to comprise an important local disease marker.

The association with negative symptoms is also interesting as negative symptoms often persist after the offset of acute psychosis and in medicated patients (Buchanan, Breier, Kirkpatrick, Ball, & Carpenter, 1998; Javitt, 2001; Tamminga, Buchanan, & Gold, 1998). As mentioned, antipsychotics operate by antagonising D2 receptors. This is in line with evidence suggesting schizophrenia manifests from downstream hyperdopaminergia through faulty striatal D2 receptors and hypodopaminergia through altered fronto-cortical D1 receptors (Howes & Kapur, 2009). However, the persistence of symptoms suggests that dopaminergic pathways may be secondary to a primary neurotransmitter imbalance, with impaired glutamatergic-GABAergic mechanisms being the supported candidates (Stone, Raffin, Morrison, & McGuire, 2010).

Abnormal task-related gamma oscillations have also been observed in certain at-risk groups, both in the visual (Kornmayer, Leicht, & Mulert, 2014; Koychev, Deakin, Haenschel, & El-Deredy, 2011) and auditory (Hall et al., 2009; Tada et al., 2014; Vernon, Haenschel, Dwivedi, & Gruzelier, 2005) cortices, suggesting local excitation-inhibition dysfunction could comprise a spectrum. Risk groups broadly fall into two categories, clinical risk and genetic risk, although these are not mutually exclusive. Individuals in clinical high-risk groups tend to have undergone clinical assessment for psychosis proneness, for example, the Comprehensive Assessment of At-Risk Mental States (CAARMS) Interview (Yung et al., 2005), or otherwise score highly on measures of schizophrenia traits such as the Schizotypy Scale (Raine & Raine, 1991).

A prominent idea is that schizotypy indexes a continuum between the normal population and schizophrenia onset (Barrantes-Vidal et al., 2015; Claridge & Beech, 2010; Grant et al., 2018). Altered gamma oscillations have also been shown to be associated with schizotypy (Reilly et al., 2018). In a review Reilly found 8 studies that had investigated schizotypy in relation to gamma. The findings were heterogeneous. For example, Kornmayer reported a positive correlation between visual gamma amplitude and the positive schizotypy dimension (Kornmayer, Leicht, & Mulert, 2014a), whereas other studies reported reductions in phase locking factor and spectral power in visual and auditory cortices respectively (Koychev et al., 2011a; Vernon, Haenschel, Dwivedi, & Gruzelier, 2005).

Schizophrenia is also a highly heritable polygenic condition (Larsen et al., 2018; review Mistry, Harrison, Smith, Escott-Price, & Zammit, 2018). Genetic risk evidence comes from familial studies and genetic association studies. For example, variation on chromosome 22 (22q11.2DS), is used as a homogeneous genetic liability model for schizophrenia and has been associated with reduced gamma in a 40Hz auditory steady state stimulus task (ASSR) (Larsen et al., 2018); a response also underpinned by excitatory-inhibitory regulation. Polygenic risk score for schizophrenia (PRS), an association score of multiple variants at low effect expressed in the healthy population, has also been associated with reduced ASSR in the gamma band (Hall et al., 2015). Furthermore, relatives of patients who had schizophrenic spectrum personality symptoms showed reduced fronto-cortical gamma ASSAR power at 40 Hz (Hong et al., 2004)

Rather than a single risk gene for schizophrenia, the known polygenic contribution of many genes distributed across the population, supports the continuous nature of schizotypy. A number of SNPs considered important in schizophrenia have been associated with schizotypy (e.g., rs4680, see Barrantes-Vidal, Grant, & Kwapil, 2015), suggesting some cross over of genetic underpinnings. However, a relationship between PRS and schizotypy does not appear to exist (Nenadić et al., 2020). It is well known that the prerequisite to psychosis onset is multifaceted and factors which lead to a high score on a schizotypy scale (e.g., developmental/ life factors), may have an environmental contribution which are not reflected in scores of genetic liability.

9.2.1 Aim and hypotheses

The aim of this chapter is to explore the relationship between clinical and genetic risk factors and visual gamma metrics, as probes of local connectivity in the VC. It is expected that 1) schizotypy and polygenic risk score for schizophrenia (PRS), will be associated with reduced visual gamma amplitude, considering findings in schizophrenia, 2) schizotypy and PRS will be associated with reduced visual gamma frequency, 3) schizotypy and PRS will not be correlated, as they may reflect different facets of schizophrenia risk.

9.3 Method

9.3.1 Participants

Participants were from the 100-Brains and MEG-Partnership cohorts. The participants were mostly undergraduate students at Cardiff University (mean age 25 years). Participants had no self-reported history of psychiatric or neurological conditions and reported no use of psychoactive drugs. Participants were homogenous in age and right-handed. Of the 185 recruited in total, 124 were female and 61 were male. Informed consent was obtained in line with university procedures. Local ethical approval was obtained through Cardiff University's School of Psychology Ethics Committee.

9.3.2 Measures

The Schizotypal Personality Questionnaire (SPQ) is a self-report measure of schizotypy traits measure, administered at the time of scanning (Raine & Raine, 1991). The questionnaire has 74 items (with a total score ranging from 0 to 74) that fall under nine subscales; ideas of reference, social anxiety, odd beliefs/magical thinking, unusual perceptual experiences, eccentric/odd behaviour and appearance, no close friends, odd speech, constricted affect and suspiciousness/paranoid ideation. Here, the total score will be used as the indicative measure of schizotypal trait in each participant.

Polygenic risk scores were created according to the procedure described by the International Schizophrenia Consortium (2009). Training data were from the most recent schizophrenia GWAS using results from the Psychiatric Genomics Consortium (PGC) schizophrenia genome-wide association studies (GWAS). SNPs were removed from all analyses if they had a low minor allele frequency ($P < 0.01$). Data were pruned for linkage disequilibrium using the clumping function (`-clump`), removing SNPs within 500 kilobase (`-clump-kb`) and $R^2 > 0.1$ (`-clump-r2`) with a more significantly associated SNP. PLINK software was used to calculate polygenic score. For the creation of the PRS for schizophrenia, SNPs associated with SZ that surpassed three GWAS thresholds ($P < 0.5$, 0.1 & 0.05) were considered. Descriptives for PRS 0.05 threshold are: range $6.2538e-04$, mean -0.0013 , std $1.1842e-04$. PRS at threshold $.05$ were used for analyses in this chapter, as it is the threshold for SNP inclusion which captures optimal variance for schizophrenia.

9.3.3 Visual gamma tasks and data acquisition

Participants in both cohorts completed a battery of MEG tasks in the scanner. The visuomotor task involving a visual grating has been previously shown to induced gamma oscillations in visual cortex (Muthukumaraswamy et al., 2010). The visuomotor tasks differed slightly between the cohorts as described below.

100-Brains

The paradigm involved 100 trials and lasted ~ 10 minutes. The visual grating stimulus was presented centrally. It comprised a vertical, stationary, maximum contrast square-wave grating with a spatial frequency of 3 cycles per degree ($8^\circ \times 8^\circ$ visual angle). The background was of mean luminescence. Stimuli were jittered between 1.5-2 seconds and followed by an inter-stimulus interval (ITI) of 2 seconds. Participants were required to push a button with their right hand every time the grating disappeared. Participants were notified if no response was detected after 750ms.

MEG-Partnership

The MEG-Partnership visuomotor task also had 100 trials in total, which lasted ~ 13 minutes. The visual stimulus presented in the lower left visual field was a stationary, vertical, maximum contrast, three cycles per minute, square-wave grating, subtended vertically and horizontally at a 4° angle. The stimulus was presented for 1.5-2 seconds, jittered, on a mean luminance background. The ITIs were either 4 seconds or 8 seconds and allocated to half of the trials, presented in random order. Participants were also required to perform a finger abduction with the index finger on the right hand whenever the grating disappeared. The tasks may be referred to as visuomotor task and visual gamma task interchangeably, though the motor component was not analysed and not of primary interest to the research questions addressed in this thesis.

Both paradigms were programmed in Matlab (2015) and presented at a refresh rate of 100Hz.

All data were acquired on the axial gradiometer (CTF-275 channel) system at CUBRIC which is placed inside a magnetically shielded room. Data were sampled at 1200Hz. Three fiducial coils

(nasion, left pre-auricular and right pre-auricular) were used for head localisation before and after the scan. For noise cancellation, data were acquired with 29 reference channels and were analysed in third-order gradiometer mode as recommended by Vrba and Robinson (2001).

9.3.4 Pre-processing

Both 100-Brains and MEG- Partnership data were pre-processed manually in DataEditor. Third-order gradient mode was applied, transforming the primary sensors for environmental noise reduction. Data were epoched into 4 second trials (-2, 2), around the stimulus onset. Trials which contained large blink, motion and muscle artefacts were excluded.

MRIs and co-registration

MRIs (1mm- isotropic, T1 weighted), were acquired on the 3 Tesla General Electric system at CUBRIC. Manual co-registration was completed on the MR image using photographs referencing the fiducial marks made on the participants during the MEG recording.

9.3.5 Visual gamma analysis

The MEG visual gamma analysis is described in full in Chapter 3, however, a summary is provided here. Beamforming was completed on 6 bilateral visual areas: Calcarine, Cuneus, Lingual, Superior Occipital, Mid Occipital and Inferior Occipital. The leadfield was constructed using a 1mm MNI sampling grid. The beamformer weights were based on the global data covariance between 30-80 Hz. Source power was projected separately for baseline and stimulus periods. A virtual sensor was inserted at the point of the peak source amplitude. The sustained period of the response was of interest and selected at 0.3s- 1.2s after stimulus onset.

9.3.6 Statistical analyses

Results were analysed in IBM SPSS (25) and JASP (0.14.1). Multiple regression models were generated with the enter method. Main predictors were schizotypy and PRS. The null models included age and gender covariates. Where the 100-Brains and MEG-Partnership data was combined, task paradigm was also coded and included as a covariate, to account for the discrepancy in tasks. Bayesian regression was implemented, post hoc, for relationships with non-significant p-values, to evaluate evidence for either the null or alternative hypotheses.

9.4 Results

The gamma amplitude and frequency descriptives, broken down by cohort, are shown in Table 9.1.

Table 9.1. Descriptive Statistics -Visual Gamma Metrics

| | Amplitude | | Frequency | |
|-------|-----------|-----|-----------|----|
| | Brains | MP | Brains | MP |
| Valid | 96 | 84 | 96 | 84 |
| Mean | 297 | 202 | 50 | 51 |
| SD | 242 | 157 | 8 | 8 |

The relationship between schizotypy scores and polygenic risk scores was investigated using correlation analysis and is shown in Figure 9.1.

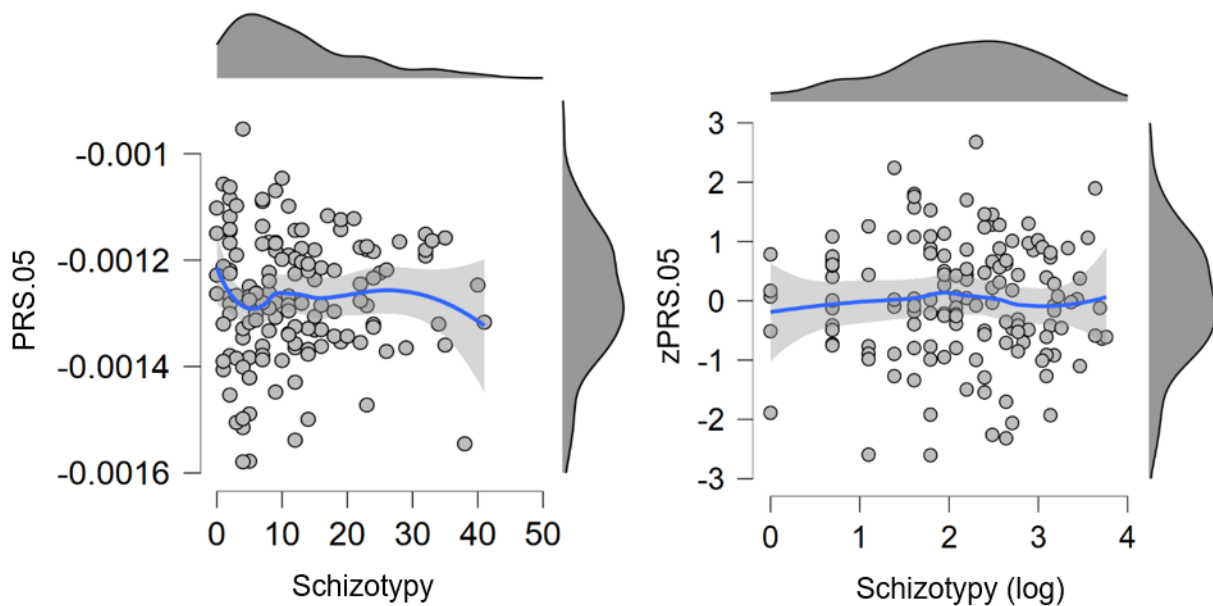


Figure 9.1. Shows the relationship between PRS and schizotypy. The left shows PRS plotted against schizotypy. The right shows normalised PRS plotted against logged schizotypy scores.

As expected, no significant relationship was found between PRS and schizotypy scores ($r=0.013$, $p=0.8$).

9.4.1 Schizotypy

A negative relationship between schizotypy and gamma amplitude can be seen in Figure 9.2. No evidence for a relationship with gamma frequency was observed.

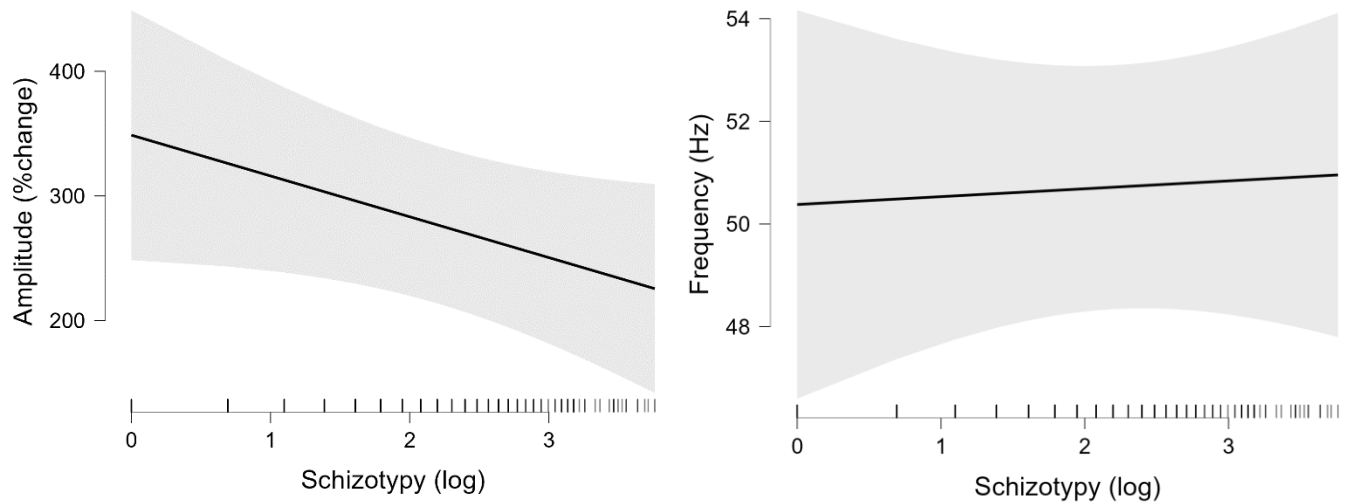


Figure 9.2. The left shows the marginal relationship between schizotypy and gamma amplitude, when age, gender and paradigm covariates were held constant. Right, shows the marginal relationship between schizotypy and gamma frequency. The grey area represents a 95% confidence interval around the line of fit.

The results of the regression model in which schizotypy was a predictor of gamma amplitude across both cohorts are shown in Table 9.2.

Table 9.2. Gamma amplitude in the combined analysis

| Model H ₁ | Adjusted R ² | Standardised beta | p | 95% CI | | BF |
|----------------------|-------------------------|-------------------|---------|---------|---------|-----|
| | | | | Lower | Upper | |
| Schizotypy | 0.095 | | | | | |
| Age | | 0.176 | 0.026 | 0.839 | 12.682 | |
| Gender | | 0.094 | 0.22 | -26.129 | 112.385 | |
| Paradigm | | -0.274 | < .001* | -184.06 | -51.686 | |
| Schizotypy | | -0.14 | 0.07 | -68.212 | 2.679 | 1.3 |

*. The effect is significant at the .05 level

Schizotypy predicted gamma amplitude at the $p = .07$ level. Bayesian regression was employed to quantify evidence for the alternative as opposed to the null i.e., that there is a relationship between schizotypy and peak gamma amplitude. A Bayes Factor (BF) value of ~ 1 is inconclusive i.e., provides no evidence either for or against the null hypothesis.

The results of the analysis in which schizotypy was a predictor of visual gamma frequency are shown in Table 9.3.

Table 9.3. Gamma frequency in the combined analysis

| Model H ₁ | Adjusted R ² | Standardised beta | p | 95% CI | |
|----------------------|-------------------------|-------------------|-------|--------|-------|
| | | | | Lower | Upper |
| Schizotypy | 0.002 | | | | |
| Age | | -0.148 | 0.074 | -0.427 | 0.02 |
| Gender | | -0.045 | 0.58 | -3.344 | 1.878 |
| Paradigm | | 0.104 | 0.208 | -0.897 | 4.094 |
| Schizotypy | | 0.018 | 0.821 | -1.183 | 1.49 |

Schizotypy was not associated with gamma frequency ($p > .05$). The Brains and MEG-Partnership cohorts were also analysed separately considering the difference in visual gamma task. Splitting the regression models did not reveal a significant relationship between schizotypy and the visual gamma metrics in either cohort. However, the negative relationship between schizotypy and gamma amplitude was larger in the 100-Brains cohort ($B = -0.184$, $p = 0.098$) than in the MEG-Partnership cohort ($B = -0.124$, $p = 0.29$).

Covariates in the schizotypy model

Age and gamma task were both significantly associated with gamma amplitude, $p < .05$.

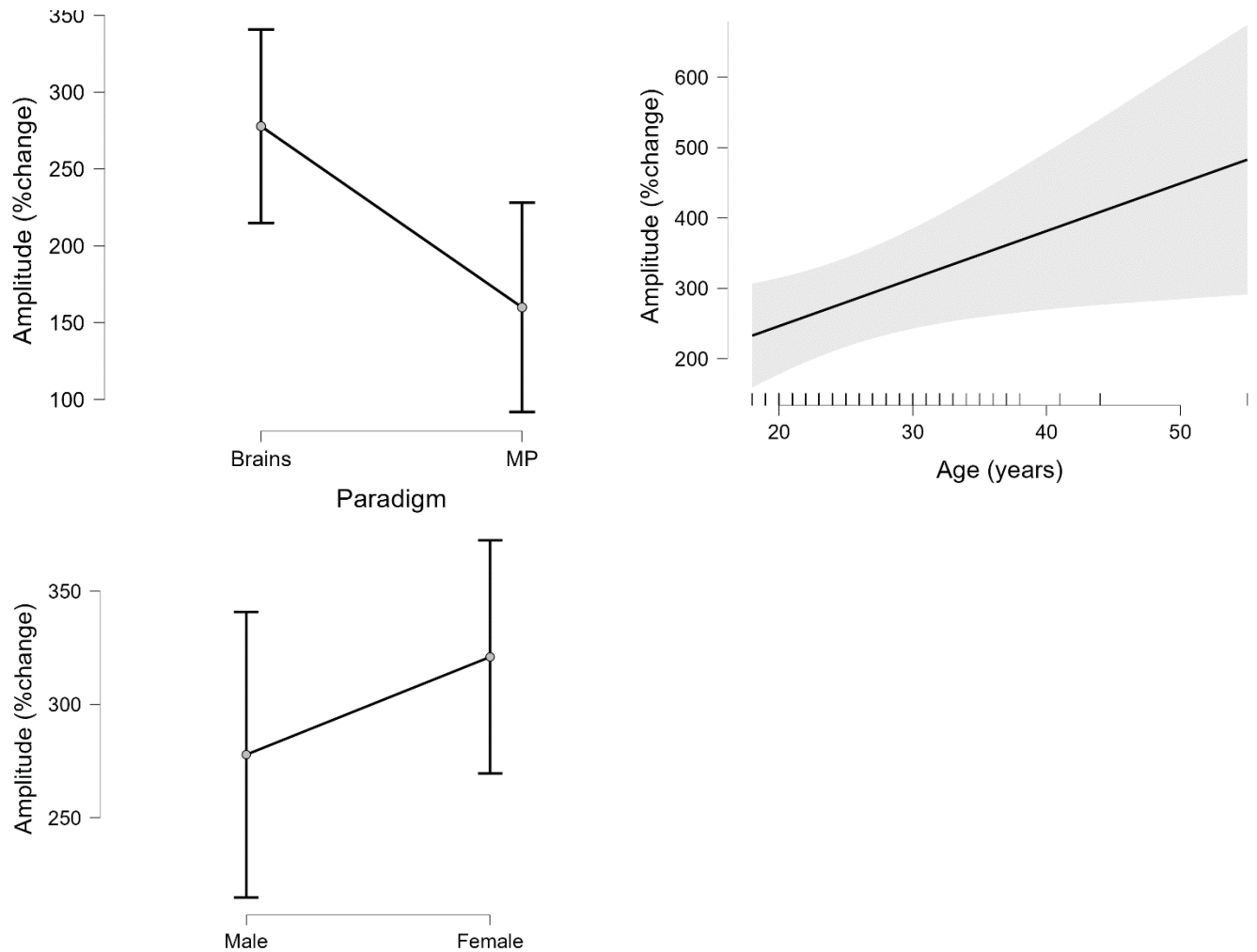


Figure 9.3. Shows the marginal effect of paradigm (top left), age (top right) and gender (bottom left) on gamma amplitude when controlling for the other variables in the regression model. The grey area represents a 95% confidence interval around the regression line.

The covariate relationships (shown in Figure 9.3) suggest that those who were older had higher gamma amplitude values. Those in the 100-Brains cohort also had higher amplitude values than those in the MEG-Partnership cohort. Females also had higher amplitude values than males, but not significantly so. None of the covariates significantly predicted gamma frequency.

9.4.2 Polygenic Risk Score

Polygenic risk score was first investigated as a predictor of gamma amplitude across both cohorts, the results of which can be seen in Table 9.4. Figure 9.4 shows a weak negative relationship between PRS and gamma amplitude, when holding age, gender and paradigm variables constant. No relationship was observed between PRS and gamma frequency in Figure 9.4.

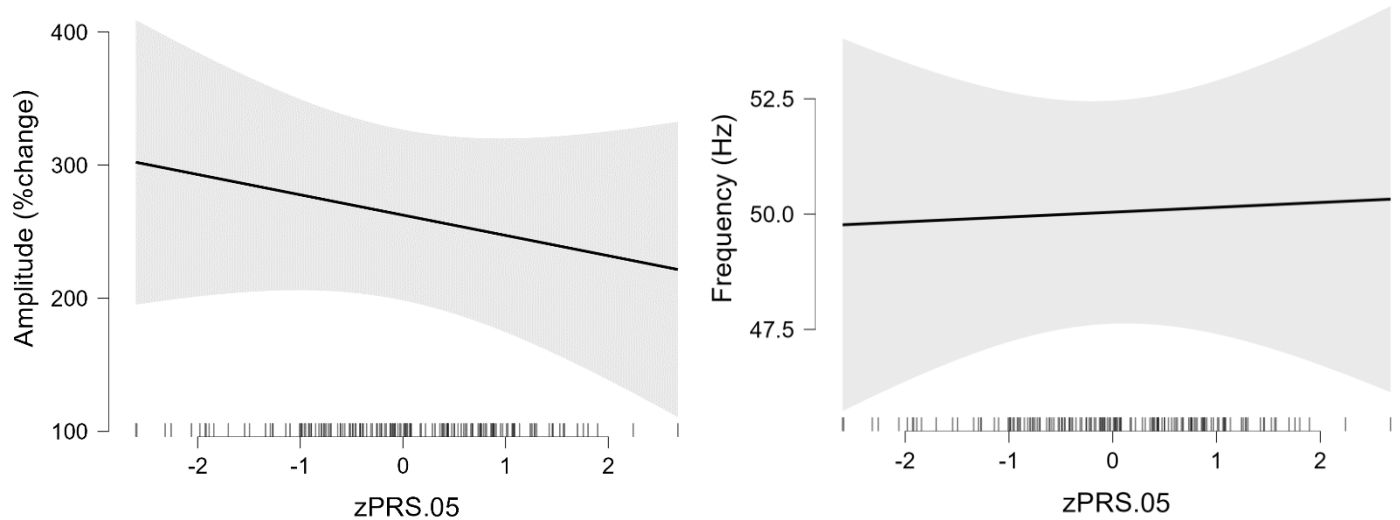


Figure 9.4. The left shows the marginal relationship between PRS and gamma amplitude, when age, gender and paradigm covariates were held constant. Right, shows the marginal relationship between PRS and gamma frequency. The grey area represents a 95% confidence interval around the regression line.

Table 9.4. Gamma amplitude in the combined analysis

| Model H ₁ | Adjusted R ² | Standardised beta | p | 95% CI | |
|----------------------|-------------------------|-------------------|---------|---------|---------|
| | | | | Lower | Upper |
| PRS | 0.097 | | | | |
| Age | | 0.195 | 0.015* | 1.619 | 14.481 |
| Gender | | 0.176 | 0.024* | 11.141 | 153.831 |
| Paradigm | | -0.289 | < .001* | -197.69 | -58.996 |
| PRS.05 | | -0.07 | 0.368 | -48.6 | 18.093 |

*. The effect is significant at the .05 level

PRS did not significantly predict gamma amplitude in the combined model, $p > .05$. The Brains and MEG-Partnership cohorts were also analysed separately considering the difference in visual gamma task, results of which can be seen in Tables 9.5 and 9.6, respectively. Interestingly, splitting the regression models revealed a significant negative relationship between polygenic risk score and visual gamma amplitude, $p = .020$, in the 100-Brains cohort, where higher PRS were associated with lower peak gamma amplitude values. However, this was not found in the MEG-Partnership cohort ($p > .05$), where a positive relationship can be seen (Figure 9.5).

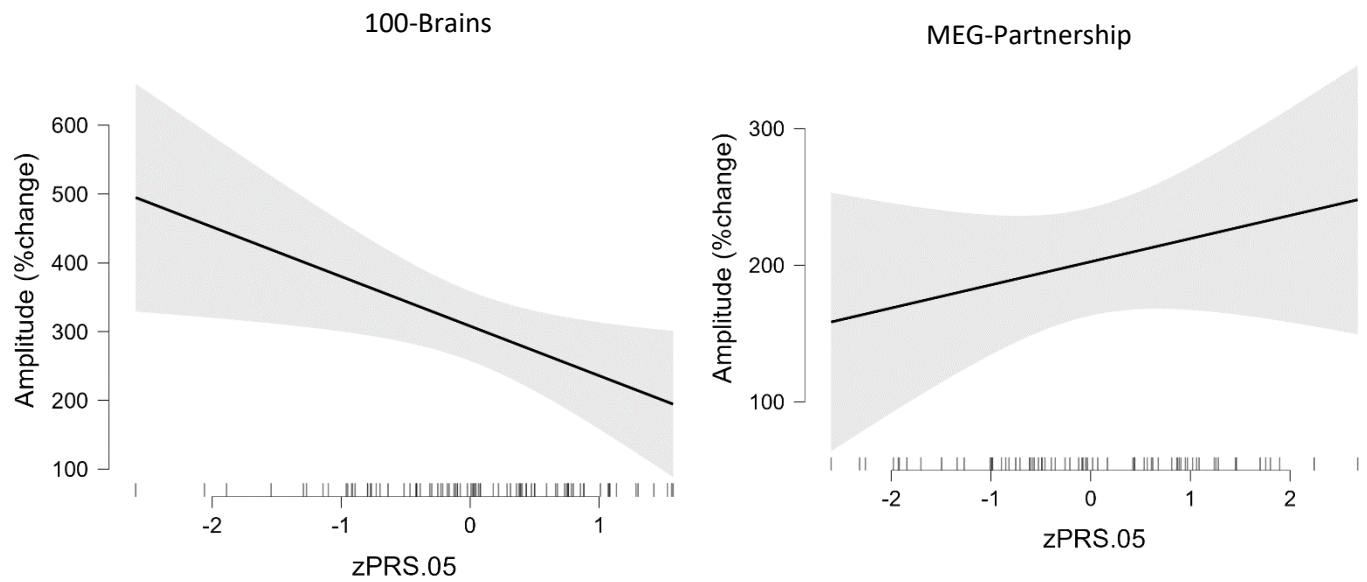


Figure 9.5. The left shows the marginal relationship between PRS and gamma amplitude in the 100-Brains cohort, when age, gender and paradigm covariates are held constant. Right, shows the marginal relationship between PRS and amplitude in the MEG-Partnership cohort. The grey area represents a 95% confidence interval around the regression line.

Table 9.5. Gamma amplitude in the 100-Brains Cohort

| Model H ₁ | Adjusted R ² | Standardised beta | p | 95% CI | | BF |
|----------------------|-------------------------|-------------------|--------|---------|---------|-------|
| | | | | Lower | Upper | |
| PRS | 0.127 | | | | | |
| Age | | 0.232 | 0.025* | 2.397 | 35.643 | |
| Gender | | 0.258 | 0.014* | 27.732 | 238.859 | |
| PRS.05 | | -0.245 | 0.02* | -132.33 | -11.836 | 4.415 |

*. The effect is significant at the .05 level

Table 9.6. Gamma amplitude in the MEG-Partnership Cohort

| Model H ₁ | Adjusted R ² | Standardised beta | p | 95% CI | | BF |
|----------------------|-------------------------|-------------------|-------|---------|---------|-------|
| | | | | Lower | Upper | |
| PRS | 0.028 | | | | | |
| Age | | 0.23 | 0.06 | -0.242 | 10.958 | |
| Gender | | 0.082 | 0.498 | -56.557 | 115.091 | |
| PRS.05 | | 0.121 | 0.315 | -16.42 | 50.266 | 0.385 |

Bayesian analyses

To further explore these results in relation to the null, i.e., that no relationship exists between PRS and gamma amplitude, or the alternative, that there is a relationship between these variables, Bayesian regression was employed. A BF above 3 is considered as support for the alternative, while a value of below 0.3 is considered support for the null (Kass & Raftery, 1995). The merit of Bayes is the provision of evidence against the null in light of a null finding. The BF for PRS in the MEG- Partnership data was .385 (.4 1dp), which is inconclusive but provides anecdotal evidence for the null (Lee & Wagenmakers, 2012). In contrast, the BF for the 100-Brains cohort was 4.415 which gives support to the alternative hypothesis, suggesting there may be a relationship between PRS and reduced gamma amplitude in the population.

Lastly, PRS was investigated as a predictor of visual gamma frequency, the results of which can be seen in Table 9.7.

Table 9.7. Gamma frequency combined analysis

| Model H ₁ | Adjusted R ² | Standardised beta | p | 95% CI | |
|----------------------|-------------------------|-------------------|-------|--------|-------|
| | | | | Lower | Upper |
| PRS | 0.001 | | | | |
| Age | | -0.159 | 0.057 | -0.479 | 0.007 |
| Gender | | -0.012 | 0.886 | -2.89 | 2.498 |
| Paradigm | | 0.086 | 0.301 | -1.243 | 3.994 |
| PRS.05 | | 0.013 | 0.869 | -1.154 | 1.364 |

PRS did not significantly predict gamma frequency in the combined or separated cohorts, $p > .05$.

Covariates in the PRS models

In the combined model, age, gender and gamma task were significantly associated with gamma amplitude ($p < .05$), in the same direction shown in Figure 9.3. None of the covariates significantly predicted gamma frequency.

9.5 Discussion

In summary, a negative relationship, approaching significance, was found between schizotypy and gamma amplitude, suggesting individuals with higher schizotypy scores had reduced gamma amplitude. However, Bayesian analysis suggested this was inconclusive, probably due to an underpowered design through the use of two different visual gamma tasks. No evidence was found for a relationship between schizotypy and gamma frequency. While PRS did not predict gamma amplitude overall, there was some evidence to suggest a relationship in the 100-Brains cohort. That is, that higher polygenic risk load was associated with reduced gamma amplitude. However, no evidence for this relationship was found in the MEG-Partnership data. No evidence for a relationship between PRS and gamma frequency was found either. In line with prediction, no evidence of a relationship between PRS and schizotypy was found.

The weak schizotypy relationships add to a body of mixed findings between schizotypy and gamma (Reilly et al., 2018). This might at least in part be due to the dimensionality of schizotypy. Schizotypy traits, like schizophrenia symptoms, can be classified into at least positive, negative and cognitive categories (Vollema & van den Bosch, 1995). Similarly, Principal Components Analysis (PCA) suggests schizotypy traits load onto three factors (social-interpersonal, cognitive-perceptual, and disorganization) with considerable cross over with schizophrenia (Calkins, Curtis, Grove, & Iacono, 2004). In the study by Kornmayer, for example, a positive relationship was found between evoked visual gamma and the positive schizotypy dimension, but no other dimensions (Kornmayer, Leicht, & Mulert, 2014b). Only a total schizotypy score was available at the time of this thesis meaning any sub-construct relationships with gamma were not elucidated.

Despite this, the negative direction of the relationship between schizotypy and visual gamma amplitude was consistent with the only other study, to the authors knowledge, that has investigated induced gamma (Vernon et al., 2005). Vernon and colleagues (2005) found high schizotypy individuals exhibited reduced sustained gamma power in the auditory cortex, using an auditory habituation task. The heterogamous nature of the existing schizotypy and gamma literature, where few findings are in VC, could suggest further research is warranted.

Though the schizotypy- gamma literature is heterogeneous the study of schizotypy is important for a number of reasons (Barrantes-Vidal et al., 2015). Firstly, schizotypy provides a platform for understanding shared aetiology of clinical presentations. For example, high positive schizotypy traits are present in individuals with schizophrenia and mood disorders with psychotic symptoms (Varghese et al., 2011), linking mood and non-mood experiences. Secondly, reports of schizotypy experiences, particularly ideas of reference and lack of close interpersonal relationships, are associated with transition to psychosis (Salokangas et al., 2013). These studies aid understanding of both risk and resilience factors in high schizotypy individuals. Moreover, the continuous nature of schizotypy compliments current National Institute of Mental Health (NIMH) initiatives. The Research Domain Criteria (RdoC), is a bottom-up approach to identifying maladaptive phenotypes in the population and is being increasingly advocated. On this basis, the continued investigation of schizotypy relationships is worthwhile. A narrative on the contextualisation of schizotypy is also superfluous to this chapter but may provide some perspective to the mixed schizotypy findings that exist.

Moreover, over the last decade, genome wide association (GWAS) studies have established schizophrenia as a polygenic condition (Ripke et al., 2014). The analyses of PRS and visual gamma was more exploratory considering the power that is required for PRS studies. For example, the UK biobank studies show associations between PRS and f/MRI measures in ~ 1000 subjects. However, a relationship between PRS and gamma amplitude, as suggested in the 100-Brains data, would be interesting considering findings of reduced gamma amplitude in schizophrenia (Gonzalez-Burgos, Fish, & Lewis, 2011; Shaw, Knight, et al., 2020; Uhlhaas & Singer, 2013). The implication being that PRS captures genetic architecture involved in the gamma reductions seen in patients and could facilitate insight into the genetic contribution to local circuitry and E-I balance in the VC.

Recently, Dimitiridis and colleagues also failed to find significant differences in narrow-band induced gamma and PRS in a genetic recall sample of ~200 participants (low and high schizotypy) (Dimitriadis et al., 2021). While amplitude in the high schizotypy group was reduced, the effect did not meet significance. This result again suggests that with improved power a relationship between PRS and visual gamma might be established. Interestingly, there

was also evidence of beta and broadband power changes with PRS in this study suggesting that it is important to look at a wider set of signals in future research.

Not all studies have found visual gamma reductions in schizophrenia disorders. For example, Brealy found increased MEG visual gamma amplitude in subjects with Schizoaffective Bipolar Disorder, using the same visual grating paradigm as in the 100-Brains cohort (Brealy et al., 2015), which is interesting considering significant genetic overlap has been shown between schizophrenia, bipolar and schizoaffective disorders (Cardno & Owen, 2014). This point may not be critically relevant to Brealy's findings, as the bipolar subtype of schizoaffective disorder may have a distinct genetic contribution (Cardno & Owen, 2014). However, simultaneous investigations of PRS as a predictor of gamma in at risk groups and patients may help further untangle these findings in regard to shared polygenic factors versus environmental or developmental factors.

Heritability of schizotypy traits has been shown at 50 percent (Linney et al., 2003). Evidence for genetic cross over with schizophrenia comes indirectly from familial studies showing family member of schizophrenia patients to score highly on schizotypy traits. Large GWAS studies have also shown correlations in linkage signals from genome-wide scans of schizophrenia and schizotypy (Fanous et al., 2007). However, this was not reflected in this chapter as no convincing relationship was found between PRS and schizotypy.

One reason is that several psycho-social and developmental factors contribute to both schizotypy and schizophrenia, for example pre- and peri-natal conditions and cannabis use have associated with psychosis risk (Compton, Chien, & Bollini, 2009; Machón et al., 2002). That being said, genetic and environmental factors are not necessarily mutually exclusive with epigenetic studies increasingly suggesting events like trauma can lead to a rapid adaption of the genome (Van Winkel, Van Nierop, Myin-Germeys, & Van Os, 2013). Findings such as these add to the multifaceted conceptualisation of schizophrenia.

Limitations and future directions

The absence of convincing relationships with amplitude and frequency prevents any meaningful conclusions or postulations being made about local neuro-circuitry and its underlying mechanisms. The main limitation of this chapter is that the power of the analysis was compromised by relatively moderate participant numbers and the inclusion of data with two different task paradigms. This is something to be addressed with larger MEG studies. However, the chapter's merit lays in the simultaneous use of different measures of risk for schizophrenia, which have been administered in the un-medicated, normal population. It was also, to the authors knowledge, the largest analysis of its kind.

Dynamic Causal Modelling is a valuable tool for probing specific connections in the micro-circuitry of the brain. DCM findings from the Cardiff MEG groups suggest that excitatory-inhibitory connections in the superficial layers of the visual cortex can be probed with visual gamma amplitude (Shaw et al., 2017). A potentially fruitful future direction would be investigating the relationship between the connections in superficial layers of visual cortex and PRS with DCM. This would provide evidence towards a specific local genotype-endotype interaction within the canonical microcircuit. This work is ongoing. Similarly, correlations with schizotypy might elucidate the relationship between clinical risk and functional visual micro-circuitry. Additionally, more recently developed measures of schizotypy exist, such as the O-LIFE (Mason & Claridge, 2006) and could be explored.

In conclusion, relationship trends between both schizotypy and polygenic risk score and reduced visual gamma amplitude were found, however these did not meet statistical significance. In line with schizophrenia findings, a significant negative relationship was found between PRS and reduced gamma amplitude in a sub-cohort, however further analyses would be needed to ratify such results. Conceptual and contextual elements of schizotypy and polygenic risk are discussed.

Chapter 10. The effect of excitatory-inhibitory (E-I) CNV status on global oscillatory connectivity and visual gamma in psychosis

10.1 Rationale

Individuals with schizophrenia have been shown to have an imbalance of excitatory and inhibitory (E-I) neural systems resulting in both local and global dysconnectivity (Committee, 2019; Friston, Brown, Siemerkus, & Stephan, 2016; Shaw, Knight, et al., 2020). GABA is the major inhibitory neurotransmitter in the brain while glutamate is the main excitatory neurotransmitter. Copy number variants (CNVs) are small genetic variants which have been strongly implicated in the etiology of schizophrenia (Bassett, Marshall, Lionel, Chow, & Scherer, 2017). MEG oscillations are sensitive to E-I processes. The aim of this research was to investigate local and long-range imaging markers, in individuals with schizophrenia with and without CNVs which impact the GABA and glutamate pathways.

10.2 Introduction

CNVs are multiplications, deletions or translocations of segments of DNA (from 1000 up to several million base pairs in length). In comparison to Single Nucleotide Polymorphisms (SNPs), where the 108 known loci/common variations contribute a very small amount to schizophrenia risk (Ripke et al., 2014), CNVs are rare and larger in terms of both size (> 500 kb) and pathological effect (odds-ratio 2-60) (Rees, O'Donovan, & Owen, 2015). Around 1500 regions of copy variation exist, constituting around 10-12% of the human genome (Redon et al., 2006). Many CNVs are specific to clinical disorders, for example, the HTT/IT15 gene in Huntington's Disease (Imarisio et al., 2008), the 7q11.23 region in Williams-Beuren syndrome (Merla, Brunetti-Pierri, Micale, & Fusco, 2010), and region 15q11-q13 in Angelman/Prader-Willi syndrome (Kalsner & Chamberlain, 2015). CNVs are mostly inherited (~99%) but can also exist *de novo*, i.e., due to mutation in meiosis (Van Ommen, 2005).

In schizophrenia no binary relationship between single-CNV carrier status and presentation has been found. Instead, CNVs are considered genetic risk factors (Kirov, Grozeva, et al., 2009;

Levinson et al., 2011; Marshall et al., 2017; Rees, Moskvina, Owen, O'Donovan, & Kirov, 2011; Rees et al., 2014). The last 15 years of research has focused on case-control association studies, implicating several CNVs within large samples (>21,000 cases & 20,000 controls; Marshall, 2017). Some of these are particularly rare, even in those with established schizophrenia prompting a review of findings by Rees (2014b), who found 11 loci robustly associated with schizophrenia. These include deletions at 1q21.1, *NRXN1*, 15q11.2 and 22q11.2 and duplications at 16p11.2 and the Angelman/Prader-Willi Syndrome region, with approximately 2.5% of patients and .09% of controls carrying these variants. Many of these regions are also implicated in disorders such as autism, epilepsy and intellectual disability (Girirajan et al., 2012; Hu et al., 2020; Olson et al., 2014; Velinov, 2019), which may provide some information on comorbidity in schizophrenia. Furthermore, *de novo* CNVs are more frequent in patients (5.1%) compared with controls (2.2%). Mutations arising *de novo* could contribute to the continuation of schizophrenia pathogenesis in the population despite the reduced fecundity in patients (Kirov et al., 2012).

Schizophrenia is known as a disorder of neural dysconnectivity (Friston, Brown, Siemerikus, & Stephan, 2016) and several studies have shown a relationship between risk-CNVs and brain structure and function. This has been made possible by the exponential growth of large genomic-imaging databases such as ENIGMA (Enhancing Neuro Imaging Genetics through Meta-Analysis: ENIGMA) and UKBioBank, where data has been collected over several MRI sites. Structural impairments associated with 22q11.2 and 16p11.2 span the insula, calcarine cortex, transverse temporal gyrus, superior and middle temporal gyri, caudate and hippocampus morphometry (Martin-Brevet et al., 2018). Reduced regional caudate, pallidum and putamen volumes have also been found (Sønderby et al., 2020).

Interestingly, in a review of CNV imaging studies, Moreau suggests pathogenic CNVs show an effect on brain related alterations that is 2-5 times larger than diagnostic studies (i.e., symptom defined) (Moreau, Ching, Kumar, Jacquemont, & Bearden, 2021). Presence of the 22q11.2 deletion, for example, increases risk for schizophrenia 20-fold and has been associated with numerous neural alterations (Sun et al., 2020), which has encouraged its use as a proxy model of

schizophrenia (Cleynen et al., 2020) and its consideration as a genetic subtype (Karayiorgou & Gogos, 2004).

Despite the abundance of functional neuroimaging schizophrenia studies that exist, functional CNV association studies are relatively sparse and have investigated large effect variants such as 22q11 and 16p11. For example, Blood Oxygen Level Dependent (BOLD) studies have shown 16p11.2 variant effects on global, thalamic-sensorimotor, frontal and temporoparietal, posterior insula, pre-supplementary motor cortex, amygdala-hippocampus complex, cerebellum, and basal ganglia connectivity (Bertero et al., 2018; Moreau et al., 2020). Additionally, 22q11 deletion carriers have consistently shown network level impairments in the Default Mode Network (DMN) and frontoparietal networks (Mattiaccio et al., 2016; Moreau et al., 2020; Schreiner et al., 2017) as well as hyper- and hypo connectivity of the thalamocortical somatomotor regions and frontoparietal associative networks (Moreau et al., 2020; Schleifer et al., 2019).

Schizophrenia is a heterogeneous disorder, where within-group variability can weaken diagnostic group effects. Therefore, CNV-control studies may have improved sensitivity to detect endophenotypes due to the homogeneity in the CNV manipulation. Variants at the same locus, i.e., deletions versus duplication, also have specificity, known as a ‘gene dosing’ effect, where opposing variants show a graded or even flipped direction of effect on connectivity in many areas (Moreau et al., 2021).

Notably, the reviewed CNV-imaging literature has utilised MRI techniques which provide high spatial but poor temporal resolution, due to metabolic dependencies, and fail to provide much information on underlying functional mechanisms. Electrophysiological papers are less abundant; however, evidence suggests that beta band oscillations are altered with 15q11.2-q13.1 duplications (Frohlich et al., 2019, 2016) and 16p11.2 deletions (Hinkley et al., 2019).

In the MEG resting-state, children with 22q11.2 deletion syndrome have been shown to have reduced oscillatory delta band activity in the medial temporal lobe and gamma activity in the occipital lobes, alongside increased gamma activity in frontal lobes, compared to controls (Doherty et al., 2021). Moreover, during the presence of a visual grating those with 22q11

deletions (7-30 years) show gamma and theta spectral power reductions in visual cortex (Mancini et al., 2022). Additionally, adults showed increased alpha/beta synchronisations in the same study.

Furthermore, another recent MEG study investigated differences in resting-state connectivity between individuals with neurodevelopmental CNVs, including deletions or duplications at 22q11.2, 15q11.2, 15q13.3, 16p11.2, 17q12, 1q21.1, 3q29, and 2p16.3, and controls (Dima et al., 2020). Decreased amplitude-amplitude connectivity between occipital, temporal, and parietal areas in the CNV group was found which was not solely driven by the 22q variant.

With the exception of 22q.11, the study of single variants has become increasingly unrewarding (Pocklington et al., 2015). Smaller CNVs are also likely to be important to function and behaviour in light of what has become known about combined genetic influences, e.g., the polygenic nature of SNPs. However, investigations have been made difficult by the rarity of many CNVs. In this respect, the approach taken by Dima and colleagues is desirable as grouping CNVs could improve sensitivity to imaging endophenotypes and presentation effects, particularly in view of the mentioned non-specificity of loci across different disorders.

In schizophrenia, functional dysconnectivity is underpinned by an imbalance of inhibitory and excitatory processes (Committee, 2019; Friston et al., 2016; Shaw, Knight, et al., 2020). GABA and glutamate, respectively, are the major inhibitory and excitatory neurotransmitters in the brain. Whilst the exact synaptic mechanisms involved in E-I imbalance are unknown, prominent theories include impaired GABAergic modulation and/or NMDA receptor (Glu) hypofunction onto GABAergic interneurons. Thus, it would seem not only important to consider CNVs associated with pathology but also those, even at small effect, involved in these neurotransmitter pathways.

In this vein, Pocklington investigated >11,000 schizophrenia cases and controls, finding both genetic evidence for disturbed glutamatergic signalling and novel causal evidence for disturbed GABAergic signalling in cases (Pocklington et al., 2015). The enrichment of NMDAR complex duplications, PSD-95 protein (post synaptic scaffold protein on excitatory neurons) and ARC

protein complex deletions found in cases in this study (Pocklington et al., 2015), in addition to denovo findings (Rees et al., 2011), polygenic (Ripke et al., 2014), animal studies (Lisman et al., 2008) and pharmacological studies (Muthukumaraswamy et al., 2015), provide very strong evidence for impaired glutamatergic function in aetiology of schizophrenia.

Regarding GABAergic neurotransmission, evidence for disturbance has been largely observational, i.e., from post-mortem and Magnetic Resonance Spectroscopy studies (Guidotti et al., 2005; Vierling-Claassen et al., 2008), where independence from glutamatergic influences has been unclear. However, Pocklington and colleagues found enrichment of GABA_A receptor complexes, independent of NMDAR complex genes in schizophrenia cases. Furthermore, the NRXN1 gene encodes the synthesis of presynaptic cell adhesion protein neurexin 1 in both GABAergic and glutamatergic synapses, and a robust association between NRXN1 deletions and schizophrenia risk has been established (Kirov, Rujescu, et al., 2009).

Box 10.1. Implicated E-I complexes in schizophrenia (Sz)

NMDA- N-Methyl-D-aspartate (NMDA) is an amino acid derivative that acts as a specific agonist at the NMDA receptor, copying the action of glutamate. Postsynaptic NMDA receptor hypofunction in Sz.

PSD-95- Postsynaptic density protein 95 (PSD-95) is an essential postsynaptic scaffolding protein in glutamatergic excitatory neurons. Disruption associated with cognitive deficits in Sz.

ARC- Activity-Regulated Cytoskeletal-associated (Arc) gene- postsynaptic signalling complex- related to NMDA. Differential Arc protein expression alters glutamate-mediated processes. ARC CNVs associated with Sz.

NRXN1- NRXNs are found presynaptically and are believed to interact with postsynaptic neuroligins (NLGNs) in excitatory (glutamatergic) and inhibitory (GABAergic) synapses in the brain. Evidence towards disturbed NRXN1 in Sz.

mGluR5- Metabotropic glutamate receptor 5 is an excitatory postsynaptic receptor, encoded by GRM5 gene. Receptor hypofunction is associated with Sz.

GABA^A – Pre and post synaptic receptors- involved in the activity activated release of inhibitory neurotransmitter GABA. Postsynaptic dysfunction associated with Sz.

As discussed elsewhere in this thesis, existing MEG analysis techniques allow local E-I circuitry in visual cortex, as well as long-range connectivity, to be probed. Using Dynamic Causal Modelling (DCM) of the canonical microcircuit in visual cortex, it has been shown that the amplitude of gamma oscillations induced with a visual grating task, is closely coupled with connectivity between excitatory superficial pyramidal cells and inhibitory interneurons (Shaw et al., 2017). This fits with the PING model (pyramidal interneuron network gamma) where gamma phenomena reflect feedback inhibition from fast-spiking cells, notably parvalbumin-positive interneurons, to pyramidal cells, and less so with the ING model (interneuron network gamma) which suggests gamma oscillations are the result of some self-inhibition processes (Gonzalez-Burgos & Lewis, 2012; Kopell, Gritton, Whittington, & Kramer, 2014).

A recent addition of a thalamo-cortical connection in the DCM model has also resulted in an alpha peak which resembles that observed in experimental data (Shaw, Muthukumaraswamy, et al., 2020; Sumner et al., 2021), supporting the idea that alpha oscillations have a thalamo-cortical drive.

Long-range connectivity measured with M/EEG also reflects E-I balance in so far as connections represent the coupled excitatory and inhibitory oscillatory fluctuations (in amplitude-amplitude correlations or phase coherence measures) between different brain areas (Siegel et al., 2012). Long-range connectivity is usually measured in the resting-state where the extraction of distance connections reveals functional networks, such as the Default Mode Network, in the alpha and beta frequency bands (Brookes, Woolrich, et al., 2011; Colclough et al., 2016; Houck et al., 2016).

10.2.1 Aim and hypotheses

Costain et al. (2013), estimate that clinically significant, large, rare structural variants occur in 1 in 13 patients. The aim of this study was to investigate the effect of GABA and glutamate CNV carrier status on temporally resolved functional imaging outcomes in schizophrenia patients. Long-range oscillatory networks were studied in the resting-state, whereas local visual circuitry was probed by a visual grating paradigm. Cases, or carriers, were defined as patients who carry GABA and glutamate CNVs, while non-cases, or non-carrier were patients without these

variants. The hypotheses were that 1) cases will show reduced visual gamma amplitude compared with non-cases and 2) cases will show increased functional dysconnectivity compared with non-cases.

10.3 Method

10.3.1 Participants

Data were collected as part of the Genetic Variants in Psychosis (GVIP) study at CUBRIC. Subjects with a diagnosis of schizophrenia Disorder, who had consented to be contacted, were recalled from the COGs and ClozUK databases at Cardiff University (Schizophrenia Working Group of the Psychiatric Genomics Consortium, 2014), which when combined comprise ~1000 schizophrenia datasets. COGs patients were originally recruited from community mental health teams in Wales and England. Diagnosis was confirmed by a SCAN interview (Wing et al., 1990) and review of case notes. DNA samples were genotyped at the Broad Institute (Cambridge, Massachusetts, United States) and at deCODE genetics (Reykjavík, Iceland).

Subjects from the ClozUk database were, at the time of recruitment, taking the antipsychotic clozapine and had received a clinical diagnosis of treatment-resistant schizophrenia. Blood samples were acquired through collaboration with Novartis (the manufacturer of a proprietary form of clozapine, Clozaril). Both studies were approved by the UK Multicentre Research Ethics Committee (MREC). Recall was approved in house, at Cardiff University, by the School of Medicine Ethics Board 16/31.

GVIP was funded by the National Alliance for Research on schizophrenia & Depression (NARSAD) and the Wellcome Trust. Participants were recalled based on having rare (<1%), relatively large (>100kb) CNVs that target GABA and glutamate pathways, specified in Table 10.1, or their matched control status. In total 22 participants were recruited, 12 carriers and 15 non-carriers. However, one of the controls was excluded as they were not properly matched, leaving 12 carriers and 14 non-carriers; 16 males: 10 females.

10.3.2 CNV calling and quality control (QC)

Raw intensity data from each dataset was processed separately in consideration of potential batch effects. SNPs were clustered and Log-R ratios and B-allele frequencies were generated using Illumina Genome Studio software (v2011.1). CNVs were then called using PennCNV, using the Hadyn Ellis MRC Centre for Neuropsychiatric Genetics and Genomics standard protocol, with GC adjustments. CNVs were called using the 666,868 probes common to all case and control

arrays. Sample outliers were excluded based on the PennCNV QC measures: LRR standard deviation, BAF drift, wave factor and total number of CNVs called per person. Duplications were removed. If the distance separating CNVs in one individual was less than 50% of their combined length, the CNVs were joined. Finally, samples were excluded if they comprised of: coverage by less than 10 probes; less than 10kb in length; overlap with low copy repeats by more than 50% of their length; probe density less than 1 probe/20kb (calculated by dividing the size of the CNV by the number of probes covering it). All CNV loci with a frequency of >1% of the total discovery sample were also excluded using PLINK10.

Selection of CNVs

The GABA and glutamate gene sets were those implicated in genetic (CNV and SNV) studies of schizophrenia (Fromer et al., 2014; Kirov et al., 2012b) and include the following gene sets: ARC, GABAA, mGluR5, NMDAR network (a full table of variants is included in Appendix B).

10.3.3 Blinding and study procedure

Researchers were blinded to the status of participants. Controls (3 or 4) were matched to carriers using a Cardiff ID, case or control status, age (within 3 years) and gender only. Patients were then contacted using details from a randomised database of carriers and non-carriers.

Patients were screened and contact with their clinical team was made to ensure suitability. Participants attended for 1 day unless individuals were unable to tolerate all scans, in which case a second day was offered. Subjects completed the Positive and Negative Syndrome Scale (PANSS) interview (Kay, Fiszbein, & Opler, 1987), MEG and 2 x MRI sessions (3 Tesla Spectroscopy and Connectom- Microstructural scans). A blood sample was also obtained.

10.3.4 Tasks and data acquisition

As both the visual gamma signal and oscillatory connectivity in the resting-state is related to E-I balance (Alamian et al., 2017; Donner & Siegel, 2011; Gonzalez-Burgos & Lewis, 2012; Shaw et al., 2017; Siegel et al., 2012), participants completed an eyes-open resting-state and a visual-motor task. The resting-state paradigm comprised a 10-minute presentation of a central fixation dot on a grey background. Participants were instructed to focus on the dot with eyes open for the

duration of the recording. The grey screen and fixation dot were projected using the same CTF Sanyo system.

The visual-motor task comprised 2 runs of 50 trials per run. Each trial consisted of presenting a square black-and-white square-wave grating (approximately 15 degrees of visual angle, 3 cycles per degree) on a mean-luminance grey background. The stimuli were stationary, subtended vertically and horizontally at a 4° angle, in the lower left visual field in relation to a central fixation dot. The stimulus was present for a jittered interval (between 1.5 s and 2 s), followed by an 8-8.5 s rest phase where the central fixation dot remained. The stimuli had been programmed in MATLAB using the Psychophysics Toolbox extensions (Brainard, 1997, Pelli, 1997, Kleiner et al., 2007), as part of the SPRING study (Gascoyne et al., 2021). The task was projected onto CTF Sanyo projector screen (framerate 60Hz), 40 cm from the participant's face. Participants were instructed to make a swift finger abduction with their right index finger when the grating disappeared. The index finger response was recorded using electromyography electrodes placed on the skin above the first dorsal interosseous muscle.

Data were acquired on the CTF-275 axial gradiometer system at CUBRIC. Participants were sat upright in the scanner in a magnetically shielded room. Electromagnetic coils were placed on the fiducial areas (nasion, right & left auricular) for head localisation. Electrodes (EMG & ECG) were also attached to the face and wrists and hands. References were placed on the elbows. Data were sampled at 1200Hz. For noise cancellation, data were acquired with 29 references channels and were analysed in third-order gradiometer mode as recommended by Vrba and Robinson (2001).

10.3.5 Pre-processing

Visual gamma data were processed manually in DataEditor. Third-order gradient mode was applied, transforming the primary sensors for environmental noise reduction. Data were epoched into 4 second trials (-2, 2), around the stimulus onset and visually inspected. Trials which contained large blink, motion and muscle artefacts were excluded. Datasets which did not have a matched MRI were also discarded.

The continuous resting-state recordings were pre-processed using a semi-automated ICA method, using fieldtrip functions. This involved ensuring 0 padding at the beginning and end of the recording and resampling at 300Hz before removing muscle artefacts using a Z threshold (default 10; manually reduced if required in an iterative process). Noisy channels were also manually extracted from the data. A 64 component ICA was then run on the original data sampled at 150Hz. Components which appeared to comprise noise were extracted from the artefact cleaned data.

The analyses were performed in Matlab (Version 2017), using in-house custom scripts implanted in Fieldtrip (2019).

Co-registration

MRIs (1mm- isotropic, T1 weighted), were acquired on the 3 Tesla General Electric system at CUBRIC. MRIs were co-registered in CTF co-ordinate space using Fieldtrip.

10.3.6 Visual gamma analysis

The visual gamma analysis was conducted using a 1mm sampling grid in the method described fully in Chapter 3, but for completeness will be summarised here. The MRIs were segmented and the outer segment (skull) was extracted. A description of the outer brain surface was generated using the semi-realistic single-shell head model method developed by Nolte (2003). The source model was generated with a 1mm sampling grid and analysis performed on a volume comprising the 6 bilateral AAL visual areas: Calcarine, Cuneus, Lingual, Superior Occipital, Mid Occipital, Inferior Occipital. A LCMV beamformer was used to solve the inverse problem. Beamformer weights were calculated based on the global covariance of the MEG data in a 30–80 Hz bandwidth. The covariance time window was set to -1.5 - 1.5 s. A regularisation procedure (lambda 5%) was applied (Treder & Nolte, 2018).

Source power was projected separately for the baseline and stimulus periods. Due to the previously established relationship between induced gamma and PING informed DCM parameters (Shaw et al., 2017), the sustained stimulus period (0.3s- 1.5s) was of interest. The coordinates of the source with the maximal percentage change in gamma power were extracted

and a virtual electrode timecourse was estimated at this location. Multi-taper and Hilbert transforms were applied to extract frequency and time-frequency metrics.

10.3.7 Resting-state Analysis

The in-house amplitude-amplitude functional connectivity pipeline (kAAL_ConnectKL) was applied to the resting-state data. In summary, the continuous data was split into 2 second trials and filtered into the canonical frequency band (delta, theta, alpha, beta, low gamma and high gamma). LCMV beamformer weights were generated using an AAL atlas which comprises 90 nodes and normalized using a vector norm (length of vector) (Hillebrand et al., 2012). Virtual sensor data for each trial was created and concatenated per voxel. A bandpass filter and Hilbert envelope was applied. A representative timecourse for each AAL region, i.e., the virtual sensor with the largest temporal variance was then selected and orthogonalisation applied (Colclough et al., 2015) to prevent source leakage. The signal was then downsampled and the Hilbert envelope conditioned to the representative timecourses. Finally, correlation matrices were generated, and a z-transform applied resulting in a 90x90 connectivity matrix for each subject.

Non-Negative Matrix Factorization (NNMF)

To reveal functional sub-networks in the data, Non-negative Matrix Factorization (NNMF) was applied to participant's MEG resting-state matrices. The method has been previously used to reveal alpha network effects in people with schizophrenia (Phalen et al., 2019). It is a mathematical approach (Lee & Seung, 1999) whereby matrices can be reduced into fundamental networks. Therefore, components reflect consistency of networks across participants, with the first component being most present. Components were selected for further analysis until certain stopping criteria were met that prevent the data from being over-fitted. The number of components for investigation are selected apriori meaning this requires caution, as components which are variable in only a few participants could be included. Conversely, a cut off that is too stringent could lead to information being missed. The stopping criteria employed here were: a maximum 20 components, every component must have a non-zero value in at least 50% of participants and, averaging across all components, the mean number of non-zero weightings should be greater than 70% of participants. NNMF components were derived separately per frequency band. Alpha (4) and beta (5) components are considered here.

10.3.8 Statistical analysis

After inspection of the available data and the described analysis steps, 25 resting datasets (11 carriers, 14 non-carrier) were brought forward for statistical analysis.

Visual gamma

There were 25 first-run visual gamma datasets (11 carriers, 14 non-carriers) and 23 second-run visual gamma datasets (10 carriers, 13 non-carriers). Carrier and non-carrier groups were compared visually for the 2 runs of the visual gamma paradigm. To utilise the power of all data a repeated measures ANOVA was employed, with run time as the within-groups variable.

Resting-state

Statistics were based on differences in Z-scored connections between carrier and non-carrier groups. Valid connections in each frequency band were selected across the cohort by selecting connections that were of mean rank $>.8$. This was done separately for the carrier and non-carrier groups to capture group effects. Connections that survived in either group were carried forward in the analysis. An unpaired (Welch's) t-test was performed at each "valid" connection and connections surviving an uncorrected $\alpha = 0.05$ were maintained.

To correct for multiple comparison, connections were also assessed with an omnibus method. This comprised 10,000 sign-shuffled iterations where the t-statistic is recomputed at each connection and the maximal t-statistic at each iteration was selected for the null distribution. The corresponding p-values were then calculated by comparing the original t-statistic per connection against this omnibus distribution.

A confidence interval for associated connections was generated using 10,000 iteration sign tests. This involved randomly comparing half of one group to half of the other group in every iteration. Connections that were consistent over 95% of the iterations were maintained. This technique shows direction of effect, i.e., reduced or increased, but not strength.

Non-Negative Matrix Factorization

Statistical analyses were based on the General Linear Model (GLM), implemented in Fieldtrip (2019). Separate GLMs were constructed for components in each frequency band. Cooks distance was set to 3, meaning individuals with values $3 * \text{mean}$ were considered outliers and rejected from the analysis. Subjects were also rejected if they had a Cook's Distance of >0.5 , which is considered large. Cooks distance is the scaled change in the coefficients due to the deletion of an observation (subject in this case) and evaluates whether a dataset (person) has a strong effect on the residuals after regression. Group comparison was also run without outlier rejection with no meaningful changes to the results.

Variants included in the visual gamma and resting-state analyses are listed in Tables 10.1 and 10.2.

Table 10.1. Visual gamma CNVs (n= 10)

| Chr | Copy number | Probes | Size | Genes | Pathways | Batch | Exonic | Type |
|-----|-------------|--------|---------|--------|-------------------------------|-----------------------|----------|-------------|
| 11 | 1 | 17 | 192414 | DLG2 | ARC, NMDAR (network), PSD-95 | ClozUK1 | Exonic | Deletion |
| 15 | 1 | 88 | 475949 | CYFIP1 | ARC | ClozUK1 | Exonic | Deletion |
| 15 | 3 | 227 | 1782296 | CYFIP1 | ARC | ClozUK1 | Exonic | Duplication |
| 2 | 1 | 18 | 56752 | NRXN1 | GABA receptor complex, PSD-95 | ClozUK2 | Exonic | Deletion |
| 2 | 1 | 24 | 64387 | NRXN1 | GABA receptor complex, PSD-95 | ClozUK2 | Exonic | Deletion |
| 2 | 1 | 12 | 42838 | NRXN1 | GABA receptor complex, PSD-95 | FinalCOGs | Intronic | Deletion |
| 2 | 1 | 27 | 55694 | NRXN1 | GABA receptor complex, PSD-95 | FinalCOGs | Intronic | Deletion |
| 9 | 1 | 143 | 86265 | GRIN1 | ARC, NMDAR (network), PSD-95 | FinalCOGs | Exonic | Deletion |
| 15 | 3 | 161 | 475949 | CYFIP1 | ARC | FinalCOGs | Exonic | Duplication |
| 15 | 3 | 460 | 1899299 | CYFIP1 | ARC | FinalCOGs/ ClozUK1 | Exonic | Duplication |

Table 10.2. Resting-state CNVs (n=11)

| Chr | Copy number | Probes | Size | Genes | Pathways | Batch | Exonic | Type |
|-----|-------------|--------|---------|---------------------------------------|--|-----------------------|----------|-------------|
| 15 | 1 | 88 | 475949 | CYFIP1 | ARC | ClozUK1 | Exonic | Deletion |
| 15 | 3 | 227 | 1782296 | CYFIP1 | ARC | ClozUK1 | Exonic | Duplication |
| 12 | 3 | 45 | 280870 | ENO2, GNB3, PHB2, TPI1, USP5 | PSD-95 (core) | ClozUK1 | Exonic | Duplication |
| 2 | 1 | 18 | 56752 | NRXN1 | GABA receptor complex, PSD-95 | ClozUK2 | Exonic | Deletion |
| 2 | 1 | 24 | 64387 | NRXN1 | GABA receptor complex, PSD-95 | ClozUK2 | Exonic | Deletion |
| 2 | 1 | 33 | 76012 | NRXN1 | GABA receptor complex, PSD-95 | ClozUK2 | Exonic | Deletion |
| 2 | 1 | 12 | 42838 | NRXN1 | GABA receptor complex, PSD-95 | FinalCOGs | Intronic | Deletion |
| 2 | 1 | 27 | 55694 | NRXN1 | GABA receptor complex, PSD-95 | FinalCOGs | Intronic | Deletion |
| 9 | 1 | 143 | 86265 | GRIN1 | ARC, NMDAR (network), PSD-95 | FinalCOGs | Exonic | Deletion |
| 15 | 3 | 161 | 475949 | CYFIP1 | ARC | FinalCOGs | Exonic | Duplication |
| 15 | 3 | 460 | 1899299 | CYFIP1 | ARC | FinalCOGs/ ClozUK1 | Exonic | Duplication |

10.4 Results

10.4.1 Visual Gamma

The trends in amplitude and frequency in CNV carriers and non-carriers, across both runs of the visual gamma paradigm, can be seen in Figure 10.1.

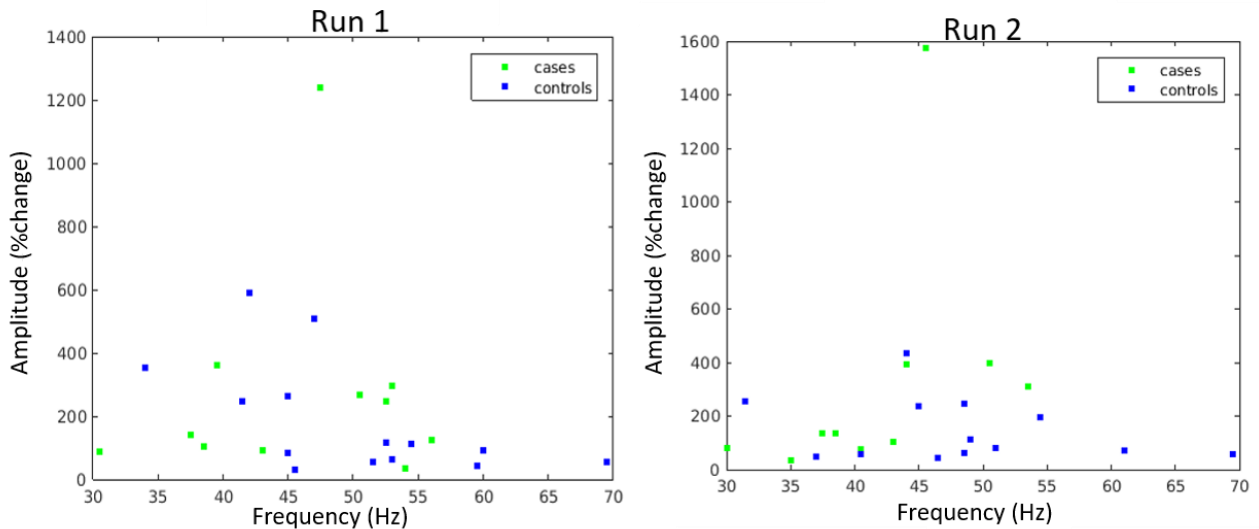


Figure 10.1. Shows peak amplitude plotted against peak frequency measures in both runs of the visual gamma task.

The mean values of amplitude and frequency in carriers and non-carriers can be seen in Figure 10.2 From the analysis of variance, no main effect of carrier status on peak amplitude was found, $F(1, 21)= 1.54, p=0.228$. Weak evidence towards an interaction between run time and carrier status was suggested $F(1, 21)=3.238, p=0.086$.

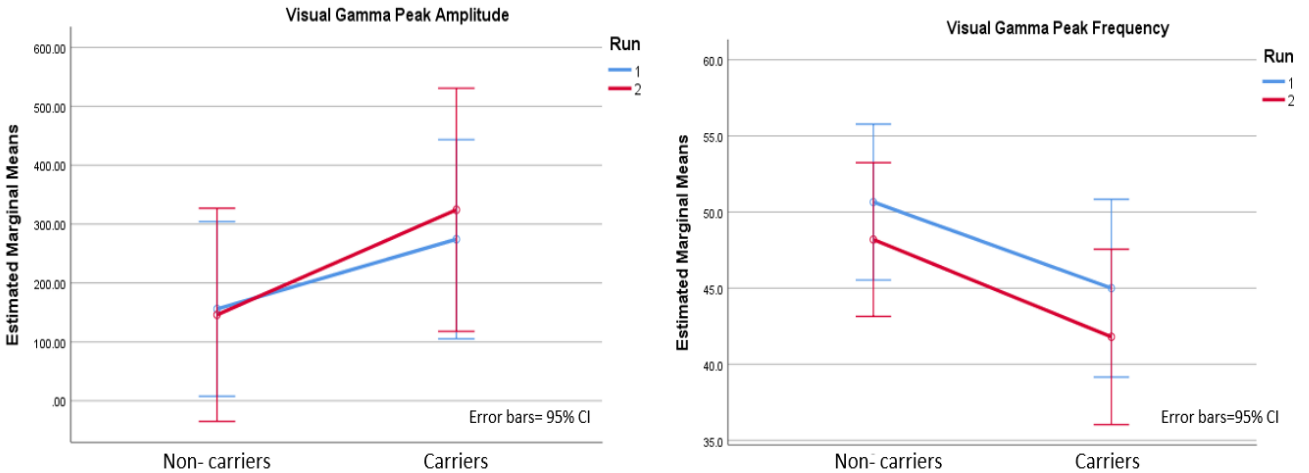


Figure 10.2. Shows the mean peak amplitude (left) and mean peak frequency values (right) values in carriers and non-carriers. Error bars are 95% confidence intervals.

No significant carrier status effect on peak frequency was found, $F(1, 21)=3.211$, $p=0.088$; nor a within participants effect of run on peak frequency $F(1,21)=3.262$, $p=0.085$.

The results suggest possible increased amplitude and reduced frequency of visual gamma response in carriers compared to non-carriers, however, differences did not meet statistical significance.

10.4.2 Resting-state Analysis- edge level connectivity

Results of the amplitude-amplitude correlation analysis in the alpha band are shown in Figure 10.3. At the uncorrected level, there was some evidence for reduced connectivity between the occipital and parietal lobes. Increased connectivity was also observed between frontal-parietal and temporal occipital areas.

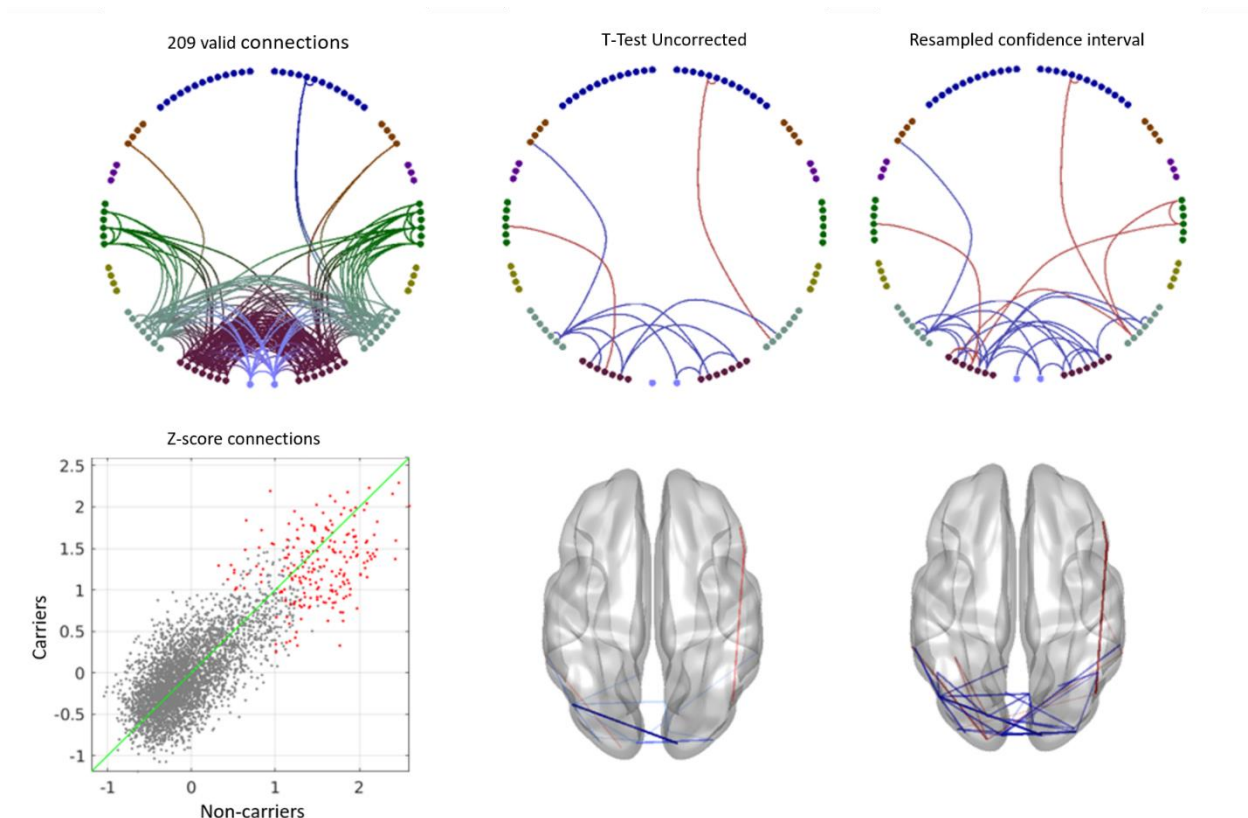


Figure 10.3. Alpha connectivity in carriers as compared to non-carriers. The first column shows the valid connections selected across the cohort (connections surviving the 80% rank threshold in either of the groups). The top left figure displays the valid connections in a circular plot with frontal regions at the top and posterior regions at the bottom. The lower left plot shows the z-score, averaged across all participants, for each connection in the carrier group plotted against the mean z-score for non-carriers. Red dots indicate the ‘valid’ connections exceeding the 80% rank threshold. That the connection values are evenly dispersed around the central line suggests that connections were not noticeably dissimilar in carriers and non-carriers.

The second column shows the connections surviving an uncorrected threshold of $\alpha = 0.05$ after running an unpaired t-test at each of the valid connections. Connections that are decreased in carriers are shown in blue, while connections that are increased in carriers are shown in red. The bottom plot shows connections plotted on a template brain.

The third column gives a 95% confidence interval on each connection and is calculated in a slightly different way to previous chapters. Across 10,000 iterations, half of one group is

subsampled randomly and compared to a random half of the second group. Increases and decreases in connectivity are generated and connections showing a consistent effect direction across 95% of iterations are considered robust and plotted (blue for decreases, red for increases). This test does not consider the magnitude of the effect, only its direction and how consistent this is across resampling.

An omnibus-corrected t-test was also run to account for multiple comparisons. After running 10,000 sign-shuffling iterations to recompute the t-statistic at each connection, the maximal t-statistic across connections is chosen from the null distribution at each iteration, and p-values are recomputed by comparing the observed t-statistics with this maximal statistic distribution. No alpha connections survived multiple comparison correction.

Results of the edge level analysis in the beta band can be seen in Figure 10.4. Some evidence for reduced connectivity in carriers between parietal and occipital lobes is shown. Some increased connections between occipital, parietal, temporal and frontal areas were also observed.

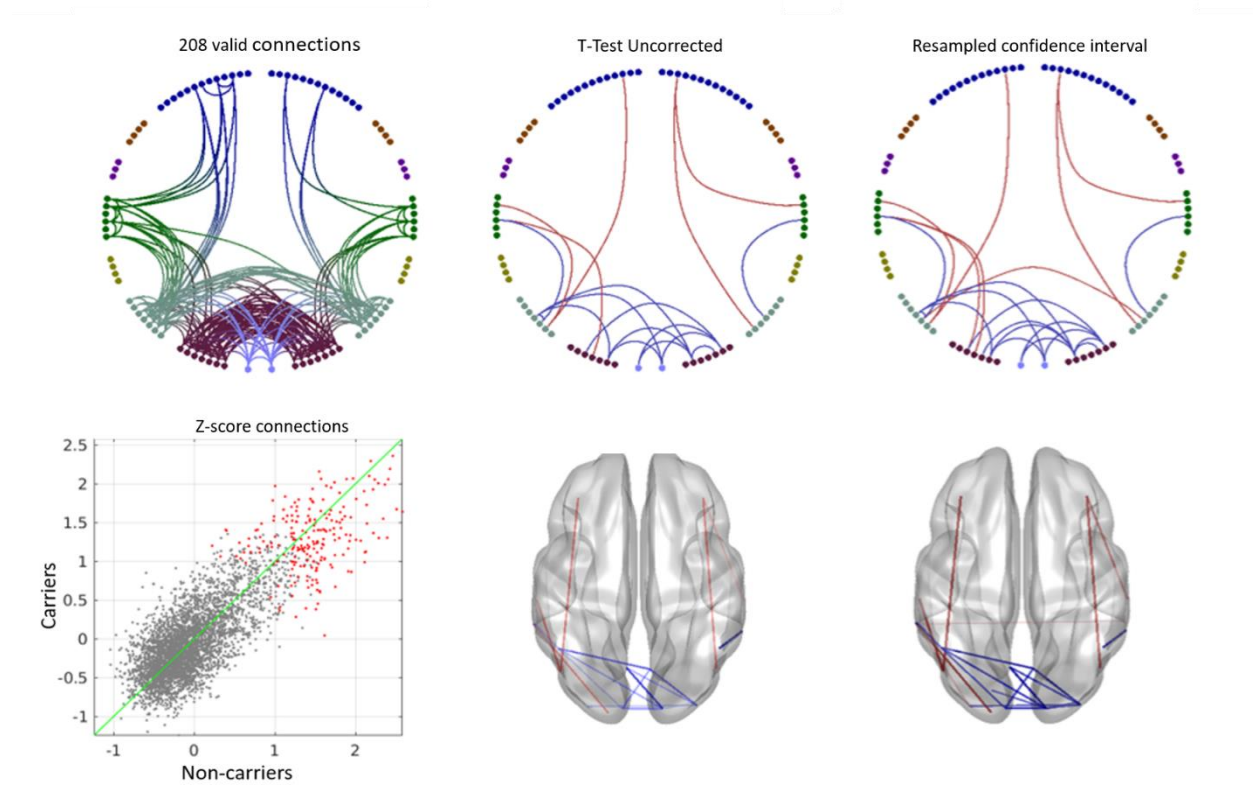


Figure 10.4. Beta connectivity in carriers as compared to non-carriers. Plots as detailed above.

No beta connections survived multiple comparison correction at the edge level.

10.4.3 Sub network analysis using Non- Negative Matrix Factorization

Functional subnetworks revealed with NNMF are shown in Figures 10.5 and 10.6. Anatomically, alpha component 1 comprises occipital and left parietal connections, alpha component 2 comprises mainly parietal temporal connections, component 3 comprises occipital and left parietal connections and component 4 comprises frontal, temporal and occipital connections.

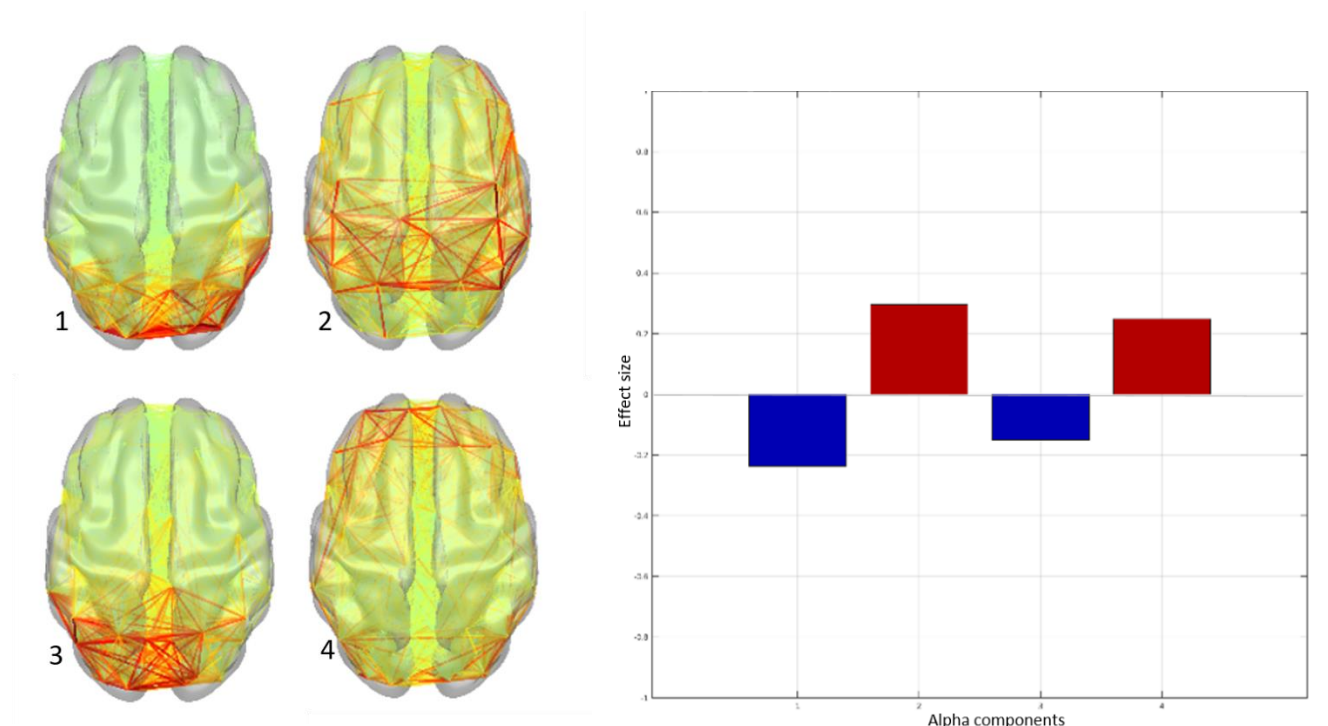


Figure 10.5. Left show the four alpha components plotted on a template brain. Right shows the effect sizes for each alpha component in relation to being a carrier of E-I CNVs.

Alpha networks 1 and 3 were reduced in carriers and networks 2 and 4 were increased. However, the none of the networks were significantly different between groups as shown in Table 10.3.

Table 10.3. Regression coefficients for each alpha component

| Alpha Component | Standard Effect | P value | Cohens ^f ² |
|-----------------|-----------------|----------|----------------------------------|
| 1 | -0.23664 | 0.249351 | 0.252263 |
| 2 | 0.29583 | 0.153945 | 0.322777 |
| 3 | -0.14998 | 0.461648 | 0.163637 |
| 4 | 0.248409 | 0.227913 | 0.271037 |

n.b. Standard effect size is standardised beta. Categorical predictor of interest is case status.

Cohen's f^2 is a scaled change in R^2 (variance explained) when the model is compared with and without the covariate of interest, as shown in equation 10.1.

$$f^2 = \frac{R_{AB}^2 - R_A^2}{1 - R_{AB}^2} \quad 10.1. \text{ (Selya, Rose, Dierker, Hedeker, \& Mermelstein, 2012)}$$

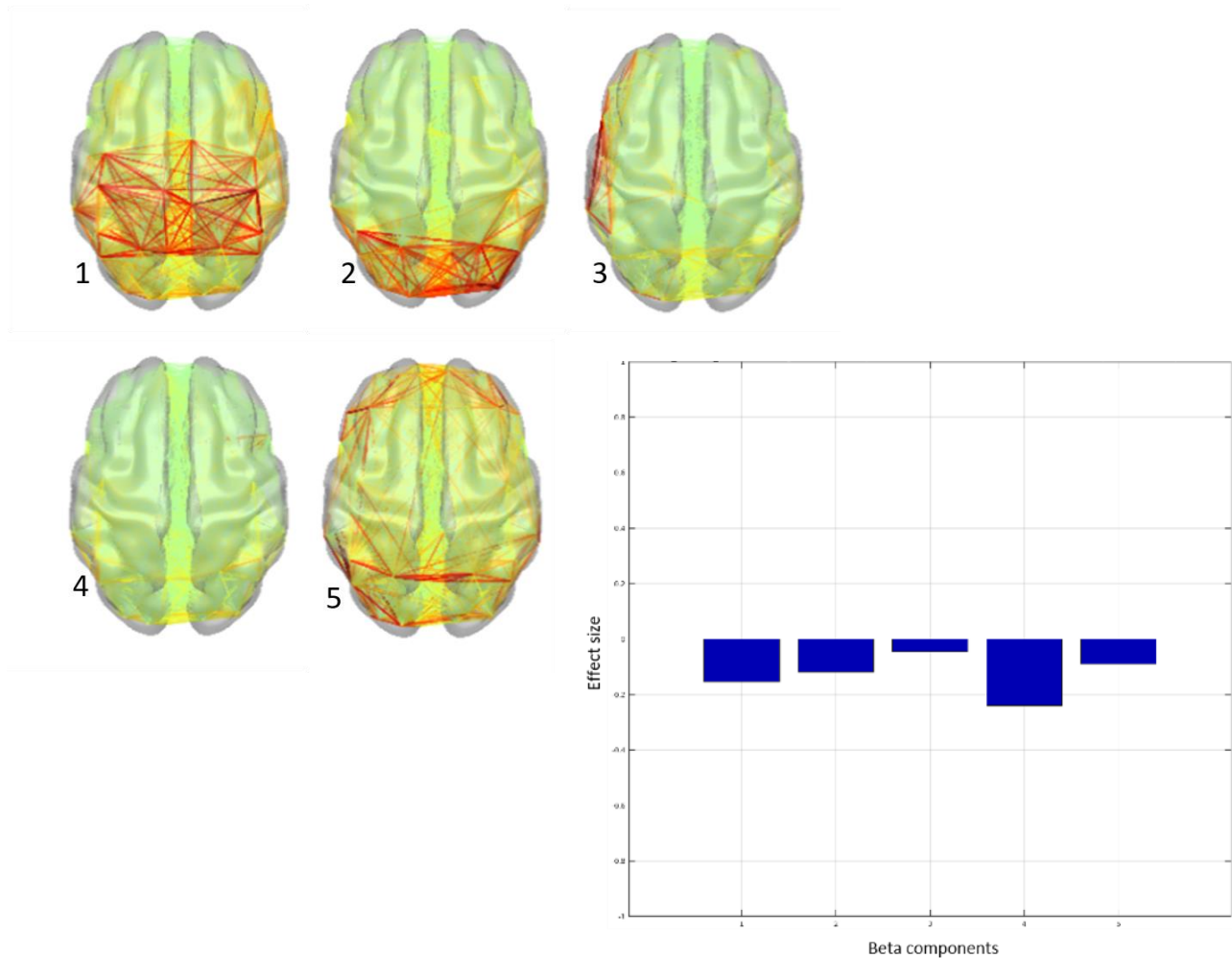


Figure 10.6. Left, beta components plotted on a template brain. Right shows effect sizes for each beta component in relation to being a carrier of E-I CNVs.

Being a carrier was negatively associated with all the beta components, suggesting carriers had reduced beta connectivity. However, none of these relationships were significant, as shown in Table 10.4.

Table 10.4. Regression coefficients for each beta component

| Beta Component | Standard Effect | P value | Cohensf² |
|-----------------------|------------------------|----------------|----------------------------|
| 1 | -0.15271 | 0.454036 | 0.17074 |
| 2 | -0.11801 | 0.56177 | 0.131938 |
| 3 | -0.04584 | 0.820839 | 0.048863 |
| 4 | -0.23906 | 0.244694 | 0.25484 |
| 5 | -0.08925 | 0.659997 | 0.097376 |

10.5 Discussion

In summary, the findings presented here cannot provide convincing evidence for a relationship between GABA and glutamate CNV carrier status and local and global MEG connectivity. However, considering the limited sample, the trends toward reduced frequency and increased amplitude of the sustained gamma response in the visual cortex, along with long-distance connectivity reductions, in the alpha and beta frequency bands, significant at uncorrected p-value thresholds, implies this is an area that needs to be further explored. This is the first study of its kind to investigate the effect of CNVs implicated in neural excitation-inhibition (E-I) on MEG electrophysiological connectivity in schizophrenia.

E-I imbalance constitutes a key element of the dysconnection theory of schizophrenia (Friston et al., 2016). Functionally, dysconnectivity appears to result in prediction errors between incoming sensory information and prior belief, which are unattenuated along the cortical hierarchy. This loss of precise inference about the world is reflected in many symptoms of schizophrenia, e.g., hallucinations and delusions. Physiologically, dysconnectivity is underpinned by faulty gain control, that is, synaptic excitability and neuromodulation, with many lines of evidence in support. For example, glutamatergic NMDA receptor hypofunction on GABAergic interneurons, as a physiological theory of schizophrenia, is well supported by pharmacological and animal studies (Anticevic et al., 2012; Ehrlichman et al., 2009; Gonzalez-Burgos & Lewis, 2012). Numerous genetic, magnetospectroscopy and post-mortem studies, in support, also exist (Cohen, Tsien, Goff, & Halassa, 2015; Kirov et al., 2012a; Rowland et al., 2016).

Importantly, there is considerable support for an interaction between gain control and neuronal oscillations. Synaptic modulation of GABAergic interneurons dictates the action of synchronous pyramidal cells, the local field potential (LFP) signal from which is measured by our electrophysiological imaging modalities. Gamma oscillations, in particular, have been linked to E-I balance at the theoretical (Gonzalez-Burgos & Lewis, 2012), cellular (Kopell, Ermentrout, Whittington, & Traub, 2000), neurotransmitter concentration (Muthukumaraswamy et al., 2009) and computational micro-circuitry levels (Shaw, Knight, et al., 2020). As frequency of gamma oscillations has been found to be associated with connections between pyramidal cells and interneurons, in the superficial layers of the cortical microcircuit in the visual cortex (Shaw,

Knight, et al., 2020), the tentative finding of reduced visual gamma frequency in GABA/Glu CNV carriers could be interesting. However, more work is needed to establish this relationship.

Moreover, the finding of increased amplitude of the visual gamma response in carriers was opposite to what was hypothesised. One plausible reason for this is by investigating the effect of carrier status, both glutamatergic and GABAergic CNVs were included, with potentially opposing effects. These glutamatergic CNVs, may have caused a disproportional enhancement of cortical excitability in some carriers which is reflected in the, overall, increased amplitude of the visual gamma signal. Considering patients generally show reduced stimulus induced amplitude, compared with controls (Whitlow, 2015; Kantrowitz & Javitt, 2010; Krishnan et al., 2005), this again warrants further investigation.

In neuroscience, an observable tension exists between viewing schizophrenia as a disorder of local dysfunction e.g., in the frontal cortex or visual cortex etc., and global dysfunction, e.g., connectivity across the whole brain (Alan Anticevic & Lisman, 2017). This is reflected in the different approaches to analysing patient imaging data. In Chapter 6 we see that measures used in this thesis appear relatively uncorrelated, apart from the negative relationship between gamma amplitude and alpha connectivity in the occipital cortex. Interestingly, in this chapter carrier status appears to be associated with reduced connectivity in the visual-parietal cortices in alpha and beta, while visual gamma amplitude is increased in carriers. The trends here were not significant and therefore further explored in terms of local and global relationships in carriers and non-carriers. However, if the trends found here are true, then the study of GABA/Glu CNV carriers and non-carriers could elucidate the effect of E-I imbalance on global functional connectivity.

The nature of the interaction between local E-I imbalance and global connectivity, as measured with current imaging modalities, is not fully clear, though contending theories include Coupled synchrony (Florin & Baillet, 2015), Communication Through Coherence (Fries, 2015) and Perceptual Binding (Tallon-Baudry & Bertrand, 1999). Similarly, the extent to which interactions across different frequency bands modulate connectivity between local and global systems is continued topic of debate. For example, considerable previous work has suggested

that alpha oscillatory connectivity has a cyclic modulatory effect on cortical excitability (Florin & Baillet, 2015; Lozano-Soldevilla et al., 2014a; Roux et al., 2013; Spaak, Bonnefond, Maier, Leopold, & Jensen, 2012). However, contrasting evidence has also been shown (Zhigalov & Jensen, 2020). A synonymous beta effect, to the authors knowledge, has not been found (Baillet, 2017). Future research with E-I CNV carriers might benefit from simultaneous use of local and global metrics to better address questions related to long-range connectivity and E-I balance.

Limitations and future directions

There were several limitations in conducting this study. Many subjects on the Cogs and Cloz UK databases were originally genotyped and screened more than 5 years ago, making recall and suitability assessments challenging, particularly considering presentation and readmission factors. Additionally, in consideration of the limited sample size, we did not control for length of illness and medication status, which have been associated with brain alterations in patient groups (Fusar-Poli et al., 2013; Zhao et al., 2018). These factors should be considered in future studies.

As previously mentioned, individuals with CNVs were grouped together under carrier status, where CNVs target both GABAergic and glutamatergic pathways. Unfortunately, the sample numbers prohibited a meaningful separation of these groups, i.e., by presence of excitatory or inhibitory CNVs. However, this is an imperative factor to consider in future, as associated synaptic actions may constitute opposing influences on cortical excitability, which could at best diminish significance. In fact, that there were more glutamatergic than GABAergic CNV carriers in the visual gamma and RSN analyses, albeit by 1 and 2 subjects respectively, suggests the group level analysis was subject to more excitatory factors and could explain the finding of increased gamma amplitude in the visual cortex in carriers.

The acquisition of larger genetic-MEG datasets will make studies, such as this, less challenging. However, open access MEG datasets, such as OMEGA (“The Open MEG Archive (OMEGA) | McConnell Brain Imaging Centre - McGill University,” n.d.), only have around 300 healthy resting-state datasets. Such a schizophrenia cohort does not exist. Thus, it would be more conceivable to investigate the role of E-I CNVs on MEG functional connectivity in the healthy population. This would be the recommended future direction.

In conclusion, these analyses suggest there might be disturbance in local visual connectivity and global lower frequency connectivity in carriers of CNVs which hit GABA and glutamate pathways. This study adds to a growing body of genetic imaging studies which will facilitate our understanding of how genetics influence the excitability of the brain in schizophrenia. While grouping the CNVs was suitable in this study, future research might consider investigating the contribution of glutamatergic and GABAergic CNVs to connectivity, separately. Implementing this methodology in the healthy population, where achieving the desired sample size would be more feasible, would be recommended at present.

10.6 Appendix B

1. GABA and glutamate CNVs in cases.

| Ch | Start | End | Copy number | Pro bes | Size | Genes | Pathways | Batch | Exonic | Type |
|----|-----------|-----------|-------------|---------|---------|------------------------------|--------------------------------------|---------------------------|----------|-------------|
| 11 | 82996986 | 83189400 | 1 | 17 | 192414 | DLG2 | ARC, NMDAR (network), PSD-95 (core) | ClozUK1_B3 | Exonic | Deletion |
| 15 | 22750305 | 23226254 | 1 | 88 | 475949 | CYFIP1 | ARC | ClozUK1_B3 | Exonic | Deletion |
| 15 | 22750305 | 24532601 | 3 | 227 | 1782296 | CYFIP1 | ARC | ClozUK1_B3 | Exonic | Duplication |
| 12 | 6884243 | 7165113 | 3 | 45 | 280870 | ENO2, GNB3, PHB2, TPI1, USP5 | PSD-95 (core) | ClozUK1_B4 | Exonic | Duplication |
| 2 | 50902931 | 50959683 | 1 | 18 | 56752 | NRXN1 | GABA receptor complex, PSD-95 (core) | ClozUK2_B1 | Exonic | Deletion |
| 2 | 50882657 | 50947044 | 1 | 24 | 64387 | NRXN1 | GABA receptor complex, PSD-95 (core) | ClozUK2_B1 | Exonic | Deletion |
| 2 | 50869459 | 50945471 | 1 | 33 | 76012 | NRXN1 | GABA receptor complex, PSD-95 (core) | ClozUK2_B1 | Exonic | Deletion |
| 2 | 51058745 | 51101583 | 1 | 12 | 42838 | NRXN1 | GABA receptor complex, PSD-95 (core) | Final COGs | Intronic | Deletion |
| 2 | 50863273 | 50918967 | 1 | 27 | 55694 | NRXN1 | GABA receptor complex, PSD-95 (core) | Final COGs | Intronic | Deletion |
| 9 | 140054136 | 140140401 | 1 | 143 | 86265 | GRIN1 | ARC, NMDAR (network), PSD-95 (core) | Final COGs | Exonic | Deletion |
| 15 | 22750305 | 23226254 | 3 | 161 | 475949 | CYFIP1 | ARC | Final COGs | Exonic | Duplication |
| 15 | 22750305 | 24649604 | 3 | 460 | 1899299 | CYFIP1 | ARC | Final COGs/ ClozUK1_B3 | Exonic | Duplication |

Chapter 11. General Discussion

11.1 Summary of findings

This thesis has investigated local and global functional and structural connectivity measures in relation to schizophrenia-risk, schizophrenia and the healthy population. Previously, it has been shown that local and long-range functional circuitry can be probed with high frequency and low frequency oscillations, respectively. Probing visual micro-circuitry with gamma oscillations requires that the best possible gamma estimates are obtained. Prior to this thesis, no formal systematic comparison of sampling resolutions for beamforming in MEG visual gamma analysis had been conducted.

In Chapter 3 different sampling grid resolutions for source localisation of the gamma signal in visual cortex during the presence of a grating stimuli, were investigated. Estimates of gamma amplitude were highest at the 1mm sampling resolution as compared with 2mm, 4mm and 6mm, suggesting the beamformer was able to reconstruct the gamma signal most precisely at 1mm resolution. In the subsequent chapters of this thesis gamma analysis was, therefore, conducted using a 1mm sampling grid with which gamma estimates are optimised.

Additionally, it is known that head-motion and participant discomfort factors have severe implications for our ability to extract robust long-range oscillatory networks with MEG. For both the participant and data quality discarding a resting-state scan, for example, would be advantageous. However, the extent to which long-range networks can be extracted from task data was previously unknown.

The key finding in Chapter 4 was that both long-range network information along with the visual gamma signal, can be extracted from data recorded during a visual paradigm. A comparison of static amplitude –amplitude networks derived from resting-state and gamma data found a high degree of similarity in the alpha, beta and to some extent theta bands also. A gamma peak in V1 was also identified in the amplitude connectivity analysis of the visual gamma data. Reducing

the number of tasks in future MEG protocols could be particularly useful in clinical studies of challenging populations, where obtaining quality data is non-trivial.

Previous studies show that individuals with schizophrenia have both local and widespread functional and structural dysconnectivity (Alamian et al., 2017; Cabral et al., 2013; Fornito, Zalesky, Pantelis, & Bullmore, 2012; Gonzalez-Burgos & Lewis, 2012; Pettersson-Yeo, Allen, Benetti, McGuire, & Mechelli, 2011; Shaw et al., 2020; Stauffer et al., 2021; Uhlhaas & Singer, 2013). However, the extent to which local abnormalities are related to global abnormalities in both schizophrenia and at-risk populations, has been largely unknown. In fact, the relationship between visual micro-circuitry and long-range connectivity in the healthy population has been thus far unclear.

In Chapter 6 a relationship between the amplitude of local gamma oscillations and reduced long-range alpha was observed with MEG, which was discussed in the context of local and global circuitry in the normative population. A relationship between gamma frequency in the visual cortex (VC) and integrity of white matter tracts in VC and across the brain was also found, which could reflect an associated increase in myelination (Winklewski et al., 2018).

Based on previous literature, the picture of functional and structural abnormalities associated with genetic and clinical risk also required further clarification. To this end, Chapters 7 and 8 investigated risk factors for schizophrenia and their relationship to global functional and structural connectivity. Robust relationships between schizotypy and reduced functional alpha connectivity and between polygenic risk score and increased diffusivity within white matter tracts, in a healthy sample, were found.

Chapter 9 investigated relationships between the aforementioned risk factors and local circuitry, as probed by visual gamma oscillations, but no significant relationships were found across the whole cohort. That being said, in line with prediction, polygenic risk score for schizophrenia predicted reduced gamma amplitude in one half of the sample.

Lastly, the effect of increased excitatory-inhibitory CNV burden on functional connectivity in the schizophrenia population was investigated in Chapter 10, where trends towards both local and global differences were shown and should be further explored.

11.2 Implications

11.2.1 A relationship between visual gamma oscillations and long-range alpha connectivity in the healthy population.

The results in this thesis are among the first to show a relationship between induced local visual gamma amplitude (V1) and reduced *at-rest* alpha oscillations beyond primary visual areas (Hirschmann et al., 2020; Zhigalov & Jensen, 2020); namely in the occipital and precuneal areas. The hippocampus was also implicated; however, this is acknowledged tentatively due to poor source imaging of deeper neural areas with MEG.

The relationship is interesting in the context of predictive error coding theory and hierarchical models of the brain (Bastos et al., 2012; Bastos et al., 2015; Friston & Kiebel, 2009). Growing evidence suggests that neural oscillations are the means by which top-down and bottom-up representations are updated, and in turn allow an accurate view of the world (Bastos et al., 2012; Friston, Brown, Siemerikus, & Stephan, 2016; Friston & Kiebel, 2009; Pinotsis et al., 2017). In this perspective, gamma oscillations are involved in feedforward processing and alpha involved in feedback processing (Kerkoerle et al., 2014).

Modelling work has shown that the generation of gamma oscillators results in low frequency inter-areal network patterns which closely correlate with BOLD resting-state networks (Cabral, Hugues, Sporns, & Deco, 2011). On this basis, and that both local and global functional measures are reduced in clinical populations (Alamian et al., 2017; Friston, Brown, Siemerikus, & Stephan, 2016; Gonzalez-Burgos & Lewis, 2012; Pettersson-Yeo, Allen, Benetti, McGuire, & Mechelli, 2010; Shaw et al., 2020), we predicted that the amplitude of local gamma might be positively correlated with the amplitude of long-range alpha and beta connectivity.

Predictive theory suggests that a trait-like relationship exists within individuals such that feedforward and feedback processes would be related. However, the direction of these

relationships was undefined. That gamma was associated with *reduced* long-range alpha connectivity in Chapter 6 required some consideration.

At the local level, in healthy volunteers, fluctuations in frequency band activity are related in that an increase in high frequency gamma power (non-phase-locked Event Related Synchronisation), due to presentation of a stimulus (auditory or visual), usually results in a concurrent suppression of low frequency power (alpha non-phase-locked Event Related Desynchronisation) (Brookes et al., 2005; Lorenz, Müller, Schlee, Hartmann, & Weisz, 2009; Strube, Rose, Fazeli, & Büchel, 2021). It might not, therefore, be too much of a leap to suggest that similar mechanisms are present over longer distances.

In support, in a recent investigation of the relationship between induced visual gamma and dynamic activity across the cortex, Hirschman and colleagues (2020) also found a within-subject association between increased gamma amplitude, using a visual gamma paradigm, and the state probability of a resting-state characterised by low alpha and beta power in several areas. Reduced gamma amplitude, in contrast, was correlated with the probability of another state characterised by high alpha and beta power in central areas.

That those who exhibit high gamma are more frequently in states of low alpha and beta oscillations in the resting-state, suggests exploring dynamical state experiences will be important in future research. Such research would also allow questions around whether a coincidence of high gamma and low alpha results from attentional factors or some other mechanism, to be addressed.

Regardless, the finding forms an excellent basis for exploring the local and long-range functional relationship in different clinical groups. In schizophrenia, after 25 years of research under the disconnection hypothesis (Friston & Frith, 1995), research is going beyond the singular connected-ness of brain regions and beginning to unpick the complex neural interactions that exist both within and between brain regions and may be disrupted in pathology. Establishing whether the gamma-alpha relationship differs in clinical groups would provide further insight into this potential hierarchical mechanism.

The study of effective connectivity, i.e., directed connectivity, provides an additional means for this. For example, Rolls and colleagues have recently shown that feedforward connectivity is weaker and feedback connectivity is stronger in schizophrenia patients versus controls, using effective modelling of the fMRI signal (Rolls et al., 2020). This is in contrast with unidirectional fMRI research which has predominantly shown reductions in long-range connectivity fMRI (Pettersson-Yeo et al., 2011), but supports MEG research which has found both increased and decreased connectivity in patients (Alamian et al., 2017b). Areas which had high effective connectivity in patients were from the precuneus and posterior cingulate cortex (PCC) to areas such as the parahippocampal, hippocampal, temporal, fusiform, and occipital cortices. Interestingly, backwards connectivity was associated with positive symptoms whereas negative and cognitive symptoms were associated with weaker connectivity. Further elucidating these relationships, therefore, has implications for better understanding symptomology.

11.2.2 The relationship between schizotypy and functional resting alpha connectivity

This thesis adds to a body of research on the clinical continuum of schizophrenia, supporting a more integrative approach to understanding neuropathology and psychological disorder (Dagleish, Black, Johnston, & Bevan, 2020; Insel, 2014; Stein, 2014). The main consistency with previous clinical literature is finding that reduced long-range alpha connectivity is robustly associated with schizotypy (Alamia & VanRullen, 2019; Alamian et al., 2017b; Phalen, Coffman, Ghuman, Sejdić, & Salisbury, 2019; Sterzer et al., 2018; Williams, 2018). Faulty representation is a key feature of schizophrenia symptomology (e.g., hallucinations, delusions, magical thinking, ideas of grandeur), and dysregulated alpha connectivity found in high schizotypy individuals might be one contributing factor to the presence of schizophrenia-like experiences in the normal population. Further exploring the positive sub-dimension of schizotypy will be important for establishing this.

If, at its core, schizophrenia symptomology is underpinned by disturbances in excitatory-inhibitory neurotransmitter systems (GABA, NMDA) as has been suggested (Friston et al., 2016; Gonzalez-Burgos, Cho, & Lewis, 2015; Gonzalez-Burgos & Lewis, 2012), these disturbances may well be reflected in reduced oscillatory alpha connectivity, as alpha oscillations have been

shown to be associated with E-I balance, although not directly (Popov et al., 2017; Zhigalov et al., 2019; Zhigalov & Jensen, 2020). That being said, alpha connectivity is thought to reflect feedback processes, which, as mentioned, have been shown to be increased in patients with effective analysis of the fMRI signal (Rolls et al., 2020). Clearly, further differentiation of effective connectivity using both fMRI and MEG methods is required.

No structural measures were associated with schizotypy. It is feasible that functional dysconnectivity in the at-risk population occurs prior to the structural dysconnectivity shown in patients. In support, with fMRI and DTI, Li and colleagues found schizophrenia had decreased functional connectivity in the ventral loop and dorsal loop, accompanied by decreased structural connectivity, whereas relatives had reduced functional connectivity in the ventral loop and the dorsal loop but no significant differences in structural connectivity (Li et al., 2020).

Notably, schizotypy has been used synonymously with clinical risk in this thesis on the basis that high schizotypy individuals are more likely to develop psychosis (Barrantes-Vidal, Grant, & Kwapil, 2015). Whether the amalgamation of these terms in relation to the underlying ‘trait’ and ‘state’ constructs is reasonable however is debatable. In support, recent factor analysis work, by Fluckiger and colleagues (2019), found schizotypy features were significantly associated with positive, negative and disorganized symptoms through cognitive disturbances using the Wisconsin Schizotypy Scales, 14 predictive basic symptoms (BS) of the schizophrenia Proneness Instrument (Schultze-Lutter, 2009), and positive, negative, and disorganized symptoms from the Structured Interview for Psychosis-Risk Syndrome (McGlashan, Walsh, & Woods, 2010). Still, that schizotypy continues to be defined across personality, quasi-clinical and clinical phenomenology is reiterated and deserves awareness in ongoing research (Grant, Green, & Mason, 2018; Mason, 2015).

11.2.3 Unclear evidence for a relationship between genetic risk and functional connectivity

Genetic research is largely free of the construct level arguments associated with the clinical literature and evidence for genetic continuity between health and disease is now well established (Hilker et al., 2018; Legge et al., 2021; Marshall et al., 2017; Purcell et al., 2009; Zhao et al., 2018). However, against prediction, relationships between polygenic risk score and both local

and long-range functional connectivity, and between CNV carrier status and connectivity in visual areas and across the cortex, did not meet significance.

Recently, the first published investigation of PRS for schizophrenia and induced gamma oscillations was circulated (Dimitriadis et al., 2021). As with the results presented here, significant differences in gamma (peak amplitude and frequency) between individuals with high (N=104) and low (N=99) polygenic load were not found. However, in an exploratory analysis, when the gamma spike (transient period) and induced signal were expressed as group averaged percentage change relative to baseline, both revealed lower gamma values in the high PRS group, suggesting gamma differences may not have been captured by the peak amplitude and frequency measures.

In this thesis, some evidence for a relationship between reduced gamma amplitude and PRS was found in one half of the cohort (100-Brains) but was diminished when grouping across both 100-Brains and MEG-Partnership samples. Employing a circular grating stimulus has been shown to induce larger gamma responses compared to the static grating stimuli used here and the work by Dimitriadis (Shaw et al., 2020). Unfortunately, the planned collection of ~200 visual gamma datasets using a circular grating was paused during this work due to uncontrollable factors. However, there is enough evidence to suggest that additional validation of the effect of PRS on induced gamma, is worth pursuing.

Beyond common polygenic variants, genetic advancements over the last 15 years have also identified both excitatory and inhibitory (E-I) CNVs as targets for exploring genotype-endotype relationships. However, a significant relationship between E-I CNV status and functional connectivity was not found, which may at least in part have been due to the nature of the recall study and availability of datasets. Only in the last 5 years, has the accumulation of data given the appropriate power for robust identification on CNVs in psychosis (Marshall et al., 2017), meaning at present the investigation of CNV–endotype relationships is in its infancy. Furthermore, that some CNVs have been implicated in both excitatory and inhibitory systems (e.g., NRXN gene, NRXN1 deletion) adds an additional level of difficulty to teasing apart their neurobiological correlates.

More broadly, the genetic picture of schizophrenia is complex, making it a challenge to capture associated dynamical imaging markers. To the author's knowledge no previous relationships have been found between PRS and long-range M/EEG networks in the adult population. However, a positive relationship between PRS score and theta and alpha connectivity in a large sample of 1,425 adolescents has been found (Meyers et al., 2021). Interestingly, the most robust associations were observed between PRS and parietal-occipital, central-parietal, and frontal-parietal alpha connectivity among males between ages 15–19 ($p < 10^{-4}$), suggesting PRS relationships exist early in life, when the onset of symptomology often occurs (Ochoa, Usall, Cobo, Labad, & Kulkarni, 2012).

That schizotypy and polygenic risk score are unrelated suggests these measures capture different risk variance despite evidence suggesting that the heritability of schizotypy is moderated by latent factors shared with schizophrenia (Grant et al., 2018). While there is no clear clinical or genetic profile for those at-risk for schizophrenia disorders at present, improved understanding of associated risk factors will be paramount for prevention in future.

On this note, elucidating the genetic trajectories of diseases is accompanied by various ethical issues going beyond individuals to the consent of the family (Knoppers & Chadwick, 2005). Clear understanding of the genetic contribution to disease also opens the door to techniques like Gene Therapy (changing the genetic architecture of DNA) which, though not yet formally implemented in humans, has its own evolutionary and social controversies. The availability and the extent to which the advantages of these procedures outweigh the risks will be addressed the coming years. However, at present, due to the complexity of schizophrenia's genetic and clinical forms, the arguments do not warrant further consideration here.

11.2.4 A relationship between PRS and structural connectivity

Findings in Chapter 8 suggest that individuals with increased polygenic load for schizophrenia have increased axial diffusivity amongst white matter tracts, which could be the result of a reduction in axonal integrity (Winklewski et al., 2018). This is consistent with a large study suggesting a link between common variants and the micro-environment in the brain (Stauffer et

al., 2021); namely, that increased diffusivity can also be pathological as it coincides with increased genetic load for schizophrenia.

In general, it has been shown that for PRS to have sufficient predictive power ~2000 subjects are required (Dudbridge & Wray, 2013). This might partly explain the lack of functional correlations already discussed; however, it also suggests that the structural finding is unlikely to be the product of type 1 error. That the relationship is shown in recent biobank research ($N_{\max} = 29,878$) also provides considerable support (Stauffer et al., 2021).

It is known that the plasticity of the brain changes from early infancy through adulthood (Guyer, Pérez-Edgar, & Crone, 2018). As PRS is associated with increased long-range functional EEG connectivity in adolescence (Meyers et al., 2021), and structural changes in adulthood (Stauffer et al., 2021), it might be postulated that PRS captures some of the variance in functional changes prior to structural changes in individuals with high polygenic load. This is not what was shown in this thesis, however, as consequently, we would expect PRS to have been correlated with both structural and functional measures in adults. In future, the implementation of non-correlational and longitudinal studies of functional and structural imaging will be fundamental to our understanding of clinical and genetic risk.

At present, establishing genetic-neurobiology-presentation relationships is challenging on account of the difficulties in imaging population samples through development. Increasing advancements in neuroimaging technologies such as Optically Pumped Magnetometers (OPMs), which allow MEG to be performed on the scalp surface, in addition to improved noise reduction techniques (Tierney et al., 2019), will soon provide the means for monitoring these neurodevelopmental factors.

11.2.6 The relationship between visual gamma frequency and structural connectivity

Finding a relationship between visual gamma frequency and structural connectivity, namely radial diffusivity and mean diffusivity, is novel and could imply gamma frequency is associated with increased myelin (Winklewski et al., 2018). Due to the correlational analyses, again, no directional assertions can be made. However, intuitively, as the primary role of myelin sheath is

to increase the conduction velocity of electrical impulses (Dean et al., 2016) and oscillatory frequency is loosely proportional to rate at which populations of neurons fire (Hämäläinen, Hari, Ilmoniemi, Knuutila, & Lounasmaa, 1993), it might be expected that the characteristics of the visual gamma signal are dependent on the integrity of structural pathways. That being said, the structural connectome appears to be necessary but not sufficient for functional connectivity (Messaritaki et al., 2021). To further explore this structure-function relationship the inverse of the radial diffusivity values ($1/RD$) might be employed in future. In retrospect this would have provided a clearer index of myelin integrity.

White matter structure facilitates the propagation of functional chemical messages, via neurotransmitters. Neurotransmitters are, therefore, an essential link between structure and function, which underpin neural plasticity and communication both within and between brain areas. Correspondingly, there has been a recent effort to unite structure and function perspectives through an investigation of the spatial distribution of chemical messengers (Hansen et al., 2021). Using a combination of Positron Emission Tomography imaging (estimation of in vivo neurotransmitter concentrations across the brain), structural MRI, fMRI and MEG resting-state recordings, Hansen and colleagues were able to curate an 18-neurotransmitter 3D atlas of the brain; neurotransmitters closely mapped onto both the structure of the neocortex and its mediated functions. This is a feat of multi-modal analysis which highlights the importance of imaging research in our understanding of the brain and a fundamental reference for on-going research.

11.2.7 Finding gamma source estimates are improved when beamforming with a finer sampling grid and alpha and beta networks can be extracted from resting-state data

The methods chapters in this thesis make a significant contribution to the MEG literature on account of the potential real-world utility of the findings therein. One of the most difficult aspects of experimental MEG design is deciding on the analysis methods due to the abundance of possible routes. It has been shown that the analysis of visual gamma data can be optimised by performing source localisation on a finer sampling grid. It is recognised, however, that because temporal and computational demands increase in a linear fashion with increased resolution, the use of a fine sampling grid is at the researcher's discretion and should align with the aims of any given study.

Additionally, visual gamma task-data can be used to extract static amplitude-amplitude coupling measures in alpha and beta networks, making a resting-state paradigm superfluous to requirement in some experiments. Static oscillatory connectivity measures have been shown to be useful markers of individual variability, disease risk, disease state and pharmacological manipulation (Dima et al., 2020; Doherty et al., 2021; Godfrey & Singh, 2020; Routley et al., 2017). This work suggests that a separate resting-state run is not needed to extract these markers. Changes made in light of these findings have the potential to improve participant comfort, increase the likelihood of identifying biomarkers and further improved data quality due the shortening of scanning sessions. If, as discussed, alpha connectivity estimates are affected by attentional factors during the resting-state, extracting long-range networks during the presence of task could also be beneficial.

11.2.8 Additional comments

Against hypotheses, no MEG predictors or schizophrenia-risk predictors were significantly associated with long-range beta connectivity. In comparison to alpha and gamma oscillations, the mechanisms driving beta oscillations are much less clear. Recent research suggests that the long-range beta oscillations measured with M/EEG are actually the result of beta bursting activity across the cortex (Barone & Rossiter, 2021). The verification of such findings could suggest that amplitude-amplitude connectivity is an inappropriate measure of beta connectivity; and subsequently contribute to the null findings in this thesis.

On a technical level, increasing interest is being given to the full Power Density Spectrum (PDS) in electrophysiological brain research. The PDS comprises the rhythmic oscillatory part of the signal, discussed at length in this thesis, as well as a continuous aperiodic part, the so called 1/f spectra, which has been suggested to reflect underlying synaptic currents (Buzsáki et al., 2012). During band pass filtering of MEG data these components are merged, which has recently been considered a problem if the aperiodic components differ between experimental conditions. Recent investigations using toolboxes like FOOOF (fitting-oscillations-and-one-over-f) suggest some spectra are more difficult to spate than others (Donoghue et al., 2020). It is expected more data will be acquired before this method is more widely implemented. However, methods like

FOOOF should give better estimates of peak amplitude and frequency as well as properties of the underlying 1/f aperiodic spectral shape. This, in turn, could facilitate the detection of better, more sensitive biomarkers.

11.3 Broader considerations

11.3.1 Genetics versus environment

Our ability to treat or prevent psychosis is largely dependent on understanding its causal mechanisms. It is known that small polygenic variants and large CNVs contribute to schizophrenia susceptibility, as discussed at length in this thesis. It is also known that numerous environmental factors are involved. For example, inflammatory factors (cytokines and c-reactive protein, Dickerson et al., 2016), bleeding, preeclampsia and asphyxia during pregnancy, as well as emergency caesarean (Canon et al., 2002) have all been associated with increased psychosis risk. Psychosocial stress, childhood adversity and cannabis use are also highly implicated (Rokita et al., 2021; Marconi et al., 2016) and may result in symptoms measured in both the clinical and healthy populations.

In the literature, heritability of schizophrenia is often treated as separate to environmental factors, however some heritability estimates could be overestimated (Zwicker et al., 2018). Twin genetic studies, for example, cannot fully account for developmental differences in utero. Similarly, because children of parents with psychosis are more likely to observe a traumatic event, untangling whether the psychosis is the results of inheritance or environment is challenging. In fact, interactions between gene and environmental factors are likely to underpin the complexity of schizophrenia and are being increasingly explored. For example, one recent but seemingly consistent finding is that the presence of the AKT1 gene increases the likelihood of developing psychosis with frequent cannabis use (Morgan et al., 2016). These results have implications for the prevention and treatment of psychosis, particularly in certain groups.

Recent research suggest that the disorganised feature of schizophrenia might be a good target for gene-environment investigations. As compared with positive and negative symptoms disorganisation is a newer concept. It refers to disorganisation of thought and behaviour and is shared in both schizophrenia and schizotypy (Kemp et al., 2021; Liddle, 2019). A number of

environmental and genetic factors have also been associated, including: history of psychosis in family, low level of insight and compliance, attention (distraction errors), lengthened P300 latency of evoked cognitive auditory potentials, low-functional alleles of genes MTHFR and DNMT3b, high level of urbanicity and psychotraumatic events at early age (Nestsiarovich et al., 2020). Continuing to target specific constructs such as disorganisation and their associated gene-environment factors, while challenging, would undoubtedly facilitate understanding of schizophrenia and schizophrenia risk in future.

11.3.2 Predictive coding and comorbidity of disorders

More broadly, increasing evidence supports the application of predictive coding theory (Friston & Kiebel, 2009) to a range of neuropathological disorders, including schizophrenia disorders, autism spectrum disorders and major depression (Kube, Schwarting, Rozenkrantz, Glombiewski, & Rief, 2020; Smith, Badcock, & Friston, 2021; Tarasi et al., 2022). One explanation for the different sensory sensitivities characteristic of autism spectrum disorders is that they result from the allocation of excessive weight to incoming sensory information, whereas the over-attribution to prior belief and internal representations might result in reality distortion symptoms in schizophrenia patients. Furthermore, negative affect in depressed individuals could also be due to an over-reliance on negative internal representations.

At present, however, these mechanistic distinctions are not clear cut as the direction of attribution i.e., excessive or diminished, has yet to be fully established in psychosis patients (Corlett et al., 2019; Sterzer et al., 2018). Moreover, the application to major depression has been criticised as broad, unspecific (Rief & Joormann, 2019) and unable to explain individual presentations, making more research necessary.

The lack of clear evidence for differences in predictive models of pathology might, at least in part, be explained in the context of co-morbidity and coexisting psychiatric conditions. For example, individuals with schizophrenia have a high prevalence of depression (~50%), substance abuse (50-70%), anxiety disorders: (18%), social anxiety disorder (10%) and obsessive-compulsive disorder (9%) (Buckley, Miller, Lehrer, & Castle, 2009; Kiran & Chaudhury, 2018; Tsai & Rosenheck, 2013; Winklbaur, Ebner, Sachs, Thau, & Fischer, 2006). Furthermore, in a

study of 3,400 individuals with autism disorders and 38,000 controls, Chien and colleagues found the incidence of schizophrenia spectrum (10%), bipolar disorder (7%), and major depressive disorder (3%) were significantly higher than for controls (Chien, Wu, & Tsai, 2021).

That there is overlap in the prescribed treatments for the aforementioned disorders, such as lithium, antidepressants, antipsychotics, and benzodiazepines, also suggests there is significant neurobiological cross-over. In turn, the grouping of individuals across diagnostic categories for the purpose of research, in contrast to traditional perspectives (American Psychiatric Association, 2013; WHO, 2018), might be the key to better understanding these conditions. The continued discovery of imaging markers that index neurobiological processes in both the healthy population and clinical groups is critical to this end.

11.4 General limitations and future directions

This thesis is subject to some general limitations. Data included was largely observational due to the completion of the work in the Covid-19 pandemic. The opportunity to collect experimental data was therefore severely restricted making it unfeasible to investigate the relationship between local and global connectivity in different clinical groups, as was an initial aim. However, this remains an ongoing interest. In view of the Positive and Negative Valence domains of the RDoc approach, a breakdown of positive and negative constructs within the clinical risk chapters would also have been beneficial.

The 100-Brains and MEG-Partnership datasets used in Chapters 3-9 had a higher number of females than males and was comprised of a population of university students meaning findings might be more reflective of females in young adulthood. The difference in visual gamma task used between the two cohorts, despite being included as a covariate, would have also led to reduced statistical power. Statistically, the use of a Bonferroni correction throughout this thesis may have been conservative on account of the assumption of independence of observations. However, considering the novel nature of some of the relationships found, a stringent multiple comparison adjustment mean results are less likely to be the product of type 1 error.

This is the first time Non-Negative Matrix Factorization (Lee & Seung, 1999) has been applied to structural connectivity matrices. This was interesting regarding the streamline components, where networks comprised a few dominant tracts at the 5% scaling threshold. In contrast, networks weighted by the DTI measures were less clear making it difficult to comment on the physiology or typology of the structural findings. In future, projecting the functional components onto the structural AAL matrices to investigate the crossover of structural and functional networks, would be beneficial.

The MEG analyses described in this thesis show an averaged static snapshot of MEG functional connectivity. Researchers are increasingly interested in dynamical methods of analysis which maximise information gained from fluctuations in the electrophysiological data over time (e.g., Hidden Markov Modelling & K-means analysis; Hirschmann et al., 2020b; Spadone, de Pasquale, Mantini, & Della Penna, 2012). Such research is likely to facilitate our understanding of schizophrenia as a disorder of dysconnectivity (Pettersson-Yeo et al., 2011).

In this vein, Sanfratello employed spatial ICA to investigate dynamic MEG and fMRI connectivity over small time windows in consideration of the temporal fluctuations of connectivity correlations (Sanfratello, Houck, & Calhoun, 2018). FMRI and MEG reveal between-group functional connectivity differences in distinct ways. FMRI revealed periods of overall dysconnectivity in schizophrenia whereas MEG analysis showed aberrant connectivity in fronto-fronto and fronto-parietal regions. Significantly more within-groups variability in connectivity in the schizophrenia group was shown, in line with previous findings (Alamian et al., 2017; Friston & Frith, 1995). One reason for the heterogeneity in schizophrenia literature is the aberrant connectivity profiles of individuals, features of which might be better revealed with dynamical connectivity analyses.

Furthermore, in relation to the extraction of functional networks from task data, a planned analysis was to explore whether the relationship between schizotypy and alpha connectivity exists with networks derived from visual gamma data. This was beyond the timeframe for this thesis but would add strong support to the obsolete nature of a resting-state run for the investigation of alpha and beta networks.

A foundation of this thesis was DCM work showing coupling between the gamma response and superficial pyramidal and interneuron connections in the visual cortex (Friston, Harrison, & Penny, 2003; Shaw et al., 2017; Shaw et al., 2020). DCM therefore provides an opportunity to explicitly investigate the relationship between the local connections in visual cortex and oscillatory connectivity across the brain. It also provides a means through which risk factors for schizophrenia can be investigated in relation to specific connections. It is hoped that by utilising DCM in future work our neurobiological understanding of these factors will be improved.

Finally, microstructural imaging makes an excellent complement to MEG imaging. This thesis suggests that functional and structural dysconnectivity could be associated with schizophrenia symptomology and genetic load, respectively, in the normal population. The further longitudinal exploration of these correlates could be highly informative. Furthermore, how function explicitly maps on to structure, also, remains an important route for future research.

11.5 Conclusion

The RDoC approach to defining pathology and psychological disorders has now been in circulation for 12 years. With increasing research, it is expected that translational markers of health and disease could be integrated into diagnostic manuals, which continue to be primary point of reference for clinicians. In line with the RDoC initiative, which seeks to provide a biologically-based framework for disorder, the aim of this thesis was to investigate structural and functional neural markers associated with health, schizophrenia risk, and schizophrenia.

Importantly, in the healthy population, schizophrenia symptomology was associated with functional dysconnectivity, whereas in the same population, increased genetic burden for schizophrenia was associated with structural dysconnectivity. Together, these findings suggest that clinical risk and polygenic risk factors capture different aspect of schizophrenia-proneness and would benefit from longitudinal exploration. The novel exploration of connectivity related to excitatory and inhibitory CNV burden in schizophrenia also provided a foundation for our future understanding of genetic-neurobiological processes involved in E-I balance.

Finding that the amplitude and frequency of the visual gamma response are correlated with reduced long-range functional connectivity and increased structural connectivity, respectively, has also provided important insight into relationships between the (local) visual cortex and the (global) rest of the brain in the healthy population. Exploring these interactions in schizophrenia groups could identify additional biomarkers and critically inform our hierarchical understanding of the brain.

Finally, enhanced methods for extracting measures of local and global connectivity with MEG have been provided which have the potential to aid the identification of biomarkers and improve the comfort of participants in future clinical studies. Overall, these findings support a new wave of schizophrenia research beyond diagnosis criteria with MEG and DTI methods.

References

- Adams, R. A., Pinotsis, D., Tsirlis, K., Unruh, L., Mahajan, A., Horas, A. M., ... Anticevic, A. (2022). Computational Modeling of Electroencephalography and Functional Magnetic Resonance Imaging Paradigms Indicates a Consistent Loss of Pyramidal Cell Synaptic Gain in Schizophrenia. *Biological Psychiatry*, *91*(2), 202–215.
- Alamia, A., & VanRullen, R. (2019). Alpha oscillations and traveling waves: Signatures of predictive coding? *PLOS Biology*, *17*(10), e3000487.
- Alamian, G., Hincapié, A.-S., Pascarella, A., Thiery, T., Combrisson, E., Saive, A.-L., ... Jerbi, K. (2017a). Measuring alterations in oscillatory brain networks in schizophrenia with resting-state MEG: State-of-the-art and methodological challenges. *Clinical Neurophysiology*, *128*(9), 1719–1736.
- American Psychiatric Association. (2013). *Diagnostic and statistical manual of mental disorders (DSM-5®)*. American Psychiatric Pub.
- Anticevic, A, Tang, Y., Cho, Y., Repovs, G., Cole, M., Savic, A., ... Xu, K. (2014). Amygdala connectivity differs among chronic, early course, and individuals at risk for developing schizophrenia. *Schizophrenia Bulletin*, *40*(5), 1105–1116.
- Anticevic, Alan, Gancsos, M., Murray, J. D., Repovs, G., Driesen, N. R., Ennis, D. J., ... Corlett, P. R. (2012). NMDA receptor function in large-scale anticorrelated neural systems with implications for cognition and schizophrenia. *Proceedings of the National Academy of Sciences of the United States of America*, *109*(41), 16720–16725.
- Anticevic, Alan, Haut, K., Murray, J. D., Repovs, G., Yang, G. J., Diehl, C., ... Cannon, T. D. (2015). Association of thalamic dysconnectivity and conversion to psychosis in youth and young adults at elevated clinical risk. *JAMA Psychiatry*, *72*(9), 882–891.
- Anticevic, A., & Lisman, J. (2017). How can global alteration of excitation/inhibition balance lead to the local dysfunctions that underlie schizophrenia?. *Biological Psychiatry*, *81*(10), 818–820.
- Baillet, S. (2017). Magnetoencephalography for brain electrophysiology and imaging. *Nature neuroscience*, *20*(3), 327–339.
- Balu, D. T. (2016). The NMDA Receptor and Schizophrenia. From Pathophysiology to Treatment. In *Advances in Pharmacology* (Vol. 76, pp. 351–382). Academic Press Inc.

- Barnes, G. R., Hillebrand, A., Fawcett, I. P., & Singh, K. D. (2004). Realistic spatial sampling for MEG beamformer images. *Human Brain Mapping, 23*(2), 120–127.
- Barone, J., & Rossiter, H. E. (2021). Understanding the Role of Sensorimotor Beta Oscillations. *Frontiers in Systems Neuroscience, 0*, 51.
- Barrantes-Vidal, N., Grant, P., & Kwapil, T. R. (2015). The role of schizotypy in the study of the etiology of schizophrenia spectrum disorders. In *Schizophrenia Bulletin* (Vol. 41, pp. S408–S416).
- Bassett, A. S., Marshall, C. R., Lionel, A. C., Chow, E. W., & Scherer, S. W. (2008). Copy number variations and risk for schizophrenia in 22q11.2 deletion syndrome. *Human molecular genetics, 17*(24), 4045-4053.
- Bassett, D. S., & Bullmore, E. D. (2006). Small-world brain networks. *The neuroscientist, 12*(6), 512-523.
- Bastos, A. M., Usrey, W. M., Adams, R. A., Mangun, G. R., Fries, P., & Friston, K. J. (2012). Canonical microcircuits for predictive coding. *Neuron, 76*(4), 695-711.
- Bastos, AndréMoraes M., Vezoli, J., Bosman, C. A., Schoffelen, J. M., Oostenveld, R., Dowdall, J. R., ... Fries, P. (2015a). Visual areas exert feedforward and feedback influences through distinct frequency channels. *Neuron, 85*(2), 390–401.
- Bastos, AndréMoraes M, Vezoli, J., Bosman, C. A., Schoffelen, J. M., Oostenveld, R., Dowdall, J. R., ... Fries, P. (2015b). Visual areas exert feedforward and feedback influences through distinct frequency channels. *Neuron, 85*(2), 390–401.
- Bertero, A., Liska, A., Pagani, M., Parolisi, R., Masferrer, M. E., Gritti, M., ... Gozzi, A. (2018). Autism-associated 16p11.2 microdeletion impairs prefrontal functional connectivity in mouse and human. *Brain, 141*(7), 2055–2065.
- Biase, M. A. Di, Cropley, V. L., Baune, B. T., Olver, J., Amminger, G. P., Phassouliotis, C., ... Zalesky, A. (2017a). White matter connectivity disruptions in early and chronic schizophrenia. *Psychological Medicine, 47*(16), 2797–2810.
- Biase, M. A. Di, Cropley, V. L., Baune, B. T., Olver, J., Amminger, G. P., Phassouliotis, C., ... Zalesky, A. (2017b). White matter connectivity disruptions in early and chronic schizophrenia. *Psychological Medicine, 47*(16), 2797–2810.
- Boashash, B. (2003). Time-Frequency Signal Analysis and Processing: A Comprehensive Reference Elsevier. In *Science*.

- Bonnefond, M., & Jensen, O. (2015). Gamma activity coupled to alpha phase as a mechanism for top-down controlled gating. *PLoS ONE*, *10*(6).
- Boozalis, T., Teixeira, A. L., Cho, R. Y.-J., & Okusaga, O. (2018). C-Reactive Protein Correlates with Negative Symptoms in Patients with Schizophrenia. *Frontiers in Public Health*, *0*, 360.
- Börger, C. (2017). Gamma Rhythms and Communication. In *An Introduction to Modeling Neuronal Dynamics* (pp. 333-337). Springer, Cham.
- Bosman, C. A., Schoffelen, J. M., Brunet, N., Oostenveld, R., Bastos, A. M., Womelsdorf, T., ... Fries, P. (2012). Attentional Stimulus Selection through Selective Synchronization between Monkey Visual Areas. *Neuron*, *75*(5), 875–888.
- Boutros, N. N., Korzyukov, O., Jansen, B., Feingold, A., & Bell, M. (2004). Sensory gating deficits during the mid-latency phase of information processing in medicated schizophrenia patients. *Psychiatry Research*, *126*(3), 203–215.
- Bowyer, S. M. (2016). Coherence a measure of the brain networks: past and present. *Neuropsychiatric Electrophysiology*, *2*(1), 1.
- Bowyer, S. M., Gjini, K., Zhu, X., Kim, L., Moran, J. E., Rizvi, S. U., ... Boutros, N. N. (2015). Potential Biomarkers of Schizophrenia from MEG Resting-State Functional Connectivity Networks: Preliminary Data. *Journal of Behavioral and Brain Science*, *05*(01), 1–11.
- Brealy, J. A., Shaw, A., Richardson, H., Singh, K. D., Muthukumaraswamy, S. D., & Keedwell, P. A. (2015). Increased visual gamma power in schizoaffective bipolar disorder. *Psychological Medicine*, *45*(4), 783–794.
- Brecht, M., Singer, W., & Engel, A. K. (1998). Correlation Analysis of Corticotectal Interactions in the Cat Visual System. *Journal of Neurophysiology*, *79*(5), 2394–2407.
- Breier, A., Buchanan, R. W., Elkashef, A., Munson, R. C., Kirkpatrick, B., & Gellad, F. (1992). Brain Morphology and Schizophrenia: A Magnetic Resonance Imaging Study of Limbic, Prefrontal Cortex, and Caudate Structures. *Archives of General Psychiatry*, *49*(12), 921–926.
- Brookes, M. J., Woolrich, M., Luckhoo, H., Price, D., Hale, J. R., Stephenson, M. C., ... Morris, P. G. (2011). Investigating the electrophysiological basis of resting state networks using magnetoencephalography. *Proceedings of the National Academy of Sciences*, *108*(40), 16783–
- Brookes, M J, Woolrich, M. W., & Barnes, G. R. (2012). Measuring functional connectivity in

- MEG: A multivariate approach insensitive to linear source leakage. *Neuroimage.*, *1*(63), 2.
- Brookes, Matthew J., Gibson, A. M., Hall, S. D., Furlong, P. L., Barnes, G. R., Hillebrand, A., ... Morris, P. G. (2005). GLM-beamformer method demonstrates stationary field, alpha ERD and gamma ERS co-localisation with fMRI BOLD response in visual cortex. *NeuroImage*, *26*(1), 302–308.
- Brookes, Matthew J., Hale, J. R., Zumer, J. M., Stevenson, C. M., Francis, S. T., Barnes, G. R., ... Nagarajan, S. S. (2011). Measuring functional connectivity using MEG: Methodology and comparison with fcMRI. *NeuroImage*, *56*(3), 1082–1104.
- Brookes, Matthew J, Tewarie, P. K., Hunt, B. A. E., Robson, S. E., Gascoyne, L. E., Liddle, E. B., ... Morris, P. G. (2016). A multi-layer network approach to MEG connectivity analysis. *NeuroImage*, (123), 425–438.
- Buckley, P. F., Miller, B. J., Lehrer, D. S., & Castle, D. J. (2009). Psychiatric Comorbidities and Schizophrenia. *Schizophrenia Bulletin*, *35*(2), 383–402.
- Buzsáki, G. (2010). Neural syntax: cell assemblies, synapsembles, and readers. *Neuron*, *68*(3), 362–385.
- Buzsaki, G., & Draguhn, A. (2004). Neuronal Oscillations in Cortical Networks. *Science*, *304*(5679), 1926–1929.
- Buzsáki, G., & Schomburg, E. W. (2015a). What does gamma coherence tell us about inter-regional neural communication? *Nature Neuroscience*, *18*(4), 484–489.
- Buzsáki, G., & Wang, X.-J. (2012a). Mechanisms of Gamma Oscillations. *Annual Review of Neuroscience*, *35*(1), 203–225.
- Cabral, J., Fernandes, H. M., Hartevelt, T. J. Van, James, A. C., Kringelbach, M. L., & Deco, G. (2013). Structural connectivity in schizophrenia and its impact on the dynamics of spontaneous functional networks. *Chaos: An Interdisciplinary Journal of Nonlinear Science*, *23*(4), 046111.
- Cabral, J., Hugues, E., Sporns, O., & Deco, G. (2011). Role of local network oscillations in resting-state functional connectivity. *NeuroImage*, *57*(1), 130–139.
- Cabral, J., Kringelbach, M. L., & Deco, G. (2017). Functional connectivity dynamically evolves on multiple time-scales over a static structural connectome: Models and mechanisms. *NeuroImage*, *160*, 84.
- Calkins, M. E., Curtis, C. E., Grove, W. M., & Iacono, W. G. (2004). Multiple Dimensions of

- Schizotypy in First Degree Biological Relatives of Schizophrenia Patients. *Schizophrenia Bulletin*, 30(2), 317–325.
- Cannon, M., Jones, P. B., & Murray, R. M. (2002). Obstetric complications and schizophrenia: historical and meta-analytic review. *American Journal of Psychiatry*, 159(7), 1080-1092.
- Canu, E., Agosta, F., & Filippi, M. (2015). A selective review of structural connectivity abnormalities of schizophrenic patients at different stages of the disease. *Schizophrenia Research*, 161(1), 19–28.
- Cardin, J. A., Carlén, M., Meletis, K., Knoblich, U., Zhang, F., Deisseroth, K., ... Moore, C. I. (2009). Driving fast-spiking cells induces gamma rhythm and controls sensory responses. *Nature*, 459(7247), 663–667.
- Cardno, A. G., & Owen, M. J. (2014). Genetic relationships between schizophrenia, bipolar disorder, and schizoaffective disorder. *Schizophrenia Bulletin*, 40(3), 504–515.
- Carlén, M., Meletis, K., Siegle, J. H., Cardin, J. A., Futai, K., Vierling-Claassen, D., ... Tsai, L. H. (2012). A critical role for NMDA receptors in parvalbumin interneurons for gamma rhythm induction and behavior. *Molecular Psychiatry*, 17(5), 537–548.
- Cetin, M. S., Houck, J. M., Rashid, B., Agacoglu, O., Stephen, J. M., Sui, J., ... & Calhoun, V. D. (2016). Multimodal classification of schizophrenia patients with MEG and fMRI data using static and dynamic connectivity measures. *Frontiers in neuroscience*, 10, 466.
- Charvet, C. J. (2020). Closing the gap from transcription to the structural connectome enhances the study of connections in the human brain. *Developmental Dynamics*, 249(9), 1047–1061.
- Chen, C.-M. A., Stanford, A. D., Mao, X., Abi-Dargham, A., Shungu, D. C., Lisanby, S. H., ... Kegeles, L. S. (2014). GABA level, gamma oscillation, and working memory performance in schizophrenia. *NeuroImage: Clinical*, 4, 531–539.
- Chen, Y.-H., Stone-Howell, B., Edgar, J. C., Huang, M., Wootton, C., Hunter, M. A., ... Cañive, J. M. (2016). Frontal slow-wave activity as a predictor of negative symptoms, cognition and functional capacity in schizophrenia. *The British Journal of Psychiatry: The Journal of Mental Science*, 208(2), 160–167.
- Chung, D. W., Fish, K. N., & Lewis, D. A. (2016). Pathological basis for deficient excitatory drive to cortical parvalbumin interneurons in schizophrenia. *The American Journal of Psychiatry*, 173(11), 1131.
- Claridge, G., & Beech, T. (1995). Fully and quasi-dimensional. *Schizotypal personality*, 192.

- Clayton, M. S., Yeung, N., & Kadosh, R. C. (2015). The roles of cortical oscillations in sustained attention. *Trends in cognitive sciences*, *19*(4), 188-195.
- Clayton, M. S., Yeung, N., & Cohen Kadosh, R. (2018). The many characters of visual alpha oscillations. *European Journal of Neuroscience*, *48*(7), 2498–2508.
- Cleynen, I., Engchuan, W., Hestand, M. S., Heung, T., Holleman, A. M., Johnston, H. R., ... Bassett, A. S. (2020). Genetic contributors to risk of schizophrenia in the presence of a 22q11.2 deletion. *Molecular Psychiatry*, 1–15.
- Cohen, A. S., Mohr, C., Ettinger, U., Chan, R. C., & Park, S. (2015). Schizotypy as an organizing framework for social and affective sciences. *Schizophrenia bulletin*, *41*(suppl_2), S427-S435.
- Cohen, M. (2014). Analyzing Neural Time Series Data. Retrieved March 3, 2021, from https://www.google.co.uk/books/edition/Analyzing_Neural_Time_Series_Data/jTskAgAAQBAJ?hl=en&gbpv=1&printsec=frontcover
- Cohen, M. X. (2014). A neural microcircuit for cognitive conflict detection and signaling. *Trends in neurosciences*, *37*(9), 480-490.
- Cohen, S. M., Tsien, R. W., Goff, D. C., & Halassa, M. M. (2015). The impact of NMDA receptor hypofunction on GABAergic neurons in the pathophysiology of schizophrenia. *Schizophrenia research*, *167*(1-3), 98-107.
- Colclough, G. L., Brookes, M. J., Smith, S. M., & Woolrich, M. W. (2015). A symmetric multivariate leakage correction for MEG connectomes. *NeuroImage*, *117*, 439–448.
- Colclough, G. L., Woolrich, M. W., Tewarie, P. K., Brookes, M. J., Quinn, A. J., & Smith, S. M. (2016). How reliable are MEG resting-state connectivity metrics? *NeuroImage*, *138*, 284–293.
- Colclough, Giles L., Smith, S. M., Nichols, T. E., Winkler, A. M., Sotiropoulos, S. N., Glasser, M. F., ... Woolrich, M. W. (2017). The heritability of multi-modal connectivity in human brain activity. *ELife*, *6*.
- Cole, M. W., Bassett, D. S., Power, J. D., Braver, T. S., & Petersen, S. E. (2014). Intrinsic and task-evoked network architectures of the human brain. *Neuron*, *83*(1), 238–251.
- Collin, G., & Keshavan, M. S. (2018). Connectome development and a novel extension to the neurodevelopmental model of schizophrenia. *Dialogues in Clinical Neuroscience*, *20*(2), 101.
- Committee, J. F. (2019). *British National Formulary. BNF*. NICE. Retrieved from

<https://bnf.nice.org.uk/drug/clozapine.html#indicationsAndDoses>

- Compton, M. T., Chien, V. H., & Bollini, A. M. (2009). Associations between past alcohol, cannabis, and cocaine use and current schizotypy among first-degree relatives of patients with schizophrenia and non-psychiatric controls. *Psychiatric Quarterly*, *80*(3), 143–154.
- Costain, G., Lionel, A. C., Merico, D., Forsythe, P., Russell, K., Lowther, C., ... Bassett, A. S. (2013). Pathogenic rare copy number variants in community-based schizophrenia suggest a potential role for clinical microarrays. *Human Molecular Genetics*, *22*(22), 4485–4501.
- COVID-19 mental health and wellbeing surveillance: report. (2021). Retrieved November 4, 2021, from <https://www.gov.uk/government/publications/covid-19-mental-health-and-wellbeing-surveillance-report>
- Daducci, Palù, D., Lemkaddem, & Thiran. (2015). COMMIT: Convex optimization modeling for microstructure informed tractography. *IEEE Transactions on Medical Imaging*, *34*(1), 246–257.
- Damoiseaux, J. S., Rombouts, S. A. R. B., Barkhof, F., Scheltens, P., Stam, C. J., Smith, S. M., & Beckmann, C. F. (2006). Consistent resting-state networks across healthy subjects. *Proceedings of the National Academy of Sciences of the United States of America*, *103*(37), 13848–13853.
- Damoiseaux, J. S., Rombouts, S. A. R. B., Barkhof, F., Scheltens, P., Stam, C. J., Smith, S. M., & Beckmann, C. F. (2006). Consistent resting-state networks across healthy subjects. *Proceedings of the national academy of sciences*, *103*(37), 13848-13853.
- De Erausquin, G. A., & Alba-Ferrara, L. (2013). What does anisotropy measure? Insights from increased and decreased anisotropy in selective fiber tracts in schizophrenia. *Frontiers in integrative neuroscience*, *7*, 9.
- de Pasquale, F., Della Penna, S., Snyder, A. Z., Lewis, C., Mantini, D., Marzetti, L., ... Corbetta, M. (2010). Temporal dynamics of spontaneous MEG activity in brain networks. *Proceedings of the National Academy of Sciences of the United States of America*, *107*(13), 6040–6045.
- Deoni, S., Matthews, L., & Kolind, S. (2013). One component? Two components? Three? The effect of including a nonexchanging “free” water component in multicomponent driven equilibrium single pulse observation of T1 and T2. *Magnetic Resonance in Medicine*, *70*(1), 147–154.

- Dhollander, T., Raffelt, D., & Connelly, A. (2016, September). Unsupervised 3-tissue response function estimation from single-shell or multi-shell diffusion MR data without a co-registered T1 image. In *ISMRM Workshop on Breaking the Barriers of Diffusion MRI* (Vol. 5, No. 5). ISMRM.
- Dickerson, F., Stallings, C., Origoni, A., Schroeder, J., Katsafanas, E., Schweinfurth, L., ... & Yolken, R. (2016). Inflammatory markers in recent onset psychosis and chronic schizophrenia. *Schizophrenia Bulletin*, *42*(1), 134-141.
- Di Lorenzo, G., Daverio, A., Ferrentino, F., Santarnecchi, E., Ciabattini, F., Monaco, L., ... & Siracusano, A. (2015). Altered resting-state EEG source functional connectivity in schizophrenia: the effect of illness duration. *Frontiers in human neuroscience*, *9*,
- Dima, D. C., Adams, R., Linden, S. C., Baird, A., Smith, J., Foley, S., ... Singh, K. D. (2020). Electrophysiological network alterations in adults with copy number variants associated with high neurodevelopmental risk. *Translational Psychiatry*, *10*(1), 1–11.
- Dimitriadis, S. I., Perry, G., Foley, S. F., Tansey, K. E., Jones, D. K., Holmans, P., ... Linden, D. E. (2021). Genetic risk for schizophrenia is associated with altered visually-induced gamma band activity: evidence from a population sample stratified polygenic risk. *Translational Psychiatry*, *11*(1).
- Dimitriadis, S. I., Routley, B., Linden, D. E., & Singh, K. D. (2018). Reliability of static and dynamic network metrics in the resting-state: a MEG-beamformed connectivity analysis. *Frontiers in neuroscience*, *12*, 506.
- Dobel, C., Junghöfer, M., & Gruber, T. (2011). The Role of Gamma-Band Activity in the Representation of Faces: Reduced Activity in the Fusiform Face Area in Congenital Prosopagnosia. *PLoS ONE*, *6*(5).
- Doesburg, S. M., Herdman, A. T., Ribary, U., Cheung, T., Moiseev, A., Weinberg, H., ... Grunau, R. E. (2010). Long-range synchronization and local desynchronization of alpha oscillations during visual short-term memory retention in children. *Experimental Brain Research*, *201*(4), 719–727.
- Doherty, J. L., Cunningham, A. C., Chawner, S. J. R. A., Moss, H. M., Dima, D. C., Linden, D. E. J., ... Singh, K. D. (2021). Alterations in resting-state activity and functional connectivity in children with 22q11.2 deletion syndrome. *MedRxiv*, 2021.09.14.21263530.
- Donner, T. H., & Siegel, M. (2011). A framework for local cortical oscillation patterns. *Trends in*

- Cognitive Sciences*, 15(5), 191–199.
- Dorph-Petersen, K. A., Pierri, J. N., Wu, Q., Sampson, A. R., & Lewis, D. A. (2007). Primary visual cortex volume and total neuron number are reduced in schizophrenia. *Journal of Comparative Neurology*, 501(2), 290–301.
- Dudbridge, F., & Wray, N. R. (2013). Power and Predictive Accuracy of Polygenic Risk Scores. *PLOS Genetics*, 9(3).
- Egerton, A., Murphy, A., Donocik, J., Anton, A., Barker, G. J., Collier, T., ... Howes, O. D. (2020). Dopamine and Glutamate in Antipsychotic-Responsive Compared With Antipsychotic-Nonresponsive Psychosis: A Multicenter Positron Emission Tomography and Magnetic Resonance Spectroscopy Study (STRATA). *Schizophrenia Bulletin*.
- Ehrlichman, R. S., Gandal, M. J., Maxwell, C. R., Lazarewicz, M. T., Finkel, L. H., Contreras, D., ... & Siegel, S. J. (2009). N-methyl-d-aspartic acid receptor antagonist–induced frequency oscillations in mice recreate pattern of electrophysiological deficits in schizophrenia. *Neuroscience*, 158(2), 705-712.
- Engel, A. K., König, P., Kreiter, A. K., & Singer, W. (1991). Interhemispheric synchronization of oscillatory neuronal responses in cat visual cortex. *Science*, 252(5009), 1177-1179.
- Esterberg, M. L., & Compton, M. T. (2009). The psychosis continuum and categorical versus dimensional diagnostic approaches. *Current Psychiatry Reports*, 11(3), 179–184.
- Ettinger, U., Meyhöfer, I., Steffens, M., Wagner, M., & Koutsouleris, N. (2014). Genetics, cognition, and neurobiology of schizotypal personality: a review of the overlap with schizophrenia. *Frontiers in psychiatry*, 5, 18.
- Eysenck, H., & Peck, R. (1962). Handbook of abnormal psychology. Retrieved from https://journals.lww.com/jonmd/Citation/1962/12000/Handbook_of_Abnormal_Psychology.13.aspx
- Fanous, A. H., Neale, M. C., Gardner, C. O., Webb, B. T., Straub, R. E., O'Neill, F. A., ... Kendler, K. S. (2007). Significant correlation in linkage signals from genome-wide scans of schizophrenia and schizotypy. *Molecular Psychiatry* 2007 12:10, 12(10), 958–965.
- Farahani, F. V., Karwowski, W., & Lighthall, N. R. (2019). Application of graph theory for identifying connectivity patterns in human brain networks: a systematic review. *frontiers in Neuroscience*, 13, 585.
- Fehr, T., Kissler, J., Moratti, S., Wienbruch, C., Rockstroh, B., & Elbert, T. (2001). Source

- distribution of neuromagnetic slow waves and MEG-delta activity in schizophrenic patients. *Biological Psychiatry*, 50(2), 108–116.
- Fehr, T., Kissler, J., Wienbruch, C., Moratti, S., Elbert, T., Watzl, H., & Rockstroh, B. (2003). Source distribution of neuromagnetic slow-wave activity in schizophrenic patients—effects of activation. *Schizophrenia Research*, 63(1–2), 63–71.
- Fitzgerald, P. J., & Watson, B. O. (2018). Gamma oscillations as a biomarker for major depression: an emerging topic. *Translational Psychiatry* 2018 8:1, 8(1), 1–7.
- Florin, E., & Baillet, S. (2015). The brain’s resting-state activity is shaped by synchronized cross-frequency coupling of neural oscillations. *NeuroImage*, 111, 26–35.
- Fond, G., Lançon, C., Korchia, T., Auquier, P., & Boyer, L. (2020). The Role of Inflammation in the Treatment of Schizophrenia. *Frontiers in Psychiatry*, 0, 160.
- Ford, J. M., Palzes, V. A., Roach, B. J., Potkin, S. G., Van Erp, T. G. M., Turner, J. A., ... Mathalon, D. H. (2015). Visual Hallucinations Are Associated With Hyperconnectivity Between the Amygdala and Visual Cortex in People With a Diagnosis of Schizophrenia. *Schizophrenia Bulletin*, 41(1), 223–232.
- Fornito, A., & Bullmore, E. T. (2015). Reconciling abnormalities of brain network structure and function in schizophrenia. *Current Opinion in Neurobiology*, 30, 44–50.
- Fornito, A., Zalesky, A., Pantelis, C., & Bullmore, E. T. (2012). Schizophrenia, neuroimaging and connectomics. *NeuroImage*, 62(4), 2296–2314.
- Fourgeaud, L., & Boulanger, L. M. (2010). Role of immune molecules in the establishment and plasticity of glutamatergic synapses. *European Journal of Neuroscience*, 32(2), 207–217.
- Fourgeaud, L., Davenport, C. M., Tyler, C. M., Cheng, T. T., Spencer, M. B., & Boulanger, L. M. (2010). MHC class I modulates NMDA receptor function and AMPA receptor trafficking. *Proceedings of the National Academy of Sciences*, 107(51).
- Freeman, W. J., Rogers, L. J., Holmes, M. D., & Silbergeld, D. L. (2000). Spatial spectral analysis of human electrocorticograms including the alpha and gamma bands. *Journal of Neuroscience Methods*, 95(2), 111–121.
- Friedman-Hill, S. (2000). Dynamics of Striate Cortical Activity in the Alert Macaque: I. Incidence and Stimulus-dependence of Gamma-band Neuronal Oscillations. *Cerebral Cortex*, 10(11), 1105–1116.
- Fries, P., Reynolds, J. H., Rorie, A. E., & Desimone, R. (2001). Modulation of oscillatory neuronal

- synchronization by selective visual attention. *Science*, 291(5508), 1560–1563.
- Fries, Pascal. (2005). A mechanism for cognitive dynamics: neuronal communication through neuronal coherence. *Trends in Cognitive Sciences*, 9(10), 474–480.
- Fries, Pascal. (2015). Rhythms for Cognition: Communication through Coherence. *Neuron*, 88(1), 220–235.
- Fries, Pascal, Schröder, J. H., Roelfsema, P. R., Singer, W., & Engel, A. K. (2002). Oscillatory Neuronal Synchronization in Primary Visual Cortex as a Correlate of Stimulus Selection. *Journal of Neuroscience*, 22(9), 3739–3754.
- Friston, K. J., & Frith, C. D. (1995). Schizophrenia: a disconnection syndrome. *Clin Neurosci*, 3(2), 89-97.
- Friston, K J., Harrison, L., & Penny, W. (2003). Dynamic causal modelling. *NeuroImage*, 19(4), 1273–1302.
- Friston, K. J. (1998). The disconnection hypothesis. *Schizophrenia research*, 30(2), 115-125..
- Friston, Karl. (2008). Hierarchical Models in the Brain. *PLoS Computational Biology*, 4(11), e1000211.
- Friston, Karl, Brown, H. R., Siemerikus, J., & Stephan, K. E. (2016). The dysconnection hypothesis (2016). *Schizophrenia Research*, 176(2–3), 83–94.
- Friston, Karl J. (2011). Functional and Effective Connectivity: A Review. *Brain Connectivity*, 1(1), 13–36.
- Friston, Karl, & Kiebel, S. (2009). Predictive coding under the free-energy principle. *Philosophical Transactions of the Royal Society B: Biological Sciences*, 364(1521), 1211–1221.
- Frohlich, J., Reiter, L. T., Saravanapandian, V., Distefano, C., Huberty, S., Hyde, C., ... Jeste, S. S. (2019). Mechanisms underlying the EEG biomarker in Dup15q syndrome. *Molecular Autism*, 10(1).
- Frohlich, J., Senturk, D., Saravanapandian, V., Golshani, P., Reiter, L. T., Sankar, R., ... Jeste, S. S. (2016). A quantitative electrophysiological biomarker of duplication 15q11.2-q13.1 syndrome. *PLoS ONE*, 11(12).
- Fromer, M., Pocklington, A. J., Kavanagh, D. H., Williams, H. J., Dwyer, S., Gormley, P., ... O'Donovan, M. C. (2014). De novo mutations in schizophrenia implicate synaptic networks. *Nature*, 506(7487),
- Fuchs, E. C., Zivkovic, A. R., Cunningham, M. O., Middleton, S., LeBeau, F. E. N., Bannerman, D.

- M. M., ... Monyer, H. (2007). Recruitment of Parvalbumin-Positive Interneurons Determines Hippocampal Function and Associated Behavior. *Neuron*, 53(4), 591–604.
- Fusar-Poli, P., Smieskova, R., Kempton, M. J., Ho, B. C., Andreasen, N. C., & Borgwardt, S. (2013). Progressive brain changes in schizophrenia related to antipsychotic treatment? A meta-analysis of longitudinal MRI studies. *Neuroscience & Biobehavioral Reviews*, 37(8), 1680-1691.
- Fusar-Poli, Paolo, Bechdolf, A., Taylor, M. J., Bonoldi, I., Carpenter, W. T., Yung, A. R., & McGuire, P. (2013). At risk for schizophrenic or affective psychoses? A meta-analysis of DSM/ICD diagnostic outcomes in individuals at high clinical risk. *Schizophrenia Bulletin*, 39(4), 923–932.
- Gandal, M. J., Edgar, J. C., Klook, K., & Siegel, S. J. (2012). Gamma synchrony: towards a translational biomarker for the treatment-resistant symptoms of schizophrenia. *Neuropharmacology*, 62(3), 1504-1518.
- Gascoyne, L. E., Brookes, M. J., Rathnaiah, M., Katshu, M. Z. U. H., Koelewijn, L., Williams, G., ... Morris, P. G. (2021). Motor-related oscillatory activity in schizophrenia according to phase of illness and clinical symptom severity. *NeuroImage: Clinical*, 29, 102524.
- Gaser, C., Nenadic, I., Buchsbaum, B. R., Hazlett, E. A., & Buchsbaum, M. S. (2004). Ventricular enlargement in schizophrenia related to volume reduction of the thalamus, striatum, and superior temporal cortex. *The American Journal of Psychiatry*, 161(1), 154–156.
- Gerster, M., Waterstraat, G., Litvak, V., Lehnertz, K., Schnitzler, A., Florin, E., ... & Nikulin, V. (2022). Separating neural oscillations from aperiodic 1/f activity: challenges and recommendations. *Neuroinformatics*, 1-22.
- Gieselmann, M. A., & Thiele, A. (2008). Comparison of spatial integration and surround suppression characteristics in spiking activity and the local field potential in macaque V1. *European Journal of Neuroscience*, 28(3), 447–459.
- Girirajan, S., Rosenfeld, J. A., Coe, B. P., Parikh, S., Friedman, N., Goldstein, A., ... Eichler, E. E. (2012). Phenotypic Heterogeneity of Genomic Disorders and Rare Copy-Number Variants. *New England Journal of Medicine*, 367(14), 1321–1331.
- Glausier, J. R., & Lewis, D. A. (2017). GABA and Schizophrenia: where we stand and where we need to go. *Schizophrenia Research*, 181, 2.
- Glöckner, A., & Moritz, S. (2008). A Fine-Grained Analysis of the Jumping to Conclusions Bias in

- Schizophrenia: Data-Gathering, Response Confidence, and Information Integration. *Judgment and Decision Making*, 4(7), 587–600.
- Godfrey, M. (2021). *The development and application of advanced methods for MEG and EEG data analysis* (Doctoral dissertation, Cardiff University).
- Godfrey, M., & Singh, K. D. (2021). Measuring robust functional connectivity from resting-state MEG using amplitude and entropy correlation across frequency bands and temporal scales. *NeuroImage*, 226, 117551.
- Gonzalez-Burgos, G., Cho, R. Y., & Lewis, D. A. (2015). Alterations in Cortical Network Oscillations and Parvalbumin Neurons in Schizophrenia. *Biological Psychiatry*, 77(12), 1031–1040.
- Gonzalez-Burgos, G., Fish, K. N., & Lewis, D. A. (2011). GABA Neuron Alterations, Cortical Circuit Dysfunction and Cognitive Deficits in Schizophrenia. *Neural Plasticity*, 2011, 1–24.
- Gonzalez-Burgos, G., & Lewis, D. A. (2012). NMDA Receptor Hypofunction, Parvalbumin-Positive Neurons and Cortical Gamma Oscillations in Schizophrenia. *Schizophrenia Bulletin*, 38(5), 950–957.
- Gramfort, A., Luessi, M., Larson, E., Engemann, D. A., Strohmeier, D., Brodbeck, C., ... & Hämäläinen, M. (2013). MEG and EEG data analysis with MNE-Python. *Frontiers in neuroscience*, 267.
- Grant, P., Green, M. J., & Mason, O. J. (2018). Models of Schizotypy: The Importance of Conceptual Clarity. *Schizophrenia Bulletin*, 44(suppl_2), S556–S563.
- Gray, C. M., & Singer, W. (1989). Stimulus-specific neuronal oscillations in orientation columns of cat visual cortex. *Proceedings of the National Academy of Sciences of the United States of America*, 86(5), 1698–1702. <https://doi.org/10.1073/pnas.86.5.1698>
- Gray, Charles M., König, P., Engel, A. K., & Singer, W. (1989b). Oscillatory responses in cat visual cortex exhibit inter-columnar synchronization which reflects global stimulus properties. *Nature*, 338(6213), 334–337. <https://doi.org/10.1038/338334a0>
- Grent-‘t-Jong, T., Rivolta, D., Sauer, A., Grube, M., Singer, W., Wibrals, M., & Uhlhaas, P. J. (2016). MEG-measured visually induced gamma-band oscillations in chronic schizophrenia: Evidence for impaired generation of rhythmic activity in ventral stream regions. *Schizophrenia Research*, 176(2–3), 177–185.
- Grent-’t-jong, T., Gross, J., Goense, J., Wibrals, M., Gajwani, R., Gumley, A. I., ... Uhlhaas, P. J. (2018). Resting-state gamma-band power alterations in schizophrenia reveal e/i-balance

- abnormalities across illness-stages. *ELife*, 7.
- Grover, V. P. B., Tognarelli, J. M., Crossey, M. M. E., Cox, I. J., Taylor-Robinson, S. D., & McPhail, M. J. W. (2015). Magnetic Resonance Imaging: Principles and Techniques: Lessons for Clinicians. *Journal of Clinical and Experimental Hepatology*, 5(3), 246.
- Grützner, C., Wibrál, M., Sun, L., Rivolta, D., Singer, W., Maurer, K., & Uhlhaas, P. J. (2013). Deficits in high- (>60 Hz) gamma-band oscillations during visual processing in schizophrenia. *Frontiers in Human Neuroscience*, 7, 88.
- Guder, S., Frey, B. M., Backhaus, W., Braass, H., Timmermann, J. E., Gerloff, C., & Schulz, R. (2020). The Influence of Cortico-Cerebellar Structural Connectivity on Cortical Excitability in Chronic Stroke. *Cerebral Cortex*, 30(3), 1330–1344.
- Guidotti, A., Auta, J., Davis, J. M., Dong, E., Grayson, D. R., Veldic, M., ... Costa, E. (2005). GABAergic dysfunction in schizophrenia: New treatment strategies on the horizon. *Psychopharmacology*, 180(2), 191–205.
- Guillem, F., & Mograss, M. (2005). Gender differences in memory processing: Evidence from event-related potentials to faces. *Brain and Cognition*, 57(1), 84–92.
- Hakami, T., Jones, N. C., Tolmacheva, E. A., Gaudias, J., Chaumont, J., Salzberg, M., ... Pinault, D. (2009). NMDA receptor hypofunction leads to generalized and persistent aberrant γ oscillations independent of hyperlocomotion and the state of consciousness. *PLoS ONE*, 4(8), e6755.
- Hämäläinen, M., Hari, R., Ilmoniemi, R. J., Knuutila, J., & Lounasmaa, O. V. (1993). Magnetoencephalography—theory, instrumentation, and applications to noninvasive studies of the working human brain. *Reviews of Modern Physics*, 65(2), 413.
- Hämäläinen, M. S., & Ilmoniemi, R. J. (1994). Interpreting magnetic fields of the brain: minimum norm estimates. *Medical & Biological Engineering & Computing*, 32(1), 35–42.
- Harrison, P. J., & Weinberger, D. R. (2005). Schizophrenia genes, gene expression, and neuropathology: on the matter of their convergence. *Molecular psychiatry*, 10(1), 40–68.
- Hasenstaub, A., Shu, Y., Haider, B., Kraushaar, U., Duque, A., & McCormick, D. A. (2005). Inhibitory postsynaptic potentials carry synchronized frequency information in active cortical networks. *Neuron*, 47(3), 423–435.
- Hayes, J. F., Picot, S., Osborn, D. P. J., Lewis, G., Dalman, C., & Lundin, A. (2019). Visual Acuity in Late Adolescence and Future Psychosis Risk in a Cohort of 1 Million Men.

Schizophrenia Bulletin, 45(3), 571–578.

- Hazlett, E. A., Goldstein, K. E., & Kolaitis, J. C. (2011). A Review of Structural MRI and Diffusion Tensor Imaging in Schizotypal Personality Disorder. *Current Psychiatry Reports* 2011 14:1, 14(1), 70–78.
- Hilbert, D. (2010). *Grundz? ge einer allgemeinen Theorie der linearen Integralgleichungen*. Рипол Классик.
- Hillebrand, A., & Barnes, G. R. (2005). Beamformer analysis of MEG data. *International review of neurobiology*, 68, 149-171.. [https://doi.org/10.1016/S0074-7742\(05\)68006-3](https://doi.org/10.1016/S0074-7742(05)68006-3)
- Hillebrand, A., Barnes, G. R., Bosboom, J. L., Berendse, H. W., & Stam, C. J. (2012). Frequency-dependent functional connectivity within resting-state networks: An atlas-based MEG beamformer solution. *NeuroImage*, 59, 3909–3921.
- Hinkley, L. B. N., Dale, C. L., Luks, T. L., Findlay, A. M., Bukshpun, P., Pojman, N., ... Nagarajan, S. S. (2019). Sensorimotor Cortical Oscillations during Movement Preparation in 16p11.2 Deletion Carriers. *Journal of Neuroscience*, 39(37), 7321–7331.
- Hinkley, L. B. N., Vinogradov, S., Guggisberg, A. G., Fisher, M., Findlay, A. M., & Nagarajan, S. S. (2011). Clinical Symptoms and Alpha Band Resting-State Functional Connectivity Imaging in Patients With Schizophrenia: Implications for Novel Approaches to Treatment. *BPS*, 70, 1134–1142.
- Hirschmann, J., Baillet, S., Woolrich, M., Schnitzler, A., Vidaurre, D., & Florin, E. (2020a). Spontaneous network activity <35 Hz accounts for variability in stimulus-induced gamma responses. *NeuroImage*, 207, 116374.
- Hirvonen, J., Wibral, M., Palva, J. M., Singer, W., Uhlhaas, P., & Palva, S. (2017). Whole-Brain Source-Reconstructed MEG-Data Reveal Reduced Long-Range Synchronization in Chronic Schizophrenia. *Eneuro*, 4(5), 0338
- Hong, L. E., Summerfelt, A., Buchanan, R. W., O'Donnell, P., Thaker, G. K., Weiler, M. A., & Lahti, A. C. (2010). Gamma and delta neural oscillations and association with clinical symptoms under subanesthetic ketamine. *Neuropsychopharmacology*, 35(3), 632–640.
- Hoonakker, M., Doignon-Camus, N., & Bonnefond, A. (2017). Sustaining attention to simple visual tasks: a central deficit in schizophrenia? A systematic review. *Annals of the New York Academy of Sciences*, 1408(1), 32–45.
- Hor, K., & Taylor, M. (2010). Suicide and schizophrenia: a systematic review of rates and risk

- factors. *Journal of psychopharmacology*, 24(4_suppl), 81-90.
- Houck, J. M., Çetin, M. S., Mayer, A. R., Bustillo, J. R., Stephen, J., Aine, C., ... Calhoun, V. D. (2016). Magnetoencephalographic and functional MRI connectomics in schizophrenia via intra- and inter-network connectivity. *NeuroImage*, 145, 96–106.
- Houck, J. M., Çetin, M. S., Mayer, A. R., Bustillo, J. R., Stephen, J., Aine, C., ... Calhoun, V. D. (2017). Magnetoencephalographic and functional MRI connectomics in schizophrenia via intra- and inter-network connectivity. *NeuroImage*, 145(Pt A), 96–106.
- Howard, M. W., Rizzuto, D. S., Caplan, J. B., Madsen, J. R., Lisman, J., Aschenbrenner-Scheibe, R., ... Kahana, M. J. (2003). Gamma Oscillations Correlate with Working Memory Load in Humans. *Cerebral Cortex*, 13(12), 1369–1374.
- Howes, O. D., & Kapur, S. (2009). The dopamine hypothesis of schizophrenia: version III—the final common pathway. *Schizophrenia bulletin*, 35(3), 549-562.
- Hu, D. K., Li, L. Y., Lopour, B. A., & Martin, E. A. (2020). Schizotypy dimensions are associated with altered resting state alpha connectivity. *International Journal of Psychophysiology*, 155, 175–183.
- Humpston, C. S., Evans, L. H., Teufel, C., Ihssen, N., & Linden, D. E. J. (2017). Evidence of absence: no relationship between behaviourally measured prediction error response and schizotypy. *Cognitive Neuropsychiatry*, 22(5), 373–390.
- Hunt, B. A., Liddle, E. B., Gascoyne, L. E., Magazzini, L., Routley, B. C., Singh, K. D., ... & Liddle, P. F. (2019). Attenuated post-movement beta rebound associated with schizotypal features in healthy people. *Schizophrenia bulletin*, 45(4), 883-891.
- Korolchuk, V., Imarisio, S., Carmichael, J., Chen, C. W., Saiki, S., Rose, C., ... & Rubinsztein, D. C. (2008). Huntington's disease: from pathology and genetics to potential therapies. *Biochemical Journal*, 412(2), 191-209
- Jaiswal, A., Nenonen, J., Stenroos, M., Gramfort, A., Dalal, S. S., Westner, B. U., ... & Parkkonen, L. (2020). Comparison of beamformer implementations for MEG source localization. *NeuroImage*, 216, 116797.
- Whitlow, L. (2016). *An investigation of the link between cortical inhibition, neural oscillations and psychophysics in schizophrenia* (Doctoral dissertation, Cardiff University).
- Jaramillo, J., Mejias, J. F., & Wang, X. J. (2019). Engagement of Pulvino-cortical Feedforward and Feedback Pathways in Cognitive Computations. *Neuron*, 101(2), 321-336.e9.

- Jenkinson, M., Beckmann, C.F., Behrens, T., Woolrich, M., & Smith, S. (2012). FSL. *NeuroImage*, 62(2), 782–790.
- Jensen, O., Goel, P., Kopell, N., Pohja, M., Hari, R., & Ermentrout, B. (2005). On the human sensorimotor-cortex beta rhythm: Sources and modeling. *NeuroImage*, 26(2), 347–355.
- Jensen, O., & Colgin, L. L. (2007). Cross-frequency coupling between neuronal oscillations. *Trends in cognitive sciences*, 11(7), 267-269.
- Jensen, Ole, & Lisman, J. E. (1996). Theta/gamma networks with slow NMDA channels learn sequences and encode episodic memory: Role of NMDA channels in recall. *Learning Memory*, 3(2–3), 264–278.
- Ma, J., & Leung, L. W. S. (2000). Relation between hippocampal γ waves and behavioral disturbances induced by phencyclidine and methamphetamine. *Behavioural brain research*, 111(1-2), 1-11.
- Jones, D. K., Knösche, T. R., & Turner, R. (2013). White matter integrity, fiber count, and other fallacies: The do's and don'ts of diffusion MRI. *NeuroImage*, 73, 239–254.
- Jones, R. S. G., & Bühl, E. H. (1993). Basket-like interneurons in layer II of the entorhinal cortex exhibit a powerful NMDA-mediated synaptic excitation. *Neuroscience Letters*, 149(1), 35–39.
- Joo, S. W., Yoon, W., Shon, S.-H., Kim, H., Cha, S., Park, K. J., & Lee, J. (2018). Altered white matter connectivity in patients with schizophrenia: An investigation using public neuroimaging data from SchizConnect. *PLOS ONE*, 13(10), e0205369.
- Josephson, B. D. (1974). The discovery of tunnelling supercurrents. *Reviews of Modern Physics*, 46(2), 251–254.
- Jurkiewicz, M. T., Gaetz, W. C., Bostan, A. C., & Cheyne, D. (2006). Post-movement beta rebound is generated in motor cortex: Evidence from neuromagnetic recordings. *NeuroImage*, 32(3), 1281–1291.
- Kalsner, L., & Chamberlain, S. J. (2015). Prader-Willi, Angelman, and 15q11-q13 duplication syndromes. *Pediatric Clinics*, 62(3), 587-606.
- Kantrowitz, J. T., & Javitt, D. C. (2010). N-methyl-d-aspartate (NMDA) receptor dysfunction or dysregulation: The final common pathway on the road to schizophrenia? *Brain Research Bulletin*, 83(3–4), 108–121.
- Karayorgou, M., & Gogos, J. A. (2004). The molecular genetics of the 22q11-associated schizophrenia. *Molecular Brain Research*, 132(2), 95-104.

- Karbasforoushan, H., & Woodward, N. D. (2013). Resting-State Networks in Schizophrenia. *Current Topics in Medicinal Chemistry*, *12*(21), 2404–2414.
- Kass, R. E., & Raftery, A. E. (1995). Bayes factors. *Journal of the American Statistical Association*, *90*(430), 773–795.
- Kay, S. R., Fiszbein, A., & Opler, L. A. (1987). The Positive and Negative Syndrome Scale (PANSS) for Schizophrenia. *Schizophrenia Bulletin*, *13*(2), 261–276.
- Keitel, C., Keitel, A., Benwell, C. S. Y., Daube, C., Thut, G., & Gross, J. (2019). Stimulus-Driven Brain Rhythms within the Alpha Band: The Attentional-Modulation Conundrum. *Journal of Neuroscience*, *39*(16), 3119–3129.
- Kelly, S., Jahanshad, N., Zalesky, A., Kochunov, P., Agartz, I., Alloza, C., ... Donohoe, G. (2017). Widespread white matter microstructural differences in schizophrenia across 4322 individuals: results from the ENIGMA Schizophrenia DTI Working Group. *Molecular Psychiatry* *2018* *23*:5, *23*(5), 1261–1269.
- Kennedy, H., Van Essen, D. C., & Christen, Y. (2016). *Research and Perspectives in Neurosciences*. Retrieved from <http://www.springer.com/series/2357>
- Kemp, K. C., Bathery, A. J., Barrantes-Vidal, N., & Kwapil, T. R. (2021). Positive, negative, and disorganized schizotypy predict differential patterns of interview-rated schizophrenia-spectrum symptoms and impairment. *Assessment*, *28*(1), 141-152.
- Kerkoerle, T. van, Self, M. W., Dagnino, B., Gariel-Mathis, M.-A., Poort, J., Togt, C. van der, & Roelfsema, P. R. (2014a). Alpha and gamma oscillations characterize feedback and feedforward processing in monkey visual cortex. *Proceedings of the National Academy of Sciences*, *111*(40), 14332–14341.
- Kerkoerle, T. van, Self, M. W., Dagnino, B., Gariel-Mathis, M.-A., Poort, J., Togt, C. van der, & Roelfsema, P. R. (2014b). Alpha and gamma oscillations characterize feedback and feedforward processing in monkey visual cortex. *Proceedings of the National Academy of Sciences*, *111*(40), 14332–14341.
- Kikinis, Z., Asami, T., Bouix, S., Finn, C. T., Ballinger, T., Tworog-Dube, E., ... Kubicki, M. (2012). Reduced fractional anisotropy and axial diffusivity in white matter in 22q11.2 deletion syndrome: A pilot study. *Schizophrenia Research*, *141*(1), 35–39.
- Kim, J. S., Shin, K. S., Jung, W. H., Kim, S. N., Kwon, J. S., & Chung, C. K. (2014). Power spectral aspects of the default mode network in schizophrenia: An MEG study. *BMC*

Neuroscience, 15(1), 104.

- Kirov, G., Pocklington, A. J., Holmans, P., Ivanov, D., Ikeda, M., Ruderfer, D., ... Owen, M. J. (2012a). De novo CNV analysis implicates specific abnormalities of postsynaptic signalling complexes in the pathogenesis of schizophrenia. *Molecular Psychiatry*, 17(2), 142–153.
- Kirov, G., George, D., Grozeva, D., Norton, N., Ivanov, D., Mantripragada, K. K., Holmans, P., ... O'Donovan, M. C. (2009). Support for the involvement of large copy number variants in the pathogenesis of schizophrenia. *Human Molecular Genetics*, 18(8), 1497–1503.
- Kirov, G., Rujescu, D., Ingason, A., Collier, D. A., O'Donovan, M. C., & Owen, M. J. (2009). Neurexin 1 (NRXN1) deletions in schizophrenia. *Schizophrenia bulletin*, 35(5), 851.
- Koelewijn, L., Bompas, A., Tales, A., Brookes, M. J., Muthukumaraswamy, S. D., Bayer, A., & Singh, K. D. (2017). Alzheimer's disease disrupts alpha and beta-band resting-state oscillatory network connectivity. *Clinical Neurophysiology : Official Journal of the International Federation of Clinical Neurophysiology*, 128(11), 2347–2357.
- Koelewijn, L., Lancaster, T. M., Linden, D., Dima, D. C., Routley, B. C., Magazzini, L., ... & Singh, K. (2019). Oscillatory hyperactivity and hyperconnectivity in young APOE-ε4 carriers and hypoconnectivity in Alzheimer's disease. *Elife*, 8, e36011.
- Kopell, N., Ermentrout, G. B., Whittington, M. A., & Traub, R. D. (2000a). Gamma rhythms and beta rhythms have different synchronization properties. *Proceedings of the National Academy of Sciences of the United States of America*, 97(4), 1867–1872.
- Kopell, N. J., Gritton, H. J., Whittington, M. A., & Kramer, M. A. (2014). Beyond the Connectome: The Dynome. *Neuron*, 83(6), 1319–1328.
- Kornmayer, L., Leicht, G., & Mulert, C. (2014a). Increased Gamma Oscillations Evoked by Physically Salient Distracters are Associated with Schizotypy. *Brain Topography 2014* 28:1, 28(1), 153–161.
- Koychev, I., Deakin, J. F. W., Haenschel, C., & El-Deredy, W. (2011a). Abnormal neural oscillations in schizotypy during a visual working memory task: Support for a deficient top-down network? *Neuropsychologia*, 49(10), 2866–2873.
- Kreiter, A. K., & Singer, W. (1996). Stimulus-dependent synchronization of neuronal responses in the visual cortex of the awake macaque monkey. *Journal of Neuroscience*, 16(7), 2381–2396.
- Krishnan, G. P., Vohs, J. L., Hetrick, W. P., Carroll, C. A., Shekhar, A., Bockbrader, M. A., &

- O'Donnell, B. F. (2005). Steady state visual evoked potential abnormalities in schizophrenia. *Clinical Neurophysiology*, *116*(3), 614–624.
- Krogmann, A., Peters, L., Hardenberg, L. von, Bödeker, K., Nöhles, V. B., & Correll, C. U. (2019). Keeping up with the therapeutic advances in schizophrenia: a review of novel and emerging pharmacological entities. *CNS Spectrums*, *24*(S1), 38–69.
- Krukow, P., Jonak, K., Grochowski, C., Plechawska-Wójcik, M., & Karakuła-Juchnowicz, H. (2020). Resting-state hyperconnectivity within the default mode network impedes the ability to initiate cognitive performance in first-episode schizophrenia patients. *Progress in Neuro-Psychopharmacology and Biological Psychiatry*, *102*, 109959.
- Kujala, J., Jung, J., Bouvard, S., Lecaigard, F., Lothe, A., Bouet, R., ... Jerbi, K. (2015). Gamma oscillations in V1 are correlated with GABAA receptor density: A multi-modal MEG and Flumazenil-PET study. *Scientific Reports*, *5*(1), 1–12.
- Kuki, T., Fujihara, K., Miwa, H., Tamamaki, N., Yanagawa, Y., & Mushiake, H. (2015). Contribution of parvalbumin and somatostatin-expressing GABAergic neurons to slow oscillations and the balance in beta-gamma oscillations across cortical layers. *Frontiers in Neural Circuits*, *9*, 6.
- Kumar, R., Chavez, A. S., Macey, P. M., Woo, M. A., & Harper, R. M. (2013a). Brain Axial and Radial Diffusivity Changes with Age and Gender in Healthy Adults. *Brain Research*, *1512*, 22.
- Kumar, R., Nguyen, H. D., Macey, P. M., Woo, M. A., & Harper, R. M. (2012). Regional brain axial and radial diffusivity changes during development. *Journal of Neuroscience Research*, *90*(2), 346–355.
- Landek-Salgado, M. A., Faust, T. E., & Sawa, A. (2015). Molecular substrates of schizophrenia: homeostatic signaling to connectivity. *Molecular Psychiatry* *2016 21:1*, *21*(1), 10–28.
- Larmor, J. J. (1897). A Dynamical Theory of the Electric and Luminiferous Medium. Part III. Relations with Material Media. *Philosophical Transactions of the Royal Society A: Mathematical, Physical and Engineering Sciences*, *190*, 205–300.
- Lawrence, S. J. D., Norris, D. G., & De Lange, F. P. (2019). Dissociable laminar profiles of concurrent bottom-up and top-down modulation in the human visual cortex. *ELife*, *8*.
- Lee, D. D., & Seung, H. S. (1999). Learning the parts of objects by non-negative matrix factorization. *Nature*, *401*(6755), 788–791.

- Lee, M. D., & Wagenmakers, E. J. (2014). *Bayesian cognitive modeling: A practical course*. Cambridge university press.
- Lee, S., & Jones, S. R. (2013). Distinguishing mechanisms of gamma frequency oscillations in human current source signals using a computational model of a laminar neocortical network. *Frontiers in Human Neuroscience*, 7(DEC).
- Legge, S. E., Santoro, M. L., Periyasamy, S., Okewole, A., Arsalan, A., & Kowalec, K. (2021). Genetic architecture of schizophrenia: a review of major advancements. *Psychological Medicine*, 51(13), 2168–2177.
- Leow, A. D., Zhan, L., Zhu, S., Hageman, N., Chiang, M. C., Barysheva, M., ... Thompson, P. M. (2009). White matter integrity measured by fractional anisotropy correlates poorly with actual individual fiber anisotropy. *Proceedings - 2009 IEEE International Symposium on Biomedical Imaging: From Nano to Macro, ISBI 2009*, 622–625.
- Leung, L. S. (1982). Nonlinear feedback model of neuronal populations in hippocampal CA1 region. *Journal of Neurophysiology*, 47(5), 845–868.
- Levinson, D. F., Duan, J., Oh, S., Wang, K., Sanders, A. R., Shi, J., ... Gejman, P. V. (2011). Copy number variants in schizophrenia: Confirmation of five previous findings and new evidence for 3q29 microdeletions and VIPR2 duplications. *American Journal of Psychiatry*, 168(3), 302–316.
- Lewis, D. A., Curley, A. A., Glausier, J. R., & Volk, D. W. (2012, January). Cortical parvalbumin interneurons and cognitive dysfunction in schizophrenia. *Trends in Neurosciences*. NIH Public Access.
- Li, P., Jing, R. X., Zhao, R. J., Shi, L., Sun, H. Q., Ding, Z., ... Fan, Y. (2020). Association between functional and structural connectivity of the corticostriatal network in people with schizophrenia and unaffected first-degree relatives. *Journal of Psychiatry & Neuroscience : JPN*, 45(6), 395.
- Li, S., Hu, N., Zhang, W., Tao, B., Dai, J., Gong, Y., ... & Lui, S. (2019). Dysconnectivity of multiple brain networks in schizophrenia: a meta-analysis of resting-state functional connectivity. *Frontiers in psychiatry*, 482.
- Li, T., Wang, Q., Zhang, J., Rolls, E. T., Yang, W., Palaniyappan, L., ... Feng, J. (2017). Brain-Wide Analysis of Functional Connectivity in First-Episode and Chronic Stages of Schizophrenia. *Schizophrenia Bulletin*, 43(2), 436.

- Liddle, P. (1987). The symptoms of chronic schizophrenia. A re-examination of the positive-negative dichotomy. *British Journal of Psychiatry*, *151*, 145–151.
- Liddle, P. F. (2019). The core deficit of classical schizophrenia: implications for predicting the functional outcome of psychotic illness and developing effective treatments. *The Canadian Journal of Psychiatry*, *64*(10), 680-685.
- Linney, Y. M., Murray, R. M., Peters, E. R., MacDonald, A. M., Rijdsdijk, F., & Sham, P. C. (2003). A quantitative genetic analysis of schizotypal personality traits. *Psychological Medicine*, *33*(5), 803–816.
- Lisman, J. E., Coyle, J. T., Green, R. W., Javitt, D. C., Benes, F. M., Heckers, S., & Grace, A. A. (2008). Circuit-based framework for understanding neurotransmitter and risk gene interactions in schizophrenia. *Trends in Neurosciences*, *31*(5), 234–242.
- Litvak, V., Mattout, J., Kiebel, S., Phillips, C., Henson, R., Kilner, J., ... Friston, K. (2011). EEG and MEG data analysis in SPM8. *Computational Intelligence and Neuroscience*, *2011*.
- Liu, T., Zhang, J., Dong, X., Li, Z., Shi, X., Tong, Y., ... Yan, T. (2019a). Occipital Alpha Connectivity During Resting-State Electroencephalography in Patients With Ultra-High Risk for Psychosis and Schizophrenia. *Frontiers in Psychiatry*, *10*, 553.
- Liu, Y., Liang, M., Zhou, Y., He, Y., Hao, Y., Song, M., ... Jiang, T. (2008). Disrupted small-world networks in schizophrenia. *Brain*, *131*(4), 945–961.
- Lopes Da Silva, F H, Pijn, J. P., Velis, D., & Nijssen, P. C. G. (1997). Alpha rhythms: noise, dynamics and models. *International Journal of Psychophysiology*, *26*, 237-249.
- Lopes Da Silva, Fernando H. (2010). Electrophysiological Basis of MEG Signals. *MEG: An Introduction to Methods*, 1–24.
- Lozano-Soldevilla, D., Ter Huurne, N., Cools, R., & Jensen, O. (2014a). GABAergic modulation of visual gamma and alpha oscillations and its consequences for working memory performance. *Current Biology*, *24*(24), 2878–2887.
- Machón, R. A., Huttunen, M. O., Mednick, S. A., Sinivuo, J., Tanskanen, A., Watson, J. B., ... & Pyhälä, R. (2002). Adult schizotypal personality characteristics and prenatal influenza in a Finnish birth cohort. *Schizophrenia research*, *54*(1-2), 7-16.
- Madsen, K. H., Krohne, L. G., Cai, X.-L., Wang, Y., & Chan, R. C. K. (2018). Perspectives on Machine Learning for Classification of Schizotypy Using fMRI Data. *Schizophrenia Bulletin*, *44*(2), 480–490.

- Magazzini, L., & Singh, K. D. (2018). Spatial attention modulates visual gamma oscillations across the human ventral stream. *NeuroImage*, *166*, 219–229.
- Mancini, V., Rochas, V., Seeber, M., Grent-‘t-Jong, T., Rihs, T. A., Latrèche, C., ... Eliez, S. (2022). Oscillatory neural signatures of visual perception across developmental stages in individuals with 22q11.2 deletion syndrome. *Biological Psychiatry*, *0*(0).
- Manzano, J. M., Munoz, J. J., Santos, J. M., Serra, A., Alonso, T. O., & Erausquin, G. de. (2017). MEG resting-state differences as a marker of clinical subtype in schizophrenia. *Neuropsychiatry*, *07*(02), 172–178.
- Maran, M., Grent-‘t-Jong, T., & Uhlhaas, P. J. (2016). Electrophysiological insights into connectivity anomalies in schizophrenia: a systematic review. *Neuropsychiatric Electrophysiology 2016 2:1*, *2*(1), 1–9.
- Marconi, A., Di Forti, M., Lewis, C. M., Murray, R. M., & Vassos, E. (2016). Meta-analysis of the association between the level of cannabis use and risk of psychosis. *Schizophrenia bulletin*, *42*(5), 1262-1269.
- Markov, N. T., Vezoli, J., Chameau, P., Falchier, A., Quilodran, R., Huissoud, C., ... Kennedy, H. (2014). Anatomy of hierarchy: Feedforward and feedback pathways in macaque visual cortex. *Journal of Comparative Neurology*, *522*(1), 225–259.
- Marshall, C. R., Howrigan, D. P., Merico, D., Thiruvahindrapuram, B., Wu, W., Greer, D. S., ... Sebat, J. (2017). Contribution of copy number variants to schizophrenia from a genome-wide study of 41,321 subjects. *Nature Genetics*, *49*(1), 27–35.
- Martin-Brevet, S., Rodríguez-Herreros, B., Nielsen, J. A., Moreau, C., Modenato, C., Maillard, A. M., ... Jacquemont, S. (2018). Quantifying the Effects of 16p11.2 Copy Number Variants on Brain Structure: A Multisite Genetic-First Study. *Biological Psychiatry*, *84*(4), 253–264.
- Mason, O., & Claridge, G. (2006). The Oxford-Liverpool Inventory of Feelings and Experiences (O-LIFE): Further description and extended norms. *Schizophrenia Research*, *82*(2–3), 203–211.
- Mattiaccio, L. M., Coman, I. L., Schreiner, M. J., Antshel, K. M., Fremont, W. P., Bearden, C. E., & Kates, W. R. (2016). Atypical functional connectivity in resting-state networks of individuals with 22q11.2 deletion syndrome: Associations with neurocognitive and psychiatric functioning. *Journal of Neurodevelopmental Disorders*, *8*(1), 1–14.
- Melloni, L., Molina, C., Pena, M., Torres, D., Singer, W., & Rodriguez, E. (2007). Synchronization

- of Neural Activity across Cortical Areas Correlates with Conscious Perception. *Journal of Neuroscience*, 27(11), 2858–2865.
- Merker, B. H. (2016). Cortical gamma oscillations: Details of their genesis preclude a role in cognition. *Frontiers in Computational Neuroscience*, 10(JUL).
<https://doi.org/10.3389/fncom.2016.00078>
- Merla, G., Brunetti-Pierri, N., Micale, L., & Fusco, C. (2010). Copy number variants at Williams-Beuren syndrome 7q11.23 region. *Hum Genet*, 128, 3–26. h
- Messaritaki, E., Foley, S., Schiavi, S., Magazzini, L., Routley, B., Jones, D. K., & Singh, K. D. (2021a). Predicting MEG resting-state functional connectivity from microstructural information. *Network Neuroscience*, 5(2), 477–504.
- Michalareas, G., Vezoli, J., van Pelt, S., Schoffelen, J. M., Kennedy, H., & Fries, P. (2016a). Alpha-Beta and Gamma Rhythms Subserve Feedback and Feedforward Influences among Human Visual Cortical Areas. *Neuron*, 89(2), 384–397.
- Mirzaei, A., Kumar, A., Leventhal, D., Mallet, N., Aertsen, A., Berke, J., & Schmidt, R. (2017). Sensorimotor Processing in the Basal Ganglia Leads to Transient Beta Oscillations during Behavior. *Journal of Neuroscience*, 37(46), 11220–11232.
- Mitra, S., Nizamie, S. H., Goyal, N., & Tikka, S. K. (2015). Evaluation of resting state gamma power as a response marker in schizophrenia. *Psychiatry and Clinical Neurosciences*, 69(10), 630–639.
- Moore, C. I., Carlen, M., Knoblich, U., & Cardin, J. A. (2010). Neocortical interneurons: from diversity, strength. *Cell*, 142(2), 184–188.
- Moran, L. V., & Hong, L. E. (2011). High vs Low Frequency Neural Oscillations in Schizophrenia. *Schizophrenia Bulletin*, 37(4), 659–663.
- Moreau, C. A., Ching, C. R., Kumar, K., Jacquemont, S., & Bearden, C. E. (2021). Structural and functional brain alterations revealed by neuroimaging in CNV carriers. *Current opinion in genetics & development*, 68, 88–98.
- Moreau, C. A., Urchs, S. G. W., Kuldeep, K., Orban, P., Schramm, C., Dumas, G., ... Jacquemont, S. (2020). Mutations associated with neuropsychiatric conditions delineate functional brain connectivity dimensions contributing to autism and schizophrenia. *Nature Communications*, 11(1), 1–12.
- Morgan, C. J., Freeman, T. P., Powell, J. C. H. V., & Curran, H. (2016). AKT1 genotype moderates the acute psychotomimetic effects of naturalistically smoked cannabis in young cannabis

- smokers. *Translational psychiatry*, 6(2), e738-e738.
- Lener, M. S., Wong, E., Tang, C. Y., Byne, W., Goldstein, K. E., Blair, N. J., ... & Hazlett, E. A. (2015). White matter abnormalities in schizophrenia and schizotypal personality disorder. *Schizophrenia bulletin*, 41(1), 300-310.
- Müller, N., Weidinger, E., Leitner, B., & Schwarz, M. J. (2015). The role of inflammation in schizophrenia. *Frontiers in Neuroscience*, 9, 372.
- Murru, A., & Carpiello, B. (2018). Duration of untreated illness as a key to early intervention in schizophrenia: A review. *Neuroscience Letters*, 669, 59–67.
- Muthukumaraswamy, S. D., Edden, R. A. E., Jones, D. K., Swettenham, J. B., & Singh, K. D. (2009). Resting GABA concentration predicts peak gamma frequency and fMRI amplitude in response to visual stimulation in humans. *Proceedings of the National Academy of Sciences of the United States of America*, 106(20), 8356–8361.
- Muthukumaraswamy, S. D., Shaw, A. D., Jackson, L. E., Hall, J., Moran, R., & Saxena, N. (2015). Evidence that subanesthetic doses of ketamine cause sustained disruptions of NMDA and AMPA-mediated frontoparietal connectivity in humans. *Journal of Neuroscience*, 35(33), 11694-11706.
- Muthukumaraswamy, S. D., Singh, K. D., Swettenham, J. B., & Jones, D. K. (2010). Visual gamma oscillations and evoked responses: Variability, repeatability and structural MRI correlates. *NeuroImage*, 49(4), 3349–3357.
- Nelson, M. T., Seal, M. L., Phillips, L. J., Merritt, A. H., Wilson, R., & Pantelis, C. (2011). An investigation of the relationship between cortical connectivity and schizotypy in the general population. *Journal of Nervous and Mental Disease*, 199(5), 348–353.
- Nenadić, I., Meller, T., Schmitt, S., Stein, F., Brosch, K., Mosebach, J., ... Kircher, T. (2020). Polygenic risk for schizophrenia and schizotypal traits in non-clinical subjects. *Psychological Medicine*, 1–11.
- Nestsiarovich, A., Obyedkov, V., Kandratsenka, H., Siniuskaya, M., Goloenko, I., & Waszkiewicz, N. (2017). Disorganization at the stage of schizophrenia clinical outcome: Clinical–biological study. *European Psychiatry*, 42, 44-48.
- Nielsen, J. D., Madsen, K. H., Wang, Z., Liu, Z., Friston, K. J., & Zhou, Y. (2017). Working Memory Modulation of Frontoparietal Network Connectivity in First-Episode Schizophrenia. *Cerebral Cortex*, 27(7), 3832–3841.

- NIMH. (2022). Schizophrenia. Retrieved February 8, 2022, from <https://www.nimh.nih.gov/health/statistics/schizophrenia>
- Nolte, G. (2003). The magnetic lead field theorem in the quasi-static approximation and its use for magnetoencephalography forward calculation in realistic volume conductors. *Physics in Medicine and Biology*, 48(22), 3637–3652.
- Nordentoft, M., Laursen, T. M., Agerbo, E., Qin, P., Høyer, E. H., & Mortensen, P. B. (2004). Change in suicide rates for patients with schizophrenia in Denmark, 1981-97: nested case-control study. *BMJ*, 329(7460), 261.
- Northoff, G., Sandsten, K. E., Nordgaard, J., Kjaer, T. W., & Parnas, J. (2021). The Self and Its Prolonged Intrinsic Neural Timescale in Schizophrenia. *Schizophrenia Bulletin*, 47(1), 170–179.
- Nuechterlein, K. H., Green, M. F., Calkins, M. E., Greenwood, T. A., Gur, R. E., Gur, R. C., ... Braff, D. L. (2015). Attention/vigilance in schizophrenia: Performance results from a large multi-site study of the Consortium on the Genetics of Schizophrenia (COGS). *Schizophrenia Research*, 163(1–3), 38–46.
- Nunez, P. L., Srinivasan, R., Westdorp, A. F., Wijesinghe, R. S., Tucker, D. M., Silberstein, R. B., & Cadusch, P. J. (1997). EEG coherency: I: statistics, reference electrode, volume conduction, Laplacians, cortical imaging, and interpretation at multiple scales. *Electroencephalography and clinical neurophysiology*, 103(5), 499-515.
- O'donnell, L. J., & Westin, C.-F. (2011). An introduction to diffusion tensor image analysis. *Neurosurg Clin N Am.*, 22(2), 185.
- Oke, O. O., Magony, A., Anver, H., Ward, P. D., Jiruska, P., Jefferys, J. G. R., & Vreugdenhil, M. (2010). High-frequency gamma oscillations coexist with low-frequency gamma oscillations in the rat visual cortex *in vitro*. *European Journal of Neuroscience*, 31(8), 1435–1445.
- Olson, H., Shen, Y., Avallone, J., Sheidley, B. R., Pinsky, R., Bergin, A. M., ... Poduri, A. (2014). Copy number variation plays an important role in clinical epilepsy. *Annals of Neurology*, 75(6), 943–958.
- Oostenveld, R., Fries, P., Maris, E., & Schoffelen, J. M. (2011). FieldTrip: Open source software for advanced analysis of MEG, EEG, and invasive electrophysiological data. *Computational Intelligence and Neuroscience*, 2011.
- Orozco, S., & Ehlers, C. L. (1998). Gender differences in electrophysiological responses to facial

- stimuli. *Biological Psychiatry*, 44(4), 281–289.
- Owen, M. J., Sawa, A., & Mortensen, P. B. (2016). Schizophrenia. *The Lancet*, 388(10039), 86–97.
- Palva, S., & Palva, J. M. (2007). New vistas for α -frequency band oscillations. *Trends in Neurosciences*, 30(4), 150–158.
- Parnanzone, S., Serrone, D., Rossetti, M. C., D'onofrio, S., Splendiani, A., Micelli, V., ... Pacitti, F. (2017). Alterations of cerebral white matter structure in psychosis and their clinical correlations: A systematic review of Diffusion Tensor Imaging studies. *Rivista Di Psichiatria*, 52(2), 49–66.
- Pascual-Marqui, R. D., Michel, C. M., & Lehmann, D. (1994). Low resolution electromagnetic tomography: a new method for localizing electrical activity in the brain. *International Journal of Psychophysiology*, 18(1), 49–65.
- Pasquale, F. de, Penna, S. Della, Snyder, A. Z., Lewis, C., Mantini, D., Marzetti, L., ... Corbetta, M. (2010). Temporal dynamics of spontaneous MEG activity in brain networks. *Proceedings of the National Academy of Sciences*, 107(13), 6040–6045.
- Paul, R. H., Goldberg, E., Williams, L. M., Clark, C. R., Lawrence, J., Cooper, N., ... Gordon, E. (2005): Developing a clinical translational neuroscience taxonomy for anxiety and mood disorder. *Article in Journal of Integrative Neuroscience*, 4(1), 63–76.
- Pettersson-Yeo, W., Allen, P., Benetti, S., Mcguire, P., & Mechelli, A. (2010). Dysconnectivity in schizophrenia: Where are we now? *Neuroscience and Biobehavioral Reviews*, 35, 1110–1124.
- Liddle, P. F. (1987). The symptoms of chronic schizophrenia: a re-examination of the positive-negative dichotomy. *The British Journal of Psychiatry*, 151(2), 145–151.
- Phalen, H., Coffman, B. A., Ghuman, A., Sejdić, E., & Salisbury, D. F. (2019). Non-negative Matrix Factorization Reveals Resting-State Cortical Alpha Network Abnormalities in the First-Episode Schizophrenia Spectrum. *Biological Psychiatry: Cognitive Neuroscience and Neuroimaging*.
- Pinikahana, J., Happell, B., Hope, J., & Keks, N. A. (2002). Quality of life in schizophrenia: A review of the literature from 1995 to 2000. *International Journal of Mental Health Nursing*, 11(2), 103–111.
- Pinotsis, D. A., Geerts, J. P., Pinto, L., FitzGerald, T. H. B., Litvak, V., Auksztulewicz, R., & Friston, K. J. (2017). Linking canonical microcircuits and neuronal activity: Dynamic

- causal modelling of laminar recordings. *NeuroImage*, 146, 355–366.
- Pocklington, A. J., Rees, E., Walters, J. T. R., Han, J., Kavanagh, D. H., Chambert, K. D., ... Owen, M. J. (2015). Novel Findings from CNVs Implicate Inhibitory and Excitatory Signaling Complexes in Schizophrenia. *Neuron*, 86(5), 1203–1214.
- Pompili, M., Amador, X. F., Girardi, P., Harkavy-Friedman, J., Harrow, M., Kaplan, K., ... Tatarelli, R. (2007). Suicide risk in schizophrenia: learning from the past to change the future. *Annals of General Psychiatry* 2007 6:1, 6(1), 1–22.
- Popov, T., Kastner, S., & Jensen, O. (2017). FEF-Controlled Alpha Delay Activity Precedes Stimulus-Induced Gamma-Band Activity in Visual Cortex. *The Journal of Neuroscience : The Official Journal of the Society for Neuroscience*, 37(15), 4117–4127.
- Power, J., Fair, D., Schlaggar, B., & Petersen, S. (2010). The development of human functional brain networks. *Neuron*, 67(5), 735–748.
- Berger, H. V. (1929). *Nach JBechterew: Die Energie des lebenden. Organismus. S* (Vol. 102). Retrieved from https://pure.mpg.de/rest/items/item_2281721/component/file_2281720/content
- Purcell, S., Wray, N., Stone, J., Visscher, P., O'Donovan, M., Sullivan, P., & Sklar, P. (2009). Common polygenic variation contributes to risk of schizophrenia that overlaps with bipolar disorder. *Nature*,
- Raichle, M. E. (2006). The Brain's Dark Energy. *Science*, 314(5803).
- Raichle, M. E., & Mintun, M. A. (2006). Brain work and brain imaging. *Annu. Rev. Neurosci.*, 29, 449-476.
- Raine, A. (1991). The SPQ: a scale for the assessment of schizotypal personality based on DSM-III-R criteria. *Schizophrenia bulletin*, 17(4), 555-564.
- Redon, R., Ishikawa, S., Fitch, K. R., Feuk, L., Perry, G. H., Andrews, T. D., ... Hurles, M. E. (2006). Global variation in copy number in the human genome. *Nature*, 444(7118), 444–454.
- Rees, E., Moskvina, V., Owen, M. J., O'Donovan, M. C., & Kirov, G. (2011). De novo rates and selection of schizophrenia-associated copy number variants. *Biological Psychiatry*, 70(12), 1109–1114.
- Rees, E., O'Donovan, M. C., & Owen, M. J. (2015). Genetics of schizophrenia. *Current Opinion in Behavioral Sciences*, 2, 8–14.

- Rees, E., Walters, J. T. R., Georgieva, L., Isles, A. R., Chambert, K. D., Richards, A. L., ... Kirov, G. (2014). Analysis of copy number variations at 15 schizophrenia-associated loci. *British Journal of Psychiatry*, *204*(2), 108–114.
- Reilly, T. J., Nottage, J. F., Studerus, E., Rutigliano, G., De Micheli, A. I., Fusar-Poli, P., & McGuire, P. (2018). Gamma band oscillations in the early phase of psychosis: a systematic review. *Neuroscience & Biobehavioral Reviews*, *90*, 381-399.
- Richardson, L. F., & Eddy, W. F. (2019). Algorithm 991: The 2d tree sliding window discrete fourier transform. *ACM Transactions on Mathematical Software (TOMS)*, *45*(1), 1-12.
- Ripke, S., Neale, B. M., Corvin, A., Walters, J. T. R., Farh, K. H., Holmans, P. A., ... O'Donovan, M. C. (2014). Biological insights from 108 schizophrenia-associated genetic loci. *Nature*, *511*(7510), 421–427.
- Robinson, S. E., & Mandell, A. J. (2015a). Mutual Information in a MEG complexity measure suggests regional hyper-connectivity in schizophrenic probands. *Neuropsychopharmacology : Official Publication of the American College of Neuropsychopharmacology*, *40*(1), 251–252.
- Robson, S. E., Brookes, M. J., Hall, E. L., Palaniyappan, L., Kumar, J., Skelton, M., ... Morris, P. G. (2016). Abnormal visuomotor processing in schizophrenia. *NeuroImage: Clinical*, *12*, 869–878.
- Rodriguez, E., George, N., Lachaux, J.-P., Martinerie, J., Renault, B., & Varela, F. J. (1999). Perception's shadow: long-distance synchronization of human brain activity. *Nature*, *397*(6718), 430–433.
- Rokita, K. I., Dauvermann, M. R., Mothersill, D., Holleran, L., Bhatnagar, P., McNicholas, Á., ... & Donohoe, G. (2021). Current psychosocial stress, childhood trauma and cognition in patients with schizophrenia and healthy participants. *Schizophrenia Research*, *237*, 115-121.
- Rolls, E. T., Cheng, W., Gilson, M., Gong, W., Deco, G., Lo, C. Y. Z., ... Feng, J. (2020). Beyond the disconnectivity hypothesis of schizophrenia. *Cerebral Cortex*, *30*(3), 1213–1233.
- Romei, V., Brodbeck, V., Michel, C., Amedi, A., Pascual-Leone, A., & Thut, G. (2008). Spontaneous fluctuations in posterior α -band EEG activity reflect variability in excitability of human visual areas. *Cerebral Cortex*, *18*(9), 2010–2018.
- Romme, I. A. C., de Reus, M. A., Ophoff, R. A., Kahn, R. S., & van den Heuvel, M. P. (2017).

- Connectome Disconnectivity and Cortical Gene Expression in Patients With Schizophrenia. *Biological Psychiatry*, 81(6), 495–502.
- Routley, B. C., Singh, K. D., Hamandi, K., & Muthukumaraswamy, S. D. (2017). The effects of AMPA receptor blockade on resting magnetoencephalography recordings. *Journal of Psychopharmacology*, 31(12), 1527–1536.
- Roux, F., Wibra, M., Singer, W., Aru, J., & Uhlhaas, P. J. (2013). The phase of thalamic alpha activity modulates cortical gamma-band activity: Evidence from resting-state MEG recordings. *Journal of Neuroscience*, 33(45), 17827–17835.
- Rowland, L. M., Summerfelt, A., Wijtenburg, S. A., Du, X., Chiappelli, J. J., Krishna, N., ... Hong, L. E. (2016). Frontal glutamate and γ -aminobutyric acid levels and their associations with mismatch negativity and digit sequencing task performance in schizophrenia. *JAMA Psychiatry*, 73(2), 166–174.
- Rutter, L., Carver, F. W., Holroyd, T., Nadar, S. R., Mitchell-Francis, J., Apud, J., ... Coppola, R. (2009). Magnetoencephalographic gamma power reduction in patients with schizophrenia during resting condition. *Human Brain Mapping*, 30(10), 3254–3264.
- Sadaghiani, S., Brookes, M., & Baillet, S. (2021a). PsyArXiv Preprints | Connectomics of Human Electrophysiology. Retrieved October 26, 2021, from <https://psyarxiv.com/dr7zh/>
- Sadaghiani, S., & Wirsich, J. (2020). Intrinsic connectome organization across temporal scales: New insights from cross-modal approaches. *Network Neuroscience*, 4(1), 1–29.
- Salokangas, R. K. R., Dingemans, P., Heinimaa, M., Svirskis, T., Luutonen, S., Hietala, J., ... Klosterkötter, J. (2013). Prediction of psychosis in clinical high-risk patients by the Schizotypal Personality Questionnaire. Results of the EPOS project. *European Psychiatry*, 28(8), 469–475.
- Samogin, J., Marino, M., Porcaro, C., Wenderoth, N., Dupont, P., Swinnen, S. P., & Mantini, D. (2020). Frequency-dependent functional connectivity in resting state networks. *Human Brain Mapping*, 41(18), 5187–5198.
- Sanfratello, L., Houck, J., & Calhoun, V. (2018). Dynamic Functional Network Connectivity In Schizophrenia With MEG And fMRI, Do Different Time Scales Tell A Different Story? *BioRxiv*, 432385.
- Satterthwaite, T. D., & Baker, J. T. (2015). How can studies of resting-state functional connectivity help us understand psychosis as a disorder of brain development? *Current Opinion in*

Neurobiology, 30, 85–91.

- Scariati, E., Schaer, M., Richiardi, J., Schneider, M., Debbané, M., Van De Ville, D., & Eliez, S. (2014). Identifying 22q11.2 Deletion Syndrome and Psychosis Using Resting-State Connectivity Patterns. *Brain Topography*, 27(6), 808–821.
- Schleifer, C., Lin, A., Kushan, L., Ji, J. L., Yang, G., Bearden, C. E., & Anticevic, A. (2019). Dissociable disruptions in thalamic and hippocampal resting-state functional connectivity in youth with 22q11.2 deletions. *Journal of Neuroscience*, 39(7), 1301–1319.
- Schreiner, M., Forsyth, J. K., Karlsgodt, K. H., Anderson, A. E., Hirsh, N., Kushan, L., ... Bearden, C. E. (2017). Intrinsic Connectivity Network-Based Classification and Detection of Psychotic Symptoms in Youth With 22q11.2 Deletions. *Cerebral Cortex*, 27(6), 3294–3306.
- Seitzman, B. A., Snyder, A. Z., Leuthardt, E. C., & Shimony, J. S. (2019). The state of resting state networks. *Topics in magnetic resonance imaging: TMRI*, 28(4), 189.
- Sekihara, K., Hild, K. E., & Nagarajan, S. S. (2006). A novel adaptive beamformer for MEG source reconstruction effective when large background brain activities exist. *IEEE Transactions on Biomedical Engineering*, 53(9), 1755–1764.
- Selya, A. S., Rose, J. S., Dierker, L. C., Hedeker, D., & Mermelstein, R. J. (2012). A practical guide to calculating Cohen's f^2 , a measure of local effect size, from PROC MIXED. *Frontiers in psychology*, 3, 111.
- Seymour, K., Stein, T., Sanders, L. L. O., Guggenmos, M., Theophil, I., & Sterzer, P. (2013). Altered Contextual Modulation of Primary Visual Cortex Responses in Schizophrenia. *Neuropsychopharmacology 2013 38:13*, 38(13), 2607–2612.
- Shaw, A. D., Moran, R. J., Muthukumaraswamy, S. D., Breal, J., Linden, D. E., Friston, K. J., & Singh, K. D. (2017). Neurophysiologically-informed markers of individual variability and pharmacological manipulation of human cortical gamma. *NeuroImage*, 161, 19–31.
- Shaw, Alexander D., Knight, L., Freeman, T. C. A., Williams, G. M., Moran, R. J., Friston, K. J., ... Singh, K. D. (2020). Oscillatory, Computational, and Behavioral Evidence for Impaired GABAergic Inhibition in Schizophrenia. *Schizophrenia Bulletin*, 46(2), 345–353.
- Shaw, Alexander D., Muthukumaraswamy, S. D., Saxena, N., Sumner, R. L., Adams, N. E., Moran, R. J., & Singh, K. D. (2020a). Generative modelling of the thalamo-cortical circuit mechanisms underlying the neurophysiological effects of ketamine. *NeuroImage*, 221,

117189.

- Shaw, Alexander D, Chandler, H. L., Hamandi, K., Muthukumaraswamy, S. D., Hammers, A., & Singh, K. D. (2020). GABAA receptor mapping in human using non-invasive electrophysiology. *BioRxiv*, 2020.05.11.087726.
- Shin, Y. W., O'Donnell, B. F., Youn, S., & Kwon, J. S. (2011, December). Gamma oscillation in schizophrenia. *Psychiatry Investigation*. Korean Neuropsychiatric Association.
- Shoham, N., Hayes, J. F., Cooper, C., Theodorsson, M., & Lewis, G. (2021). Association Between Childhood Visual Acuity and Late Adolescent Psychotic Experiences: A Prospective Birth Cohort Study. *Schizophrenia Bulletin*.
- Siegel, M., Donner, T. H., & Engel, A. K. (2012). Spectral fingerprints of large-scale neuronal interactions. *Nature Reviews Neuroscience*, 13(2), 121–134.
- Siegel, M., Engel, A. K., & Donner, T. H. (2011). Cortical Network Dynamics of Perceptual Decision-Making in the Human Brain. *Frontiers in Human Neuroscience*, 5, 21.
- Sikkens, T., Bosman, C. A., & Olcese, U. (2019). The role of top-down modulation in shaping sensory processing across brain states: implications for consciousness. *Frontiers in systems neuroscience*, 31.
- Singh, K. D., Barnes, G. R., & Hillebrand, A. (2003). Group imaging of task-related changes in cortical synchronisation using nonparametric permutation testing. *NeuroImage*, 19(4), 1589–1601.
- Smith, S. M. (2002). Fast robust automated brain extraction. *Human Brain Mapping*, 17(3), 143–155.
- Smith, S. M., Fox, P. T., Miller, K. L., Glahn, D. C., Fox, P. M., Mackay, C. E., ... Beckmann, C. F. (2009). Correspondence of the brain's functional architecture during activation and rest. *Proceedings of the National Academy of Sciences of the United States of America*, 106(31), 13040–13045.
- Smith, S. M., Hyvärinen, A., Varoquaux, G., Miller, K. L., & Beckmann, C. F. (2014). Group-PCA for very large fMRI datasets. *NeuroImage*, 101, 738–749.
- Smith, S. M., Miller, K. L., Moeller, S., Xu, J., Auerbach, E. J., Woolrich, M. W., ... Ugurbil, K. (2012). Temporally-independent functional modes of spontaneous brain activity. *Proceedings of the National Academy of Sciences of the United States of America*, 109(8), 3131–3136.

- Sohal, V. S., Zhang, F., Yizhar, O., & Deisseroth, K. (2009). Parvalbumin neurons and gamma rhythms enhance cortical circuit performance. *Nature*, *459*(7247), 698–702.
- Sønderby, I. E., Gústafsson, Ó., Doan, N. T., Hibar, D. P., Martin-Brevet, S., Abdellaoui, A., ... Andreassen, O. A. (2020). Dose response of the 16p11.2 distal copy number variant on intracranial volume and basal ganglia. *Molecular Psychiatry*, *25*(3), 584–602.
- Song, S., Sun, S., Ju, W., Lin, S., Cross, A., & Neufeld, A. (2003). Diffusion tensor imaging detects and differentiates axon and myelin degeneration in mouse optic nerve after retinal ischemia. *NeuroImage*, *20*(3), 1714–1722.
- Spaak, E., Bonnefond, M., Maier, A., Leopold, D. A., & Jensen, O. (2012). Layer-specific entrainment of gamma-band neural activity by the alpha rhythm in monkey visual cortex. *Current Biology*, *22*(24), 2313–2318.
- Spadone, S., de Pasquale, F., Mantini, D., & Della Penna, S. (2012). A K-means multivariate approach for clustering independent components from magnetoencephalographic data. *NeuroImage*, *62*(3),
- Spencer, K. M. (2008). Visual gamma oscillations in schizophrenia: implications for understanding neural circuitry abnormalities. *Clinical EEG and Neuroscience*, *39*(2), 65–68.
- Spencer, K. M., Nestor, P. G., Perlmuter, R., Niznikiewicz, M. A., Klump, M. C., Frumin, M., ... McCarley, R. W. (2004). Neural synchrony indexes disordered perception and cognition in schizophrenia. *Proceedings of the National Academy of Sciences of the United States of America*, *101*(49), 17288–
- Spencer, K. M., Niznikiewicz, M. A., Shenton, M. E., & McCarley, R. W. (2008). Sensory-Evoked Gamma Oscillations in Chronic Schizophrenia. *Biological Psychiatry*, *63*(8), 744–747.
- Spencer, K. M., Salisbury, D. F., Shenton, M. E., & McCarley, R. W. (2008). γ -Band Auditory Steady-State Responses Are Impaired in First Episode Psychosis. *Biological Psychiatry*, *64*(5), 369–375.
- Spencer, M. E., Leahy, R. M., Mosher, J. C., & Lewis, P. S. (1992). Adaptive filters for monitoring localized brain activity from surface potential time series. In *Conference Record - Asilomar Conference on Signals, Systems and Computers* (pp. 156–161). IEEE Computer Society.
- Sperling, W., Martus, P., Kober, H., Bleich, S., & Kornhuber, J. (2002). Spontaneous, slow and fast magnetoencephalographic activity in patients with schizophrenia. *Schizophrenia Research*, *58*(2–3),

- Sperling, Wolfgang, Kornhuber, J., & Bleich, S. (2003). Dipole elevations over the temporoparietal brain area are associated with negative symptoms in schizophrenia. *Schizophrenia Research*, *64*(2–3), 187–188.
- Spitzer, B., & Haegens, S. (2017). Beyond the Status Quo: A Role for Beta Oscillations in Endogenous Content (Re)Activation. *ENeuro*, *4*(4).
- Stauffer, E.-M., Bethlehem, R. A. I., Warrier, V., Murray, G. K., Romero-Garcia, R., Seidlitz, J., & Bullmore, E. T. (2021). Grey and white matter microstructure is associated with polygenic risk for schizophrenia. *Molecular Psychiatry* *2021*, 1–10.
- Sterzer, P., Adams, R. A., Fletcher, P., Frith, C., Lawrie, S. M., Muckli, L., ... Corlett, P. R. (2018). The Predictive Coding Account of Psychosis. *Biological Psychiatry*, *84*(9), 634–643.
- Stone, J. M. (2011). Glutamatergic antipsychotic drugs: A new dawn in the treatment of schizophrenia? *Therapeutic Advances in Psychopharmacology*. SAGE Publications.
- Stone, J. M., Raffin, M., Morrison, P., & McGuire, P. K. (2010, July). Review: The biological basis of antipsychotic response in schizophrenia. *Journal of Psychopharmacology*.
- Sumner, R. L., Spriggs, M. J., & Shaw, A. D. (2021). Modelling thalamocortical circuitry shows that visually induced LTP changes laminar connectivity in human visual cortex. *PLOS Computational Biology*, *17*(1), e1008414.
- Sun, D., Ching, C. R. K., Lin, A., Forsyth, J. K., Kushan, L., Vajdi, A., ... Bearden, C. E. (2020). Large-scale mapping of cortical alterations in 22q11.2 deletion syndrome: Convergence with idiopathic psychosis and effects of deletion size. *Molecular Psychiatry*, *25*(8), 1822–1834.
- Sun, S., Liang, H., Trinkaus, K.T., Cross, A., Armstrong, R., & Song, S. (2006). Noninvasive detection of cuprizone induced axonal damage and demyelination in the mouse corpus callosum. *Magnetic Resonance in Medicine*, *55*(2), 302–308.
- Tadel, F., Baillet, S., Mosher, J. C., Pantazis, D., & Leahy, R. M. (2011). Brainstorm: A user-friendly application for MEG/EEG analysis. *Computational Intelligence and Neuroscience*, *2011*.
- Tait, L., Ozkan, A. A., Szul, M. J., & Zhang, J. (2020). Cortical source imaging of resting-state MEG with a high resolution atlas: An evaluation of methods. *BioRxiv*, 2020.01.12.903302.
- Tallon-Baudry, & Bertrand. (1999). Oscillatory gamma activity in humans and its role in object representation. *Trends in Cognitive Sciences*, *3*(4), 151–162.

- Tallon-Baudry, C, Bertrand, O., Delpuech, C., & Pernier, J. (1996). Stimulus specificity of phase-locked and non-phase-locked 40 Hz visual responses in human. *The Journal of Neuroscience : The Official Journal of the Society for Neuroscience*, *16*(13), 4240–4249.
- Tallon-Baudry, C, Bertrand, O., Peronnet, F., Pernier, J., Lindner, M., Maurer, K., & Rodriguez, E. (1998). Induced gamma-band activity during the delay of a visual short-term memory task in humans. *The Journal of Neuroscience : The Official Journal of the Society for Neuroscience*, *18*(11), 4244–4254.
- Tallon-Baudry, Catherine. (2009). The roles of gamma-band oscillatory synchrony in human visual cognition. *Frontiers in Bioscience*, *14*, 321.
- Tallon-Baudry, Catherine, Bertrand, O., Hénaff, M.-A., Isnard, J., & Fischer, C. (2005). Attention Modulates Gamma-band Oscillations Differently in the Human Lateral Occipital Cortex and Fusiform Gyrus. *Cerebral Cortex*, *15*(5), 654–662.
- Tarcijonas, G., & Sarpal, D. K. (2019). Neuroimaging markers of antipsychotic treatment response in schizophrenia: An overview of magnetic resonance imaging studies. *Neurobiology of Disease*, *131*, 104209.
- Teufel, C., Subramaniam, N., Dobler, V., Perez, J., Finnemann, J., Mehta, P. R., ... Fletcher, P. C. (2015). Shift toward prior knowledge confers a perceptual advantage in early psychosis and psychosis-prone healthy individuals. *Proceedings of the National Academy of Sciences of the United States of America*, *112*(43), 13401–13406.
- Tewarie, P., Abeysuriya, R., Byrne, Á., O'Neill, G. C., Sotiropoulos, S. N., Brookes, M. J., & Coombes, S. (2019). How do spatially distinct frequency specific MEG networks emerge from one underlying structural connectome? The role of the structural eigenmodes. *NeuroImage*, *186*, 211–220.
- Tewarie, P., Prasse, B., Meier, J. M., Santos, F. A. N., Douw, L., Schoonheim, M. M., ... Hillebrand, A. (2020). Mapping functional brain networks from the structural connectome: Relating the series expansion and eigenmode approaches. *NeuroImage*, *216*, 116805.
- The Open MEG Archive (OMEGA) | McConnell Brain Imaging Centre - McGill University. (n.d.). Retrieved June 18, 2021, from <https://www.mcgill.ca/bic/resources/omega>
- Thomson, D. J. (1982). Spectrum Estimation and Harmonic Analysis. *Proceedings of the IEEE*, *70*(9), 1055–1096.
- Tiesinga, P., & Sejnowski, T. J. (2009, September 24). Cortical Enlightenment: Are Attentional

- Gamma Oscillations Driven by ING or PING? *Neuron*. Howard Hughes Medical Institute.
- Trajkovic, J., Di Gregorio, F., Ferri, F., Marzi, C., Diciotti, S., & Romei, V. (2021). Resting state alpha oscillatory activity is a valid and reliable marker of schizotypy. *Scientific Reports*, *11*(1), 1–13.
- Traub, R. D., Kopell, N., Bibbig, A., Buhl, E. H., Lebeau, F. E. N., & Whittington, M. A. (2001). Gap junctions between interneuron dendrites can enhance synchrony of gamma oscillations in distributed networks. *Journal of Neuroscience*, *21*(23), 9478–9486.
- Traub, R. D., Whittington, M. A., Stanford, I. M., & Jefferys, J. G. R. (1996). A mechanism for generation of long-range synchronous fast oscillations in the cortex. *Nature*, *383*(6601), 621–224.
- Tsai, G., & Coyle, J. T. (2002). Glutamatergic mechanisms in Schizophrenia. *Annual Review of Pharmacology and Toxicology*, *42*(1), 165–179.
- Tsuchimoto, R., Kanba, S., Hirano, S., Oribe, N., Ueno, T., Hirano, Y., ... Onitsuka, T. (2011). Reduced high and low frequency gamma synchronization in patients with chronic schizophrenia. *Schizophrenia Research*, *133*(1–3), 99–105.
- Tzourio-Mazoyer, N., Landeau, B., Papathanassiou, D., Crivello, F., Etard, O., Delcroix, N., ... Joliot, M. (2002). Automated anatomical labeling of activations in SPM using a macroscopic anatomical parcellation of the MNI MRI single-subject brain. *NeuroImage*, *15*(1), 273–289.
- Uhlhaas, P.J., Haenschel, C., Nikolić, D., & Singer, W. (2008). The role of oscillations and synchrony in cortical networks and their putative relevance for the pathophysiology of schizophrenia. *Schizophrenia Bulletin*, *34*(5), 927–943.
- Uhlhaas, Peter J., & Singer, W. (2010a). Abnormal neural oscillations and synchrony in schizophrenia. *Nature Reviews Neuroscience*, *11*(2), 100–113.
- Uhlhaas, Peter J., & Singer, W. (2013a). High-frequency oscillations and the neurobiology of schizophrenia. *Dialogues in Clinical Neuroscience*, *15*(3), 301–313.
- Uhlhaas, Peter J. (2013). Dysconnectivity, large-scale networks and neuronal dynamics in schizophrenia. *Current Opinion in Neurobiology*.
- Uhlhaas, Peter J, Linden, D. E. J., Singer, W., Haenschel, C., Lindner, M., Maurer, K., & Rodriguez, E. (2006). Neurobiology of Disease Dysfunctional Long-Range Coordination of Neural Activity during Gestalt Perception in Schizophrenia. *Neurobiology of Disease*, (26),

- Van Den Heuvel, P. M., & Fornito, A. (2014). Brain Networks in Schizophrenia.
- Van Ommen, G. J. B. (2005, April). Frequency of new copy number variation in humans [2]. *Nature Genetics*. Nat Genet.
- Van Veen, B. D., & Buckley, K. M. (1988). Beamforming: A Versatile Approach to Spatial Filtering. *IEEE ASSP Magazine*, 5(2), 4–24.
- van Vugt, M. K., Sederberg, P. B., & Kahana, M. J. (2007). Comparison of spectral analysis methods for characterizing brain oscillations. *Journal of Neuroscience Methods*, 162(1–2), 49.
- Van Winkel, R., Van Nierop, M., Myin-Germeys, I., & Van Os, J. (2013). Childhood trauma as a cause of psychosis: Linking genes, psychology, and biology. *Canadian Journal of Psychiatry*. Canadian Psychiatric Association.
- Varghese, D., Scott, J., Welham, J., Bor, W., Najman, J., O’Callaghan, M., ... McGrath, J. (2011). Psychotic-like experiences in major depression and anxiety disorders: A population-based survey in young adults. *Schizophrenia Bulletin*, 37(2), 389–393.
- Velinov, M. (2019). Genomic Copy number variations in the autism clinic—work in progress. *Frontiers in cellular neuroscience*, 13, 57.
- Vernon, D., Haenschel, C., Dwivedi, P., & Gruzelier, J. (2005). Slow habituation of induced gamma and beta oscillations in association with unreality experiences in schizotypy. *International Journal of Psychophysiology*, 56(1), 15–24.
- Vierling-Claassen, D., Siekmeier, P., Stufflebeam, S., & Kopell, N. (2008). Modeling GABA Alterations in Schizophrenia: A Link Between Impaired Inhibition and Altered Gamma and Beta Range Auditory Entrainment. *Journal of Neurophysiology*, 99(5), 2656–2671.
- Vijayan, S., Ching, S. N., Purdon, P. L., Brown, E. N., & Kopell, N. J. (2013). Thalamocortical mechanisms for the anteriorization of alpha rhythms during propofol-induced unconsciousness. *Journal of Neuroscience*, 33(27), 11070–11075.
- Vijayan, S., & Kopell, N. J. (2012). Thalamic model of awake alpha oscillations and implications for stimulus processing. *Proceedings of the National Academy of Sciences of the United States of*
- Vollema, M. G., Sitskoorn, M. M., Appels, M. C. M., & Kahn, R. S. (2002). Does the Schizotypal Personality Questionnaire reflect the biological-genetic vulnerability to schizophrenia?

- Schizophr Res.*, 1(54), 1–2.
- Vollema, M. G., & van den Bosch, R. J. (1995). The Multidimensionality of Schizotypy. *Schizophrenia Bulletin*, 21(1), 19–31.
- Volpe, U., Federspiel, A., Mucci, A., Dierks, T., Frank, A., Wahlund, L.-O., ... Maj, M. (2008). Cerebral connectivity and psychotic personality traits. *European Archives of Psychiatry and Clinical Neuroscience* 2008 258:5, 258(5), 292–299.
- von Stein, A., & Sarnthein, J. (2000). Different frequencies for different scales of cortical integration: from local gamma to long range alpha/theta synchronization. *International Journal of Psychophysiology : Official Journal of the International Organization of Psychophysiology*, 38(3), 301–313.
- Vrba, J., & Robinson, S. E. (2001). Signal processing in magnetoencephalography. *Methods*, 25(2), 249–271.
- Waltmann, M., O'Daly, O., Egerton, A., McMullen, K., Kumari, V., Barker, G. J., ... Modinos, G. (2019). Multi-echo fMRI, resting-state connectivity, and high psychometric schizotypy. *NeuroImage. Clinical*, 21, 101603.
- Wang, X. J., & Buzsáki, G. (1996). Gamma oscillation by synaptic inhibition in a hippocampal interneuronal network model. *Journal of Neuroscience*, 16(20), 6402–6413.
- Wang, Y. M., Cai, X. L., Zhang, R. T., Zhang, Y. J., Zhou, H. Y., Wang, Y., ... & Chan, R. C. (2020). Altered brain structural and functional connectivity in schizotypy. *Psychological Medicine*, 1-10.
- Wang, X., Jiao, Y., Tang, T., Wang, H., & Lu, Z. (2013). Investigating univariate temporal patterns for intrinsic connectivity networks based on complexity and low-frequency oscillation: A test–retest reliability study. *Neuroscience*, 254, 404–426.
- Wang, Yi, Ettinger, U., Meindl, T., & Chan, R. C. K. (2018). Association of schizotypy with striatocortical functional connectivity and its asymmetry in healthy adults. *Human Brain Mapping*, 39(1), 288–299.
- Wang, Yong-ming, Cai, X., Zhang, R., Zhang, Y., Zhou, H., Wang, Y., ... Chan, R. C. K. (2020). Altered brain structural and functional connectivity in schizotypy. *Psychological Medicine*, 1–10.
- Wang, Yong ming, Zhang, Y. jing, Cai, X. lu, Yang, H. xue, Shan, H. di, Cheung, E. F. C., & Chan, R. C. K. (2020). Altered grey matter volume and white matter integrity in individuals

- with high schizo-obsessive traits, high schizotypal traits and obsessive-compulsive symptoms. *Asian Journal of Psychiatry*, 52, 102096.
- Wespatat, V., Tennigkeit, F., & Singer, W. (2004). Phase Sensitivity of Synaptic Modifications in Oscillating Cells of Rat Visual Cortex. *Journal of Neuroscience*, 24(41), 9067–9075.
- Whittington, M. A., Traub, R. D., Kopell, N., Ermentrout, B., & Buhl, E. H. (2000). Inhibition-based rhythms: experimental and mathematical observations on network dynamics. *International journal of psychophysiology*, 38(3), 315-336.
- Williams, G. (2018). *An exploration of functional connectivity and GABA in schizophrenia and related conditions* (Doctoral dissertation, Cardiff University).
- Williams, S., & Boksa, P. (2010). Gamma oscillations and schizophrenia. *Journal of psychiatry & neuroscience: JPN*, 35(2), 75.
- Winklewski, P. J., Sabisz, A., Naumczyk, P., Jodzio, K., Szurowska, E., & Szarmach, A. (2018). Understanding the physiopathology behind axial and radial diffusivity changes—what do we know?. *Frontiers in neurology*, 9, 92.
- Winterer, G., & Weinberger, D. R. (2004). Genes, dopamine and cortical signal-to-noise ratio in schizophrenia. *Trends in Neurosciences*, 27(11), 683–690.
- Wulff, P., Ponomarenko, A. A., Bartos, M., Korotkova, T. M., Fuchs, E. C., Bähner, F., ... & Monyer, H. (2009). Hippocampal theta rhythm and its coupling with gamma oscillations require fast inhibition onto parvalbumin-positive interneurons. *Proceedings of the National Academy of Sciences*, 106(9), 3561-3566.
- Xue, M., Atallah, B. V., & Scanziani, M. (2014). Equalizing excitation-inhibition ratios across visual cortical neurons. *Nature*, 511(7511), 596–600.
- Yamamoto, M., Kushima, I., Suzuki, R., Branko, A., Kawano, N., Inada, T., ... Ozaki, N. (2018). Aberrant functional connectivity between the thalamus and visual cortex is related to attentional impairment in schizophrenia. *Psychiatry Research: Neuroimaging*, 278, 35–41.
- Yang, E., Tadin, D., Glasser, D. M., Hong, S. W., Blake, R., & Park, S. (2013). Visual context processing in schizophrenia. *Clinical Psychological Science : A Journal of the Association for Psychological Science*, 1(1), 5–15.
- Yaralian, P. S., Raine, A., Lencz, T., Hooley, J. M., Bihle, S. E., Mills, S., & Ventura, J. (2000). Elevated levels of cognitive-perceptual deficits in individuals with a family history of schizophrenia spectrum disorders. *Schizophrenia Research*, 46(1), 57–63.

- Yoon, J. H., Maddock, R. J., Cui, E. D., Minzenberg, M. J., Niendam, T. A., Lesh, T., ... & Carter, C. (2020). Reduced in vivo visual cortex GABA in schizophrenia, a replication in a recent onset sample. *Schizophrenia research*, *215*, 217-222.
- Yoon, J. H., Maddock, R. J., Rokem, A., Silver, M. A., Minzenberg, M. J., Ragland, J. D., & Carter, C. S. (2010). GABA Concentration Is Reduced in Visual Cortex in Schizophrenia and Correlates with Orientation-Specific Surround Suppression. *Journal of Neuroscience*, *30*(10), 3777–3781.
- Yu, Q., A. Allen, E., Sui, J., R. Arbabshirani, M., Pearlson, G., & D. Calhoun, V. (2012). Brain Connectivity Networks in Schizophrenia Underlying Resting State Functional Magnetic Resonance Imaging. *Current Topics in Medicinal Chemistry*, *12*(21), 2415–2425.
- Yu, Q., A. Allen, E., Sui, J., R. Arbabshirani, M., Pearlson, G., & D. Calhoun, V. (2013). Brain Connectivity Networks in Schizophrenia Underlying Resting State Functional Magnetic Resonance Imaging. *Current Topics in Medicinal Chemistry*, *12*(21), 2415–2425.
- Zacharopoulos, G., Hanel, P. H. P., Lancaster, T. M., Ihssen, N., Drakesmith, M., Foley, S., ... Linden, D. E. J. (2017). Nonlinear associations between human values and neuroanatomy. *Social Neuroscience*, *12*(6), 673–684.
- Zhang, X., Wang, Y.-T., Wang, Y., Jung, T. P., Huang, M., Cheng, C. K., & Mandell, A. J. (2015). Ultra-slow frequency bands reflecting potential coherence between neocortical brain regions. *Neuroscience*, *289*, 71–84.
- Zhao, C., Zhu, J., Liu, X., Pu, C., Lai, Y., Chen, L., ... Hong, N. (2018). Structural and functional brain abnormalities in schizophrenia: A cross-sectional study at different stages of the disease. *Progress in Neuro-Psychopharmacology and Biological Psychiatry*, *83*, 27–32.
- Zhigalov, A., Herring, J. D., Herpers, J., Bergmann, T. O., & Jensen, O. (2019). Probing cortical excitability using rapid frequency tagging. *NeuroImage*, *195*, 59–66.
- Zhigalov, A., & Jensen, O. (2020). Alpha oscillations do not implement gain control in early visual cortex but rather gating in parieto-occipital regions.
- Zhou, Y., Liang, M., Tian, L., Wang, K., Hao, Y., Liu, H., ... Jiang, T. (2007). Functional disintegration in paranoid schizophrenia using resting-state fMRI. *Schizophrenia Research*, *97*(1–3), 194–205.
- Zhu, Y., Tang, Y., Zhang, T., Li, H., Tang, Y., Li, C., ... Wang, J. (2017). Reduced functional connectivity between bilateral precuneus and contralateral parahippocampus in schizotypal

personality disorder. *BMC Psychiatry*, 17(1), 1–7.

Zink, N., Mückschel, M., & Beste, C. (2021). Resting-state EEG Dynamics Reveals Differences in Network Organization and its Fluctuation between Frequency Bands. *Neuroscience*, 453, 43–56.

Zwicker, A., Denovan-Wright, E. M., & Uher, R. (2018). Gene–environment interplay in the etiology of psychosis. *Psychological medicine*, 48(12), 1925-1936.